Physics Library
QC
1
.P5812
V.56
no.9

# THE PHYSICAL REVIEW

VOLUME 56 *Second Series* NUMBER 9

NOVEMBER 1, 1939

*Published for the*

AMERICAN PHYSICAL SOCIETY

*by the*

AMERICAN INSTITUTE OF PHYSICS
Incorporated

LANCASTER, PA., AND NEW YORK, N. Y.

UNIVERSITY OF MICHIGAN LIBRARIES

# THE PHYSICAL REVIEW

*A journal of experimental and theoretical physics established by E. L. Nichols in 1893*

Published by the American Institute of Physics for the

**American Physical Society**

**OFFICERS**

*President*

JOHN T. TATE
University of Minnesota
Minneapolis, Minnesota

*Vice President*

JOHN ZELENY
Yale University
New Haven, Connecticut

*Secretary*

W. L. SEVERINGHAUS
Columbia University
New York, New York

*Treasurer*

G. B. PEGRAM
Columbia University
New York, New York

*Local Secretary for the Pacific Coast*

PAUL KIRKPATRICK
Stanford University
California

*Editor*

JOHN T. TATE
University of Minnesota
Minneapolis, Minnesota

**BOARD OF EDITORS**

JOHN T. TATE, *Editor* — J. W. BUCHTA, *Assistant Editor*

*Associate Editors*

| | | |
|---|---|---|
| K. T. BAINBRIDGE | A. L. HUGHES | W. BLEAKNEY |
| H. P. ROBERTSON | T. H. JOHNSON | G. BREIT |
| H. B. WAHLIN | F. A. JENKINS | D. M. DENNISON |

Manuscripts for publication should be submitted to John T. Tate, University of Minnesota, Minneapolis, Minnesota.

Proof and all correspondence concerning papers in the process of publication, should be addressed to the Publications Manager, American Institute of Physics, 175 Fifth Avenue, New York, New York.

**Subscription Price**

*United States and Possessions and Canada* . . . . . $15.00
*Foreign* . . . . . $16.50

**Back Numbers**

*Complete set:* Series 2,[1] Vol. 1, 1913–Vol. 54, 1938—$390.00
*Yearly rate:* $16.50
*Single copies:* $1.50 each prior to July, 1929; $.75 each after July, 1929.

Subscriptions and orders for back numbers should be addressed to Prince and Lemon Streets, Lancaster, Pennsylvania, or to the American Institute of Physics, 175 Fifth Avenue, New York, New York.

Advertising is not accepted for the *Physical Review* but attention is called to the *Review of Scientific Instruments* and the *Journal of Applied Physics*, companion publications of the Institute, and media through which the field of physics can be reached most effectively. Rates and other information will be furnished on request.

Changes of address in the case of members of the American Physical Society, should be addressed to the Treasurer; in the case of other subscribers, to the Publications Manager.

[1] For Series 1 inquire of Physics Department, Cornell University, Ithaca, N. Y.

The Physical Review is published semi-monthly at Prince and Lemon Streets, Lancaster, Pennsylvania.

Entered at the Post Office at Lancaster, Pennsylvania, as second class matter.

Acceptance for mailing at special rate of postage provided for in section 1103, Act of October 3, 1917, authorized September 6, 1926.

Physics
Physics-LSA
Library
QC1.P5
Replaces,

THE
PHYSICAL REVIEW

*A Journal of Experimental and Theoretical Physics Established by E. L. Nichols in 1893*

VOL. 56, No. 9 NOVEMBER 1, 1939 SECOND SERIES

# The Internally Converted Gamma-Rays of Several Radioactive Elements

G. E. VALLEY* AND R. L. MCCREARY
*University of Rochester, Rochester, New York*

(Received September 7, 1939)

The conversion electron spectra of a number of radioactive elements produced by proton and deuteron bombardment in the cyclotron have been investigated. The beta-ray spectrograph was designed to allow rapid replacement of the source and photographic film so that successive fresh samples of short period activities could be used for a single exposure. The results may be summarized as follows: $Br^{80}$ (4.4 hr.) three conversion lines observed corresponding to two gamma-rays, one of 48.9±0.4 kev and a second of either 37.1 or 25.3 kev, both arising in the isomeric transition to the 18-min. state. $Br^{78}$ (6.3 min., $e^+$) $K$ and $L_1$ conversions in Se of two gamma-rays of 45.8±0.4 and 107.7±0.9 kev; $Cd^{107 \text{ or } 109}$ (6.4 hr., $K$ capture) $K$, $L_1$ and $M_1$ conversions of a gamma-ray of 92.6±0.8 kev. In this case there is an anomalously high $L_1$ conversion since the $K$ and $L_1$ lines have nearly equal intensity. Also a 530-kev gamma-ray, possibly annihilation radiation, although no positrons are observed. $Ga^{67}$ (78 hr., $K$ capture) $K$ and $L_1$ conversions of a gamma-ray of 92.5±0.8 kev; $Ga^{70}$ (18.5 min., $e^-$ and possible $K$ capture) $K$ and $L_1$ conversions of a gamma-ray of 53.8±0.5 kev and probably a second line of about 117 kev.

## INTRODUCTION

THE low energy line spectra of electrons emitted by radioactive isotopes are of interest in giving information about the mode of decay, the gamma-ray spectra and the process of internal conversion. Studies of such spectra for the radioactive isotopes $Br^{80}$, $Br^{78}$, $Cd^{107}$ (or $Cd^{109}$), $Ga^{67}$ and $Ga^{70}$ are reported in this paper. The results are summarized in Table I.[1]

## PROCEDURE

The beta-ray spectrograph used is shown in Fig. 1. It was developed after observations of the behavior of two previous instruments which indicated, that insofar as the sharpness of the line spectra were concerned, electron scattering could be neglected in such an arrangement. Accordingly the simplest design which would allow quick and accurate replacement of both source and photographic plate or film was sought.

TABLE I. *Conversion electron and gamma-ray energies.*

| RADIOACTIVE NUCLEUS | HALF-LIFE | $H\rho$ (GAUSS-CM) | ELECTRON ENERGY (KEV) | CONVERSION SHELL | GAMMA-RAY ENERGY (KEV) |
|---|---|---|---|---|---|
| $Br^{80}$ | 4.4 hr. | 524 | 23.6 | Br $K$ or $L_1$ | 37.1 or 25.3 |
| | | 646 | 35.5 | Br $K$ | 48.9±0.4 |
| | | 749 | 47.2 | Br $L_1$ | |
| $Br^{78}$ | 6.7 min. | 619 | 32.7 | Se $K$ | 45.8±0.4 |
| | | 725 | 44.3 | Se $L_1$ | |
| | | 1090 | 95.5 | Se $K$ | 107.7±0.9 |
| | | 1150 | 105.4 | Se $L_1$ | |
| $Cd^{107}$ (or $Cd^{109}$) | 6.4 hr. | 897 | 66.4 | Ag $K$ | 92.6±0.8 |
| | | 1053 | 89.6 | Ag $L_1$ | |
| | | 1065 | 91.5 | Ag $M_1$ | |
| $Ga^{67}$ | 78 hr. | 1006 | 82.4 | Zn $K$ | 92.5±0.8 |
| | | 1066 | 91.7 | Zn $L_1$ | |
| $Ga^{70}$ | 18.5 min. | 721 | 43.8 | Zn $K$ | 53.8±0.5 |
| | | 794 | 52.7 | Zn $L_1$ | |
| | | 1160 | 107.1 | Zn $K$ (?) | 117.0±1.0 |

* Now at Harvard University, Cambridge, Massachusetts.

[1] The values of the natural constants used in computation were those appearing in the publication of J. W. M. DuMond, Phys. Rev. **56**, 153 (1939); namely, $e_0=4.80290\times10^{-10}$ e.s.u.; $m_0=9.11096\times10^{-28}$ gram; $h_0=6.62602\times10^{-27}$ erg sec.

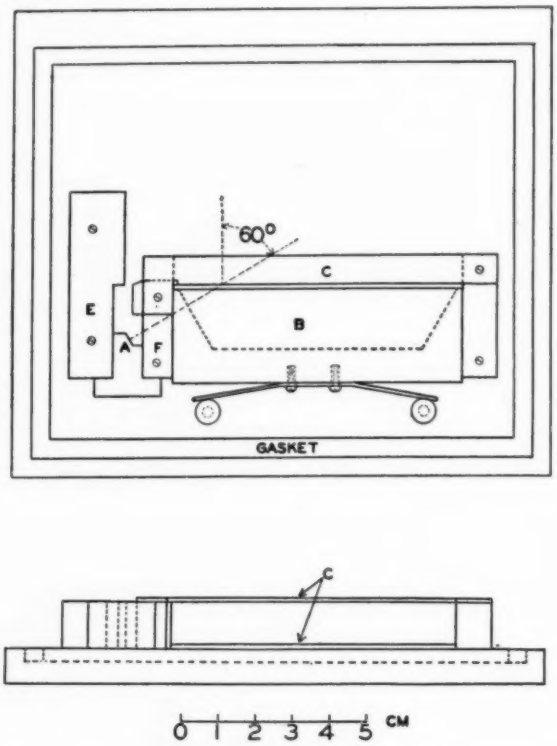


FIG. 1. Magnetic spectrograph. The radioactive source is placed on the inclined face of the removable block, *A*. The film or plate is clamped between the stationary members *C* and the sliding block, *B*. The elevation is drawn without *B*.

The first condition was met by mounting the radioactive source on the inclined face of the removable block *A*, which fits between the slit jaws consisting of two aluminum blocks *E* and *F*. The sources themselves were thin foils from 1 to 3 mm wide and 11 mm long. Several blocks similar to *A* were available. When high resolution was desired to determine line energies, the inclined face of *A* was tilted at 60 degrees as shown in Fig. 1. In this case, the sources were 1 mm wide and fastened to *A* so that the source edge nearest the photographic plate lay on a line through the center of the slit and normal to its plane. If this is not the case, the high energy side of the lines is not formed by exactly semi-circular trajectories and a small error results. For higher intensity with lower resolution, the source was tilted at an angle of 45 degrees and made 2 to 3 mm wide.

The photographic film or plate is clamped between the longitudinal members, *C* and the block *B*. *B* is pushed against the back of the film by the flat spring shown.

All of the parts shown in Fig. 1, including the base plates, are of aluminum except the block *B* which is a brass case filled with lead. A loosely hinged cover of brass, the beveled edges of whose sides fit the gasket shown, is held tight by atmospheric pressure. A sufficiently good vacuum was produced by a Megavac pump.

The magnet was constructed of Armco Ingot iron with pole face dimensions of eight by fourteen inches. The field produced was sufficiently uniform to make corrections unnecessary over the area occupied by the instrument of Fig. 1. The precision of our results is limited only by the constancy of the direct-current supply. The field was observed to vary over a maximum range $\pm 0.5$ percent during a run of 24 hours. Unless otherwise indicated, our measurements of $H\rho$ represent the mean values from several plates. No deviations from the mean greater than 0.5 percent were observed.

The field meter was a small direct-current generator driven by a synchronous motor. It is quite similar to the design published by Cole,[2] except that the part of the rotating shaft inserted between the magnet poles is made of lucite instead of brass. The average voltage produced by such a device is proportional to the magnetic field. This voltage was measured by a potentiometer. The generator and potentiometer was checked for linearity over the range of fields used with a pair of Helmholtz coils excited by storage batteries. No departure from linearity greater than 0.1 percent in the range of 100 to 500 gauss was observed.

To calibrate this field meter, the prominent *F* line from the thorium B·C transition was used for which line Ellis[3] gives the value 1385.8 gauss-cm.[4]

Both Eastman and Agfa "No Screen" x-ray films were used and developed for 8 minutes in Eastman D-19 developer at 66 degrees F. No significant difference between these two films was found in the range of opacities covered. These films are emulsion coated on both sides, a feature which served only to raise the background fog in the present work, since none of

[2] R. H. Cole, Rev. Sci. Inst. **9**, 215 (1938).
[3] C. D. Ellis, Proc. Roy. Soc. **A138**, 318 (1932).
[4] We wish to thank Professor T. R. Wilkins for preparing the thorium B sources for us.

the electron groups had sufficient energy to penetrate the film base.

The films were photometered at 0.2-mm intervals in the region of the lines. Wherever these measurements are significant they are plotted here as opacity *vs.* distance along the plate, with a superimposed $H\rho$ scale. The opacity of the plates is used instead of the density since with proper choice of development time this quantity is a linear function of the exposure.[5] To check this, a plot of line intensity *vs.* exposure was obtained from seven plates exposed to the same source of $Ga^{67}$ for various periods of time. It was found that the intensity of the $K$ line, measured either as the opacity of the peak of the line or as the area under the line, was a linear function of the exposure, provided the peak opacity was less than five. We have accordingly worked in this region.

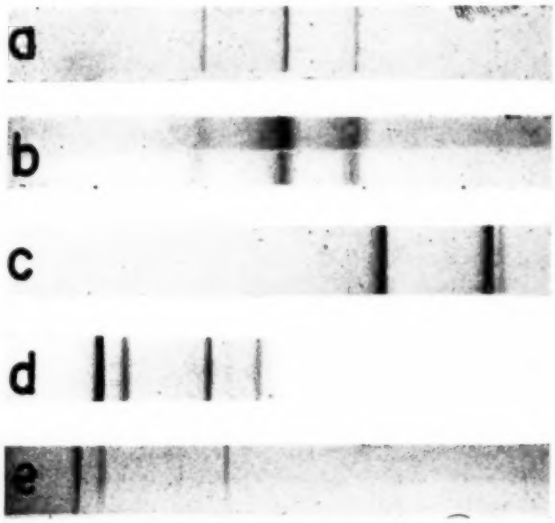


FIG. 2. (a) and (b) Plates of the 4.4-hour $Br^{80}$. (a) Plate from which energy measurements were taken. Source 1 mm inclined at 60 degrees. (b) Shielded plate. Source 2 mm inclined at 45 degrees. Upper section exposed 48 min. beginning immediately after bombardment; lower section exposed 55 min. beginning 48 min. after bombardment. (c) Plate of 6.4-hour $Cd^{107 \text{ or } 109}$. Thin silver films evaporated on aluminum foil and bombarded with protons used as sources. Sources 1 mm and inclined at 60 degrees. (d) and (e) Plates of 18-min. $Ga^{70}$ and 78-hour $Ga^{67}$ from bombardment of zinc with deuterons. (d) Plate from which energy measurements were taken. Plate was exposed for 75 min. to each of four sources of thin zinc foils 1 mm inclined at 60 degrees. (e) Shielded plate. Upper section exposed continually; lower section exposed for 26 min. beginning 21 min. after bombardment. Sources 2 mm inclined at 45 degrees.

[5] Cf. C. D. Ellis and W. A. Wooster, Proc. Roy. Soc. **A114**, 266 (1927).

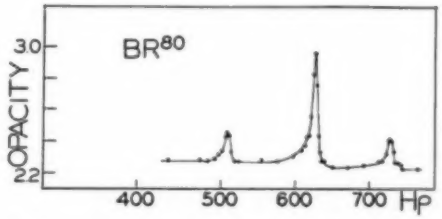


FIG. 3. Photometer record of plate shown in Fig. 2(a).

**$Br^{80}$, $Br^{78}$**

Since our previous communication[6] on the spectrum of $Br^{80}$, we have so improved our technique as to make desirable a more careful repetition of these experiments. The measurements were all made with sources produced by the deposition of thin films of selenium on aluminum foil by evaporation in a vacuum. The selenium-coated foils were cut to the correct size for the spectrograph, placed in an evacuated bombarding cup, which was cooled with dry ice in butyl-alcohol, and mounted on the exit port of the cyclotron chamber behind a 0.0005-inch aluminum window. During the bombardment the beam was sufficiently focused so that about 75 percent of the total current was intercepted by a foil 3 by 11 mm in size.

Figure 2(a) and (b) show two of the many spectra taken with selenium targets bombarded for various lengths of time and for different exposure times. Figure 2(a) is a spectrum such as was used to determine accurately the energies of the lines previously reported. Here the source was 1 mm wide and inclined at an angle of 60 degrees. The photometer measurements of this plate are shown in Fig. 3. Three lines at $H\rho$ values of 524, 646, 749 gauss-cm are clearly evident. The corresponding energies are 23.6, 35.5, 47.2 kev. These values supplant those previously given. The difference between the energies of the two highest lines is 11.7 kev agreeing within limits of error with the energy difference of 11.8 kev between the $K$ and $L_1$ absorption edges of Br. The difference between the two lowest lines is 11.9 kev. It seems safe to ascribe the lines at 646 and 749 $H\rho$ to the $K$ and $L_1$ conversion of a gamma-ray of $48.9 \pm 0.4$ kev. The line at 524 $H\rho$ may be the result either of a $K$ conversion of a gamma-ray of about

[6] G. E. Valley and R. L. McCreary, Phys. Rev. **55**, 666 (1939).

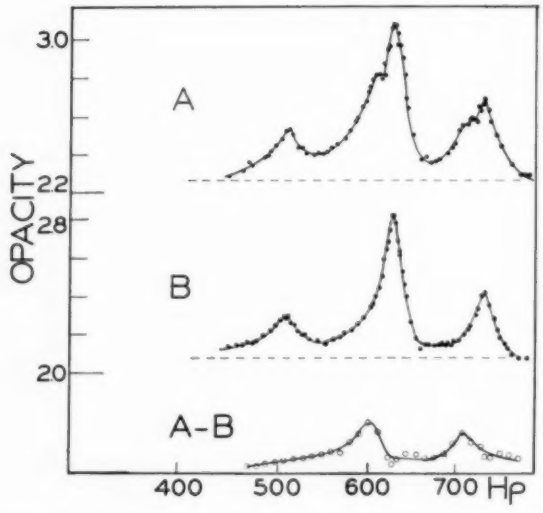


FIG. 4. Photometer records of plate shown in Fig. 2(b). *A*, record of the upper section; *B*, record of the lower section; *A*–*B*, difference curve.

37 kev (the $L_1$ conversion group being hidden in the large peak at 646 $H\rho$ [7]), or the $L_1$ conversion of a gamma-ray of about 25 kev. In the latter case there should be a $K$ conversion line at 12 kev, but we shall show some evidence below in support of the supposition of Ellis[3] that the sensitivity of photographic emulsions decreases sharply with decrease in energy in this region so that such a line would not be registered. For this reason also, no good estimate of the relative intensities of these lines can be given.

It remains to establish that these lines all come from 4.4-hour period of $Br^{80}$. Buck[8] has shown that Se when activated by protons of 6.5 Mev exhibits the following radioactive periods: 6.3 min. ($Br^{78}$, $e^+$), 18 min., and 4.4 hours ($Br^{80}$) and 33 hours ($Br^{82}$, $e^-$). We have excluded the 33-hour period by exposing another plate to a source which had already produced the lines previously. This second exposure of twenty hours beginning twenty hours after bombardment should have revealed the same spectrum with 0.65 times the intensity of Fig. 3 if $Br^{82}$ were responsible. Actually, two exposures of this type showed no evidence for any lines whatever.

It was next of great importance to determine whether this spectrum was due entirely or in part to the 18-minute isomer of $Br^{80}$. The procedure was to bombard a selenium covered foil for 90 minutes with a beam of 1.5 microamp. of 6.5-Mev protons. This target was placed in the spectrograph within 90 seconds after the end of bombardment and an exposure of 48 minutes taken with the lower section of the photographic plate shielded longitudinally with 0.5-mm aluminum strip. The exposure was then interrupted for one minute while the lower section of the plate was uncovered and the upper section shielded. The exposure then continued for 55 minutes. Meanwhile a second source was being bombarded, to which the same plate was exposed in turn with the same procedure. This was repeated with six sources in order to get the lines sufficiently dark for reliable photometry. Since it was found necessary to use sources about 2 mm wide inclined at only 45 degrees in order to increase the intensity, the resolution is not as good as that obtained previously. This plate is shown in Fig. 2(b) and the photometry measurements of both longitudinal sections in Fig. 4. Here $A$ is the section exposed for the first period of 48 minutes and $B$ is the section exposed for the second period of 55 minutes. If any of these lines occur only in the 18-minute period they should be about seven times as strong in $A$ as in $B$, while if they come from the 4.4-hour period their opacities should be the same for the two sections. There remains the possibility that one or more of these lines accompany both the isomeric periods, 18 min. and 4.4 hr. However, from Buck's[8] measurements of the cross section of the two periods under similar conditions, it is found that at the end of this bombardment there would be about 35 times as many 18-minute atoms as there are 4.4-hour atoms. Hence a line common to both periods would give relative intensities in sections $A$ and $B$ about the same as if they came from the 18-minute period alone.

After subtracting out the backgrounds, indicated by the dashed lines in Fig. 4, it is found that the peak opacities of the lines on the two sections are equal to within 4 percent, which is satisfactory proof that the lines at 525, 646 and 749 $H\rho$ come from the 4.4-hour half-life only.

The situation is complicated, however, by the doublet structure which appears on the low

[7] Cf. also C. D. Ellis, reference 3, who gives two instances of this curious phenomenon in thorium.
[8] J. H. Buck, Phys. Rev. **54**, 1025 (1938).

energy side of the lines at 646 and 749 $H\rho$. That this is a new pair of lines was revealed by making the ordinates of $A$ exactly equal to those of $B$ at the peak of the 646 $H\rho$ line and subtracting $B$ from $A$. This reveals a pair of lines at 620 and 725 $H\rho$. It was obvious that these do not come from the 4.4-hour half-life alone. The possibilities were then that they came from (1) the 6.3-minute $Br^{78}$, or (2) the 18-minute period, or (3) the 18-minute and the 4.4-hour half-lives. Accordingly, the above experiment was repeated in faster tempo to settle this point.

A source was bombarded for 12 minutes and exposed to the upper section for 7 minutes with the lower section shielded, immediately after which the lower section was exposed for 8 minutes with the upper section shielded. This procedure, as in the previous experiment, was repeated for 8 sources with the same conditions prevailing for each source. Under these conditions, lines from the 6.3-minute period should be twice as strong in the upper as in the lower section, whereas lines from the 18-minute, (or the 18-minute and 4.4-hour) period should appear equally strong. The photometer tracings of this plate appear in Fig. 5. This shows that these lines as well as two more of higher energy come from the 6.3-minute period of $Br^{78}$. Because of the low intensity and resolution (2-mm sources inclined at 45 degrees) the $H\rho$ values of the new lines could not be determined accurately. However, the following are approximate values for the four lines of the 6.3-minute period: 619, 725, 1090 and 1150 gauss-cm, corresponding to energies of 32.7, 44.3, 95.5 and 105.4 kev, respectively. These can be interpreted as the $K$ and $L_1$ conversions, in the product nucleus Se, of gamma-rays of $45.8\pm0.4$ and $107.7\pm0.9$ kev.

### Significance of the $Br^{78, 80}$ lines

Segrè *et al.*[9] have shown that the 4.4-hour $Br^{80}$ isomer decays into the 18-minute isomer with the emission of internally converted gamma-rays. These are the gamma-rays which have been detected. The absence of any others from the 18-minute period alone confirms this view since these would be impossible if there is such a genetic relationship. If some of these lines appeared in both periods, it would mean merely that they came from an excited state of the product nucleus, $Kr^{80}$. This is, however, not the case with these gamma-rays. The much harder gamma-rays detected by Buck[8] in both periods are probably from the excited $Kr^{80}$.

The existence of the two gamma-ray lines associated with the 4.4-hour $Br^{80}$ requires that there be an additional level in this nucleus between the 4.4-hour and the 18-minute levels. Transitions between the latter two levels give rise to the 48.9-kev gamma-ray while transitions from the 4.4-hour level to an intermediate level give rise to the 37.1 (or 25.3) kev line. The succeeding transition from the intermediate to the lower (18-minute) level either is not internally converted to any appreciable extent or (in case 25.3 kev is the correct value), gives lines nearly coinciding with the first transition. It is also possible, but less probable in view of the necessary spin differences, that the two gamma-rays are emitted in cascade, the total energy difference between the upper and lower states being 86.0 (or 74.2) kev. In this case direct transitions might be expected, but are not observed.

The group of conversion electron lines from the positron emitting $Br^{78}$ (6.3 minute) is of interest. They might be ascribed to transitions from a hitherto unobserved isomeric state of this nucleus of much shorter period, or more probably to excited levels in the product nucleus $Se^{78}$. (The accuracy is not sufficiently great to distinguish between the $K-L_1$ differences for Br and Se.) In the latter case this would suggest a fine structure in the upper limit of the positron

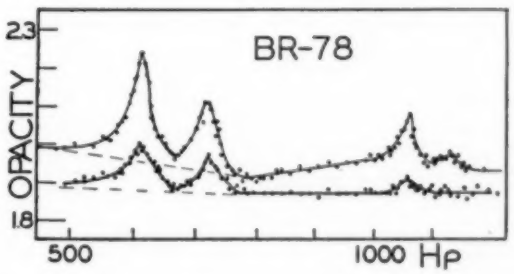


FIG. 5. Photometer records of both upper and lower sections of the 6.3-min. $Br^{78}$ plate. Top curve shows section exposed for 7 min. beginning immediately after bombardment; bottom curve shows section exposed for 8 min. beginning 7 min. after bombardment.

[9] E. Segrè, R. S. Halford and G. T. Seaborg, Phys. Rev. **55**, 321 (1939).

spectrum which is at 2.3 Mev.[10] This fine structure would not be directly observed by present methods, but might be of interest in connection with the theory of beta-decay.

**6.4-hour Cd**

Figure 2(c) shows the spectrum obtained after bombarding silver deposited on 0.0005-in. aluminum foil to a thickness of 0.48 mg/cm². Fig. 6 shows the photometer measurements of this plate. There are three lines whose $H\rho$ values are: 897, 1053 and 1065 gauss-cm, corresponding to energies of 66.4, 89.6 and 91.5 kev, respectively. These correspond within experimental error to the $K$, $L_1$ and $M_1$ conversions of a gamma-ray of $92.6\pm0.8$ kev. The lines corresponding to the $K$ and $L_1$ conversions are seen to have equal opacities. It is highly improbable that any corrections for the decreased sensitivity of the plate at lower energies, can possibly make the line at 897 $H\rho$ more than twice the intensity of that at 1053 $H\rho$. This is still a fourfold discrepancy from the usual ratio of 8 to 1 for $K$ and $L_1$ conversions. W. T. Harris[11] of Princeton University has also measured these lines and confirms the fact that the two lowest energy lines appear equally strong. Further, as will be shown below, the $K$ and $L_1$ lines from $Ga^{67}$, at about the same energy, appear to have about the correct relative opacities (8 to 1) which rules out any large correction for the change in sensitivity of the plate with $H\rho$.

It is difficult to understand the large difference in the ratio $K$ to $L_1$ conversion between this Cd activity (ratio approximately one) and $Ga^{67}$ (ratio approximately eight), the gamma-rays being about the same energy. One might assume that these two lines are both $K$ conversions of two different gamma-rays. One has then to explain why there is no line corresponding to the $L_1$ conversion of the second gamma-ray. Attempts to observe this have been made without success. In making the choice between anomalously high and anomalously low $L_1$ conversion, the former has been chosen because of the presence of the low intensity ($M_1$) line at 1065 gauss-cm.

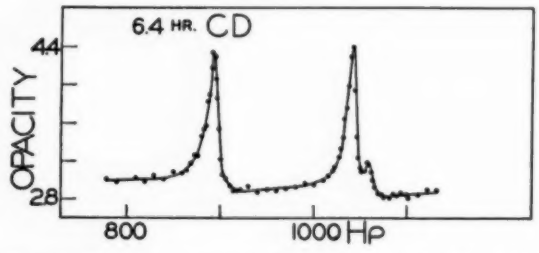


FIG. 6. Photometer record of plate shown in Fig. 2(c).

Since this nucleus gives off large quantities of x-rays which arise from $K$ capture as well as from the high internal conversion of the 92.6-kev gamma-ray and since the fluorescent yield in silver is about 0.75, the Auger electrons should be of sufficient number to be observed. From Ilford Q2 plates[12] as well as the usual x-ray emulsions, no evidence was found for these electrons. It is concluded that electrons of energy less than 20 kev have very little effect upon these photographic emulsions as compared to those of two or three times that energy. It is for this reason that no statement can be made concerning the relative intensities of the conversion groups from the $Br^{80}$.

Delsasso *et al.*[13] also report a hard gamma-ray accompanying this decay. A thick piece of silver was bombarded for two hours with 1.5 microamp of 6.7-Mev protons. This gave a source sufficiently intense so that the decay was followed over a half-life with the radiation filtered by 1.89 g/cm² of lead. This decay is shown in Fig. 7. At the same time the absorption curve in lead, which is also shown in Fig. 7 was taken. From this the mass absorption coefficient was found to be 0.146 g/cm², corresponding to a gamma-ray of 0.53 Mev, according to Gentner's[14] compilation. This immediately suggests the annihilation of positrons. Positrons were looked for by placing a specimen, several hours after bombardment, in a cloud chamber. No positrons were seen in 250 pictures although several thousand short range tracks of the conversion electrons were noted. However, a few positrons with an energy of 100 kev or less might have escaped observation because at this energy

[10] A. H. Snell, Phys. Rev. **52**, 1007 (1937).
[11] W. T. Harris, private communication.

[12] We wish to thank Professor K. T. Bainbridge for the gift of these plates.
[13] L. A. Delsasso, L. N. Ridenour, R. Sherr and M. G. White, Phys. Rev. **55**, 113 (1939).
[14] W. Gentner, Physik. Zeits. **38**, 836 (1937).

scattering has more to do with track direction than the magnetic field.

Silver, 0.01 in. thick has been bombarded as an internal target in the cyclotron chamber[15] for approximately six hours at 20 microamp. With this source possible annihilation radiation was searched for by measuring the coincidence counting rate when the source was placed alternately between and above two Geiger counters. No conclusive evidence for annihilation radiation was found. The experiment is made difficult, however, by the very low intensity of this 530-kev gamma-ray compared to the other very intense radiations which accompany this decay.

The 32-minute half-life which appears in Fig. 7, was shown not to be cadmium by chemical separation. Less than one percent of sulphur impurity would produce sufficient $Cl^{34}$ to appear here. There is, therefore, no evidence sufficient to fix the assignment of the 6.4-hour period to either $Cd^{107}$ or $Cd^{109}$.

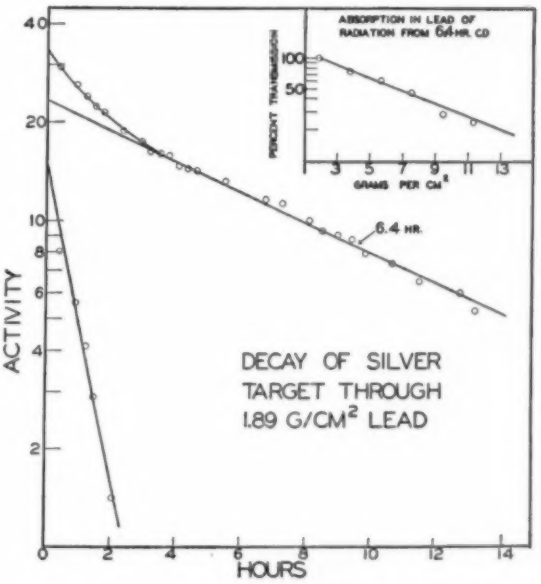


FIG. 7. Decay and absorption in lead of $Cd^{107}$ or $^{109}$.

### $Ga^{67}$, $Ga^{70}$

The zinc radioactivities with half-lives of 57 minutes and 13.8 hours have been shown by Livingood and Seaborg[16] to be isomers of $Zn^{69}$. These have about the same beta-ray upper limits. Since this is a necessary condition for the isomers to be related genetically, zinc has been bombarded with 4.3-Mev deuterons and observed for internal conversion spectra arising from the isomeric transitions. Several lines were found, but none can be attributed to either period of $Zn^{69}$. This confirms the result of the absorption measurements of Livingood and Seaborg.[16]

Figures 8 and 9 show the decay of gallium and zinc, the two elements having been chemically separated after bombardment of zinc with 4.3-Mev deuterons. The gallium periods are 18.5 minutes, 69.5 minutes and 78 hours corresponding to the isotopes, previously reported by Buck,[8] or $Ga^{70}$, $Ga^{68}$ and $Ga^{67}$, respectively. The zinc separation (which included any other elements which may have been present) shows only the periods of $Zn^{69}$ plus a trace of the long-lived $Zn^{65}$ (245 days) which has been subtracted out from Fig. 9.

To determine the source of the observed lines, zinc foils were bombarded for 75 minutes with 0.8 microamp. of 4.3-Mev deuterons. These foils were obtained by rolling out spectroscopically pure zinc crystals (from the New Jersey Zinc Co.) to the thickness of 0.0006 inches. Four such sources were exposed in the spectrograph, each for 75 minutes, in order to attain sufficient density on the plate. The plate is shown in Fig. 2(d) and the accompanying photometer curves in Fig. 10, curve *A*. Another piece of this zinc was bombarded for 6 hours at 1.2 microamp. of 4.3-Mev deuterons and two successive two-hour exposures, Fig. 10, curves *B* and *C*, were taken. These three plates taken together show five lines, three at $H\rho$ values of 721, 794 and 1160 gauss-cm accompanying a half-life of less than two hours, the other two at $H\rho$ values of 1006 and 1057 gauss-cm accompanying a much longer half-life.

Commercial zinc was bombarded as an internal target in the cyclotron for six hours at about 20 microamp. of 4.3-Mev deuterons. From this source thirteen exposures of various lengths of time were made during the course of ten days. Two of these, the first exposed for two hours beginning four hours after the end of bombardment, the second exposed for six hours beginning

[15] R. R. Wilson and M. D. Kamen, Phys. Rev. **54**, 1031 (1938).
[16] J. J. Livingood and G. T. Seaborg, Phys. Rev. **55**, 457 (1939).

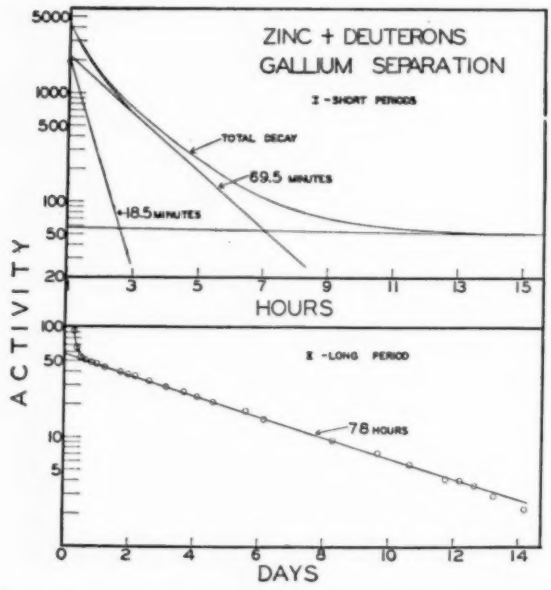


FIG. 8. Decay curves of gallium separation from zinc bombarded with deuterons.

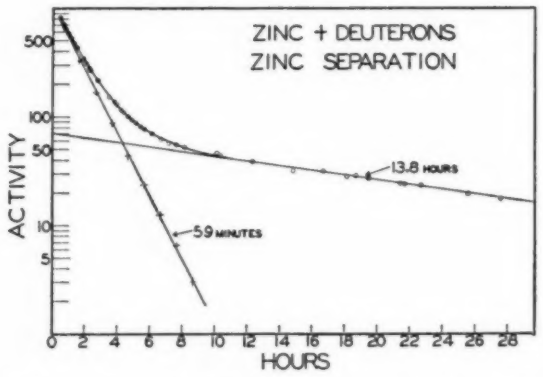


FIG. 9. Decay curve of zinc separation from zinc bombarded with deuterons.

224 hours after bombardment, exhibit the line at 1006 gauss-cm with the peak opacities above background of 0.9 and 0.36, respectively. It was assumed that the plate responded linearly between these values the decay period of this line was computed giving a value of about 75 hours. This indicates that this is the $K$ line accompanying the decay of $Ga^{67}$. Having ascertained this, it was felt justifiable to calculate the exposures to the other plates using the known period of $Ga^{67}$ and thus obtaining the exposure *vs.* intensity data previously mentioned.

The lines at $H\rho$ values of 1006 and 1066 gauss-cm, corresponding to electron energies of 82.4 and 91.7 kev, respectively, accompany the decay of the long life $Ga^{67}$. Since this is a well-known case of decay by $K$-electron capture previously reported by Alvarez,[17] these energies correspond to the internal conversion in the Zn $K$ and $L_1$ shells, respectively, of a gamma-ray of $92.5 \pm 0.8$ kev. This is in fair agreement with the gamma-ray reported by him.

The lines at $H\rho$ values of 721 and 794 gauss-cm, corresponding to electron energies of 43.8 and 52.7 kev, respectively, were shown definitely to be associated with $Ga^{70}$ in a manner similar to that employed in investigating $Br^{80}$. Zinc was bombarded with deuterons for 40 minutes and the upper section of the plate exposed for a period of 47 minutes; the lower section was shielded for the first 21 minutes after bombardment. The shield was then removed and this section was then exposed for a period of 26 minutes. This schedule was repeated with five sources. This plate is shown as Fig. 2(e). Fig. 11, curve $A$, shows the photometer record of the upper section of this plate. Here since the plate shows a large background increasing toward the low energy end, an interpolated background was subtracted and these relative opacities above background were plotted for the upper and lower sections as Fig. 11, curves $B_1$ and $B_2$, respectively. The curve $B_1$ shows the lines at $H\rho$

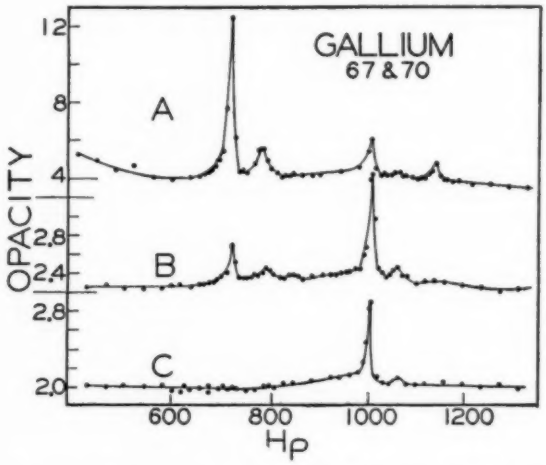


FIG. 10. Photometer records of $Ga^{67}$ and $Ga^{70}$ plates. $A$, record of the plate shown in Fig. 2(d); $B$ and $C$, records of plates of successive two-hour exposures to a strongly activated zinc source by deuterons. Plates for $B$ and $C$ are not shown.

[17] L. W. Alvarez, Phys. Rev. **54**, 486 (1938).

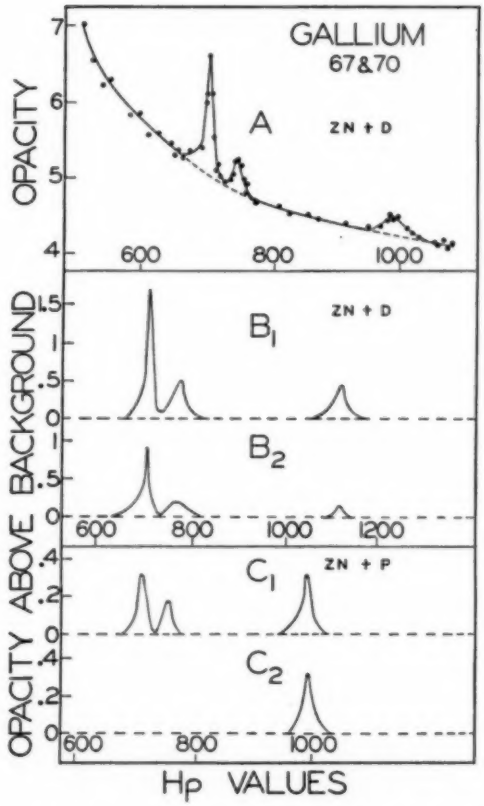


FIG. 11. Photometer records of $Ga^{67}$ and $Ga^{70}$ plates. $A$, record of the upper section of the plate shown in Fig. 2(e); $B_1$ and $B_2$, records from which the background has been subtracted out of the plate shown in Fig. 2(e). $C_1$ and $C_2$, records of plate exposed to zinc bombarded with protons. $C_1$ is upper section exposed for 46 min. beginning immediately after bombardment; $C_2$ is lower section exposed for 48 min. beginning 46 min. after bombardment.

values of 721 and 794 gauss-cm twice as strong as does curve $B_2$. This is about what one would expect for an 18-minute decay. The line at 1160 also seems to come from a half-life shorter than 20 minutes.

Since the only activity of the required short half-life which we have detected was the 18-minute $Ga^{70}$, we tried the experiment of bombarding 0.0002-inch zinc foil with 6.7-Mev protons. Buck[8] has previously established the reaction $Zn^{70}(p, n)Ga^{70}$. The sample was bombarded for a period of 90 minutes; the upper section of the plate was exposed for a period of 46 minutes after bombardment and subsequently the lower section for a period of 48 minutes. Several sources were exposed. This plate is not shown, but the photometer records, from which the background has been subtracted out, are shown as Fig. 11, curves $C_1$ and $C_2$. Curve $C_1$, which is the upper section, shows the lines at $H\rho$ values of 721, 794 and 1006 gauss-cm. Curve $C_2$ shows only the line at 1006 gauss-cm, which is the $Ga^{67}$ $K$ line. This is conclusive evidence for the existence of the lines at 721 and 794 gauss-cm in $Ga^{70}$. However, the failure to observe the line at 1160 gauss-cm by bombardment of zinc with protons, renders the assignment of it doubtful.

Mann[18] reports the existence of 4.9-Mev negative electrons accompanying the decay of $Ga^{70}$ to stable $Ge^{70}$. Since Buck found the threshold for the formation of $Ga^{70}$ by bombardment of zinc with protons to be below 1.6 Mev, this would indicate a surprisingly high mass difference between $Ga^{70}$ and $Ge^{70}$. Zinc was bombarded with protons for a period of 9 minutes behind sufficient aluminum to reduce the beam energy to 2 to 3 Mev which is above the threshold for $Ga^{70}$, but below that of the short period positron emitting isotopes of Ga. With such a bombardment the 18-minute $Ga^{70}$ should be much more intense than any other gallium periods formed. Such a source, however, showed no high energy electron tracks in the cloud chamber, although there were a number of positrons from other weak activities. This suggests that $Ga^{70}$ decays mainly by $K$ capture to $Zn^{70}$, though the emission of a few beta-rays is not excluded. The electron lines at $H\rho$ values of 721 and 794 gauss-cm are then interpreted as arising from the internal conversion in the Zn $K$ and $L_1$ shells of a gamma-ray of $53.8 \pm 0.5$ kev.

In conclusion we wish to thank Professor L. A. DuBridge and Dr. S. W. Barnes for suggesting some of these investigations, and Dr. S. N. VanVoorhis who has most graciously given us his assistance. We are indebted to Dr. C. V. Strain for the use of his Geiger counters and ionization chamber, and to the Institute of Optics for the use of their photometer. This work was supported in part by a grant from the Research Corporation.

[18] W. B. Mann, Phys. Rev. **54**, 649 (1938).

# Radioactivities Produced by Proton Bombardment of Palladium

T. ENNS
*The University of Rochester, Rochester, New York*
(Received September 11, 1939)

Proton bombardment of Pd produces the three known Ag periods of 2.3 min. ($Ag^{108}$), 25 min. and 8 days ($Ag^{106}$), and three new periods of 16.3 min. (+), 73 min. (+) and 45 days (*K* capture). The latter are assigned tentatively to $Ag^{102}$, $Ag^{104}$, and $Ag^{105}$, respectively. Excitation functions for the isomeric 25-min. and 8-day periods give *p-n* thresholds of 3.8 and 3.9 Mev, respectively. The former agrees with the known positron spectrum of the short period. The higher threshold for the 8-day period indicates that this state lies above the 25-min. state. This activity is accompanied by probably three gamma-rays of which two of 0.62 and 1.06 Mev have been identified with a beta-ray spectrograph. Since no positrons accompany this activity it must decay mainly by *K*-electron capture to $Pd^{106}$ rather than to the lower isomeric state. Four gamma-rays of about 0.29, 0.42, 0.50, and 0.69 Mev accompany the 45-day period.

BOMBARDMENT of Pd by fast protons produces six radioactive periods. Decay curves from which these are obtained are shown in Figs. 1 and 2. The half-lives are 2.3 min., 16.3 min., 25 min., 73 min., 8 days, and 45 days. All of them have been assigned to Ag isotopes. Fig. 3 shows the radioactive Ag isotopes (circles) and the Rh, Pd, Ag, and Cd stable isotopes (squares).

The 2.3-min., 25-min., and 8-day periods have been reported by previous observers[1] and assignments fixed by several reactions. The 2.3-min. activity ($e^-$) is due to $Ag^{108}$ while the 25-min. and 8-day periods have been assigned to isomers of $Ag^{106}$. The 25-min. state emits positrons whose maximum energy is 2.0 Mev.[1, 2] The 8-day activity has been reported[1, 2, 3] as emitting electrons, a much smaller number of positrons, and gamma-rays. A further study of its radiations will be reported in this paper.

It should be possible to produce the 22-sec. period assigned to $Ag^{110}$ by proton bombardment of $Pd^{110}$ (Fig. 3). No trace of this period was found even when observations began within 2 min. after bombardment. It is easily observed after slow neutron bombardment of Ag. If the cross section of this activity at 6.5 Mev were of the order of magnitude of other short period cross sections, the period would have been observed. The *p-n* threshold, therefore, must be quite high.

### THE 16.3-MIN. AND 73-MIN. PERIODS

These periods have been assigned to $Ag^{104}$ and $Ag^{102}$, respectively, since they are probably formed by *p-n* reactions. The assignments were made in this way since the abundance of these isotopes gave yield values of the order of magnitude of those for the 25-min. period. These periods have not been produced by other reactions. $Ag^{102}$ cannot be produced by any other known type of reaction but $Ag^{104}$ could be formed by $Cd^{106}$ $(d, \alpha)$.

The activities probably consist of positrons though no accurate sign determinations could be made because of the other short periods of both signs.

The 16.3-min. activity is too strong to be assigned to an impurity. There is however some doubt concerning the assignment of the 73-min. period. This activity appeared in the Pd foils obtained from the American Platinum Works. The purity was given as 99.8 percent and the impurities listed as Pt, Rh, and Ir. None of these elements show *p-n* reactions at an energy of 6.6 Mev. The period also appeared in Pd obtained from another source. If the period is due to impurities, it must be composed of several periods from low atomic number elements occuring as 0.1 percent or less in all Pd targets.

[1] M. L. Pool, Phys. Rev. **53**, 116 (1938).
[2] N. Feather and J. V. Dunworth, Proc. Roy. Soc., **168**, 566 (1938).
[3] J. R. Richardson, Phys. Rev. **55**, 609 (1939).

### The 8-day and 45-day Periods

Analysis of the long period activities of the Ag produced from Pd gives an 8-day and a 45-day activity. The 45-day period was determined from the curves of Fig. 2 and from other measurements extending over three months.

Considering the possible products of *p-n* reactions, $Ag^{105}$ was the unassigned isotope of odd mass number closest to the stable Ag isotopes (Fig. 3). Hence the longest of the periods was assigned to it. It should be possible to produce this period from $Pd^{104}$ by a *d-n* reaction. The activity would be small and may have escaped observation.

Both long period activities are composed of x-rays, $\gamma$-rays, and conversion electrons. These were separated and identified from absorption measurements. The electrons were stopped by covering the target with 2 mm. of Be. From absorption measurements in aluminium the x-ray and $\gamma$-ray components were separated and are plotted in Fig. 2.

The x-ray absorption coefficient of the 45-day activity is equal to that expected for Pd $K\alpha$. This isotope probably decays by $K$-electron capture followed by $\gamma$-ray emission in a manner similar to that assigned to the 8-day period in Fig. 6.

The 8-day period x-ray absorption curves also have the Pd $K\alpha_1$ slope. The activity was too small however to make definite differentiation from x-rays of neighboring elements.

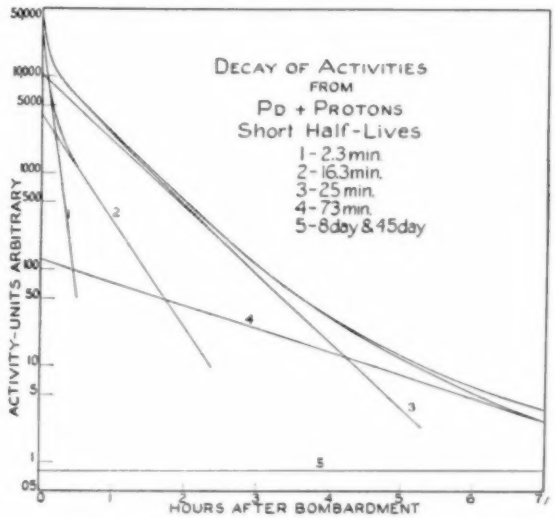


Fig. 1. Short period decay curve for activated Pd.

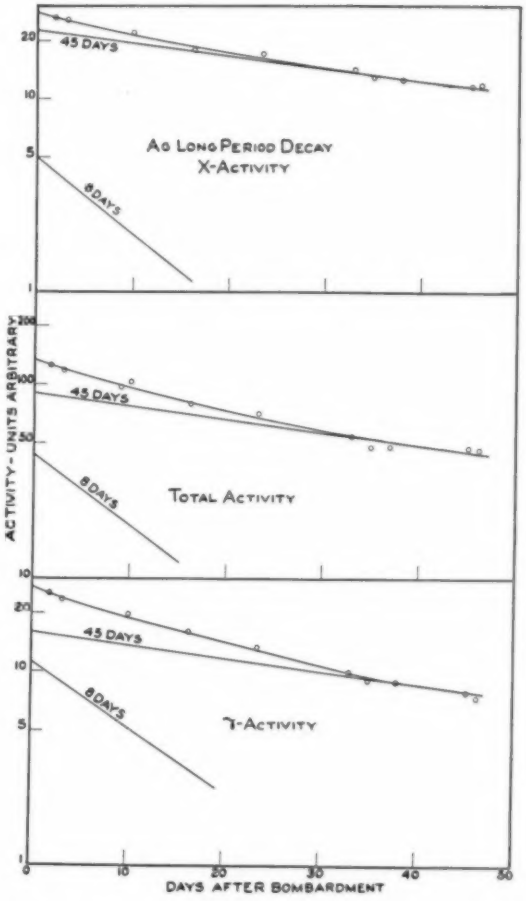


Fig. 2. Long period decay curve for activated Pd.

From the curves of Fig. 2 and the sensitivity ratio, the ratio of electrons to x-ray quanta was found to be 1 : 5 for the 8-day period and 1 : 10 for the 45-day period. The low energy electrons recently reported by Richardson[3] for the 8-day period are undoubtedly secondaries produced by the x-rays.

Gamma-ray spectra of the two long periods were obtained by covering the sample with lead foil and mounting in a $\beta$-ray spectrograph to obtain spectra of the photoelectrons. One 6-day

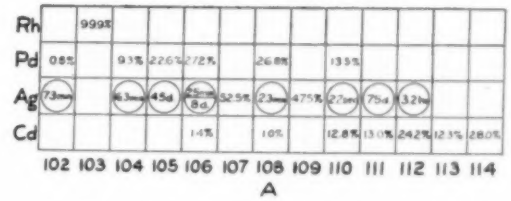


Fig. 3. Stable and radioactive isotopes of Ag and neighboring elements.

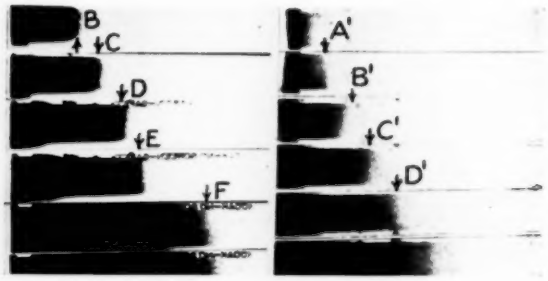


FIG. 4. Long period $\gamma$-ray spectra.

exposure was begun 3 days after bombardment and a second 7-day exposure began 38 days after bombardment. The sample was the same one used to get the decay curves of Fig. 2. Exposure 1 should show spectra of both periods, but exposure 2 should show only the 45-day period. Lack of contrast in the films made high contrast prints necessary for their analysis. Prints were made on Kodalith film and developed in a special high contrast developer prepared by Mr. T. W. Finucane of the Institute of Optics. The edges in the spectra were brought out by varying the exposures of the Kodalith film. No edge was assigned unless it appeared on several prints of different exposures. Normal contact prints of some of the Kodalith films are shown in Fig. 4. The high energy edges are on the right side of the prints.

Table I gives the $H\rho$ values of the observed edges and the corresponding $\gamma$-ray energy values. It is seen that the 45-day spectrum consists of four gamma-rays of 0.29 Mev, 0.42 Mev, 0.51 Mev, and 0.62 Mev. The 8-day spectrum shows two gamma-rays of 0.69 Mev and 1.06 Mev.

## EXCITATION DATA

Table II gives the thick target yields and thin target cross sections for the reactions observed. The yields are expressed as radioactive atoms formed per proton for a thick target of the pure isotope with incident protons of 6.3 Mev energy. The cross sections were calculated from thin film excitation measurements using stacked foils with incident protons of 6.63 Mev.

The 8-day period and 45-day period cross sections are calculated for $K$-electron capture, the number of radioactive atoms decaying being taken equal to the number of x-ray quanta. The fraction of the initial activity of 8-day and 45-day periods caused by x-rays was obtained from the data of Fig. 2, and the same ratios assumed for the thin targets. The ionization chamber was calibrated for x-rays by observing the deflection caused by a known number of In x-ray quanta from radioactive[4] $Sn^{113}$. The ionization produced by one x-ray quantum was found to be 1/25 of that for one $\beta$-ray.

The excitation curves of Fig. 5 were obtained from observations on stacked Pd foils 0.2 mil thick. The energy intervals were increased in some cases by placing Al foils between the targets. To make possible a closer examination of the long period thresholds, a bombardment was made on 0.1-mil foils without intermediate Al foils.

Energy determinations were made by measuring the visible range in air of the proton beam. This value was corrected for temperature and pressure, and assumed to be the extrapolated range. The mean range was calculated and the energy read from the curves given by M. S. Livingston and H. A. Bethe.[5] The energy values used were thus maxima rather than average

TABLE I. *Gamma-rays from 8-day and 45-day periods of Ag.*

| EXPOSURE | LINE NO. | $H\rho$ IN GAUSS-CM | $h\nu$ IN MEV |
|---|---|---|---|
| 1 | *A* | 1650 | 0.29±0.03 |
| | *B* | 2260 | 0.43± .04 |
| | *C* | 2620 | 0.52± .04 |
| | *D* | 2980 | 0.62± .04 |
| | *E* | 3270 | 0.69± .05 |
| | *F* | 4560 | 1.06± .05 |
| 2 | *A'* | 1610 | 0.29± .03 |
| | *B'* | 2140 | 0.40± .04 |
| | *C'* | 2470 | 0.49± .04 |
| | *D'* | 2990 | 0.62± .04 |

TABLE II. *Yields for p-n reactions yielding silver isotopes.*

| ISOTOPE AND EMITTED PARTICLE | HALF-LIFE | YIELD RAD. ATOMS PER $10^6$ PROTONS | $\sigma$ IN $CM^2$ $\times 10^{28}$ |
|---|---|---|---|
| $Ag^{108}(e^-)$ | 2.3±0.2 min. | 4.5±0.5 | 8.1 ±0.8 |
| $Ag^{106}(e^+)$ | 25.0±0.5 min. | 2.7± .3 | 5.5 ±0.6 |
| $Ag^{106}(K)$ | 8.2±0.2 days | | 0.13±0.05 |
| $Ag^{105}(K)$ | 45 ±5 days | | 3.7 ±1.0 |
| $Ag^{104}(e^+)$ | 16.3±0.7 min. | 2.6±1.0 | 1.8 ±0.9 |
| $Ag^{102}(e^+)$ | 73 ±10 min. | 2.1±1.0 | |

[4] S. W. Barnes, Phys. Rev. **56**, 414 (1939).
[5] M. S. Livingston and H. A. Bethe, Rev. Mod. Phys. **9**, 245 (1937).

values. This was desirable as threshold determinations were the main object of the measurements.

The 25-min. threshold was established as $3.8 \pm 0.1$ Mev. The 8-day period and 45-day period thresholds are probably within 0.4 Mev of each other. A composite excitation curve taken within 4 days of the end of the bombardment time has been plotted. This shows a 3.9-Mev threshold. At 3.8 Mev the foils showed no activity. At 4.3 Mev the activity had a period of about 20 days. The 8-day period threshold was therefore between these limits.

## The Isomers of $Ag^{106}$

Energy level diagrams for the decay of the 25-min. and 8-day $Ag^{106}$ isomers to $Pd^{106}$ are shown in Fig. 6. The $Pd^{106}$ energy is taken as the ground level. The $Ag^{106}$ energies are obtained by subtracting the $n$-$p$ mass difference ($\sim 0.8$ Mev) from the observed $p$-$n$ thresholds.

The 25-min. period belonging to the lower state must decay directly to the ground state of $Pd^{106}$ by positron emission, the threshold measurements being in agreement with the known positron spectrum. Since the 8-day period is accompanied by few if any positrons, and since the gamma-rays accompanying it are

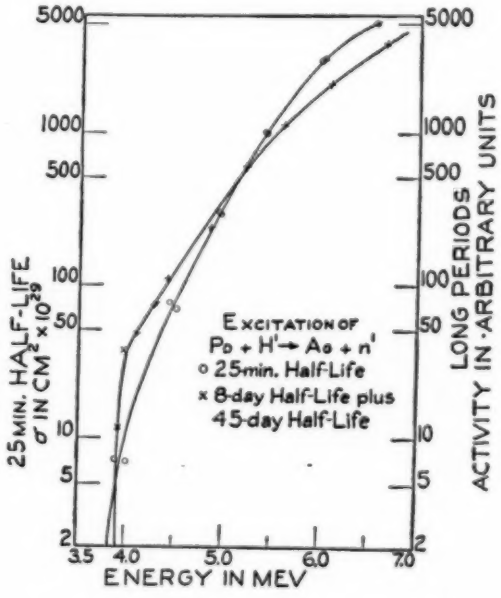


FIG. 5. Excitation curves for protons on Pd.

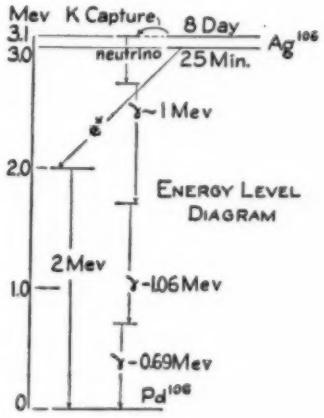


FIG. 6. Energy level diagram for $Ag^{106}$ and $Pd^{106}$.

of much higher energy than the 0.1 to 0.2 Mev threshold difference, it is necessary to assume that this state decays by $K$-electron capture and gamma-ray emission directly to $Pd^{106}$ rather than to the lower 25-min. state. Since a total of 3 Mev must be assigned to neurino and gamma-radiation and since two gamma-ray lines of 0.69 and 1.06 Mev have been identified it is evident that at least three gamma-ray quanta must be emitted in cascade in the process. Coincidence counter measurements by Feather and Dunworth[2] have previously indicated 3 to 5 quanta emitted simultaneously. It is probable that there are two quanta, unresolved on our plates, of about 1 Mev as shown in Fig. 6. Measurements of the relative ionization produced by the x-rays and gamma-rays also indicate about one x-ray quantum to three or four gamma-rays.

Since the electrons which accompany this period can be assumed to be conversion electrons, and since no continuous negative $\beta$-ray spectrum has been established,[3] it is unnecessary to postulate that electron decay to $Cd^{106}$ occurs to any appreciable extent.

Although our cloud-chamber observations showed no positrons accompanying this period a small number of positrons was reported by Pool. These may be due to occasional direct positron emission from this state or to decay from the 8-day to the 25-min. state followed by positron emission.

The $p$-$n$ cross section for the 25-min. period is about 30 to 40 times as great as for the 8-day

period (Table II). Pool[1] reports that for the $n$-$2n$ reaction the 8-day period cross section is greater than the 25-min. period cross section.

The author is grateful to Professor L. A. DuBridge for suggestion of the problem, and valuable advice. He is also grateful to Dr. S. N. Van Voorhis and Dr. S. W. Barnes for advice and assistance. The $Sn^{113}$ used for x-ray calibration was prepared by Dr. Barnes. The high contrast development of the spectrograph prints was kindly done by Mr. T. W. Finucane of the Institute of Optics. Other members of the department kindly assisted in operating the cyclotron and $\beta$-ray spectrograph.

This work was supported in part by a grant from the Research Corporation.

---

NOVEMBER 1, 1939 PHYSICAL REVIEW VOLUME 56

# Disintegration of Beryllium by Electrons

GEORGE B. COLLINS, BERNARD WALDMAN AND EUGENE GUTH
*University of Notre Dame, Notre Dame, Indiana*

(Received August 18, 1939)

The beryllium nucleus has been disintegrated by fast electrons whose energies exceeded the photoelectric threshold. The source of the electrons was a 1.8-Mv Van de Graaff generator. As was predicted by Guth, neutrons were produced, and the radioactivity which these neutrons induced in silver was used as a measure of the rate of disintegration. The possibility that the observed disintegration was not due to the direct action of the electrons, but resulted from stray x-rays, or x-rays produced in the beryllium by the electrons was eliminated. The yield curve for disintegration by electrons was obtained, and fixed the threshold for this process at $1.63\pm0.05$ Mev. At 1.73 Mev the cross section was found to be $10^{-31}$ cm², in good agreement with theory.

The yield curve for photodisintegration by continuous x-radiation was also obtained, and the threshold was found to be identical with that for disintegration by electrons.

SEVERAL attempts have been made in the past to disintegrate atomic nuclei with electrons.[1] Cathode rays and positrons with energies up to 800 kev have been used to irradiate a wide variety of elements, but no evidence of nuclear disintegration has been reported. Recently, however, one of us[2] has presented a theoretical treatment of this problem and has indicated clearly the conditions under which disintegration by electrons may be expected to take place. His theory points out a similarity between this process and that of photodisintegration and states that before disintegration by electrons may occur the energy of the electrons must exceed the photoelectric threshold of the nucleus.

It was to be expected then, that disintegration by electrons would be most likely to succeed with the element beryllium, since it has the lowest known photoelectric threshold. The threshold has been estimated[3] to be about 1.6 Mev which fortunately is somewhat lower than the maximum potential of our Van de Graaff generator. The reaction predicted is the following

$$Be^9+e_v\rightarrow Be^8+n+e_{v'},$$

where $v$ and $v'$ indicate energies of electrons before and after disintegration. If $Be^8$ is unstable, on which point there is some disagreement,[4] it would soon disintegrate into two low energy helium nuclei. The cross section of this process for electrons having energies a few 100 kilovolts above the threshold is estimated[2] to be about $10^{-31}$ cm². It was decided to allow the neutrons produced by the above process to induce radioactivity in another element and to use this induced radioactivity as a measure of the rate of disintegration by electrons. Considera-

[1] J. J. Livingood and A. H. Snell, Phys. Rev. **48**, 851 (1935); W. B. Lewis and W. E. Burcham, Camb. Phil. Soc. Proc. **32**, 503 (1936); G. P. Thomson and J. A. Saxton, Phil. Mag. **23**, 241 (1937).

[2] E. Guth, Phys. Rev. **55**, 412 (1939).

[3] J. Chadwick and M. Goldhaber, Proc. Roy. Soc. **151**, 479 (1935).

[4] Allison, Skaggs, Smith, Phys. Rev. **56**, 288 (1939).

tions involving the expected cross section for the process, the strength of the available electron beam, which was equivalent to the $\beta$-rays from about 20 kilograms of radium, and the sensitivity of the detecting method indicated that measurable activities would result.[5]

## Apparatus

### High voltage generator

Inasmuch as a detailed description of the generator has not been published, a brief account will be given here. The generator is of the Van de Graaff type, mounted on a tripod similar to that of Tuve, Hafstad and Dahl[6] and housed in a 40-foot cubical room. The high voltage electrode consists of two hemispherical shells 12 feet in diameter joined by a 2-foot cylindrical section. (See Fig. 1.) The shells were made by tacking thin copper sheeting to a wood framework. The supporting tripod is constructed from Textolite tubing 12 inches in diameter, $\frac{3}{8}$ inch thick and 24 feet long.

Charge is carried to the copper shell by two belts, each 30 inches wide and 70 feet endless length. Various types of materials were used; including paper, balloon silk and conveyor belting. The black rubber 3-ply conveyor belting, 8 ounces per square foot, has been very satisfactory. The spray voltage is supplied by a transformer Kenotron rectifier set and may be varied from 10 kv to 30 kv. The charging current is strongly dependent upon the humidity and during normal winter conditions (relative humidity about 30 percent) is about 200 $\mu$a per belt with a belt speed of 70 feet per second.

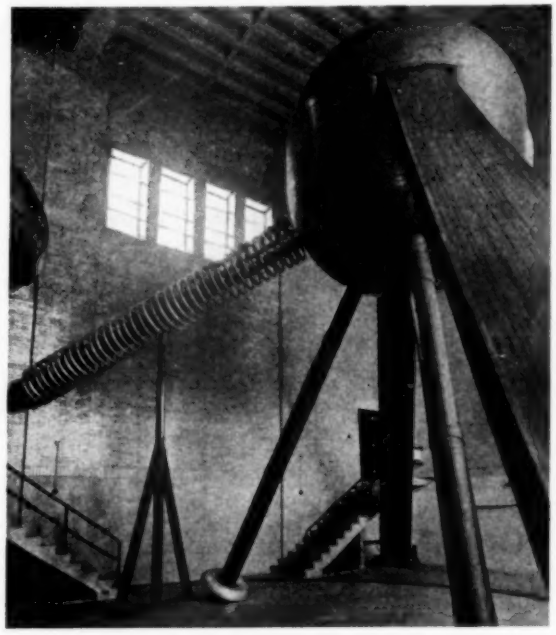

Fig. 1. View of 1.8-Mv generator and accelerating tube.

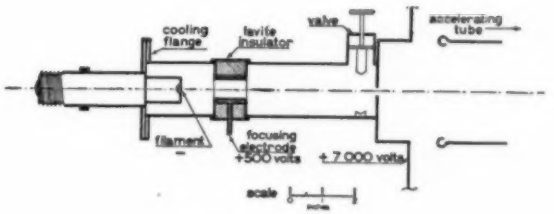


Fig. 2. The electron source.

The accelerating tube consists of six, 4-foot sections of 9-inch Pyrex glass tubing supported by a 4″×6″-redwood beam, which was kiln dried and coated with Victron varnish. Twenty cylindrical brass electrodes are used to accelerate the electron beam. These electrodes are connected to alternate aluminum hoops which surround the supporting beam and accelerating tube. Each hoop (there are some 40 in all) carries 3 pins pointing to the adjacent lower ring so that negative point-to-positive plane corona results. The first two accelerating electrode potentials are varied by adjusting the corresponding pins which provides an excellent control of the focusing of the electron beam.

The electron gun is illustrated in Fig. 2. The filament assembly is from an old x-ray tube. A rheostat operated by strings from the observation room controls the filament current and hence the electron current down the accelerating tube. The voltages for focusing and accelerating the electrons in the gun are produced by a small transformer Kenotron set operating on 110 volts a.c. generated by a rotary converter run from storage batteries. Currents up to 150 $\mu$a can be obtained and focused to a $\frac{1}{4}$-inch spot on the target.

The lower end of the accelerating tube passes through the wall of the generator room into the adjacent observation room. A large solenoid, 18 inches long fits over the last section of the ac-

[5] Collins, Waldman and Polye, Phys. Rev. **55**, 412 (1939).
[6] Tuve, Hafstad and Dahl, Phys. Rev. **48**, 315 (1935).

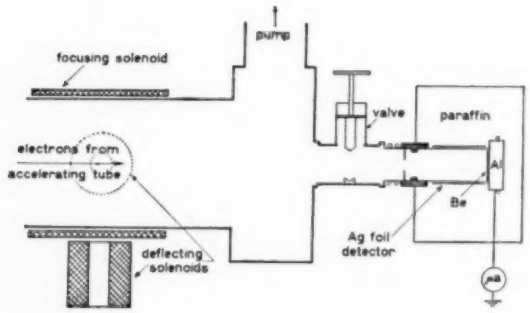


FIG. 3. Target arrangement.

celerating tube. This solenoid concentrates the focal spot from 1 inch to $\frac{1}{4}$ inch in diameter. Two small solenoids, with their axes perpendicular to each other and the accelerating tube, are used to control the position of the beam on the target.

The pumping system consists of a 4-inch oil diffusion pump, backed by a 2-inch oil diffusion pump and a Hypervac. The normal operating pressure is approximately $10^{-5}$ mm of mercury.

### Voltage measurement

A generating voltmeter, fastened to the ceiling directly above the copper shell, is used to measure the voltage. The voltmeter operates on a balancing principle with a null detector, the details of which will be published soon. The voltmeter was calibrated over its entire range by direct measurement of the deflection of an electron beam in a magnetic field. The absolute value of the voltage is known to within 50 kv. A grounded set of corona points, whose distance from the copper shell is adjustable, controls the potential of the generator.

It was found necessary to swing the earth's magnetic field parallel to the axis of the accelerating tube in order to avoid a deflection of the electron beam. This was accomplished, following a suggestion of Dr. Breit, by constructing two pairs of Helmholtz coils 30 feet in diameter and placing one set on the walls and the other set on the roof and floor of the generator room. About 1000 ampere turns for each coil were necessary.

The maximum voltage obtainable is 1.75 Mv to 1.8 Mv depending upon the number of sparks per minute permissible. These discharges occurred along the belts and down the legs of the generator. Sparks along the belts can be prevented by reducing the spray voltage on the charging circuit, though this also reduces the available electron current if the voltage is to remain constant.

The magnetic deflection chamber used to calibrate the voltage afforded a means of determining the homogeneity of the beam. The maximum spread in energy of the beam was estimated to be 10 kev and was due almost entirely to fluctuations of the generator voltage.

### Target arrangement

Figure 3 shows the target arrangement. The focused electron beam impinged on the beryllium plate (placed at the end of the Faraday cage) which was soldered to an aluminum block for cooling. The neutrons emitted in the reaction were diffused by the paraffin and induced activity in the detector (usually silver). The activity of the silver was measured with a thin-walled glass Geiger-Müller tube coupled to a scale-of-16 vacuum tube recorder[7] by the Neher-Harper circuit. The background count was about 16 per minute inside 2 inches of lead.

The bombarding current ranged from 5 to 15 $\mu$a and the time of irradiation for a silver detector was one minute. Fifteen seconds elapsed between the cessation of bombardment and the recording of the activity of the detector. The activity is expressed in net counts per 10 $\mu$a during the first minute of recording.

## RESULTS

In every case when the beryllium target was bombarded with electrons whose energy exceeded 1.63 Mev, activity was induced in the detectors, either silver, rhodium, or indium, which decayed with the appropriate period. A typical run with rhodium as a detector gave 126 net counts in the first minute, and a similar run, with silver gave 208 counts. In both cases 8 microamperes of 1.75-Mev electrons bombarded the beryllium for 50 seconds.

Numerous runs were made under widely different conditions as regards voltages, activation times, and beam currents, and consistent data were obtained. A run with the beryllium removed gave negative results. There is thus no doubt

[7] H. Lifschutz and J. L. Lawson, Rev. Sci. Inst. 9, 83 (1938).

that the disintegration of beryllium had occurred with the emission of neutrons.

The possibility existed, however, that the observed activity was not due to the direct action of the electrons on the beryllium, but resulted from photoneutrons produced by the action of x-rays induced in the beryllium by the fast electrons. Considerable care was taken to eliminate this possibility and the following paragraphs are concerned with this question.

Two methods of attack were used to determine which process was responsible for the activity. The first consisted of interposing thin targets of lead, aluminum and carbon before the beryllium, and comparing the resulting activities induced in the silver detector. These targets were thick enough to reduce the energy of the electrons to a value less than the threshold of beryllium. Their purpose was to eliminate the direct effect of the electrons and produce x-rays of varying intensity by a change in the atomic number of the target. Table I gives the results of this experiment and shows the activity induced in a silver detector for two electron energies. The thickness of the beryllium was 0.20 cm.

The high activity obtained with the lead target was interpreted as being due to the photoneutrons produced by the relatively strong x-rays set up in the lead. The activity obtained with targets of aluminum and carbon is seen to be less, as would be expected because less intense x-rays were produced in these targets of lower atomic number. If the activity observed upon exposing the beryllium was due entirely to photoneutrons from beryllium, the activity obtained should have been still less, because the atomic number of beryllium is less than that of carbon. The observed increase (column 5) must then be attributed to the disintegration of beryllium by electrons. Changes in geometry could not have accounted for the increase in activity obtained because the size of the beryllium sheet was large compared with the size of the focal spot of the electrons.

Additional evidence that the electrons were directly responsible for the disintegration of the beryllium was obtained in the following manner. Since many centimeters of beryllium would be needed to absorb appreciably these hard x-rays, the photodisintegration process should be proportional to the thickness of the beryllium target. On the other hand, since the effective range for disintegration of 1.75-Mev electrons in beryllium is only about 0.035 cm, the disintegration by electrons should not increase for thicknesses above this value. This difference in the behavior of x-rays and electrons then provided a means of distinguishing between the two effects. Additional trials were then made on a thin beryllium target with a thickness (0.038 cm) about equal to the effective range of the electrons. Table II is a comparison of the results of these trials with those obtained using the thick target (0.20 cm). It will be noted that nearly identical activities were obtained from the thick and thin targets showing clearly that the activity was essentially all due to the direct action of the electrons.

The experimental cross section for the process has been obtained by means of a calibration experiment to determine the sensitivity of the detecting method. 71 millicuries of radon in glass were placed in the center of 30 grams of beryllium and this was surrounded by the silver foil and paraffin blocks used to obtain the data given in Table II. Assuming that $2.8\times10^{7}$ effective gamma-rays are emitted from one millicurie of radon per second, and that the cross section for photodisintegration by these gamma-rays is $3\times10^{-28}$ cm$^2$ it was calculated that the sensitivity of the detecting apparatus is such that 300 neutrons per second produce 1 count per minute from the silver foil. At 1.73 Mev and 10 $\mu$a 79 counts per minute were obtained from the thin target. These data combined with the sensitivity

TABLE I. *Activities induced in a silver detector with various targets placed in front of 0.20 cm of beryllium. The last column gives the induced activity with the beryllium exposed.*

| Electron Energy | Type of Target | | | |
|---|---|---|---|---|
| | Pb | Al | C | |
| 1.73 Mev | 2880 | 72 | 12 | 80 |
| 1.69 | 300 | — | 14 | 24 |

TABLE II. *Comparison of activities induced in silver by electron bombardment of thick and thin targets of beryllium.*

| Electron Energy Mev | Induced Activity | |
|---|---|---|
| | 0.20 cm Be | 0.038 cm Be |
| 1.75 | 228 | 260 |
| 1.73 | 80 | 79 |
| 1.69 | 24 | 28 |

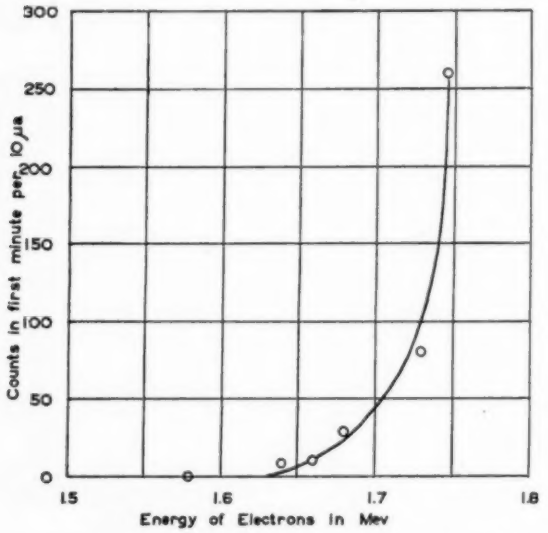


FIG. 4. Yield curve for disintegration of Be by electrons.

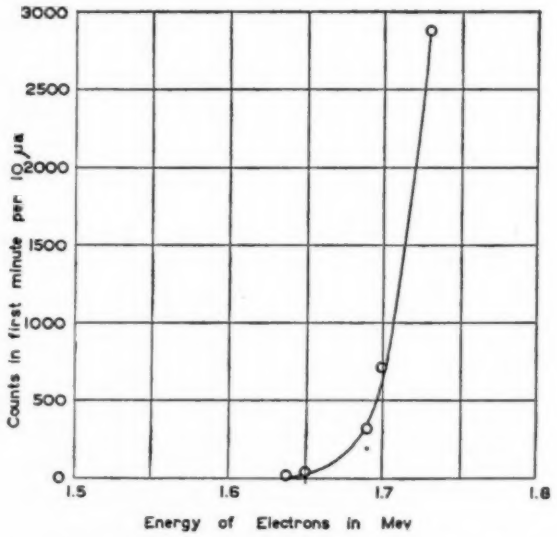


FIG. 5. Yield curve for photodisintegration of Be.

stated above and an effective beryllium thickness of 0.030 cm yield a cross section of $1\times10^{-31}$ cm$^2$. It is probably significant only as far as order of magnitude is concerned, but is in excellent agreement with the theoretical value predicted by Guth. As may be seen from Fig. 4 this cross section is very sensitive to the electron energy.

Figure 4 is the yield curve for electron disintegration obtained by bombarding the 0.038-cm beryllium target with electrons of various energies. From this curve the threshold for the process is fixed at $1.63\pm0.05$ Mev. Uncertainties in the voltage measurement prevent one from attaching too much significance to its exact shape. Its steep rise however may be explained by the cross section and effective range of the electrons, both of which increase with increasing electron energy.

The disintegration of beryllium by continuous x-radiation has been reported by Brasch and co-workers.[8] They used however a surge generator to accelerate the electrons which made it impossible to obtain an excitation curve or an exact threshold for the process. We repeated the experiment under more favorable conditions by bombarding a lead target placed before a 0.20-cm beryllium plate with "monochromatic" electrons of various energies. The detecting arrangement was the same as that used for the electron-disintegration experiments. Fig. 5 is the yield curve obtained in which the silver activities are plotted against the energy of the electrons which corresponds to the maximum energy of the x-rays. From this curve the threshold for photodisintegration is fixed at $1.63\pm0.05$ Mev which is the same as the threshold for electron-disintegration. It also agrees very well with the value $1.62\pm0.02$ obtained by Skaggs[9] from mass and energy relationships based on experiments involving the proton bombardment of beryllium. It is noteworthy that for the same electron energy and current one obtains ten times the activity from photodisintegration as is obtained from electron-disintegration. This is due principally to the greater amount of beryllium available for the photodisintegration process, since for a given electron current the cross section for electron-disintegration times the number of electrons is about equal to the cross section for photodisintegration times the number of effective x-ray quanta produced.

The authors wish to acknowledge the important assistance given by Mr. Richard S. Schager and Mr. Alex A. Petrauskas whose work was essential to the successful operation of the generator.

[8] Brasch, Lange Waly, Banks, Chalmers, Szilard and Hopwood, Nature **134**, 880 (1934).

[9] L. S. Skaggs, Phys. Rev. **56**, 24 (1939).

# On the Scattering of Neutrons from the C+D Reaction

E. AMALDI, D. BOCCIARELLI, F. RASETTI AND G. C. TRABACCHI
*Istituto di Sanità Pubblica, Rome, Italy*

(Received August 10, 1939)

The scattering cross section for neutrons emitted by bombarding carbon with 600-kev deuterons was measured for 39 elements.

## I. INTRODUCTION

IN recent years in measurements of the scattering and absorption of fast neutrons the neutron source has usually been either the D+D reaction[1] (neutron energy between 2.5 and 3 Mev) or photoelectric neutrons[2,3] (neutron energy between 0.14 and 0.2 Mev).

As the properties of neutrons of energy of the order of $10^5$ ev seem very interesting, we have undertaken to perform scattering experiments on the neutrons obtained by bombarding carbon with deuterons, as carried out by Tuve and Hafstad[4] for the case of hydrogen. Bonner and Brubaker[5] have shown that the neutrons from carbon bombarded with 0.9-Mev deuterons, consist of three groups of maximum energies 5.6, 1.8, and 0.35 Mev, whose intensities are in the ratio 1 : 3 : 300. On account of the weak intensity of the high energy groups, in most cases it is sufficient to consider only the group of lowest energy. This, according to the above authors, arises from the reaction

$$ {}_6C^{12}+D={}_7N^{13}+n+Q, \tag{1}$$

where

$$ Q=-0.37 \text{ Mev}. \tag{2}$$

However, Livingston and Bethe,[6] on the evidence of the measurements of Cockcroft and Lewis,[7] consider as more probable the lower value

$$ Q=-0.28 \text{ Mev}. \tag{2'}$$

## II. EXPERIMENTAL ARRANGEMENT AND METHOD

Our neutrons were produced by bombarding a target of Acheson graphite with deuterons accelerated in the high voltage tube of the Istituto di Sanità Pubblica.[8] The unanalyzed ion current was of the order of 50$\mu$a, as deduced by comparing the power dissipated in the target (measured calorimetrically) with the accelerating voltage. The latter quantity was measured by means of a $4\times10^9$-ohm resistor connected in series with a microammeter. The voltage calibration has been often checked during the measurements by comparison, up to 200 kv, with the readings on a Schroeder electrostatic voltmeter.

During the measurements, the voltage was kept constant at 600 kv. The voltage fluctuation due to the load was of the order of one-tenth of one percent, and therefore negligible.

From the applied voltage and the value of the reaction energy, it follows that the neutrons emitted at 90° to the direction of the incident deuterons, as used in our experiments, had a maximum energy of 0.13 or 0.21 Mev, according to whether one assumes for $Q$ the value (2) or (2'). From the steepness of the excitation curve[9] of reaction (1), we may conclude that most neutrons have energies only slightly lower than either of these values. In the following, we shall assume the average effective energy of the neutrons to be either 0.10 or 0.18 Mev.

[1] E. T. Booth and C. Hurst, Proc. Roy. Soc. **161**, 248 (1937); R. Ladenburg and M. H. Kanner, Phys. Rev. **52**, 911 (1937); W. H. Zinn, S. Seely and V. W. Cohen, Phys. Rev. **53**, 921 (1938); **55**, 679 (1939); **56**, 260 (1939); S. Kikuchi and H. Aoki, Phys. Rev. **55**, 108 (1939); Scient. Papers of the I.P.C.R. **34**, 864 (1938).

[2] M. Goldhaber, Nature **137**, 824 (1936).

[3] A. Leipunski, L. Rosenkewitsch and D. Timoshuk, Physik. Zeits. Sowjetunion **10**, 625 (1936); **10**, 751 (1936); E. Fedorow and N. Perfilieva, Physik. Zeits. Sowjetunion **11**, 660 (1937); G. I. Satkoverzky, Physik. Zeits. Sowjetunion **11**, 664 (1937).

[4] M. A. Tuve and L. R. Hafstad, Phys. Rev. **50**, 308 (1936).

[5] J. W. Bonner and W. M. Brubaker, Phys. Rev. **50**, 308 (1936).

[6] M. S. Livingston and H. A. Bethe, Rev. Mod. Phys. **9**, 334 (1937).

[7] J. D. Cockcroft and W. B. Lewis, Proc. Roy. Soc. **154**, 261 (1936).

[8] G. C. Trabacchi, E. Amaldi, D. Bocciarelli and F. Rasetti, Ric. Scient., in press.

[9] E. Amaldi, L. R. Hafstad and M. A. Tuve, Phys. Rev. **51**, 896 (1937).

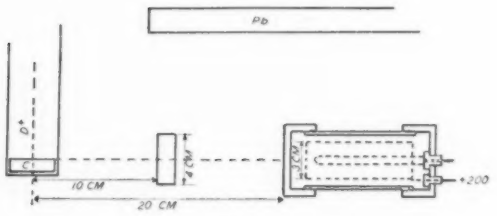


FIG. 1. Experimental arrangement.

The neutrons emitted at 90° were recorded by means of an ionization chamber filled with hydrogen at 20 atmospheres, and an Edelmann electrometer; the sensitivity of the latter instrument being 20 divisions per volt.

The effective diameter of the cylindrical ionization chamber was 3 cm, while the average distance between the target and the chamber was 26 cm. The geometry of the experiment is clearly apparent from Fig. 1.

By taking into account the solid angle subtended by the scatterers and by the ionization chamber, we estimated that in the case of isotropic scattering (which applies to all elements except hydrogen) the error due to the imperfect geometry was of the order of five percent. We therefore corrected by that amount the experimental values, assuming that for neutrons of energy of the order of $10^5$ ev, scattering prevails over true absorption. In the case of hydrogen (paraffin), the correction for the geometry is larger, as the scattering takes place mostly in the forward direction. A rough evaluation indicates that the true mean free path should be about 15 percent shorter than the one directly measured.

Under our conditions, the ionization chamber recorded, besides the neutrons coming directly from the target, a background of neutrons scattered by the walls and also x-rays coming from the upper part of the tube. The intensity of the latter was reduced as much as possible by means of lead screens. In order to determine the residual background to be subtracted from our measurements, we placed a paraffin cylinder 4 cm in diameter and 15 cm in length between the neutron source and the ionization chamber. This scatterer was estimated to reduce the direct neutron intensity to about one percent. The residual ionization, measured under such conditions, amounted to one-third of the total one. A check of this value of the background ionization is provided by the fact that the scattering curves obtained with different thicknesses of all substances investigated are exponential to a fairly high degree of accuracy.

The neutron intensity remained constant, within a few percent, over a period of several hours. Nevertheless, we recorded each scattering curve at least six times, changing the order of succession of the different thicknesses.

The scatterers were shaped in the form of cylinders 4 cm in diameter and of convenient thickness. Powders were sufficiently compressed to form compact cylinders. Liquids were placed in convenient containers, the scattering effect of the walls being taken into account.

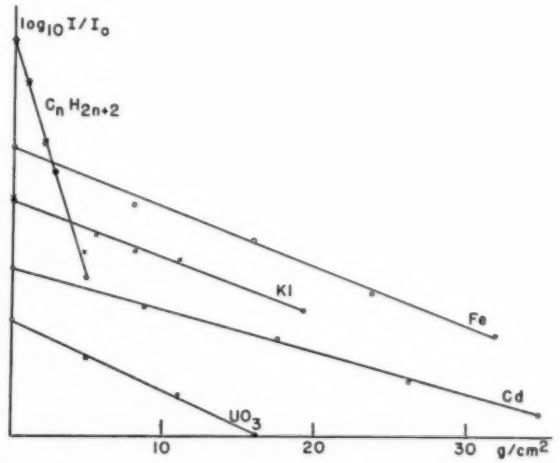


FIG. 2. Scattering curves of selected substances. Crosses and dots refer to two series of measurements.

## III. EXPERIMENTAL RESULTS

Figure 2 shows, for a few selected substances, the scattering curves on a logarithmic scale. Table I gives the values of the reciprocal scattering coefficient in g/cm² and of the atomic cross section. Both these values have been corrected for the imperfect geometry as explained above. In the last column we give for comparison the values of the scattering cross section as found by the Russian experimenters[3] using photoelectric neutrons of 0.15 Mev energy.

Where elements were not available, the atomic cross section was deduced by subtraction from that of a convenient compound. Such values are, of course, subject to a larger error than the

others. A question mark indicates those cross sections which appear to be particularly uncertain, either because only two points of the scattering curve could be measured, or because their values were deduced by subtraction from more than two measured cross sections of compounds.

As appears from Fig. 3, there is no simple relation between the cross section for neutron scattering and the atomic number, although a generally increasing trend of the cross section towards the heavy elements is apparent. This result is similar to that found by other experimenters using homogeneous neutrons.[1, 2] As we see from Table I, there is poor agreement between our values and those found by Leipunski and others.[3] Probably the disagreement can be at least partly explained by taking into account the much higher homogeneity of photoneutrons as compared with neutrons of reaction (1).

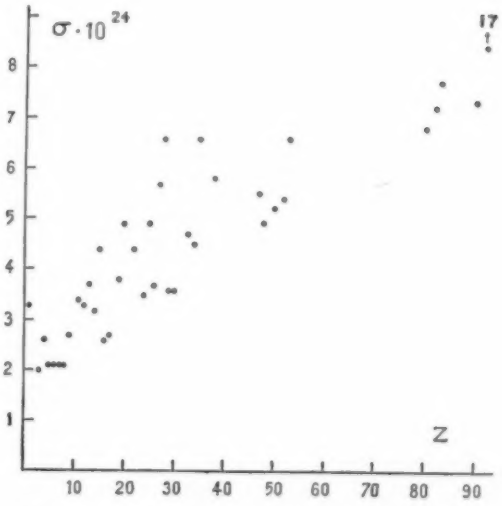


FIG. 3. Scattering cross section plotted against atomic number.

TABLE I. *Cross sections for neutron scattering.*

| ELEMENT | SUBSTANCE USED | THICKNESS FOR REDUCTION TO $1/e$ IN G/CM² | CROSS SECTION IN CM² $\times 10^{24}$ | CROSS SECTION IN CM² $\times 10^{24}$ BY LEIPUNSKI AND OTHERS |
|---|---|---|---|---|
| 1 H | $CH_2$ | 2.7 | 3.3 | 8 |
| 3 Li | Li | 5.9 | 2.0 | 1 |
| 4 Be | Be | 5.7 | 2.6 | 2.9 |
| 5 B | B | 8.2 | 2.1 | 3.8 |
| 6 C | C | 9.5 | 2.1 | 1.5 |
| 7 N | $NaN_3$ | 8.6 | 2.1 | 1.6 |
| 8 O | MgO | 12.4 | 2.1 | 1.8 |
| 9 F | NaF | 11.6 | 2.7 | 6.3 |
| 11 Na | Na | 11.4 | 3.4 | 3.6 |
| 12 Mg | Mg | 12.4 | 3.3 | 8.4 |
| 13 Al | Al | 12.4 | 3.7 | 4.0 |
| 14 Si | Si | 14.6 | 3.2 | 1.4 |
| 15 P | P | 11.7 | 4.4 | |
| 16 S | S | 20 | 2.6 | 1 |
| 17 Cl | NaCl | 16 | 2.7 | 3.6 |
| 19 K | KCl | 19 | 3.8? | |
| 20 Ca | $CaF_2$ | 12.6 | 4.9? | |
| 22 Ti | $TiO_2$ | 15 | 4.4 | |
| 24 Cr | $Cr_2O_3$ | 19 | 3.5 | |
| 25 Mn | $MnO_2$ | 16 | 4.9 | |
| 26 Fe | Fe | 26 | 3.7 | 2.7 |
| 27 Co | CoO | 17 | 5.2? | |
| 28 Ni | NiO | 14.3 | 6.6 | |
| 29 Cu | Cu | 29 | 3.6 | 4.2 |
| 30 Zn | Zn | 30 | 3.6 | 4.0 |
| 33 As | As | 27 | 4.7 | |
| 34 Se | Se | 29 | 4.5 | |
| 35 Br | NaBr | 17 | 6.6 | |
| 38 Sr | SrO | 22 | 5.8 | |
| 47 Ag | Ag | 33 | 5.5 | |
| 48 Cd | Cd | 38 | 4.9 | |
| 50 Sn | Sn | 37 | 5.2 | 5.2 |
| 51 Sb | Sb | 37 | 5.4 | |
| 53 I | KI | 27 | 6.6? | |
| 80 Hg | Hg | 50 | 6.8 | |
| 82 Pb | Pb | 48 | 7.2 | 7.3 |
| 83 Bi | Bi | 46 | 7.7 | |
| 90 Th | $ThO_2$ | 38 | 7.3? | |
| 92 U | $UO_3$ | 22 | 17 | |

The largest cross section was found for uranium ($\sigma = 17 \times 10^{-24}$ cm²), and it may be interesting to notice that it is practically equal to the scattering cross section found for neutrons of thermal energies.[10]

The cross section found for hydrogen from paraffin ($\sigma = 3.3 \times 10^{-24}$ cm² after applying the correction for geometry and subtracting the cross section of carbon) may throw some doubt on the correctness of the whole experiment, since there appears to be a considerable disagreement with the theoretically expected value. If our neutrons were really homogeneous of either 0.10 or 0.18 Mev energy, the cross section calculated according to the formula of Bethe and Peierls[11] (assuming 0.12 Mev as the energy of the singlet $S$ state of the deuteron) should be either $9.4 \times 10^{-24}$ or $7.9 \times 10^{-24}$ cm². It seems impossible to explain such a large difference as due to insufficient correction for the geometry. On the other hand, the neutron groups of 1.8 and 5.6 Mev (in our case, 1.5 and 5.3) are so weak that, even taking into account the larger ionization produced by their recoil protons, they must contribute only 2.5 percent and 5 percent, respectively, to the total ioniza-

[10] H. H. Goldsmith, V. W. Cohen and J. R. Dunning, Phys. Rev. **55**, 1124 (1939).

[11] See, for instance, H. A. Bethe and R. F. Bacher, Rev. Mod. Phys. **8**, 117 (1936).

tion. The evaluation of the efficiency of the chamber for these groups was calculated by means of the formula of Bethe and Peierls.

We must also keep in mind the possibility of an emission of D+D neutrons due to a deuterium contamination of the target surface. This objection seems to be ruled out by our conditions being similar to those of Bonner and Brubaker, who observed only a negligible number of neutrons corresponding to the D+D reaction. It appears moreover, unlikely that a red hot graphite target, under a pressure of $7\times10^{-5}$ mm, as in the tube during our experiments, could adsorb an amount of deuterium (of the order of one-tenth of one percent within the effective thickness of the target) sufficient to give an average cross section of the order of the one observed by us.

Finally, the possible explanation that our small value of the cross section is due to an admixture of neutrons of higher energies does not appear to be consistent with the exponential form of the scattering curve.

A similar result was found by Goldhaber[2] using photoneutrons. The value (from 3.7 to $4.7\times10^{24}$) found by Tuve and Hafstad[4] for the neutrons from the C+D reaction appears to be also somewhat lower than theoretically expected. Instead, Leipunski, Rosenkewitsch and Timoshuk,[3] using photoelectric neutrons of 0.15 Mev energy, found the theoretically expected value.

We intend to investigate further this point in order to understand why the scattering cross section in hydrogen in our experiments was much smaller than we expected.

---

NOVEMBER 1, 1939 PHYSICAL REVIEW VOLUME 56

# Effects of Shape of Potential Energy Wells Detectable by Experiments on Proton-Proton Scattering

L. E. HOISINGTON, S. S. SHARE AND G. BREIT
*University of Wisconsin, Madison, Wisconsin*

(Received September 5, 1939)

The shapes of several types of potential wells giving approximate agreement with proton-proton scattering experiments are discussed. The somewhat poor agreement of the $K_0$, $E$ curve for the exponential well with experimental data is shown to be due to the "tail" of the well at large radii. In the case of the meson potential well the effect of very large values of the potential at small distances counteracts the effect of the tail. The experimental dependence of phase shift on energy is not reproduced by the inverse square potential well. The maximum theoretically admissible depth of this potential fits experiment at about 1 Mev. A series expansion is developed which gives the change of the phase shift caused by a given change in the potential well, and an example of the use of the formula is given. The approximate equality of the proton-proton and proton-neutron interactions is discussed, and the close agreement in the case of the meson potential is shown to be due to the large attraction at small distances.

THE first experiments[1] on the scattering of protons by protons determined the *s*-wave anomaly in the energy range 600–900 kev and have indicated the rather close equality of the proton-proton and proton-neutron interactions on the assumption of the same shape of potential well.[2] The energy range covered was insufficient, however, to determine the range of force except very qualitatively and the shape of the nuclear potential curve was also left quite undetermined. The newer experiments[3] have increased the energy region in which the *s* anomaly is known

[1] W. H. Wells, Phys. Rev. **47**, 591 (1935); M. G. White, Phys. Rev. **47**, 573 (1935); M. A. Tuve, N. P. Heydenburg and L. R. Hafstad, Phys. Rev. **49**, 402 (1936); **50**, 806 (1936); L. R. Hafstad, N. P. Heydenburg and M. A. Tuve, Phys. Rev. **51**, 1023 (1937); **53**, 239 (1938).

[2] G. Breit, E. U. Condon and R. D. Present, Phys. Rev. **50**, 842 (1936).

[3] R. G. Herb, D. W. Kerst, D. B. Parkinson and G. J. Plain, Phys. Rev. **55**, 998 (1939); N. P. Heydenburg, L. R. Hafstad and M. A. Tuve, Phys. Rev. **55**, 603(A) (1939). For analysis of data see BTE, pp. 1035–36.

and have also increased the precision. For some assumed potential energy curves of fixed shape but adjustable width and depth, one finds now disagreement between theoretical and experimental values even though width and depth are adjusted to represent experiment at two energies. It is possible to distinguish between different shapes of potential energy curves, and the present note is intended to show some examples illustrative of the features in the shape which may cause experimentally observable effects. For relativistic reasons it is impossible to believe in a potential energy well as an ultimate description of the interaction and the wells which agree with experiment are not necessarily advocated as having a fundamental significance. It will be seen, however, that the meson potential agrees satisfactorily with experiment, and among the potentials tried is the only one giving agreement of proton-proton and proton-neutron interactions

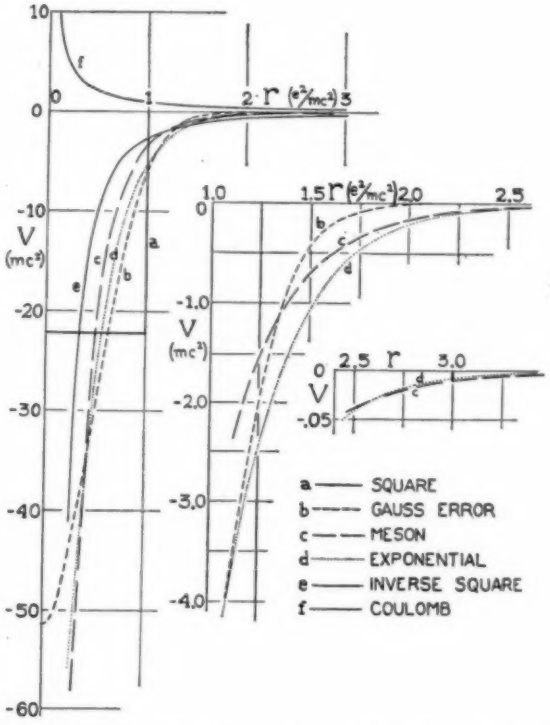


FIG. 1. Potential energy in $mc^2$ plotted against the radius in $e^2/mc^2$ for the following: (a) square well of depth 22.15 $mc^2$ and width $e^2/mc^2$, (b) Gauss error well $Ae^{-\alpha r^2}$ where $A=51.44\ mc^2$ and $\alpha=21.59\ Mmc^2/\hbar^2$, (c) meson well $Ce^{-r/a}/(r/a)$ where $C=89.65\ mc$ and $a=0.42\ e^2/mc^2$, (d) exponential well $Be^{-2r/b}$ where $B=137.6\ mc^2$ and $b=0.193\ \hbar(Mmc^2)^{-\frac{1}{2}}$, (e) inverse square well $B/r^2$ where $B=\frac{1}{4}$ and (f) the Coulomb potential. The "tails" are shown in the two smaller insets.

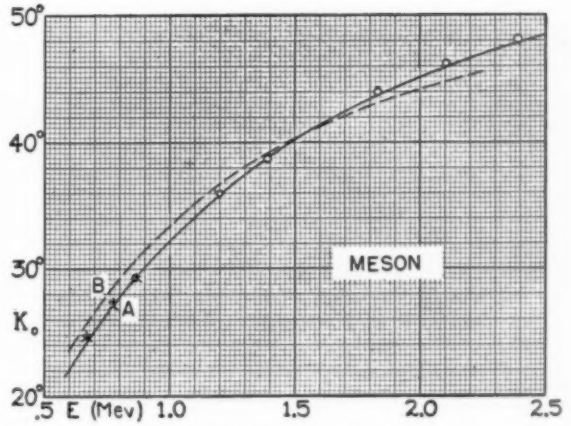


FIG. 2. Phase shift $K_0$ plotted against the energy of the incident protons, for the meson potential well, $Ce^{-r/a}/(r/a)$. $A$, $C=89.65\ mc^2$, $a=0.42\ e^2/mc^2$ (this corresponds to a meson mass of 326 m). $B$, $C=34.15\ mc^2$, $a=\frac{2}{3}\ e^2/mc^2$ (corresponding to a meson mass of 206 m). The potential $-Ce^{-r/a}/(r/a)$ is superposed on the Coulomb potential. Points ⊙ correspond to the data of Herb, Kerst, Parkinson and Plain, points + to the data of Heydenburg, Hafstad and Tuve (see BTE[6], pp. 1035–6), and points ∧ to the data of HHT as analyzed by Mr. E. C. Creutz using least squares in work to be published shortly.

to within the accuracy of scattering experiments.

In Fig. 1 are shown potential energy curves for (a) square well of depth 22.15 $mc^2$ and range $e^2/mc^2$, (b) Gauss error potential well $Ae^{-\alpha r^2}$ where $A=51.44\ mc^2$ and $\alpha=21.59\ Mmc^2/\hbar^2$, (c) meson,[4] $Ce^{-r/a}/(r/a)$ where $C=89.65\ mc^2$, $a=0.42\ e^2/mc^2$, (d) exponential[5] potential well $Be^{-2r/b}$ where $B=137.6\ mc^2$, $b=0.193\ \hbar(Mmc^2)^{-\frac{1}{2}}$, and (e) inverse square $B/r^2$ with $B=\hbar^2/4M$. All potential wells except (a) are cut off at $r=3e^2/mc^2$ and in all cases the potentials are supposed to be superposed on the Coulombian potential (f). The potentials in this figure are chosen so as to represent the data approximately. It is seen from the figure that the potentials (b), (c), (d) are not very different from $r=0.5$ to $r=1.25\ e^2/mc^2$. The square well intersects each of the other three curves twice also in the same region. The values of the depth at $r=0$ are quite different in the four cases, covering a range from 22.15 $mc^2$ to $\infty$. These values of depth have no direct simple significance since $\mathfrak{F}$ ($r$ times the radial wave function) is too small close to $r=0$.

In Figs. 2 and 3 the phase shift ($K_0$) is plotted against energy for the potentials (c) and (d).

[4] S. S. Share, L. E. Hoisington and G. Breit, Phys. Rev. **55**, 1130(A) (1939).

[5] W. Rarita and R. D. Present, Phys. Rev. **51**, 793 (1937).

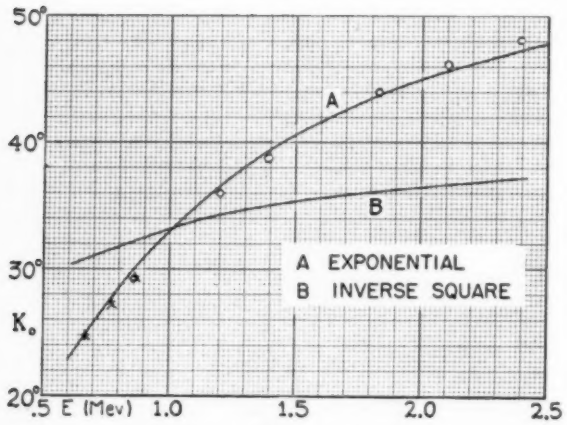


FIG. 3. Phase shift $K_0$ plotted against the energy of the incident protons. $A$, for the exponential well $Be^{-2r/b}$, where $B=137.6\ mc^2$ and $b=0.193\ \hbar(Mmc^2)^{-\frac{1}{2}}$. $B$, for the inverse square well, $B/r^2$, where $B=\frac{1}{4}$. Each well is superposed on the Coulomb potential. Points ⊙, + and ∧ are as in Fig. 2.

(For (a) and (b) see Fig. 10 of BTE.)[6] It is seen in Fig. 3 that the exponential potential gives relatively too high values of $K_0$ at 1200 kev and too low values at 2400 kev even though it is fitted to experiment at 670 kev. At 1200 kev $K_0$ is too high by $\sim 0.7°$, which amounts to $\sim 5$ percent of the measured scattering at a scattering angle of 45°. At 2400 kev the deviation of $-0.7°$ in $K_0$ corresponds to $\sim -3$ percent of the scattering at 45°. The consistency with which the experimental curve deviates from that calculated for the exponential potential is striking. To explain it one would need to assume a systematic error varying suitably with energy. The disagreement could be decreased by fitting the potential to intersect the experimental curve at a higher energy than 670 kev. The fit of the square and the Gauss error potentials (a) and (b) (Fig. 10 of BTE[6]) is seen, however, to be practically as good as that of the exponential well at 700 kev and much better at higher energies. The deviation from experiment for the exponential potential is due to a too high curvature of the theoretical $K_0$, $E$ curve, and a change in range affects primarily the slope rather than the curvature.

The depth and width of the exponential well used here are those obtained by Rarita and Present.[5] It is remarkable that this potential agrees approximately with proton-proton scattering up to 2400 kev as well as with the binding energies of $H^3$ and $H^2$. Yet it does not agree[5] with the energy of $He^4$. The comparison of curve $A$ of Fig. 3 with curve $A$ of Fig. 2 is not quite fair to the exponential potential because in Fig. 2 the experimental point at 670 kev lies above the theoretical curve.

The qualitative explanation of the difference in shape of the $K_0$, $E$ curve for the exponential potential as compared with the Gauss error or square well potentials lies in the fact that the exponential potential has a "tail." As can be seen in Fig. 1, this potential well (d) is deeper than the Gauss error well (b) for $r>1.1\ e^2/mc^2$ and is appreciable even out to $r=3\ e^2/mc^2$. But the function $\mathfrak{F}$ differs little for the three wells (a) (b) and (d), and the first-order effect due to a small change of potential at a given distance is proportional to $\mathfrak{F}^2E^{-\frac{1}{2}}$ (see Eq. (3)). Curves of $\mathfrak{F}^2E^{-\frac{1}{2}}$ plotted against $E$ are shown in Fig. 4(a). Up to 1 Mev $\mathfrak{F}$ increases so rapidly with energy that $\mathfrak{F}^2E^{-\frac{1}{2}}$ also does the same, but above 1 Mev the slope is seen to be negative for the larger radii. Thus the effect of increasing the proton-proton attraction at a distance of about $2\ e^2/mc^2$ is to increase $K_0$ by a larger amount at lower energies than at 2.6 Mev. Therefore when a potential well is fitted to data at approximately 1 Mev, the tail makes it unnecessary to use as large a depth as one would if it were not present. There is, therefore, less dependence of $K_0$ on energy of the type shown by the curve labeled $r=0.5$ and more of the type shown in the curve labeled $r=3$ in Fig. 4(a). The negative slope of the $r=3$ curve gives a smaller slope of the $K_0$, $E$ curve above 1 Mev as the result of the tail.

The increase in slope at low energies can also be seen from the sensitivity curves as well as from the fact that the tail when extending to the outskirts of the Coulomb barrier should give a rapid increase of $K_0$ with $E$ somewhat below that energy at which barrier penetration becomes unimportant. The result of the increase in slope below 1 Mev and decrease above 1 Mev is the bulge in the phase shift curve around 1.4 Mev which is apparent in Fig. 3 for the potential (d) and which is responsible for the disagreement with experiment.

The meson potential (c) has a tail which is similar to that of the exponential potential (d), as is seen in Fig. 1. The bulge at intermediate

[6] G. Breit, H. M. Thaxton and L. Eisenbud, Phys. Rev. **55**, 1057 (1939).

energies is absent, however. This is due to the rather large values of the potential energy for (c) at radii smaller than $e^2/2\,mc^2$. For these small distances the slope of $\mathfrak{F}^2E^{-\frac{1}{2}}$ against $E$ remains nearly constant from 1 Mev to higher energies, while for $r>e^2/mc^2$ the slope in this energy region becomes negative. Increasing the attraction at small distances decreases the bulge of the $K_0$, $E$ curve which is present for the exponential well. These considerations are only approximate, since they neglect the distortion of the wave function due to large interactions at small $r$ for well (c). The main effect of this distortion is to change the relative scale of curves for different $r$ in Fig. 4(a) which does not affect the above qualitative argument.

For the well (e) of type $B/r^2$ (potential energy $=-B/r^2$) there are again compensating effects of tail and large values at small distances. In this case there is no exponential decrease of depth with distance. The phase shift can be computed[7] analytically as the argument of a gamma-function. For $B<+\hbar^2/4M$ there is no regular solution of the equation for $\mathfrak{F}$ so that $\mathfrak{F}$ is undefined. The singularity is then too strong. For $B=+\frac{1}{4}$ nuclear units (i.e., $+\hbar^2/4M$ in c.g.s. units) the solution $\mathfrak{F}$ and $K_0$ can be defined. The $K_0$, $E$ graph corresponding to this is shown in Fig. 3. The order of magnitude is correct through most of the experimental region. The slope of the $K_0$, $E$ curve is too small, however. The effect of the tail is seen to be predominant. In the absence of a Coulomb potential the phase shift is independent of energy, the asymptotic form of the regular solution of $\{d^2/d\rho^2+[1-L(L+1)/\rho^2]\}\mathfrak{F}=0$ being $\sin(\rho-L\pi/2)$. The value $B=+\frac{1}{4}$ nuclear units corresponds to $L=-\frac{1}{2}$ and in this case would give $K_0=\pi/4$ at all energies. In the absence of Coulomb field the solution for $\mathfrak{F}$ becomes const. $\rho^{\frac{1}{2}}J_0(\rho)$ and an irregular solution is const. $\rho^{\frac{1}{2}}Y_0(\rho)$. The irregular solution has only a logarithmic singularity at $\rho=0$ and the distinction between regular and irregular solutions appears to be only artificial in this case.[8] One should require, however, that $\mathfrak{F}^2\rho^{-2}$ be integrable at $\rho=0$. Since for small $\rho$ one has $\mathfrak{F}\sim$const. $\rho^{L+1}$ it is necessary for $\rho^{2L+1}$ to be finite at $\rho=0$, so that $L>-\frac{1}{2}$.

[7] We understand that unpublished calculations with this potential have been made in a thesis with Professor Hoyt at the University of Chicago.

[8] N. F. Mott and H. S. W. Massey, *The Theory of Atomic Collisions* (Oxford, 1933), p. 30.

## Expansion Showing Effects of Local Changes in Potential

The explanation of the effect of the tail has been tested by using an expansion for $K_0$ in terms of a small change in potential which will be called $\delta V$. The differential equation is

$$(d^2/d\rho^2+1-V/E'-\lambda\delta V/E')\mathfrak{F}=0.$$

The quantities $V$, $\delta V$ are functions of $\rho$ and the phase shift is expanded in powers of $\lambda$. The solution $\mathfrak{F}$ is supposed to be known for $\lambda=0$, and the value of the phase shift $K_0$ for $\lambda=0$ is also supposed to be known. For the higher order corrections one needs also the irregular solution $\mathfrak{G}$ of the above differential equation. $\mathfrak{F}$ and $\mathfrak{G}$ are supposed to be normalized to unit amplitude at

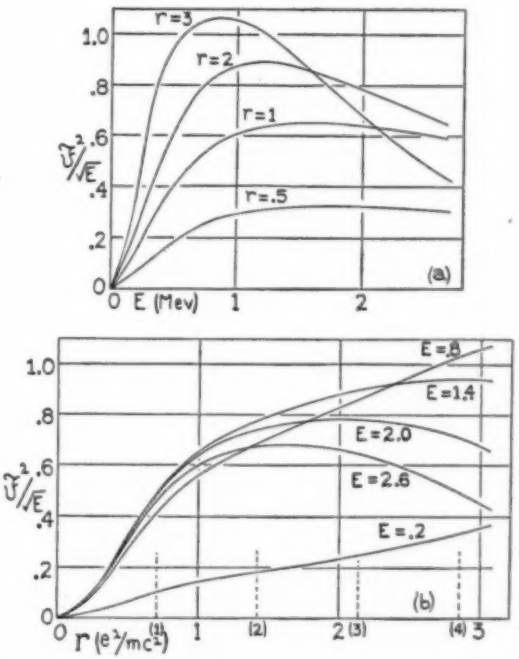


FIG. 4. (a) $\mathfrak{F}^2E^{-\frac{1}{2}}$ plotted for different radii as a function of energy of the incident protons. (b) $\mathfrak{F}^2E^{-\frac{1}{2}}$ plotted for different energies as a function of the radius. The small numbers in parentheses along the $r$ axis in (b) give the values of $x=(20\,Mmc^2/\hbar^2)^{\frac{1}{2}}r$. $E$ is in Mev and $r$ is in $e^2/mc^2$. $\mathfrak{F}$ is for the Gauss error potential $Ae^{-\alpha r^2}$ where $A=47.17\,mc^2$ and $\alpha=20\,Mmc^2/\hbar^2$. $\mathfrak{F}^2E^{-\frac{1}{2}}$ at any radius measures the sensitivity of the phase shift $K_0$ to a change in potential at that radius. These sensitivity curves are not changed much if other potentials, fitting experiment approximately, are used for calculating $\mathfrak{F}$ because $\mathfrak{F}$ is approximately determined by $K_0$.

$\rho=\infty$ and the phase of $\mathfrak{G}$ is $\pi/2$ plus the phase of $\mathfrak{F}$. Because of $\lambda$ there is an addition to the phase shift which will be called $\delta K$. It is found that

$$\tan(\delta K)=-\mathfrak{F}^2[\lambda y_\lambda+\lambda^2(y_{\lambda\lambda}/2-\mathfrak{F}\mathfrak{G}y_\lambda^2)+\lambda^3(y_{\lambda\lambda\lambda}/6-\mathfrak{F}\mathfrak{G}y_\lambda y_{\lambda\lambda}+\mathfrak{F}^2\mathfrak{G}^2y_\lambda^3)+\cdots], \quad (1)$$

where

$$y=d\mathfrak{F}/d\rho$$

and successive differentiation of $y$ with respect to $\lambda$ is denoted by suffixes. In the differentiation $\mathfrak{F}$ is supposed to be varied with $\lambda$. Considering $\mathfrak{F}$ and $\mathfrak{G}$ as $\mathfrak{F}(\lambda,\rho)$, $\mathfrak{G}(\lambda,\rho)$ the values in Eq. (1) are $\mathfrak{F}(0,\rho)$, $\mathfrak{G}(0,\rho)$, and similarly $y_\lambda$, $y_{\lambda\lambda}$, $\cdots$ are evaluated for $\lambda=0$. To derive the formula it is sufficient to remember that the phase shift $\delta K$ can be computed with reference to $K$ by exactly the same procedure as $K$ can be computed with reference to the phase existing in the absence of the nuclear potential (the latter is part of $V$); only $\mathfrak{F}$, $\mathfrak{G}$ should be used instead of the Coulomb functions $F$, $G$ and the quantity $dF/Fd\rho-d\mathfrak{F}/\mathfrak{F}d\rho$ should be replaced by $d\mathfrak{F}/\mathfrak{F}d\rho-d\mathfrak{F}_m/\mathfrak{F}_md\rho$, where $\mathfrak{F}_m$ is $\mathfrak{F}$ modified by using $V+\lambda\delta V$ instead of $V$. This difference in logarithmic derivatives when expanded into Taylor's series in $\lambda$ gives Eq. (1). The quantities $y_\lambda$, $y_{\lambda\lambda}$, $\cdots$ can be evaluated by means of Eqs. (9.1) of BTE[6] by substituting $\rho$ for $x$, $-\delta V/E'$ for $\varphi$ and $\mathfrak{F}$ for $F$. With the abbreviation

$$-\mathfrak{F}^2y_\lambda=I(\rho)=-\int_0^\rho(\delta V\mathfrak{F}^2E'^{-1})d\rho,$$

the expansion (1) becomes

$$\tan\delta K=\lambda I+\lambda^2\left(\int_0^\rho\mathfrak{F}^{-2}I^2d\rho+\mathfrak{G}I^2/\mathfrak{F}\right)+\lambda^3\left(2\int_0^\rho\mathfrak{F}^{-2}I\left[\int_0^\rho\mathfrak{F}^{-2}I^2d\rho\right]d\rho+2\mathfrak{G}\mathfrak{F}^{-1}I\left[\int_0^\rho\mathfrak{F}^{-2}I^2d\rho\right]+\mathfrak{G}^2I^3/\mathfrak{F}^2\right)+\cdots. \quad (2)$$

The first term is essentially Taylor's approximation. The second represents the effect of the distortion of the wave function on the first-order effect. The expansion converges rapidly if the distortion of the wave function is not too large. It applies for all $L$ and can be used for other phase shifts than those in proton-proton scattering.

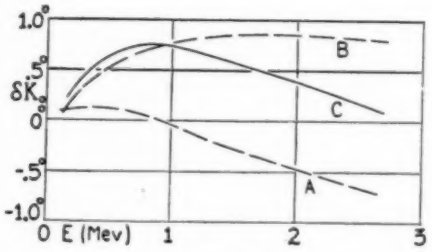


FIG. 5. The changes in phase shift $K_0$ caused by changing from the Gauss error potential $Ae^{-\alpha r^2}$ where $A=47.17\ mc^2$ and $\alpha=20\ Mmc^2/\hbar^2$ to the exponential potential $Be^{-2r/b}$ where $B=137.6\ mc^2$ and $b=0.193\ \hbar(Mmc^2)^{-\frac{1}{2}}$ as calculated by Eq. (2). $A$, first-order effect; $B$, second-order effect; $C$, the sum of first- and second-order effects.

For proton-proton scattering the first-order effect becomes, for $\lambda=1$,

$$\delta K=-0.618\int_0^r\delta V\mathfrak{F}^2E^{-\frac{1}{2}}d(rmc^2/e^2), \quad (3)$$

where $\delta V$ and $E$ are in Mev.

The above expansion was used to compute $K_0$ for the exponential potential (d) using numerical integrations for the Gauss error potential $Ae^{-\alpha r^2}$ with $A=47.17\ mc^2$, $\alpha=20\ Mmc^2/\hbar^2$. The results were compared with direct calculations for the exponential potential. The latter were made by numerical integration of the differential equation at 600, 1400 kev and expansion of $y$ by Eqs. (9.1) of BTE as a function of $E$, the results interchecking in the overlapping region. These calculations for the exponential potential differ from those obtained by the expansion (1) by 0.01° at 300 kev, 0.02° at 1400 kev, −0.01° at 2000 kev, and 0.01° at 2600 kev. At 200 kev the difference is larger and is 0.07°. In Fig. 5 the first- and second-order effects are represented graphically. The second-order effect is practically constant from 800–2600 kev and the first-order effect gives a fair idea of the change in shape of the $K_0$, $E$, curve in this region.

## COMPARISON OF THE PROTON-PROTON AND PROTON-NEUTRON INTERACTIONS

The experiments on proton-proton scattering and the older experiments on proton-neutron scattering[9] indicated that the proton-neutron

[9] V. W. Cohen, H. H. Goldsmith and J. Schwinger, Phys. Rev. **55**, 106(L) (1939).

interaction was a little stronger than that between two protons; that is, if the two interactions were considered as due to the same shape and range of potential well, the proton-neutron interaction required a slightly greater depth. Although this difference was small, it was definitely outside the apparent limits of experimental error. The newer experiments,[10] however, have given a lower proton-neutron cross section. The required difference in depth changed[11] to about 1.5 percent for the square and Gauss error wells and corresponds to a difference of $\sim 4\times10^{-24}$ cm² in a total slow neutron-proton scattering cross section of $\sim 15\times10^{-24}$ cm².

In the case of the meson well, however, the difference is within experimental error. Simons' value for the proton-neutron scattering cross section $\sigma_{\tau\tau}$ is $14.8\times10^{-24}$ cm² so that $\sigma_{th}=59.2\times10^{-24}$ cm², and assuming $12\ \pi a_3^2=12.9\times10^{-24}$, this gives $46.3\times10^{-24}$ cm² $=4\ \pi a_1^2$. (For notation see BTE.*) The best fit to proton-proton data was obtained for the meson well $Ce^{-r/a}/(r/a)$ where $C=89.65\ mc^2$ and $a=0.42\ e^2/mc^2$. By numerical integration it was found that for these values of $C$ and $a$ $4\pi a_1^2=43.85\times10^{-24}$ cm². The value of $12\pi a_3^2$ was not calculated for the meson well, but this quantity does not change much with change of type of potential, so the value $12.9\times10^{-24}$ cm² found for the square well (BTE p. 1057) was used. This gives $\sigma_{th}=56.7\times10^{-24}$ cm², which agrees with the experimental value $59.2\times10^{-24}$ cm² to within the experimental error.

Numerical integrations to find $\mathfrak{F}$ were made for the meson wells with $a=0.42\ e^2/mc^2$ and $C=89.648$, 91.020, and 92.696 $mc^2$. These integrations gave values of $4\pi a_1^2$ equal to 43.85, 65.38, and $122.87\times10^{-24}$ cm², respectively. If $C$ is plotted against $(4\pi a_1^2)^{-\frac{1}{2}}$, the resulting curve is almost a straight line, and it is easy to see what value of $C$ is required to give $4\pi a_1^2=46.3\times10^{-24}$ cm², which is expected from Simons' experiments. The required value of $C$ is only 0.2 percent greater than 89.65 $mc^2$, the value which fits proton-proton scattering data.

The reason that the agreement between the proton-proton and proton-neutron interactions is better for the meson well than for the Gauss error or square potentials is the very large depth of the meson well at small radii, as will now be discussed. Since the calculations show that the proton-neutron experimental data are fitted by a meson well which is the same to within experimental error as the meson well fitting the proton-proton data, it will be assumed that the two wells are identical. It will follow from this assumption that for a square well the proton-neutron attraction is greater than that between protons. By means of Eq. (3) one can obtain the depth of a square well of radius $e^2/mc^2$ from the depth of the meson potential. To the first order one has to adjust the square well depth so that

$$\int \mathfrak{F}_{\tau\tau}^2 E^{-\frac{1}{2}} \delta V_{\tau\tau} dr = 0,$$

where $\delta V_{\tau\tau}$ = (square well potential) − (meson potential) and $\mathfrak{F}_{\tau\tau}$ is the function for the meson well for the proton-neutron singlet state scattering problem. In the same way, starting from the same meson well, one can find a square well of the same width and of such a depth that it fits the proton-proton scattering data and there is no change of phase shift $K_0$; i.e., such values of $\delta V_{\tau\tau}$ are found that

$$\int \mathfrak{F}_{\tau\tau}^2 E^{-\frac{1}{2}} \delta V_{\tau\tau} dr = 0,$$

where $\mathfrak{F}_{\tau\tau}$ is the function for the meson well for the proton-proton scattering problem. Since

$$\delta K = \text{const.} \int \mathfrak{F}_{\tau\tau}^2 \delta V_{\tau\tau} dr = 0$$

and only $\mathfrak{F}_{\tau\tau}$ inside the well is important for the integral, one can make $\mathfrak{F}_{\tau\tau}$ equal to $\mathfrak{F}_{\tau\tau}$ at some radius by multiplying $\mathfrak{F}_{\tau\tau}$ by a constant and, to the first-order approximation,

$$\int \mathfrak{F}_{\tau\tau}^2 \delta V_{\tau\tau} dr = 0$$

will remain unchanged. Suppose that $\mathfrak{F}_{\tau\tau}$ is made equal to $\mathfrak{F}_{\tau\tau}$ at some very small radius; then at small radii they will be almost equal, but since $\mathfrak{F}_{\tau\tau}$ is less bent, because of the presence of the Coulomb potential, it will become increasingly

[10] L. Simons, Phys. Rev. **55**, 792(L) (1939).
[11] G. Breit, L. E. Hoisington, S. S. Share and H. M. Thaxton, Phys. Rev. **55**, 1103(L) (1939).
* Reference 6, pp. 1043, 1057.

larger than $\mathfrak{F}_{pp}$ as the radius increases. Because of the small difference between $\mathfrak{F}_{nn}$ and $\mathfrak{F}_{np}$ from $r=0$ to $r=0.5\ e^2/mc^2$, and because of the small value of $\delta V$ from $r=1$ to $r=3\ e^2/mc^2$, the most important region for the comparison of the two integrals is from $r=0.5$ to $r=1\ e^2/mc^2$. Since $\mathfrak{F}_{nn}$ is larger than $\mathfrak{F}_{np}$, $|\delta V_{nn}|$ must be smaller than $|\delta V_{np}|$ in this region in order that the integral be zero. To compensate for the very large depth from $r=0$ to $r=0.5\ e^2/mv^2$, the meson well is comparatively shallow from $r=0.5$ to $r=1$ $e^2/mc^2$, so that in this interval $\delta V$ is negative, and a smaller $|\delta V_{nn}|$ means a raising of the bottom of the square well, so that the square well fitting proton-proton scattering is not as deep as that fitting proton-neutron scattering. The argument would be the same in comparing the meson and Gauss error wells.

As a test, the required difference of square well depth was calculated very roughly in the above manner, and was found to be 0.3 (5) Mev, which was considered to be good agreement with the difference 0.1 (7) Mev found by direct fitting to the experimental data.

That locating the main part of the attractive potential at shorter radii should give better agreement between the proton-proton and proton-neutron interactions can also be seen from the equation

$$\frac{\rho\mathfrak{F}'}{\mathfrak{F}}=y\frac{X+(2\ln 2y+f)\Phi_0^*}{\Psi_0+y(2\ln 2y+f)\Phi_0}. \qquad (4)$$

(Eq. (7.5) of BCP[2].) This formula gives the value of the logarithmic derivative of $\mathfrak{F}$ at the edge of a well of width $ay$ for a given phase shift $K_0$. Here $a=2\hbar^2/Me^2$. As the well becomes narrower, i.e., as $y$ becomes smaller, $X$ approaches 2; $\Phi_0^*$, $\Phi_0$ and $\Psi_0$ approach unity, and $f$ remains unchanged, so that because of the $2\ln 2y$ term in the numerator the logarithmic derivative becomes smaller and can be made equal to zero. This corresponds to an increase of the theoretically expected proton-neutron scattering cross section from 0 to $\infty$. One would expect, therefore, that a suitably narrow range could be found that would make the well depth required for proton-proton scattering at a fixed energy just equal to that required for proton-neutron scattering.

It may be significant that the meson potential well fits the proton-proton experiments and that for it the proton-proton and proton-neutron interactions are equal within the experimental error of scattering experiments. The value $a=0.42\ e^2/mc^2$, however, corresponds to a meson mass of 326 $m$, and it is apparent from Fig. 2 that a lighter meson of mass $\sim$180 m will not give results fitting proton-proton scattering data. It may be that calculations using higher orders of the meson field theory will result in a smaller calculated mass, or perhaps the interaction is caused by a praticle actually having the heavier mass. If the interaction is due to neutral mesons as is apparently indicated by Bethe's[12] calculations of the deuteron quadrupole moment, no direct information about the mass would be obtained from cosmic rays. It would nevertheless be strange if the mass of the neutral meson were almost twice as large as that of the charged meson.

The partial success of the meson potential in the above attempts to fit experiment is far from being a definite encouragement for the meson theory of nuclear forces. The promising features are the rather good fit to the experimental $K_0$, $E$ curve and the internal consistency of the "symmetric Hamiltonian" point of view indicated by the agreement of the proton-proton and proton-neutron interactions. The discouraging feature is the very poor agreement of the mass of the meson as obtained from proton-proton scattering and from cosmic-ray evidence. It is conceivable that improvements in the meson theory will affect the slope of the theoretical $K_0$, $E$ curve more than the order of magnitude of the expected quadrupole moment of the deuteron and it is also imaginable that the mass of the particle responsible for nuclear forces is greater than that of the particle seen in cosmic rays. More fundamental work on these questions is obviously needed and it is clear that quantitative applications of the meson theory to problems of nuclear structure are still very questionable.

[12] H. A. Bethe, Phys. Rev. **55**, 1261 (1939).

# Scattering of Photoneutrons from Deuterium by the Nuclei of Atoms of Light Elements

T. Goloborodko and A. Leipunski
*Ukrainian Physico-Technical Institute, Kharkov, U. S. S. R.*
(Received May 29, 1939)

In 1937 measurements of cross sections for the scattering of photoneutrons Ra-Be by the nuclei of atoms of light elements were carried out in this laboratory.[1] The measurements show that these cross sections do not increase approximately monotonously as the cross sections for fast Ra-Be neutrons,[2] but that they exhibit irregular fluctuations.

As we believe this phenomenon to be of considerable interest for the theory of the interaction of neutrons with atomic nuclei, we undertook a systematic investigation of the cross sections for the scattering of photoneutrons of different energies by atomic nuclei. This communication reports the first results of this research.

The photoneutrons from deuterium (50 cm³ of 99.6 percent $D_2O$) irradiated by gamma-rays from RaTh (125 mC in a thin glass ampoule 1.5 mm diameter, 6 mm high) were scattered by the nuclei of light elements from hydrogen to calcium. After scattering they were slowed down to thermal velocities by a paraffin sphere of 13 cm diameter in the center of which were placed two cylindrical dysprosium detectors. The detectors were irradiated to saturation and their activity was then measured (for 3 hours without interruption) by a Geiger-Müller counter. The measurements were made alternately with and without the scatterer. The counting apparatus was checked by measuring the uranium standard after the activity measurements of the detectors were finished. The activities of the detectors with and without the scatterer were compared only when the readings of the standard in the two cases were within the statistical error. The background of the counter was likewise measured for 3 to 5 hr. after the measurements of the activity of the detectors were finished. Because the counters were shielded on all sides by 10 cm lead the background amounted on the average to 10 counts per minute and never exceeded 10 percent of the total activity of the detectors. The fluctuations of the background during the course of the measurements were not more than 1 percent of the total activity. The statistical error in measuring the ratio

$$\frac{a}{b}=\frac{\text{number of counts with scatterer}}{\text{number of counts without scatterer}}$$

varied from 1.7 to 2 percent. The experimental arrangement is represented in Fig. 1.

The scatterers had the shape of disks of equal size (8 cm in diameter) and consisted of powder thoroughly desiccated to remove absorbed water and enclosed in hermetically soldered thin iron boxes. Potassium, sodium, lithium and phosphorus were placed in such boxes; magnesium, aluminum and sulphur were shaped into disks. Hydrogen, chlorine, oxygen and fluorine were used in their compounds $H_2O$, $PbCl_2$, $CaF_2$ and $SiO_2$. The scattering in lead was measured separately.

The scattering cross sections $\sigma$ were calculated by the formula

$$\sigma=\frac{1}{N\delta}\ln\frac{1-\alpha}{(a/b)-\alpha}, \qquad (1)$$

where $N$ is the number of atoms or molecules in 1 cm³ of the scatterer, $\delta$ is the thickness of the scatterer, and

$$\alpha=\omega_1\omega_2/4\pi\omega_0 \qquad (2)$$

is the correction for the geometry of the arrangement. Here $\omega_1$, $\omega_2$ and $\omega_0$ are the solid angles subtended by the scatterer at the source, by the

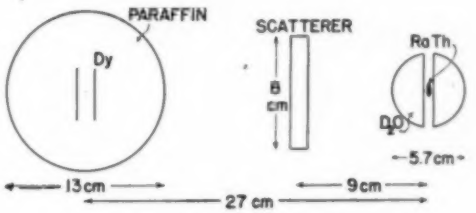


Fig. 1.

[1] Fedorov and Perfilieva, Sowietphys. 2, 660 (1937).
[2] Dunning, Pegram, Fink and Mitchell, Phys. Rev. 48, 277 (1935).

paraffin sphere at the scatterer and by the paraffin sphere at the source, respectively.

The measured values of $a/b$ were about 0.85. The correction terms $\alpha$ were practically constant for all measurements and equal to 0.1.

As the sphere containing $D_2O$ could not be regarded as a point, a correction for the shortening of the distances from the center of the neutron beam to the scatterer and the detector was calculated, according to which all the cross sections $\sigma$ had to be increased by $0.3\times10^{-24}$ cm$^2$. But, on the other hand, considering the scattering by the iron boxes[3] all the cross sections ought to be reduced by $0.33\times10^{-24}$ cm$^2$, so that one correction counterbalanced the other.

The results of the measurements are given in Table I and in Fig. 2.

As seen from the diagram (Fig. 2) within the precision of the measurements there is close

TABLE I. *Cross sections for the scattering of neutrons.*

| ELEMENTS | AT. WEIGHT | $\sigma\times10^{24}$ cm$^2$ PHOTONEUTRONS OF RaTh+D | $\sigma\times10^{24}$ cm$^2$ PHOTONEUTRONS OF Ra+Be |
|---|---|---|---|
| H | 1.008 | 5.0±1.0 | — |
| Li | 6.94 | 2.2±0.4 | 1.0±0.3 |
| Be | 9.02 | 2.8±0.2 | 2.9±0.5 |
| B | 10.82 | 4.2±0.5 | 3.8±0.5 |
| C | 12.00 | 4.8±0.5 | — |
| N | 14.01 | — | 1.6±0.3 |
| O | 16.00 | 3.0±1.0 | 1.8±0.4 |
| F | 19.00 | 6.4±1.3 | 6.3±1.6 |
| Na | 23.00 | 3.2±0.6 | 3.5±0.8 |
| Mg | 24.32 | 3.9±0.4 | 8.4±2.8 |
| Al | 26.97 | 3.8±0.4 | 4.0±0.4 |
| Si | 28.06 | 7.2±0.9 | 1.4±0.7 |
| P | 31.02 | 2.4±0.4 | — |
| S | 32.06 | 2.3±0.4 | 1.0±0.3 |
| Cl | 35.46 | 3.8±1.6 | 3.5±2.1 |
| K | 39.10 | 7.4±1.4 | — |
| Ca | 40.07 | 4.1±1.1 | — |

[3] The scattering by iron was measured and calculated for the weight of a box which was the same for all the scatterers.

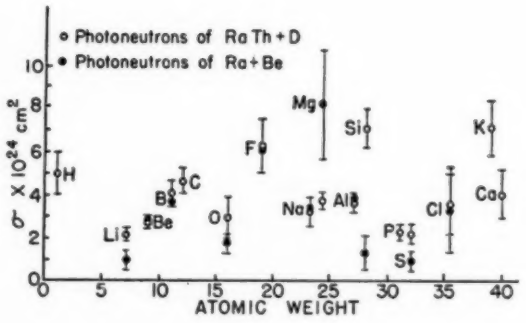


FIG. 2.

parallelism between the fluctuations of the cross section values for the photoneutrons RaTh+D and Ra+Be. The latter are taken from the work of Fedorov and Perfilieva.[1] However Mg and Si display a sharp anomaly. Slight disagreements are also observed with Li and S.

Assuming the energy of the gamma-rays of RaTh to be 2.62 Mev and the threshold of excitation for deuterium to be 2.20 Mev,[4] we get for the energy of the photoneutrons of deuterium a value of 210 kev. In the disintegration of beryllium nuclei the active lines of the spectrum of gamma-rays of radium are probably those with the energies 1.75 Mev and 2.2 Mev.[5]

Assuming the excitation threshold of the beryllium nucleus to be 1.6 Mev,[6] we get for the photoneutrons from beryllium 133 kev and 530 kev.

The measurements are being carried on. Full results of the measurements of cross sections for the scattering by the nuclei of elements from calcium to uranium will be published shortly.

[4] H. A. Bethe, Phys. Rev. **53**, 313 (1938).
[5] A. Alichanov and G. Latyschev, Bulletin de l'académie des Sciences de l'union des Répub. Soviet. Social. (Russian) **20**, 429 (1938).
[6] J. Chadwick and M. Goldhaber, Proc. Roy. Soc. **A151**, 479 (1935).

# Analysis of Proton-Proton Scattering Data

E. CREUTZ*
*University of Wisconsin, Madison, Wisconsin*
(Received August 21, 1939)

THE analysis by Breit, Thaxton and Eisenbud[1] of the proton-proton scattering data of Heydenberg, Hafstad and Tuve[2] indicated a value of $K_0$, the phase shift for the $S$ wave, which appeared too large at 670 kev to fit the theoretical curve deduced from a square and a Gauss error potential well which gave good agreement with the experiments of Herb, Kerst, Parkinson and Plain[3] at higher energies. In the same analysis the values of $K_0$ at 776 and 867 kev were somewhat doubtful because (1) the values of $\mathfrak{R}$, the ratio of the observed scattering to that given by Mott's formula, were read off the curve drawn by Heydenberg, Hafstad and Tuve, rather than being computed from the actual numbers of counts; (2) the coefficients of $\sin^2 K_0$ and $\sin K_0 \cos K_0$ in the theoretical expression for the scattering had been computed only for every 100 kev from 500 to 1000 kev and interpolations made to the experimental energies; and (3) those coefficients had been computed only for every 5° in the value of $\Theta$, the scattering angle, while the experiments were made in most cases at every $2\frac{1}{2}$°.

The present work consisted first in extending the table of coefficients to include every 50 kev and every $2\frac{1}{2}$° from 15° to 45°, and second in fitting the data of Heydenberg, Hafstad and Tuve in the sense of least squares, allowing for the possible effect of scattering of the $P$ wave, i.e., considering terms in $K_1$ in the theoretical expansion of the scattering.

Since the value of $K_1$ that might fit the data was expected to be small, of the order of a few tenths of a degree at most, the term in $\sin^2 K_1$ was dropped and the term in $\sin K_1 \cos K_1$ assumed proportional to $K_1$. The theoretical value of $\mathfrak{R}$ was then $\mathfrak{R}_0+aK_1$ where $\mathfrak{R}_0$ is the value of $\mathfrak{R}$ computed for some $K_0$ chosen near that arrived at by Breit, Thaxton and Eisenbud and $a$ is the coefficient of $\sin K_1 \cos K_1$, computed from the formulas given by Breit, Condon and Present.[4] The percentage difference between $\mathfrak{R}_0+aK_1$ and the experimental $\mathfrak{R}$ was squared and summed over all scattering angles. This sum was then minimized with respect to $K_1$ and the corresponding "best" $K_1$ was found for the particular $K_0$ chosen. Another $K_0$ was then used, and the same procedure repeated, giving a new best $K_1$ and a new sum of squared differences between experiment and theory.

The values of these sums of squares were then plotted against their $K_0$ and the abscissa of the minimum point of the parabola-shaped curve was taken as the $K_0$ which best fits the data, along with the corresponding $K_1$.

An important source of error in scattering experiments is the wobbling of the beam, and since this affects $\mathfrak{R}$ more at small than at large scattering angles it was thought advisable to weight the data in evaluating $K_0$ and $K_1$. This was done by graphically evaluating the logarithmic derivative of the yield as function of $\Theta$ and using the reciprocal of this quantity, ie., $Yd\Theta/dY$, as the weighting factor, to multiply $(\mathfrak{R}_{\text{experiment}}-\mathfrak{R}_0-aK_1)$. The $K_0$ as found from the unweighted data varied from that found in this manner by about $-0.03$°, $-0.03$°, and $+0.02$° at 867, 776, and 670 kev, respectively. By both methods the $K_1$ found was accurately a linear function of the $K_0$ chosen.

In Fig. 1 is plotted as a solid line the percentage variation of experiment, from $\mathfrak{R}$ calculated with the "best" $K_0$ and $K_1$ determined as explained above; and as a dotted line a typical fit in which a value of $K_0$ alone and no $K_1$ is used. A better fit is obtained at practically all points by the use of a small amount of $K_1$ than can be gotten by the use of $K_0$ alone, as is expected, since the number of parameters is thereby increased. The fact that the $K_1$ which gives the

* Now at Princeton University.
[1] G. Breit, H. M. Thaxton and L. Eisenbud, Phys. Rev. **55**, 1018 (1939).
[2] L. R. Hafstad, N. P. Heydenberg and M. A. Tuve Phys. Rev. **51**, 1023 (1937); **53**, 239 (1938).
[3] R. G. Herb, D. W. Kerst, D. B. Parkinson and G. J. Plain, Phys. Rev. **55**, 998 (1939).
[4] G. Breit, E. U. Condon and R. D. Present, Phys. Rev. **50**, 825 (1936).

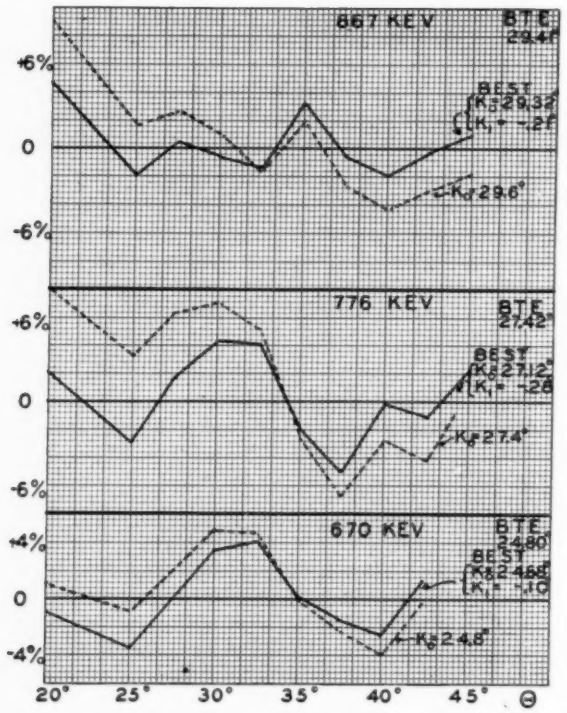


FIG. 1. Solid line: Percentage deviation of experimental values of $\mathfrak{R}$ from value obtained with the $K_0$ and $K_1$ which give the best fit in the sense of least squares. Dotted line: a typical fit in which a value of $K_0$ alone and no $K_1$ is used. Values of $K_0$ given by Breit, Thaxton and Eisenbud are indicated by BTE.

best fit is not a smooth function of energy but is greater at 776 kev than at 670 or 867 kev probably indicates that no meaning should be attached to it as a real scattering anomaly, but only that the experimental errors are such as to increase the apparent $\mathfrak{R}$ at small angles more than at large. For the "best" $K_1$ the difference between experiment and theory is of the same order of magnitude as for $K_1=0$, and the dips in the full drawn curves in the figure occur at about the same scattering angle at the three energies. If these dips are due to systematic errors, the apparent $K_1$ may be due to them as well. It appears somewhat inconsistent, therefore, to introduce $K_1$ into the analysis without bringing in $K_2$ as well. The latter seems to be improbable theoretically. It should also be mentioned that[1] the data of Herb, Kerst, Parkinson and Plain[3] do not indicate the necessity of $K_1$. The data are insufficient to render the suggestion of a possible resonance in $K_1$ in the neighborhood of 776 kev due to the formation of an excited $He^2$ any more than a mere speculation. It is of interest, however, that this more thorough analysis of the data provides values for $K_0$ in good agreement with the theoretical values of Breit, Thaxton and Eisenbud, lowering the low energy part of the experimental $K_0$, $E$ curve.

Table I gives the expansions in powers of $1/E$,

TABLE I. *Series expansions in powers of 1/E, E being the energy in Mev, for* $\mathbf{X}$, $-2\mathbf{Y}/\eta$, *and* $\mathfrak{M}$.

| | 22½° | 27½° | 32½° | 37½° |
|---|---|---|---|---|
| $\mathbf{X}$ | 8.000<br>$-0.3154/E$<br>$+0.00242/E^2$ | 5.961<br>$-0.1410/E$<br>$+0.0007/E^2$ | 4.870<br>$-0.0689/E$<br>$+0.0002/E^2$ | 4.287<br>$-0.0375/E$<br>$+0.00007/E^2$ |
| $-2\mathbf{Y}/\eta$ | 26.61<br>$-0.4034/E$<br>$+0.00186/E^2$ | 15.107<br>$-0.1444/E$<br>$+0.00043/E^2$ | 9.565<br>$-0.0558/E$<br>$+0.000107/E^2$ | 6.828<br>$-0.0233/E$<br>$+0.000027/E^2$ |
| $\mathfrak{M}$ | 40.00<br>$+0.3108/E$<br>$-0.002011/E^2$ | 17.65<br>$+0.1270/E$<br>$-0.000451/E^2$ | 9.106<br>$+0.0495/E$<br>$-0.000084/E^2$ | 5.518<br>$+0.01504/E$<br>$-0.000009/E^2$ |

$E$ being the energy in Mev, for $\mathbf{X}$, $-2\mathbf{Y}/\eta$, and $\mathfrak{M}$ for values of $\Theta$ not given in the tables of Breit, Thaxton and Eisenbud.[5] The expansions were checked for several values by direct trigonometric substitution in formulas (1) and (2.2) of the above paper. The author wishes to express his appreciation to Professor Breit for suggesting this work and to Mr. R. Davies who checked some of the calculations.

[5] Reference 1, pages 1024–1025.

# The Rotation-Vibration Energies of Tetrahedrally Symmetric Pentatomic Molecules. I

WAVE H. SHAFFER, HARALD H. NIELSEN AND L. H. THOMAS
*Mendenhall Laboratory of Physics, Ohio State University, Columbus, Ohio*

(Received June 29, 1939)

A complete theory for the rotation-vibration energies of tetrahedrally pentatomic molecules has been derived to second degree of approximation for certain vibration states. In this discussion the elements of the matrix $H$ are given for the states $V_1\nu_1$, $\nu_2$, $V_1\nu_1+\nu_3$, $V_1\nu_1+\nu_4$, $\nu_2+\nu_3$ and $\nu_2+\nu_4$. The selection rules governing what transitions may take place have been determined with relations for the intensities.

## I. INTRODUCTION

THE band spectra of tetrahedrally symmetric molecules, of which methane is a typical example, have long been known to possess anomalies in their rotational structure. Not only does the value of the moment of inertia $A_0$, computed from the rotational line separation $\Delta\nu$ by the relation $A_0=(h/4\pi^2\Delta\nu)$, vary from band to band, but recent measurements[1] have shown that the rotation lines themselves are not single lines, but show multiplet structure. The first effect has been explained in a theory originally proposed by Teller[2] and subsequently enlarged upon by Johnston and Dennison[3] which shows that the Coriolis interactions between rotation and the threefold degenerate oscillations yield corrections to the energies of these states so significant that the relation for $A_0$ becomes $(\zeta h/4\pi^2\Delta\nu)$ where $\zeta$ is a constant, varying from band to band, which depends upon the nature of the normal vibration and may be substantially different from unity. The second effect has, for the frequency $\nu_4$, been accounted for by Jahn[4] who attributes this splitting principally to a Coriolis interaction between the optically active frequency $\nu_4$ and the optically inactive vibration $\nu_2$. The work of Jahn does not, however, take into account any of the other kinds of interactions which may be present, such as the centrifugal expansion of the molecule, the Coriolis interactions between more remotely separated vibration frequencies and the effects of the anharmonicity of the oscillational motion, all of which are indicated by experiment to be of considerable importance. Jahn's work serves essentially to emphasize the importance of obtaining a complete theory for the energies of such polyatomic models where all second-order effects are taken into account.

In a recent paper[5] we have made just such calculations for non-linear triatomic molecules and have given explicit expressions for the elements of the energy matrix for the general rotation-vibration state. In principle it is possible to make such calculations also for the tetrahedrally symmetric model, but in practice it is not feasible to do so and it becomes necessary to treat each vibration state as a separate case. We have determined the elements of the energy matrix accurately to second order of approximation for the states $V_1\nu_1$, $\nu_2$, $V_1\nu_1+\nu_3$, $V_1\nu_1+\nu_4$, $\nu_2+\nu_3$, $\nu_2+\nu_4$, $2\nu_3$, $2\nu_4$ and $\nu_3+\nu_4$. In this paper we desire to set down our results for the first six of the above states, leaving for a Part II the discussion of the states $2\nu_3$, $2\nu_4$ and the combination states between $\nu_3$ and $\nu_4$.

## II. DERIVATION OF THE SCHRÖDINGER EQUATION

The orientation is a system of body-fixed coordinates $x$, $y$, $z$ of the model which we shall refer to herein is illustrated in Fig. 1. In their equilibrium positions, the four identical $Y$

[1] W. B. Steward and H. H. Nielsen, Phys. Rev. **47**, 878 (1935); W. B. Steward and H. H. Nielsen, Phys. Rev. **48**, 862 (1935); A. H. Nielsen and H. H. Nielsen, Phys. Rev. **48**, 864 (1935).
[2] E. Teller, *Hand und Jahrbuch Chem. Phys.* **9**, II, 43 (1934).
[3] M. Johnston and D. M. Dennison, Phys. Rev. **48**, 868 (1935).
[4] H. A. Jahn, Proc. Roy. Soc. **A168**, 469 (1938).
[5] W. H. Shaffer and H. H. Nielsen, Phys Rev. **56**, 188 (1939).

particles of masses $m_1$ lie at the corners of a regular tetrahedron, of which the edges have a length $2(2)^{\frac{1}{2}}a$, and the $X$ particle of mass $m_5$ is situated at the center of mass of the $Y$ particles. From Fig. 1 the equilibrium positions of the five particles will be seen to be the following: 1, $(a, -a, -a)$; 2, $(-a, a, -a)$; 3, $(-a, -a, a)$; 4, $(a, a, a)$; 5, $(0, 0, 0)$.

The kinetic energy of the molecule expressed in the coordinates $x$, $y$ and $z$ will be:

$$T=\tfrac{1}{2}\{\sum_{s=1}^{5}m_s(\dot{x}_s^2+\dot{y}_s^2+\dot{z}_s^2)+\sum_{\alpha}A_\alpha\omega_\alpha^2 -\sum_{\alpha\beta}{}'D_{\alpha\beta}\omega_\alpha\omega_\beta+2\sum_{\alpha}\Omega_\alpha\omega_\alpha\}, \quad (1)$$

$\alpha$ and $\beta$ being summed over the values $x$, $y$ and $z$ and the prime associated with the summation $\alpha\beta$ meaning that $\alpha\neq\beta$. In the above the $x_s$, $y_s$ and $z_s$ are the instantaneous values of the coordinates of the particles; $A_\alpha$ and $D_\alpha$ are respectively the moments and products of inertia; $\Omega_\alpha$ are the internal angular momenta, their values being:

$$A_\alpha=\sum_{s=1}^{5}m_s(\beta_s^2+\dot{\gamma}_s^2), \quad D_{\alpha\beta}=\sum_{s=1}^{5}m_s\alpha_s\beta_s,$$
$$\Omega_\alpha=\sum_{s=1}^{5}m(\dot{\beta}_s\delta\gamma_s-\dot{\gamma}_s\delta\beta_s). \quad (2)$$

The $\omega_\alpha$ are the components of the angular velocities along the axes $x$, $y$ and $z$ and the $\delta\alpha$ in the above are the displacements of the atoms from their rest positions in the $x$, $y$ and $z$ directions.

To be useful in deriving the Schrödinger equation Eq. (1) must be expressed in terms of the normal coordinates. To obtain these it will be necessary briefly to consider the problem of the oscillation of the molecule in the body-fixed coordinates. There are in all nine degrees of oscillational freedom for this type of molecule so that the above coordinates are not all independent. It is convenient, therefore, to introduce the nine intermediate coordinates which are related to the $x_s$, $y_s$ and $z_s$ by the relations:

$$\begin{aligned}
x_1&=a+\tfrac{1}{2}(\mu_1/m_1)\xi_1+\tfrac{1}{2}\zeta_1-\tfrac{1}{2}\eta_3-\tfrac{1}{2}\eta_2,\\
x_2&=-a+\tfrac{1}{2}(\mu_1/m_1)\xi_1-\tfrac{1}{2}\zeta_1+\tfrac{1}{2}\eta_3-\tfrac{1}{2}\eta_2,\\
x_3&=-a+\tfrac{1}{2}(\mu_1/m_1)\xi_1-\tfrac{1}{2}\zeta_1+\tfrac{1}{2}\eta_3+\tfrac{1}{2}\eta_2,\\
x_4&=a+\tfrac{1}{2}(\mu_1/m_1)\xi_1+\tfrac{1}{2}\zeta_1-\tfrac{1}{2}\eta_3+\tfrac{1}{2}\eta_2,\\
x_5&=-2(\mu_1/m_5)\xi_1.
\end{aligned} \quad (3)$$

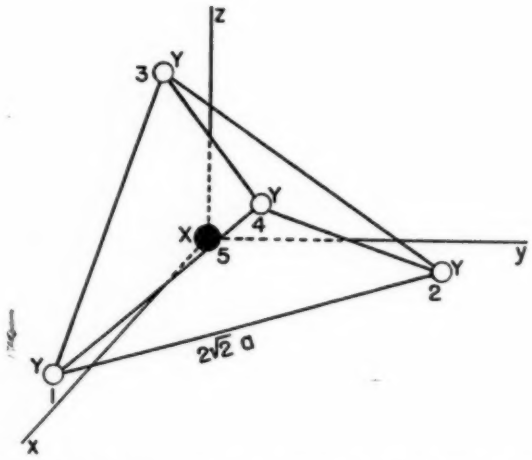


FIG. 1. The orientation in a system of body-fixed coordinates $x$, $y$, $z$ of the pentatomic molecule.

The corresponding $y_s$ and $z_s$ are obtained from (3) simply by replacing the coordinates $(\xi_1, \zeta_1, \eta_3, \eta_2)$ by $(\xi_2, \eta_3, \zeta_2, \eta_1)$ and $(\xi_3, \eta_2, \eta_1, \zeta_3)$, respectively, with appropriate changes in the equilibrium coordinates. In the above $\mu_1$ is substituted for $m_1m_5/(4m_1+m_5)$. It may readily be verified that these conform to the usual requirements that the centroid shall remain fixed and that to zeroth approximation the angular momentum in the coordinates $x$, $y$ and $z$ shall be zero.

We must next select a function for the harmonic portion of the potential energy. To do so we proceed as follows: We denote by $S_{ij}$ the distance between two particles $i$ and $j$ and by $\delta_{ij}$ their relative displacements from their positions of equilibrium so that $S_{ij}=S_{ij}^0+\delta_{ij}$. We shall adopt the perfectly general quadratic function of the displacement coordinates $\delta_{ij}$

$$\begin{aligned}
V_0=\tfrac{1}{2}\{&\tfrac{1}{2}K_1\sum_{i=1}^{4}\sum_{j=1}^{4}{}'\delta_{ij}^2+K_2\sum_{k=1}^{4}\delta_{k5}^2\\
&+\tfrac{1}{4}K_3\sum_{i=1}^{4}\sum_{j=1}^{4}{}'\sum_{k=1}^{4}{}''\delta_{ij}(\delta_{ik}+\delta_{jk})\\
&+\tfrac{1}{2}K_4\sum_{j=1}^{4}\sum_{k=1}^{4}{}'\delta_{j5}\delta_{k5}+\tfrac{1}{2}K_5\sum_{i=1}^{4}\sum_{j=1}^{4}{}'\delta_{ij}(\delta_{j5}+\delta_{i5})\\
&+\tfrac{1}{4}K_6\sum_{i=1}^{4}{}'\sum_{j=1}^{4}{}''\sum_{k=1}^{4}{}'''\sum_{l=1}^{4}{}''''\delta_{ij}\delta_{kl}\\
&+\tfrac{1}{2}K_7\sum_{i=1}^{4}\sum_{j=1}^{4}{}'\sum_{k=1}^{4}{}''\delta_{ij}\delta_{k5}\}
\end{aligned} \quad (4)$$

as the one suitable for our problem. In (4) the single and double primes are used to indicate that no two indices may simultaneously take the same values. The $K$'s are the force constant factors. When $\delta_{ij}$ are expressed in the intermediate coordinates one obtains for (4):

$$V_0=\tfrac{1}{2}\{k_1\sum_{i=1}^{3}\xi_i^2+2k_2\sum_{i=1}^{3}\eta_i\xi_i+k_3\sum_{i=1}^{3}\eta_i^2 +k_4\sum_{i=1}^{3}\zeta_i^2+k_5\sum_{i=1}^{3}{}'\sum_{j=1}^{3}\zeta_i\zeta_j\}, \quad (5)$$

where the constants

$$\begin{aligned}
k_1&=(K_2/3)-(K_4/6),\\
2k_2&=(4K_2/3)-(2K_4/3)+(4K_5/6^{\frac{1}{2}})-(4K_7/6^{\frac{1}{2}}),\\
k_3&=4K_1+(4K_2/3)-2K_3-(2K_4/3)\\
&\quad+(8K_5/6^{\frac{1}{2}})-2K_6-(8K_7/6^{\frac{1}{2}}), \quad (6)\\
k_4&=2K_1+(K_2/3)+3K_3+\tfrac{1}{2}K_4\\
&\quad+(4K_5/6^{\frac{1}{2}})+K_6+(4K_7/6^{\frac{1}{2}}),\\
2k_5&=2K_1+7K_3+K_4+(8K_5/6^{\frac{1}{2}})\\
&\quad+K_6+(8K_7/6^{\frac{1}{2}}).
\end{aligned}$$

The actual normal coordinates, which we shall designate by $q_1, q_2, \cdots q_9$, are simple linear combinations of the intermediate coordinates (3). In fact it is readily verified that oscillational kinetic and potential energies take the following simple form

$$T_v+V_0=\tfrac{1}{2}\{\sum_{i=1}^{3}(\dot{q}_i^2/\omega_3+\omega_3 q_i^2)+\sum_{j=4}^{6}(\dot{q}_j^2/\omega_4+\omega_4 q_j^2) +\sum_{k=7}^{8}(\dot{q}_k^2/\omega_2+\omega_2 q_k^2)+(\dot{q}_9^2/\omega_1+\omega_1 q_9^2), \quad (7)$$

where the intermediate coordinates $\xi_i$, $\eta_i$ and $\zeta_i$ are taken to be the following linear combinations of $q_i$:

$$\begin{aligned}
\xi_l&=(\mu_1)^{-\frac{1}{2}}(q_l\cos\gamma/\omega_3^{\frac{1}{2}}+q_{l+3}\sin\gamma/\omega_4^{\frac{1}{2}}),\\
\eta_l&=(2m_5)^{-\frac{1}{2}}(-q_l\sin\gamma/\omega_3^{\frac{1}{2}}+q_{l+3}\cos\gamma/\omega_4^{\frac{1}{2}}), \quad (7)\\
\zeta_l&=(3m_5)^{-\frac{1}{2}}(u_\alpha(2)^{\frac{1}{2}}+q_9/\omega_1^{\frac{1}{2}}),
\end{aligned}$$

where the index $l$ takes the values 1, 2 and 3 and $\alpha$ takes, respectively, the values $x$, $y$ and $z$. For the sake of brevity the following notation has been adopted: $u_\alpha=\omega_2^{-\frac{1}{2}}(q_7\cos\epsilon_l+q_8\sin\epsilon_l)$, $\epsilon_l=\epsilon_1+2\pi(l-1)/3$ where $\epsilon_1$ is arbitrary;

$$\left.\begin{matrix}\sin\gamma\\ \cos\gamma\end{matrix}\right\}=\mp(2)^{-\frac{1}{2}}\{1\mp[(2m_5k_1-\mu_1k_3)^2/(8\mu_1m_5k_2^2-(2m_5k_1-\mu_1k_3)^2)]^{\frac{1}{2}}\}^{\frac{1}{2}},$$

$$\omega_{1,2}=2\pi\nu_{1,2}=\{[k_4+(k_5/2)(1\pm3)]/m_5\}^{\frac{1}{2}},$$

$$\omega_{3,4}=2\pi\nu_{3,4}=\{((\mu_1k_3+2m_5k_1)\pm[(\mu_1k_3-2m_5k_1)^2+8\mu_1m_5k_2^2]^{\frac{1}{2}})/4\mu_1m_5\}^{\frac{1}{2}}.$$

To carry our calculations to the desired approximation, contributions to the energy from the anharmonic terms in the potential energy, cubic and quartic in the coordinates must be taken into account. These have also been chosen as perfectly general functions of the coordinates which are tetrahedrally symmetric. They have been designated by $V_1$ and $V_2$ and are the following:

TABLE I. *Basic transformation functions $S_\rho$ required to remove the types of terms occurring in $H^{(1)\prime}$ together with the corresponding values of $i(H^0S_\rho-S_\rho H^{(0)})$.*

| $\rho$ | $S_\rho$ | $i(H^{(0)}S_\rho-S_\rho H^{(0)})$ |
|---|---|---|
| 1 | $(-p_k/h\nu_k)$ | $q_k$ |
| 2 | $(q_k/h\nu_k)$ | $p_k$ |
| 3 | $(-2/h\nu_k)(p_k^3/3+\tfrac{1}{2}q_kp_kq_k)$ | $q_k^3$ |
| 4 | $(1/h)(\nu_sq_rq_s+\nu_rp_rp_s)/(\nu_r^2-\nu_s^2)$[1] | $q_rp_s$ |
| 5 | $-\{(2\nu_r^2-\nu_s^2)q_r^2p_s+\nu_r\nu_s(q_rp_r+p_rq_r)q_s+2\nu_r^2p_r^2p_s\}/h\nu_s(4\nu_r^2-\nu_s^2)$ | $q_r^2q_s$ |
| 6 | $-\{\nu_r(\nu_r^2-\nu_s^2-\nu_t^2)p_rq_sq_t+\nu_s(\nu_s^2-\nu_r^2-\nu_t^2)q_rp_sq_t-2\nu_r\nu_s\nu_tp_rp_sp_t +\nu_t(\nu_t^2-\nu_r^2-\nu_s^2)q_rq_sq_t\}h^{-1}(\nu_r^4+\nu_s^4+\nu_t^4-2\nu_r^2\nu_s^2-2\nu_t^2\nu_s^2-2\nu_r^2\nu_t^2)^{-1}$ | $q_rq_sq_t$ |
| 7 | $(q_rq_s+p_rp_s)/h(\nu_r-\nu_s)$ | $q_rp_s-p_rq_s$ |

[1] $S_4$ is the function which removes from $H^{(1)}$ the Coriolis interaction terms which are of the type $(q_rp_s-p_rq_s)P_\alpha$. When these terms originate with degenerate oscillations the difference $\nu_r-\nu_s$ occurring in the denominator vanishes. Obviously such terms cannot be removed from $H^{(1)}$ by this method.

$$V_1 = C_1q_1q_2q_3 + C_2(q_1q_2q_6 + q_1q_3q_5 + q_2q_3q_4) + C_3(q_1q_5q_6 + q_2q_4q_6 + q_3q_4q_5) + C_4q_4q_5q_6 + C_5(q_1^2 + q_2^2 + q_3^2)q_9$$
$$+ C_6(q_1q_4 + q_2q_5 + q_3q_6)q_9 + C_7(q_4^2 + q_5^2 + q_6^2)q_9 + C_8(u_xq_1^2 + u_yq_2^2 + u_zq_3^2)$$
$$+ C_9(u_xq_1q_4 + u_yq_2q_5 + u_zq_3q_6) + C_{10}(u_xq_4^2 + u_yq_5^2 + u_zq_6^2) + C_{11}q_9^3$$
$$+ C_{12}(u_x^2 + u_y^2 + u_z^2)q_9 + C_{13}u_xu_yu_z,$$
$$V_2 = d_1(q_1^4 + q_2^4 + q_3^4) + d_2(q_1^3q_4 + q_2^3q_5 + q_3^3q_6) + d_3(q_1^2q_4^2 + q_2^2q_5^2 + q_3^2q_6^2) + d_4(q_1q_4^3 + q_2q_5^3 + q_3q_6^3)$$
$$+ d_5(q_4^4 + q_5^4 + q_6^4) + d_6(q_1^2q_2^2 + q_2^2q_3^2 + q_1^2q_3^2) + d_7(q_1q_4q_2^2 + q_1^2q_2q_5 + q_2q_5q_3^2 + q_2^2q_3q_6$$
$$+ q_3q_6q_1^2 + q_3^2q_1q_4) + d_8(q_1q_2q_4q_5 + q_2q_3q_5q_6 + q_3q_1q_4q_6) + d_9(q_4^2q_2q_5 + q_1q_4q_5^2 + q_2q_5q_6^2 + q_3q_5^2q_6$$
$$+ q_3q_6q_4^2 + q_6^2q_1q_4) + d_{10}(q_4^2q_5^2 + q_5^2q_6^2 + q_4^2q_6^2) + d_{11}(q_1^2q_5^2 + q_1^2q_6^2 + q_2^2q_6^2 + q_2^2q_4^2 + q_3^2q_4^2 + q_3^2q_5^2)$$
$$+ d_{12}q_9(q_1q_2q_3) + d_{13}(q_2q_3q_4 + q_1q_3q_5 + q_1q_2q_6)q_9 + d_{14}(q_3q_4q_5 + q_2q_4q_6 + q_1q_5q_6)q_9 + d_{15}q_4q_5q_6q_9$$
$$+ d_{16}(u_xq_2q_3q_4 + u_yq_1q_3q_5 + u_zq_1q_2q_6) + d_{17}(u_xq_1q_5q_6 + u_yq_2q_4q_6 + u_zq_3q_4q_5) + d_{18}q_9^2(q_1^2 + q_2^2 + q_3^2)$$
$$+ d_{19}q_9^2(q_1q_4 + q_2q_5 + q_3q_6) + d_{20}q_9^2(q_4^2 + q_5^2 + q_6^2) + d_{21}(u_x^2q_1^2 + u_y^2q_2^2 + u_z^2q_3^2)$$
$$+ d_{22}[u_x^2(q_2^2 + q_3^2) + u_y^2(q_1^2 + q_3^2) + u_z^2(q_1^2 + q_2^2)] + d_{23}(u_xu_yq_3^2 + u_xu_zq_2^2 + u_yu_zq_1^2)$$
$$+ d_{24}(u_x^2q_1q_4 + u_y^2q_2q_5 + u_z^2q_3q_6) + d_{25}[u_x^2(q_1q_5 + q_3q_6) + u_y^2(q_3q_6 + q_1q_4) + u_z^2(q_1q_4 + q_2q_5)]$$
$$d_{26}(u_xu_yq_3q_6 + u_xu_zq_2q_5 + u_yu_zq_1q_4) + d_{27}(u_x^2q_4^2 + u_y^2q_5^2 + u_z^2q_6^2) + d_{29}(u_xu_yq_6^2 + u_xu_zq_5^2 + u_yu_zq_4^2)$$
$$+ d_{28}(u_x^2(q_5^2 + q_6^2) + u_y^2(q_4^2 + q_6^2) + u_z^2(q_4^2 + q_5^2)) + d_{30}q_9^4 + d_{31}q_9^2(u_x^2 + u_y^2 + u_z^2)$$
$$+ d_{32}u_xu_yu_zq_9 + d_{33}(u_x^4 + u_y^4 + u_z^4). \tag{8}$$

When the complete kinetic and potential energies have been written down in terms of the normal coordinates and expressed in the Hamiltonian form, one may proceed directly to obtain the Schrödinger equation. We have made use of the method of Wilson and Howard[6] and later verified the results by the variational method of Schrödinger. We shall give none of the intermediate details here, but set down directly the appropriate quantum mechanical Hamiltonian expressed in orders of magnitude. It is the following:

$$H^0 = (P^2/2A_0) + \pi\nu_3\sum_{i=1}^{3}(p_i^2 + q_i^2) + \pi\nu_4\sum_{j=4}^{6}(p_j^2 + q_j^2) + \pi\nu_2\sum_{k=7}^{8}(p_k^2 + q_k^2) + \pi\nu_1(p_9^2 + q_9^2), \tag{9a}$$

where $p_s$ is the differential operator $-i\hbar(\partial/\partial q_s)$, $P$, the total angular momentum operator and $A_0$ the constant part of the moments of inertia.

$$H^{(1)} = -(\sum_\alpha p_\alpha P_\alpha/A_0) + \sum_\alpha E_\alpha P_\alpha^2 + \tfrac{1}{2}\sum_{\alpha\beta}{}' F_{\alpha\beta}(P_\alpha P_\beta) - i\hbar(3\pi\nu_1/A_0)^{\frac{1}{2}}p_9 + V_1. \tag{9b}$$

The summation $\alpha$ and $\beta$ is over $x$, $y$, $z$, and the prime indicating that no two indices may at the same time take the same value. In the above $E_\alpha = (3A_0^3)^{-\frac{1}{2}}[\omega_2^{-\frac{1}{2}}u_\alpha - 2(2\omega_1)^{-\frac{1}{2}}q_9]$ and $F_{\alpha\beta} = F_{\beta\alpha} = (m_5/2A_0^3)^{\frac{1}{2}}\eta_r$, $r$ taking the values 1, 2 and 3 with $\alpha\beta$ equal to $yz$, $xz$ and $xy$, respectively. The quantity $p_z$ is equal to:

$$p_z = \zeta_3(q_2p_3 - q_3p_2) + \zeta_4(q_5p_6 - q_6p_5) + \zeta_{34}[(\nu_4/\nu_3)^{\frac{1}{2}}(q_2p_6 - q_6p_2) + (\nu_3/\nu_4)^{\frac{1}{2}}(q_5p_3 - q_6p_2)]$$
$$+ \zeta_{23}[(\nu_3/\nu_2)^{\frac{1}{2}}v_zp_1 - (\nu_2/\nu_3)^{\frac{1}{2}}q_1p_{v_z}] - \zeta_{24}[(\nu_4/\nu_2)^{\frac{1}{2}}v_zp_4 - (\nu_2/\nu_4)^{\frac{1}{2}}q_4p_{v_z}],$$

$p_y$ and $p_z$ being, respectively, obtained by cyclicly rotating the coordinates $q_1$, $q_2$, $q_3$; the coordinates $q_4$, $q_5$, $q_6$; the momenta $p_1$, $p_2$, $p_3$ and $p_4$, $p_5$, $p_6$ in the relation $p_x$. For the sake of brevity the notation

[6] E. Bright Wilson and J. B. Howard, J. Chem. Phys. **4**, 260 (1936).

$v_\alpha = q_7 \sin \epsilon_r - q_8 \cos \epsilon_r$ and $p_{v_\alpha} = p_7 \sin \epsilon_r - p_8 \cos \epsilon_r$, $\zeta_3 = (1-(3/2)\sin^2\gamma)$, $\zeta_4 = (1-(3/2)\cos^2\gamma)$, $\zeta_{23} = \sin\gamma$, $\zeta_{24} = \cos\gamma$ and $\zeta_{34} = (3/2)\zeta_{23}\zeta_{24}$ is introduced.

$$H^{(2)} = C + \sum_\alpha G_\alpha P_\alpha^2 + \tfrac{1}{2}\sum_{\alpha\beta}{}' H_{\alpha\beta} P_\alpha P_\beta + \sum_\alpha I_\alpha P_\alpha + \sum_\alpha (p_\alpha^2/2A_0) + V_2, \tag{9c}$$

where

$$C = (i\hbar/4A_0)\{(q_1p_1+q_2p_2+q_3p_3)\zeta_{23}^2 + (q_4p_4+q_5p_5+q_6p_6)\zeta_{24}^2 - (4/3)\zeta_{34}[(\nu_3/\nu_4)^{\frac{1}{2}}(q_4p_1+q_5p_2+q_6p_3) + (\nu_4/\nu_3)^{\frac{1}{2}}(q_1p_4+q_2p_5+q_3p_6)] + q_7p_7+q_8p_8+4q_9p_9\},$$

$$G_x = (4\pi A_0{}^2)^{-1}\{(\zeta_{23}^2/\nu_3)(q_1^2-(q_2^2/4)+(3q_3^2/4)) + (\zeta_{24}^2/\nu_4)(q_4^2-(q_5^2/4)+(3q_6^2/4)) + (u_x^2/\nu_2) + (2/\nu_1)q_9^2 + (4/3)(\nu_3\nu_4)^{-\frac{1}{2}}\zeta_{34}(-q_1q_4+(1/4)q_2q_5-(3/4)q_3q_6) - 2(2/\nu_1\nu_2)^{\frac{1}{2}}u_xq_9\},$$

$$H_{xy} = (4\pi A_0{}^2)^{-1}\{(-\zeta_{34}/2)(\nu_3\nu_4)^{-\frac{1}{2}}(q_1q_5+q_2q_4) + (3\zeta_{23}^2/4\nu_3)q_1q_2 + (3\zeta_{24}/4\nu_4)q_4q_5 - [(\zeta_{24}^2/\nu_4)^{\frac{1}{2}}q_6 - (\zeta_{23}^2/\nu_3)^{\frac{1}{2}}q_3][(6/\nu_1)^{\frac{1}{2}}q_9 + (3/4\nu_2)^{\frac{1}{2}}u_z]\},$$

$$I_x = -(2\pi A_0{}^3)^{-\frac{1}{2}}\{[(4/3\nu_2)^{\frac{1}{2}}u_x - (8/3\nu_1)^{\frac{1}{2}}q_9]p_x + [(\zeta_{24}^2/\nu_4)^{\frac{1}{2}}q_6 - (\zeta_{23}^2/\nu_3)^{\frac{1}{2}}q_3]p_y + [(\zeta_{24}^2/\nu_4)^{\frac{1}{2}}q_5 - (\zeta_{23}^2/\nu_3)^{\frac{1}{2}}q_2]p_z\}.$$

The quantities $G_y$, $G_z$, $H_{yz}$, $H_{xz}$, $I_y$ and $I_z$ may be obtained from the above by cyclically rotating $u_x, u_y, u_z$; $p_x, p_y, p_z$; $q_1, q_2, q_3$; $q_4, q_5, q_6$.

## III. Determination of the Eigenfunctions and Eigenvalues

The Schrödinger equation corresponding to (9a) is separable in the coordinates and has the eigenfunction:

$$\Psi^0(n_1,n_2,\text{—}n_9, J,K,M) = N\,R(J,K,M)\Phi(n_1,n_2,n_3) \times\Phi(n_4,n_5,n_6)\Phi(n_7,n_8)\Phi(n_9) \tag{10}$$

where $R(J, K, M)$ is the wave function of the spherical top, $\Phi(n_1, n_2, n_3)$ and $\Phi(n_4, n_5, n_6)$ the eigenfunctions of two three-dimensionally isotropic oscillators of frequencies $\nu_3$ and $\nu_4$, respectively; $\Phi(n_7, n_8)$, the wave function of a two-dimensionally isotropic oscillator of frequency $\nu_2$ and $\Phi(n_9)$ is the wave function of a linear oscillator. The $n_s$ are all integers and may be regarded as the vibration quantum numbers associated with the coordinates $q_s$. $N$ is a normalization factor. The zeroth order eigenvalues become:

$$E^0(V_1, V_2, V_3, V_4, J) = (V_1+\tfrac{1}{2})h\nu_1 + (V_2+1)h\nu_2 + (V_3+\tfrac{3}{2})h\nu_3 + (V_4+\tfrac{3}{2})h\nu_4 + J(J+1)h^2/8\pi^2A_0, \tag{11}$$

where for convenience the substitution $V_1 = n_9$, $V_2 = n_7+n_8$, $V_3 = n_1+n_2+n_3$ and $V_4 = n_4+n_5+n_6$ is made.

The evaluation of the corrections to the energy contributed by $H^{(1)}$ and $H^{(2)}$ may be effected by perturbation methods, but is a formidable undertaking when one considers the large number of terms included in $H^{(1)}$ and $H^{(2)}$ and the high degree of degeneracy of the zeroth order energies. The only terms in $H^{(1)}$ which can contribute in first approximation are the Coriolis terms arising from the oscillations $\nu_3$ and $\nu_4$ and a linear combination of the functions (10) can always be found such that the matrix of these will have elements only along the principal diagonal. This suggests the effectiveness of transforming $H$ by a contact transformation[7] $THT^{-1}$ into $H^{(0)\prime} + H^{(1)\prime} + H^{(2)\prime}$ so that $H^{(1)\prime}$ will, to second approximation, contain only the above Coriolis terms. The evaluation of the second-order energies will thus, in principle, be reduced to a first-order perturbation calculation where the wave functions to be used are the stabilized wave functions of $H^{(0)\prime}$, i.e., the linear combination of the functions (10) which diagonalize $H^{(0)\prime}+H^{(1)\prime}$.

We shall denote by $T(\lambda)$ the transformation function $e^{i\lambda S}$ (and by $T^{-1}(\lambda) = e^{-i\lambda S}$ its inverse)

[7] See for example, J. H. Van Vleck, Phys. Rev. **33**, 467 (1929); O. M. Johrdahl, Phys. Rev. **45**, 87 (1934).

which to second approximation may be written:

$$T=1+i\lambda S-\tfrac{1}{2}\lambda^2S^2-(i/6)\lambda^3S^3+\cdots. \quad (12)$$

The transformed Hamiltonian will become to second approximation $THT^{-1}=H'=H^{(0)\prime}+\lambda H^{(1)\prime}+\lambda^2H^{(2)\prime}$ where $H=H^{(0)}+\lambda H^{(1)}+\lambda^2H^{(2)}$. When (12) is used for $T$ (and $T^{-1}$) in the above indicated transformation one obtains by equating together like powers of $\lambda$:

$$\begin{aligned}H^{(0)\prime}&=H^{(0)},\\ H^{(1)\prime}&=H^{(1)}-i(H^{(0)}S-SH^{(0)}),\\ H^{(2)\prime}&=H^{(2)}+(i/2)[S(H^{(1)}+H^{(1)\prime})\\ &\qquad -(H^{(1)}+H^{(1)\prime})S].\end{aligned} \quad (13)$$

The portion of $H^{(1)}$ which we wish to remove consists of terms each of which is a function of the normal coordinates $q_k$ (or the conjugate momenta $p_k$) multiplied by a coefficient which is either a constant or a function of the angular momentum operators $P_\alpha$, for example $ap_k$ and $q_kP_x^2$. When, as in the latter case, the coefficients are functions of $P_\alpha$ they may still be treated merely as constants since the rotational part of $H^{(0)}$ is proportional directly to the square of $P$, which commutes with all functions of $P_\alpha$ so that $(H^{(0)}P_\alpha-P_\alpha H^{(0)})=0$. In Table I is given the basic transformation functions $S_\rho$ required to remove the types of terms occurring in $H^{(1)\prime}$ together with the corresponding values of $i(H^0S_\rho-S_\rho H^{(0)})$. The complete $S$ function will be a sum of terms, each of which will be a basic $S_\rho$ multiplied by an appropriate coefficient. It will contain as many elements as there are terms to be removed; each element in $S$ being chosen to remove a single term in $H^{(1)}$.

The transformed Hamiltonian $H'$ written in orders of magnitude becomes:

$$H^{(0)\prime}=H^{(0)}, \quad (14a)$$

$$H^{(1)\prime}=-(\zeta_3/A_0)[(q_2p_3-q_3p_2)P_x+(q_3p_1-q_1p_3)P_y+(q_1p_2-q_2p_1)P_z]$$
$$-(\zeta_4/A_0)[(q_5p_6-q_6p_5)P_x+(q_6p_4-q_4p_6)P_y+(q_4p_5-q_5p_4)P_z], \quad (14b)$$

$$H^{(2)\prime}=H^{(2)}+(i/2)[S(H^{(1)}+H^{(1)\prime})-(H^{(1)}+H^{(1)\prime})S], \quad (14c)$$

where

$$(i/2)[S(H^{(1)}+H^{(1)\prime})-(H^{(1)}+H^{(1)\prime})S]=\bar{V}_2+\sum_\alpha G'_\alpha P_\alpha{}^2+\sum'_{\alpha\beta}H'_{\alpha\beta}P_\alpha P_\beta+\tau_{\alpha\alpha\alpha\alpha}\sum_\alpha P_\alpha{}^4$$
$$+\tau_{\alpha\alpha\beta\beta}\sum'_{\alpha\beta}(P_\alpha{}^2P_\beta{}^2)+\tau_{\alpha\beta\alpha\beta}\sum'_{\alpha\beta}(P_\alpha P_\beta+P_\beta P_\alpha)^2+\sum_{\alpha\beta\gamma\beta}\tau_{\alpha\beta\gamma\beta}[(P_\alpha P_\beta+P_\beta P_\alpha)(P_\gamma P_\beta+P_\beta P_\gamma)$$
$$-(P_\gamma P_\beta+P_\beta P_\gamma)(P_\alpha P_\beta+P_\beta P_\alpha)]+\tau_0P^2. \quad (14c')$$

In the above:

$$\bar{V}_2=(3\hbar^2/4A_0)+B(\nu_3)+B(\nu_4)+C(\nu_3)+C(\nu_4)+J(\nu_3)+J(\nu_4)+K(\nu_3)+K(\nu_4)$$
$$-(c_6{}^2/4\pi)(\nu_1{}^4+\nu_3{}^4+\nu_4{}^4-2\nu_1{}^2\nu_3{}^2-2\nu_1{}^2\nu_4{}^2-2\nu_3{}^2\nu_4{}^2)^{-1}\{\nu_3(\nu_3{}^2-\nu_4{}^2-\nu_1{}^2)q_9{}^2(q_4{}^2+q_5{}^2+q_6{}^2)$$
$$+\nu_4(\nu_4{}^2-\nu_3{}^2-\nu_1{}^2)q_9{}^2(q_1{}^2+q_2{}^2+q_3{}^2)+\nu_1(\nu_1{}^2-\nu_3{}^2-\nu_4{}^2)(q_1q_4+q_2q_5+q_3q_6)^2+\tfrac{3}{2}i\hbar\nu_1\nu_3\nu_4$$
$$-2\nu_1\nu_3\nu_4[p_1p_4(q_2q_5+q_3q_6)+p_2p_5(q_1q_4+q_3q_6)+p_3p_6(q_1q_4+q_2q_5)]\}-(c_9{}^2/4\pi)(\nu_2{}^4+\nu_3{}^4+\nu_4{}^4$$
$$-2\nu_3{}^2\nu_2{}^2-2\nu_2{}^2\nu_4{}^2-2\nu_3{}^2\nu_4{}^2)^{-1}\{\nu_3(\nu_3{}^2-\nu_4{}^2-\nu_2{}^2)(u_x{}^2q_4{}^2+u_y{}^2q_5{}^2+u_z{}^2q_6{}^2)$$
$$+\nu_4(\nu_4{}^2-\nu_3{}^2-\nu_2{}^2)(u_x{}^2q_1{}^2+u_y{}^2q_2{}^2+u_z{}^2q_3{}^2)+\nu_2(\nu_2{}^2-\nu_4{}^2-\nu_3{}^2)(q_1{}^2q_4{}^2+q_2{}^2q_5{}^2+q_3{}^2q_6{}^2-q_1q_2q_4q_5$$
$$-q_1q_3q_4q_6-q_2q_3q_5q_6)+\tfrac{3}{2}i\hbar\nu_2\nu_3\nu_4+\nu_2\nu_3\nu_4[p_1p_4(q_2q_5+q_3q_6)+p_1p_5(q_1q_4+q_3q_6)$$
$$+p_3p_6(q_1q_4+q_2q_5)]\}-(ic_{11}{}^2/\hbar\nu_1)\{(1/3)(p_9{}^3q_9{}^3-q_9{}^3p_9{}^3)+\tfrac{1}{2}(q_9p_9q_9{}^4-q_9{}^4p_9q_8)\}$$
$$-(9c_{12}{}^2/8\pi\nu_1(4\nu_2{}^2-\nu_1{}^2))\{(2\nu_2{}^2-\nu_1{}^2)(q_7{}^2+q_8{}^2)^2+2\nu_2{}^2(p_7{}^2q_8{}^2+q_7{}^2p_8{}^2)+4\nu_1\nu_2q_9{}^2(q_7{}^2+q_8{}^2)$$

*Formula continued on following page*

$$+\nu_2^2(p_7^2q_7^2+q_7^2p_7^2+p_8^2q_8^2+q_8^2p_8^2)\}-(c_{13}^2/4\pi\nu_2)\{(i/48\hbar)(p_7^3q_7^3-q_7^3p_7^3+p_8^3q_8^3-q_8^3p_8^3)$$
$$+(3/8)q_7^2q_8^2+(3/32)(q_7^4+q_8^4)-(3/16)[p_8(p_7q_7^2+q_7^2p_7)+p_7(p_8q_8^2+q_8^2p_8)+p_7^2q_8^2+p_8^2q_7^2]$$
$$+(3i/16\hbar)[p_7^2q_7^2p_8q_8-q_8p_8q_7^2p_7^2+p_7^2q_7p_8q_8^2-q_8^2p_8q_7p_7^2+p_8^2q_8p_7q_7^2-q_7^2p_7q_8p_8^2+p_7q_7p_8^2q_8^2$$
$$-q_8^2p_8^2q_7p_7]\}-((c_1c_3/2\pi\nu_3)+(c_2c_4/2\pi\nu_4))(q_1q_2q_4q_5+q_1q_3q_4q_6+q_2q_3q_5q_6)-(c_5c_7/2\pi\nu_1)(q_1^2+q_2^2+q_3^2)$$
$$\times(q_4^2+q_5^2+q_6^2)-((3c_5c_{11}/2\pi\nu_1)q_9^2+(3c_5c_{12}/4\pi\nu_1)(q_7^2+q_8^2))(q_1^2+q_2^2+q_3^2)-((3c_7c_{11}/2\pi\nu_1)q_9^2$$
$$+(3c_7c_{12}/2\pi\nu_1)(q_7^2+q_8^2))(q_4^2+q_5^2+q_6^2)-(c_8c_{10}/2\pi\nu_2)[q_4^2(q_1^2-\tfrac{1}{2}q_2^2-\tfrac{1}{2}q_3^2)+q_5^2(q_2^2-\tfrac{1}{2}q_1^2-\tfrac{1}{2}q_3^2)$$
$$+q_6^2(q_3^2-\tfrac{1}{2}q_1^2-\tfrac{1}{2}q_2^2)]-(9c_{11}c_{12}/4\pi\nu_1)q_9^2(q_7^2+q_8^2),$$

where

$$B(\nu_3)=(-c_1^2/12\pi\nu_3)\{q_1^2q_2^2+q_1^2q_3^2+q_2^2q_3^2+(2i/\hbar)(p_1q_1p_2q_2p_3q_3-q_1p_1q_2p_2q_3p_3)\},$$

$$C(\nu_3)=(c_2^2/4\pi\nu_4)(\nu_4^2-4\nu_3^2)^{-1}\{[(q_2q_6+q_3q_5)^2+(q_1q_6+q_3q_4)^2+(q_1q_5+q_2q_4)^2]\nu_3\nu_4$$
$$-(q_1^2q_2^2+q_2^2q_3^2+q_1^2q_3^2)(\nu_4^2-2\nu_3^2)+(2i\nu_3^2/\hbar)(p_1q_1p_3q_3p_5q_5+p_1q_1p_2q_2p_6q_6+p_2q_2p_3q_3p_4q_4$$
$$-q_1p_1q_3p_3q_5p_5-q_1p_1q_2p_2q_6p_6-q_2p_2q_3p_3q_4p_4)\},$$

$$J(\nu_3)=(-c_5^2/4\pi\nu_1)(4\nu_3^2-\nu_1^2)^{-1}\{(2\nu_3^2-\nu_1^2)(q_1^2+q_2^2+q_3^2)^2+4\nu_1\nu_3q_9^2(q_1^2+q_2^2+q_3^2)$$
$$+2\nu_3^2[p_1^2(q_2^2+q_3^2)+p_2^2(q_1^2+q_3^2)+p_3^2(q_1^2+q_2^2)]+(2i\nu_3^2/\hbar)[(p_1^2q_1^2+p_2^2q_2^2+p_3^2q_3^2)p_9q_9$$
$$-q_9p_9(q_1^2p_1^2+q_2^2p_2^2+q_3^2p_3^2)]\},$$

$$K(\nu_3)=(-c_8^2/4\pi\nu_2)(4\nu_3^2-\nu_2^2)^{-1}\{(2\nu_3^2-\nu_2^2)(q_1^4+q_2^4+q_3^4-q_1^2q_2^2-q_1^2q_3^2-q_2^2q_3^2)$$
$$+4\nu_2\nu_3(u_x^2q_1^2+u_y^2q_2^2+u_z^2q_3^2)-\nu_3^2[p_1(q_2^2+q_3^2)+p_2(q_1^2+q_3^2)+p_3(q_1^2+q_2^2)]$$
$$+\nu_3^2[p_1^2q_1^2-q_1^2p_1^2+p_2^2q_2^2-q_2^2p_2^2]\}.$$

The corresponding quantities for $\nu_4$ are obtained, respectively, by replacing $c_1^2$ by $c_4^2$; $c_2^2$ by $c_3^2$; $c_5^2$ by $c_7^2$ and $c_8^2$ by $c_{10}^2$ and in addition by interchanging $\nu_3$ by $\nu_4$ and the coordinates and momenta $q_1$, $q_2$, $q_3$, $p_1$, $p_2$, $p_3$, respectively, by $q_4$, $q_5$, $q_6$, $p_4$, $p_5$, $p_6$. Other quantities which occur in (14c′) are

$$\tau_{aaaa}=(-12\pi^2A_0^3)^{-1}(1/\nu_2^2+2/\nu_1^2),\quad \tau_{aa\beta\beta}=(2/\nu_1^2-1/2\nu_2^2),\quad \tau_{a\beta a\beta}=(-1/32\pi^2A_0^3)(\zeta_{24}^2/\nu_4^2+\zeta_{23}^2/\nu_3^2),$$
$$\tau_{xyzz}=(-i/16\pi hA_0^3)\{(\zeta_{24}p_6/\nu_4^{\frac{1}{2}}-\zeta_{23}p_3/\nu_3^{\frac{1}{2}})(\zeta_{24}q_5/\nu_4^{\frac{1}{2}}-\zeta_{23}q_2/\nu_3^{\frac{1}{2}})-(\zeta_{24}p_5/\nu_4^{\frac{1}{2}}-\zeta_{23}p_2/\nu_3^{\frac{1}{2}})$$
$$\times(\zeta_{24}q_6/\nu_4^{\frac{1}{2}}-\zeta_{23}q_3/\nu_3^{\frac{1}{2}})\};$$

$$\tau_0=\{2c_5(q_1^2+q_2^2+q_3^2)+2c_7(q_4^2+q_5^2+q_6^2)+6c_{11}q_9^2+3c_{12}(q_7^2+q_8^2)\}(4\pi A_0^{\frac{1}{2}}(3\pi\nu_1)^{\frac{1}{2}})^{-1},$$
$$G_x'=\{(a_1/\nu_2)(q_1^2-\tfrac{1}{2}q_2^2-\tfrac{1}{2}q_3^2)+(a_2/\nu_2)(q_4^2-\tfrac{1}{2}q_5^2-\tfrac{1}{2}q_6^2)+(\zeta_{34}^2/(\nu_3^2-\nu_4^2))[(\nu_4^2+\nu_3^2)((q_5^2+q_6^2)/\nu_4$$
$$-(q_2^2+q_3^2)/\nu_3)+2\nu_4(p_5^2+p_6^2)-2\nu_3(p_2^2+p_3^2)]+(\zeta_{23}^2/(\nu_2^2-\nu_3^2))[(\nu_3^2+\nu_4^2)(q_1^2/\nu_3-v_x/\nu_2)$$
$$-2\nu_2p_{v_x}^2+2\nu_3p_1^2]+(\zeta_{24}^2/(\nu_2^2-\nu_4^2))[(\nu_2^2+\nu_4^2)(q_4^2/\nu_3-v_x^2/\nu_2)-2\nu_2p_{v_x}+2\nu_4p_4^2],$$
$$H_{xy}'=\{(3a_6/\nu_3)-(a_7/\nu_4)+a_{10}/(\nu_3\nu_4)^{\frac{1}{2}}+(\zeta_{34}^2/(\nu_3^2-\nu_4^2))(\nu_4^2+3\nu_3^2)/\nu_3\}q_1q_2+\{(3a_9/\nu_4)+(a_8/\nu_3)$$
$$+a_{11}/(\nu_3\nu_4)^{\frac{1}{2}}-(\zeta_{34}^2/(\nu_3^2-\nu_4^2)(3\nu_4^2+\nu_3^2)/\nu_4\}q_4q_5,$$

where for the sake of brevity the substitutions have been made:

$$a_1=-c_8(A_0/6\pi\nu_2)^{\frac{1}{2}},\qquad a_2=-c_{10}(A_0/6\pi\nu_2)^{\frac{1}{2}},\qquad a_6=(c_1\zeta_{23}/6)(A_0/2\pi\nu_3)^{\frac{1}{2}},$$
$$a_7=(c_2\zeta_{24}/6)(A_0/2\pi\nu_4)^{\frac{1}{2}},\quad a_8=(c_3\zeta_{23}/2)(A_0/2\pi\nu_3)^{\frac{1}{2}},\quad a_9=(-c_4\zeta_{24}/6)(A_0/2\pi\nu_4)^{\frac{1}{2}},$$

$$a_{10}=-\tfrac{1}{2}(A_0/2\pi)^{\frac{1}{2}}[(c_2\zeta_{24}/\nu_4^{\frac{1}{2}})(\nu_3/\nu_4)^{\frac{1}{2}}-(c_1\zeta_{23}/\nu_3^{\frac{1}{2}})(\nu_4/\nu_3)^{\frac{1}{2}}],$$

$$a_{11}=-\tfrac{1}{2}(A_0/2\pi)^{\frac{1}{2}}[(c_4\zeta_{24}/\nu_4^{\frac{1}{2}}(\nu_3/\nu_4)^{\frac{1}{2}}-(c_1\zeta_{23}/\nu_3^{\frac{1}{2}})(\nu_4/\nu_3)^{\frac{1}{2}}].$$

$\tau_{yxyz}$, $\tau_{zxzy}$, $G_y'$, $G_z'$, $H_{yz}'$, $H_{zz}'$ are obtained from the above by cyclic rotation of $q_1$, $q_2$, $q_3$; $p_1$, $p_2$, $p_3$; $q_4$, $q_5$, $q_6$; $p_4$, $p_5$, $p_6$; $v_x$, $v_y$, $v_z$; $p_{v_x}$, $p_{v_y}$, $p_{v_z}$.

We are now in a position to calculate by perturbation theory the alterations of the energy caused by the second-order Hamiltonian. We shall treat each of the states $V_1\nu_1$, $\nu_2$, $V_1\nu_1+\nu_3$, $V_1\nu_1+\nu_4$, $\nu_2+\nu_3$ and $\nu_2+\nu_4$ separately. In doing so we shall employ the degenerate perturbation methods for while certain degeneracies have been removed those in the quantum numbers $K$ and $M$ still exist. The matrix $H^{(2)\prime}$ will be a step matrix with a step for each value of $J$. Each step will have $2J+1$ rows and columns corresponding to the $2J+1$ values of the quantum number $K$ for a given $J$ value. Since $H^{(2)\prime}$ contains terms which are functions of $P_\alpha$ the degeneracy in $K$ is removed in this approximation so that these steps will contain elements which are nondiagonal. The elements of the matrix $H^{(2)\prime}$ are obtained for any one of the above states by evaluating the integrals

$$(\nu_j : K|H^{(2)\prime}|\nu_j : K')=\int \bar{\Psi}_{JKM}(\nu_j, s)H^{(2)\prime}\Psi_{JKM}(\nu_j, s)dv, \tag{15}$$

where $\Psi_{JKM}(\nu_j : s)$ is the stabilized wave function for the state in question.

The state $V_1\nu_1$, of which the normal state may be regarded as a special case, is entirely nondegenerate in the vibrational coordinates and the functions $\Psi_{JKM}(\nu, s)$ is simply the function (10) where all the quantum numbers $V$, save $V_1$, are set equal to zero. For these states, the only nonvanishing matrix elements are the $(K|K)$ and $(K|K\pm4)$ elements which are given below:

$$(K|H^{(2)\prime}|K)_{V_1\nu_1}=(\hbar^2/2A_0)\{R_0(V_1\nu_1)+J(J+1)R_1(V_1\nu_1)+J^2(J+1)^2R_2(V_1\nu_1)$$
$$+[6J(J+1)K^2-5K^2-7K^4]R_3(V_1\nu_1)\}, \tag{16}$$

where

$$R_0(V_1\nu_1)=(1/4)\{27/2[(\omega_3/\omega_4)+(\omega_4/\omega_3)]\zeta_{23}^2\zeta_{24}^2+3[(\omega_2/\omega_3)+(\omega_3/\omega_2)]\zeta_{23}^2+3[(\omega_2/\omega_4)+(\omega_4/\omega_2)]\zeta_{24}^2$$
$$-27\zeta_{23}^2\zeta_{24}^2-9\}+(3A_0/2)\{3d_1+d_3+3d_5+d_6+d_{10}+2d_{11}+d_{21}+d_{22}-\tfrac{1}{2}(d_{23}+d_{29})+d_{27}$$
$$+d_{28}+3d_{33}+(2V_1+1)(d_{18}+d_{20}+d_{31})+(2V_1^2+2V_1+1)d_{30}\}-(A_0/4)\{c_1^2/3\omega_3$$
$$+3c_2^2/(2\omega_3+\omega_4)+3c_3^2/(2\omega_4+\omega_3)+c_4^2/3\omega_3+3(12\omega_3^2-5\omega_1^2)c_5^2/\omega_1(4\omega_3^2-\omega_1^2)$$
$$+18(c_5c_7+c_5c_{12}+c_7c_{12})/\omega_1+3c_6^2[\omega_1(\omega_1^2-\omega_3^2-\omega_4^2)+2\omega_1\omega_3\omega_4]/(\omega_1^4+\omega_3^4+\omega_4^4-2\omega_1^2\omega_3^2$$
$$-2\omega_1^2\omega_4^2-2\omega_3^2\omega_4^2)+3(12\nu_4^2-5\nu_1^2)c_7/\omega_1(4\omega_4^2-\omega_1^2)+6c_8^2/(2\omega_3+\omega_2)+6c_{10}^2/(2\omega_4+\omega_2)$$
$$+36(2\omega_2^2-\omega_1^2)c_{12}^2/\omega_1(4\omega_2^2-\omega_1^2)+5c_{13}^2/16\omega_2+3c_9^2[\omega_3(\omega_3^2-\omega_4^2-\omega_2^2)+\omega_4(\omega_4^2-\omega_1^2-\omega_2^2)$$
$$+\omega_2(\omega_2^2-\omega_3^2-\omega_4^2)+2\omega_2\omega_3\omega_4]/(\omega_2^4+\omega_3^4+\omega_4^4-2\omega_2^2\omega_3^2-2\omega_3^2\omega_4^2-2\omega_2^2\omega_4^2)\}$$
$$-(2V_1+1)(A_0/2)\{9(c_5+c_7+c_{12})(c_{11}/\nu_1)+6\omega_3c_5^2/(4\omega_3^2-\omega_1^2)+6\omega_4c_7^2/(4\omega_4^2-\omega_1^2)$$
$$+18\omega_2c_{12}^2/(4\omega_2^2-\omega_1^2)+(3c_6^2/2)[\omega_3(\omega_3^2-\omega_4^2-\omega_1^2)+\omega_4(\omega_4^2-\omega_3^2-\omega_1^2)]/(\omega_1^4+\omega_3^4+\omega_4^4$$
$$-2\omega_1^2\omega_3^2-2\omega_1^2\omega_4^2-2\omega_3^2\omega_4^2)\}-(A_0c_{11}^2/4\omega_1)(30V_1^2+30V_1+11),$$

$$R_1(V_1\nu_1)=(\hbar/A_0)\{(5\omega_2^2-\omega_2\omega_3+2\omega_3^2)\zeta_{23}^2/4\omega_2\omega_3(\omega_2+\omega_3)+(2V_1+1)/\omega_1+(1/2\omega_2)$$
$$+(5\omega_2^2-\omega_2\omega_4+2\omega_4^2)\zeta_{24}^2/4\omega_2\omega_4(\omega_2+\omega_4)+\zeta_{34}^2(\omega_3-\omega_4)^2/\omega_3\omega_4(\omega_3+\omega_4)$$
$$+(3A_0/2\omega_1^3)^{\frac{1}{2}}[c_5+c_7+c_{12}+(2V_1+1)c_{11}]+(\hbar/2A_0\omega_2^2)\},$$

$$R_2(V_1\nu_1)=(-\hbar^2/6A_0^2)\{(8/\omega_1^2)+(5/2\omega_2^2)+(3/4)(\zeta_{23}^2/\omega_3^2+\zeta_{24}^2/\omega_4^2)\},$$

$$R_3(V_1\nu_1)=(\hbar^2/4A_0^2)\{(1/\omega_2^2)-\tfrac{1}{2}(\zeta_{23}^2/\omega_3^2+\zeta_{24}^2/\omega_4^2)\}$$

and

$$(K|H^{(2)\prime}|K\pm4)=\{[f-K(K\pm1)][f-(K\pm1)(K\pm2)][f-(K\pm2)(K\pm3)]$$
$$\times[f-(K\pm3)(K\pm4)]\}^{\frac{1}{2}}(\hbar^2/4A_0)R_3(V_1\nu_1). \quad (17)$$

We have for the sake of brevity introduced the notation $f=J(J+1)$ and $\hbar=(h/2\pi)$.

The state $\nu_2$ becomes excited when $V_2$ is set equal to unity. This may take place in two ways, i.e., by setting $n_7=1$, $n_8=0$ or $n_7=0$, $n_8=1$, so that this frequency is twofold degenerate. It, also, is uneffected by the presence of $H^{(1)\prime}$ and the stabilized form for that part of the wave function characteristic of $\nu_2$ is readily formed to be:

$$\left.\begin{matrix}U(\nu_2)\\V(\nu_2)\end{matrix}\right\}=2^{-\frac{1}{2}}\{\Phi(n_7=1,\ n_8=0)\mp\Phi(n_7=0,\ n_8=1)\}. \quad (18)$$

The degeneracy in $\nu_2$ is removed by $H^{(2)\prime}$ and its matrix breaks up into two nearly identical steps in the vibration coordinates with the elements $U_{JKM}\,\vdots\,U_{JK'M}$ and $V_{JKM}\,\vdots\,V_{JK'M}$. The elements $U_{JKM}\,\vdots\,V_{JK'M}$ vanish identically. These steps will again be diagonal in all the rotation quantum numbers save $K$ and the nonvanishing elements are the elements $(K|K)$ and $(K|K\pm4)$, the values of which are given below:

$$(K|H^{(2)\prime}|K)_{\nu_2}=(\hbar^2/2A_0)\{R_0(\nu_2:1,2)+J(J+1)R_1(\nu_2:1,2)+J^2(J+1)^2R_2(\nu_2:1,2)$$
$$+[6J(J+1)K^2-5K^2-7K^4]R_3(\nu_2:1,2)+K^2R_4(\nu_2:1,2)\}, \quad (19)$$

where

$$R_0(\nu_2:1,2)=R_0(0)+(3/4)\{[(\omega_2/\omega_3)+(\omega_3/\omega_2)]\zeta_{23}^2+[(\omega_2/\omega_4)+(\omega_4/\omega_2)]\zeta_{24}^2\}$$
$$+(3A_0/2)\{d_{21}+2d_{22}+(\tfrac{1}{2}-2^{\frac{1}{2}}/6)(d_{23}+d_{29}+d_{27}+3d_{28}+d_{31}+6d_{33})\}$$
$$-(A_0/4)\{18c_7c_{12}/\omega_1+12\omega_3c_8^2/(4\omega_3^2-\omega_2^2)+12\omega_4c_{10}^2/(4\omega_4^2-\omega_2^2)+18c_{11}c_{12}/\omega_1$$
$$+36(3\omega_2+2\omega_1)c_{12}^2/\omega_1(2\omega_2+\omega_1)+(42\mp12)c_{13}^2/16\omega_2+c_9^2[\omega_3(\omega_3^2-\omega_4^2-\omega_2^2)$$
$$+\omega_4(\omega_4^2-\omega_3^2-\omega_2^2)]/(\omega_2^4+\omega_3^4+\omega_4^4-2\omega_2^2\omega_3^2-2\omega_2^2\omega_4^2-2\omega_3^2\omega_4^2)\},$$

$$R_1(\nu_2:1,2)=R_1(0)+(\hbar/A_0\omega_2)\{(1\mp1/8)-(\tfrac{1}{2}\pm1/8)[(3\omega_2^2+\omega_3^2)\zeta_{23}^2/(\omega_2^2-\omega_3^2)$$
$$+(3\omega_2^2+\omega_4^2)\zeta_{24}^2/(\omega_2^2-\omega_4^2)]\},$$

$$R_2(\nu_2:1,2)=R_2(V_1\nu_1);\quad R_3(\nu_2:1,2)=R_3(V_1\nu_1),$$

$$R_4(\nu_2:1,2)=\pm(3\hbar/8A_0\omega_2)\{(3\omega_2^2+\omega_3^2)\zeta_{23}^2/(\omega_2^2-\omega_3^2)+(3\omega_2^2+\omega_4^2)\zeta_{24}^2/(\omega_2^2-\omega_4^2)+1\}$$

and

$$(K|H^{(2)\prime}|K\pm4)_{\nu_3}=(K|H^{(2)\prime}|K\pm4)_{V_1\nu_1}. \quad (20)$$

The state $\nu_3$ is excited when $V_3$ takes the value unity. This may take place in three different ways, namely; when one of the three quantum numbers $n_1$, $n_2$, $n_3$ is set equal to one, so that the state $\nu_3$ is threefold degenerate. This degeneracy is removed by $H^{(1)\prime}$ and the wave functions which we shall require for our second-order calculations are just the linear combinations of the basic functions (10) which will diagonalize $H^{(1)\prime}$. It is not difficult to show that the appropriate linear combinations of

these[8] are of the form:

$$\Psi_{JKM}(\nu_3 : s)=\{a_s F(\nu_3)R(K+1)+b_s G(\nu_3)+c_s H(\nu_3)R(K-1)\}\Psi(V_1V_2V_4), \quad s=I, II, III \tag{21}$$

where $F(\nu_3)$, $G(\nu_3)$ and $H(\nu_3)$ are the three linear combinations of the functions $(n_1n_2n_3)$:

$$\left.\begin{matrix}F(\nu_3)\\H(\nu_3)\end{matrix}\right\}=2^{-\frac{1}{2}}\{\Phi(n_1=1,\ n_2=n_3=0)\pm i\Phi(n_1=n_3=0,\ n_2=1)\},$$
$$G(\nu_3)=\Phi(n_1=n_2=0,\ n_3=1), \tag{22}$$

which will be recognized as the three wave functions for the three-dimensionally isotropic oscillator treated in spherical polar coordinates. The coefficients $a_s$, $b_s$ and $c_s$ are the following quantities:

$$a_I=\left\{\frac{(J-K)(J-K+1)}{2(J+1)(2J+1)}\right\}^{\frac{1}{2}}, \quad b_I=\left\{\frac{(J-K+1)(J+K+1)}{(J+1)(2J+1)}\right\}^{\frac{1}{2}}, \quad c_I=-\left\{\frac{(J+K)(J+K+1)}{2(J+1)(2J+1)}\right\}^{\frac{1}{2}},$$

$$a_{II}=\left\{\frac{(J-K)(J+K+1)}{2J(J+1)}\right\}^{\frac{1}{2}}, \quad b_{II}=\left\{\frac{K^2}{J(J+1)}\right\}^{\frac{1}{2}}, \quad c_{II}=\left\{\frac{(J+K)(J-K+1)}{2J(J+1)}\right\}^{\frac{1}{2}},$$

$$a_{III}=\left\{\frac{(J+K)(J+K+1)}{2J(2J+1)}\right\}^{\frac{1}{2}}, \quad b_{III}=-\left\{\frac{(J+K)(J-K)}{J(2J+1)}\right\}^{\frac{1}{2}}, \quad c_{III}=-\left\{\frac{(J-K)(J-K+1)}{2J(2J+1)}\right\}^{\frac{1}{2}}$$

and $R(K')$ are the wave functions of the spherical top. These functions lead to the well-known values for the first-order energy corrections

$$E_I^{(1)}=J\zeta_3\hbar^2/A_0, \quad E_{II}^{(1)}=-\zeta_3\hbar^2/A_0 \quad \text{and} \quad E_{III}^{(1)}=-(J+1)\zeta_3\hbar^2/A_0.$$

With the aid of the function (21) where $\Psi(V_1V_2V_4)$ is set equal to $\Phi(V_1)\Phi(n_7=n_8=0)\Phi(V_4=0)$ we now evaluate the elements of the second-order matrix $H^{(2)'}$ for the states $V_1\nu_1+\nu_3$ of which the fundamental state is a special case where $V_1=0$. For these states the matrix $H^{(2)'}$ breaks up into three-step matrices with the elements $\Psi_{JKM}(V_1\nu_1+\nu_3 : s)\,\vdots\,\Psi_{JKM}(V_1\nu_1+\nu_3 : s)$. This will be true because the functions $\Psi_{JKM}(V_1\nu_1+\nu_3 : I, II, III)$ are the eigenfunctions of $H^{(0)}+H^{(1)'}$ in which $\nu_3$ is nondegenerate so that to this approximation the elements $\Psi_{JKM}(V_1\nu_1+\nu_3 : s)\,\vdots\,\Psi_{JKM}(V_1\nu_1+\nu_3 : r)$, $r\neq s$, may be neglected. Each step will again be diagonal in the quantum numbers $J$ and $M$ and will have the following nonvanishing elements in $K$:

$$\begin{aligned}(K|H^{(2)'}|K)_{V_1\nu_1+\nu_3}=(\hbar^2/2A_0)\{&R_0(V_1\nu_1+\nu_3)+fR_1(V_1\nu_1+\nu_3)+[(a_i^2+c_i^2)(f-K^2-1)-2K(a_i^2-c_i^2)\\&+2b_i^2K^2]R_3(V_1\nu_1+\nu_3)+a_ic_i[f-K(K-1)]^{\frac{1}{2}}[f-K(K+1)^{\frac{1}{2}}](R_3+R_4)\\&+2^{\frac{1}{2}}b_i[(2K+1)a_i(f-K(K+1))^{\frac{1}{2}}+(2K-1)c_i[f-K(K-1)]^{\frac{1}{2}}]R_4\\&+[6fK^2-5K^2-7K^4+2(a_i^2+c_i^2)(3f-6-21K^2)\\&+2(a_i^2-c_i^2)K(6f-19-14K^2)]R_5-[(a_i^2+c_i^2)(24K^2+9-4f)\\&+(a_i^2-c_i^2)K(8K^2+25-4f)]R_6+2^{-\frac{1}{2}}b_i[(2f-6K^2-6K-3)a_i\\&\times(f-K(K+1))^{\frac{1}{2}}-(2f-6K^2+6K-3)c_i(f-K(K-1))^{\frac{1}{2}}]R_6\},\end{aligned} \tag{23}$$

[8] The transformation matrix which transforms functions (10) into (21) may be obtained from Condon and Shortley, *The Theory of Atomic Spectra* (Cambridge Univ. Press, 1935), p. 76, when their discussion is made applicable to our problem. This is not surprising since the case here under consideration is just a trivial case of the vector addition of angular momenta in quantum mechanics. This method is particularly useful in obtaining the wave functions for combination states between $\nu_3$ and $\nu_4$ as well as for the overtones of $\nu_3$ and $\nu_4$.

$$(K|H^{(2)\prime}|K+2)=(\hbar^2/2A_0)\{-a_ia_i(+2)[f-(K+1)(K+2)]^{\frac{1}{2}}[f-(K+2)(K+3)]^{\frac{1}{2}}$$
$$+2b_ib_i(+2)[f-K(K+1)]^{\frac{1}{2}}[f-(K+1)(K+2)]^{\frac{1}{2}}c_ic_i(+2)[f-K(K-1)]^{\frac{1}{2}}$$
$$\times[f-K(K+1)]^{\frac{1}{2}}+a_ic_i(+2)[2f-6(K+1)^2]\}(A_0\omega_3R_6/4\hbar), \quad (24)$$

$$(K+2|H^{(2)\prime}|K)=(K|H^{(2)\prime}|K+2),$$

$$(K|H^{(2)\prime}|K+4)=(\hbar^2/2A_0)\{[f-(K+1)(K+2)]^{\frac{1}{2}}[f-(K+2)(K+3)]^{\frac{1}{2}}\}\{a_ic_i(+4)$$
$$\times[(R_3/2)-(R_6/4)]+2^{-\frac{1}{2}}[f-(K+3)(K+4)]^{\frac{1}{2}}a_ib_i(+4)(R_6/4)$$
$$-2^{-\frac{1}{2}}[f-K(K+1)]^{\frac{1}{2}}b_ic_i(+4)(R_6/4)-[f-(K+3)(K+4)]^{\frac{1}{2}}$$
$$\times[f-(K+4)(K+5)]^{\frac{1}{2}}a_ia_i(+4)(R_5/2)-[f-K(K+1)]^{\frac{1}{2}}[f-(K+3)$$
$$\times(K+4)]^{\frac{1}{2}}b_ib_i(+4)(R_5/2)-[f-K(K-1)]^{\frac{1}{2}}[f-K(K+1)]^{\frac{1}{2}}c_ic_i(+4)(R_5/2)\};$$

$$(K+4|H^{(2)\prime}|K)=(K|H^{(2)\prime}|K+4), \quad (25)$$

where

$$R_0(V_1v_1+v_3)=(1/4)[18\zeta_{23}^4-24\zeta_{23}^2-1+5((\omega_2/\omega_3)+(\omega_3/\omega_2))\zeta_{23}^2+3((\omega_2/\omega_4)+(\omega_4/\omega_2))\zeta_{24}^2$$
$$-27\zeta_{23}^2\zeta_{24}^2+(45/2)((\omega_4/\omega_3)+(\omega_3/\omega_4))\zeta_{23}^2\zeta_{24}^2]+(A_0/2)\{21d_1+5d_3+9d_5+7d_6$$
$$+3d_{10}+10d_{11}+3(2V_1+1)[d_{20}+d_{31}+(5d_{18}/3)]+5d_{21}+10d_{22}-(5d_{23}/2)+3d_{27}+6d_{28}$$
$$-3d_{29}+3(2V_1^2+2V_1+1)d_{30}+9d_{33}\}-(A_0/4)\{(5c_1^2/3\omega_3)+(7\omega_4+4\omega_3)c_2^2/\omega_4(\omega_4+2\omega_3)$$
$$+(3\omega_3-10\omega_4)c_3^2/(\omega_3^2-4\omega_4^2)+(c_4^2/3\omega_4)+[(2V_1+1)(3\omega_3(\omega_3^2-\omega_4^2-\omega_1^2)$$
$$+5\omega_4(\omega_4^2-\omega_3^2-\omega_1^2))+5\omega_1(\omega_1^2-\omega_3^2-\omega_4^2)+6\omega_1\omega_3\omega_4]c_6^2(\omega_1^4+\omega_3^4+\omega_4^4-2\omega_1^2\omega_3^2$$
$$-2\omega_1^2\omega_4^2-2\omega_3^2\omega_4^2)^{-1}+[100\omega_3^2-35\omega_1^2+20(2V_1+1)\omega_1\omega_3]c_5^2/\omega_1(4\omega_3^2-\omega_1^2)$$
$$+[3\omega_3(\omega_3^2-\omega_4^2-\omega_2^2)+5\omega_4(\omega_4^2-\omega_3^2-\omega_1^2)+5\omega_2(\omega_2^2-\omega_3^2-\omega_4^2)+6\omega_2\omega_3\omega_4]$$
$$\times(\omega_2^4+\omega_3^4+\omega_4^4-2\omega_2^2\omega_3^2-2\omega_2^2\omega_4^2-2\omega_3^2\omega_4^2)^{-1}+(3c_7^2/\omega_1)[4(2V+1)\omega_1\omega_4-5\omega_1^2$$
$$+12\omega_4^2]/(4\omega_4^2-\omega_1^2)+2(4\omega_3+7\omega_2)c_8^2/\omega_2(\omega_2+2\omega_3)+6c_{10}^2/(\omega_2+2\omega_4)$$
$$+(30V_1^2+30V_1+11)c_{11}^2/\omega_1+(5/16)c_{13}^2/\omega_2+18[4\omega_2^2-2\omega_1^2+2(2V_1+1)\omega_1\omega_2]c_{12}^2$$
$$/\omega_1(4\omega_2^2-\omega_1^2)+(2V_1+1)(30c_5+18c_7+18c_{12})(c_{11}^2/\omega_1)+30(c_7+c_{12})c_5/\omega_1+18c_7c_{12}/\omega_1\},$$

$$R_1(V_1v_1+v_3)=(\hbar/2A_0)\{(\omega_3^2+3\omega_2^2)\zeta_{23}^2/\omega_2\omega_3(\omega_2+\omega_3)+3\zeta_{24}^2/2\omega_4+(c_8/\omega_2)(A_0/3\omega_2)^{\frac{1}{2}}+2(2V_1+1)/\omega_1$$
$$+(1/\omega_2)+2\zeta_{34}^2(\omega_3^3-6\omega_3^2\omega_4+3\omega_3\omega_4^2-2\omega_4^3)/\omega_3\omega_4(\omega_3^2-\omega_4^2)+(\hbar/A_0\omega_2^2)$$
$$+2(2A_0/3\omega_1^3)^{\frac{1}{2}}(5c_5+3c_7+3c_{11}+3c_{12})\},$$

$$R_2(V_1v_1+v_3)=R(V_1v_1),$$

$$R_3(V_1v_1+v_3)=(\hbar/2A_0)\{[(3/4)(7\omega_2^2+5\omega_3^2)\zeta_{23}^2/\omega_3(\omega_2^2-\omega_3^2)]-(3A_0/\omega_2)^{\frac{1}{2}}(c_8/2\omega_2)$$
$$+[(\omega_4^2+3\omega_3^2)\zeta_{34}^2/\omega_3(\omega_3^2-\omega_4^2)]\},$$

$$R_4(V_1v_1+v_3)=(\hbar/A_0)\{(3\zeta_{23}^2/4\omega_3)+\zeta_{23}c_1(A_0/\omega_3^3)^{\frac{1}{2}}-\zeta_{24}c_2(A_0/\omega_4^3)^{\frac{1}{2}}+[(\omega_4^2+3\omega_3^2)\zeta_{34}^2/\omega_3(\omega_3^2-\omega_4^2)]\},$$

$$R_5(V_1v_1+v_3)=R_3(V_1v_1),$$

$R_6(V_1v_1+v_3)=(\zeta_{23}^2\hbar^2/4A_0^2\omega_3^2)$; the subscript $i$ assumes the three values of $s$ in (21).

The coefficients $a_s$, $b_s$, $c_s$ which have already been defined are always to be associated with the quantum

number $K=K$. In (24) and (25) a notation $a(+2)$, $b(+2)$, etc. is introduced to denote the values of the coefficients $a_s$, $b_s$ and $c_s$ where the quantum number $K$ is replaced by $K+2$.

In the same manner by setting $\Psi(V_1V_2V_3)$ equal to $\Phi(V_1=0)U(\nu_2)$ and $\Phi(V_1=0)V(\nu_2)$ we may determine also the matrix $H^{(2)'}$ for the state $\nu_2+\nu_3$. From the foregoing it will become apparent that for this state the matrix will split up into three sets of two nearly identical steps which are diagonal in $J$ and $M$, but have elements nondiagonal in $K$. The $(K|K)$ elements are identical in form with (23) where the parameters $R_0(V_1\nu_1+\nu_3)$, etc., are replaced by $R_0(\nu_2+\nu_3)$, etc. These are given below:

$$\begin{aligned}R_0(\nu_2+\nu_3 : i: 1, 2) &= R_0(\nu_3)+(1/8)(10\pm1\mp3b_i^2)\zeta_{23}^2[(\omega_2/\omega_3)+(\omega_3/\omega_2)]+(A_0/4)\{(10\mp1\pm3b_i^2)d_{21}\\ &+(20\pm1\mp3b_i^2)d_{22}-(5\pm1\mp3b_i^2)d_{23}+6d_{27}+12d_{28}+6d_{31}+36d_{33}\}\\ &-(A_0/8)\{(30c_5+18c_7)(c_{12}/\omega_1)+(10\pm1\pm3b_i^2)[2\omega_3c_8^2/(4\omega_3^2-\omega_2^2)]\\ &+[12\omega_4c_{10}^2/(4\omega_4^2-\omega_2^2)]+36(3\omega_2+2\omega_1)[c_{12}^2/\omega_1(2\omega_2+\omega_1)]+(7\pm2)(3c_{13}^2/8\omega_2)\\ &+[15\omega_3(\omega_3^2-\omega_4^2-\omega_2^2)+\tfrac{1}{2}(10\mp1\pm3b_i^2)\omega_4(\omega_4^2-\omega_3^2-\omega_2^2)]c_9^2\\ &/[\omega_2^4+\omega_3^4+\omega_4^4-2\omega_2^2\omega_3^2-2\omega_2^2\omega_4^2-2\omega_3^2\omega_4^2]\},\end{aligned}$$

$$\begin{aligned}R_1(\nu_2+\nu_3 : 1, 2) &= R_1(\nu_3)+(\hbar/2A_0)\{(6A_0/\omega_1^3)^{\frac{1}{2}}c_{12}+(1\mp1/4)/\omega_2\\ &-(1\pm1/4)\zeta_{24}^2[(3\omega_2^2+\omega_4^2)/\omega_2(\omega_2^2-\omega_4^2)]\},\end{aligned}\quad (26)$$

$$R_2(\nu_2+\nu_3)=R_2(\nu_3),$$

$$R_3(\nu_2+\nu_3 : 1, 2)-R_3(\nu_3)=R_4(\nu_2+\nu_3 : 1, 2)-R_4(\nu_3)=-(1\pm1/4)(\zeta_{23}^2\hbar/2A_0)[(3\omega_2^2+\omega_3^2)/\omega_2(\omega_2^2-\omega_3^2)],$$

$$\begin{aligned}R_5(\nu_2+\nu_3 : 1, 2)-R_5(\nu_3) &= R_8(\nu_2+\nu_3 : 1, 2)-R_8(\nu_3)\\ &=\pm(3\omega_2\hbar/2A_0)\{[\zeta_{23}^2/(\omega_2^2-\omega_3^2)]+[\zeta_{24}^2(\omega_2^2-\omega_4^2)]\},\end{aligned}$$

$$R_6(\nu_2+\nu_3)=R_6(\nu_3);\quad R_7(\nu_2+\nu_3)=R_7(\nu_3);\quad R_9(\nu_2+\nu_3)=R_9(\nu_3);\quad R_{10}(\nu_2+\nu_3)=R_{10}(\nu_3)$$

and

$$\begin{aligned}(K|H^{(2)'}|K+2)=(K+2|H^{(2)'}|K) &= (\hbar^2/2A_0)\{[2f-6(K+1)^2]a_ic_i(+2)R_{11}+[f-K(K+1)]^{\frac{1}{2}}\\ &\times[f-(K+1)(K+2)]^{\frac{1}{2}}b_ib_i(+2)(2R_{11}-R_{15})\}+(\hbar^2/?A_0)(R_{11}+R_{15})\\ &\times\{[f-K(K-1)]^{\frac{1}{2}}[f-K(K+1)]^{\frac{1}{2}}c_ic_i(+2)-[f-(K+1)(K+2)]^{\frac{1}{2}}\\ &\times[f-(K+2)(K+3)]^{\frac{1}{2}}a_ia_i(+2)\},\end{aligned}\quad (27)$$

where

$$R_{11}(\nu_2+\nu_3)=R_{11}(\nu_3);\quad 2R_{15}(\nu_2+\nu_3 : 1, 2)=R_5(\nu_2+\nu_3 : 1, 2)-R_5(\nu_3)$$

and $(K|H^{(2)'}|K\pm4)$ which are entirely identical with those for the state $\nu_3$ given in (25).

Since the nature of the frequency $\nu_4$ is entirely analogous to $\nu_3$ the elements of the matrix $H^{(2)'}$ for the states $V_1\nu_1+\nu_4$ and $\nu_2+\nu_3$ may be obtained from the relations (23) to (27) simply by replacing $R_s(V_1\nu_1+\nu_3)$ by $R_s(V_1\nu_1+\nu_4)$ and $R_s(\nu_2+\nu_3)$ by $R_s(\nu_2+\nu_4)$ where these may be obtained by replacing in $R_s(\nu_j+\nu_3)$ the following quantities which are included in parentheses: $(\zeta_{23}, \zeta_{24})$, $(\omega_3, \omega_4)$, $(d_1, d_5)$, $(d_6, d_{10})$, $(d_{18}, d_{20})$, $(d_{21}, d_{27})$, $(d_{22}, d_{28})$, $(d_{23}, d_{29})$, $(c_1, c_4)$, $(c_2, c_3)$, $(c_5, c_7)$, $(c_8, c_{10})$. Thus for example $R_{11}(V_1\nu_1+\nu_4)$ becomes $(\hbar\zeta_{24}^2/8A_0\omega_4)$.

The actual values of the rotation-vibration energies for the above states may be had by diagonalizing the corresponding matrices $H$. This is most readily accomplished by solving for the roots of the secular determinant $|(K|H|K')-E\delta_{K'K}|$, $\delta_{K'K}$ being the Kronecker symbol. The actual unperturbed wave functions $\chi_{JM}(\nu_j : s)$ for a rotation-vibration state $\tau$, $\tau$ being simply an index number running from $-J$ to $+J$, which are the limiting values of the actual perturbed wave functions may now be written as an expansion in terms of the wave

functions $\Psi_{JKM}(v_j : s)$:

$$\chi_{JM}(v_j : s) = \sum_{K=-J}^{+J} A_{JM}^{(K)} \Psi_{JKM}(v_j : s), \quad (28)$$

where the coefficients $A_{JM}^{(K)}$ are the normalized first minors of the secular determinant.

## IV. The Selection Rules and Intensities

To determine the selection rules we have to determine what are the nonvanishing matrix elements of the electric moment. To second approximation the classical expression for the body fixed components of this are the quantities:

$$\Pi_x = A_1 q_1 + A_2 q_4 + B_1 q_2 q_3 + B_2(q_2 q_6 + q_3 q_5)$$
$$+ B_3 q_5 q_6 + B_5 q_1 q_9 + B_6 q_4 q_9 + B_7 q_1 u_x + B_8 q_4 u_x,$$

$\Pi_y$ and $\Pi_z$ being obtained by cyclic rotation of $q_1, q_2, q_3; q_4, q_5, q_6; u_x, u_y$ and $u_z$. The matrix elements of the electric moment are given by the integrals

$$\int \bar{\chi}_{JKM}(v_j : s) \Pi_\beta \bar{\chi}_{J'K'M'}(v_j' : s') dv$$

where $\Pi_\beta$ are the components of $\Pi$ along the spaced fixed axes; $\chi_{J,K,M}(v_j : s)$ and $\chi_{J'K'M'} \times (v_j', s')$ the wave functions of the initial and final states. The function $\chi_{JKM}(v_j : s)$ may to a good approximation be replaced by $\Psi_{JKM}(v_j : s)$ in computing the intensities because the actual splitting of the rotation levels is small so that all the $A_{J\tau M}^{(K)}$, except the one where $\tau = K$, will be small.

Inspection of the quantity $\Pi$ shows it to have no linear terms in $q_7$, $q_8$ or $q_9$. For the frequencies $\nu_1$ and $\nu_2$ the above integral will therefore vanish and they will consequently be optically inactive, giving no bands in the infra-red. For transitions from the normal state to the states $V_1\nu_1 + \nu_3$ and $\nu_2 + \nu_3$ the above integral will not vanish so that these frequencies may be expected to occur in the spectrum.

In evaluating the integral for the electric moment it is found that the selection rules for the rotational quantum numbers are the same for $\nu_3$, $\nu_1+\nu_3$ and $\nu_2+\nu_3$, from which the inference may be drawn that also for higher combination frequencies of this type the selection rules will be the same. For $J$ the selection rule is $\Delta J = +1$, 0 or $-1$ as the transition is from the normal state to the states $\nu_{3,\,I}$, $\nu_{3,\,II}$ or $\nu_{3,\,III}$, respectively, which verifies the conclusions drawn by other investigators. In addition we have the selection rules for $M$ and $K$, $\Delta M = \pm 1$, 0 and $\Delta K = 0$. An interesting result which prevails is that the quantum mechanical amplitudes are independent of the quantum numbers $J$ and $K$. One obtains for the square of the electric moment $\Pi^2$, which is $\Pi_{x'}^2 + \Pi_{y'}^2 + \Pi_{z'}^2$, simply

$$(J \mid \Pi^2 \mid J) = (J \mid \Pi^2 \mid J \pm 1) = 1. \quad (29)$$

The actual intensity of a spectral line, ignoring all symmetry properties, will very nearly be proportional to

$$I(J, K; J', K') = N(J)(J' \mid \Pi^2 \mid J)(g_{J'}/g_J), \quad (30)$$

where $N(J)$ is the number of molecules in the state $J$ and $g_J$ and $g_{J'}$ are the statistical weights of the state $J$ and $J'$, respectively. For the three cases $\Delta J = -1$, 0 and $+1$ the relation (30) will become

$$\begin{aligned} I(J, K; J-1, K) &= (2J-1) \\ &\quad \times \exp(-E(JK)/kT), \\ I(J, K; J, K) &= (2J+1) \\ &\quad \times \exp(-E(JK)/kT), \\ I(J, K; J+1, K) &= (2J+3) \\ &\quad \times \exp(-E(JK)/kT). \end{aligned} \quad (31)$$

These results appear to be in agreement with those of Jahn derived from other considerations.

To arrive at the actual intensities the relations (31) must be multipled by the appropriate spin factor. This problem has been considered by Wilson[9] for the cases where the four $Y$ particles are protons and deuterons and need not here be discussed. For these cases the actual nuclear spin factors for the various rotation states have been evaluated and may be obtained by reference to this work.

[9] E. Bright Wilson, Jr., J. Chem. Phys. **3**, 276 (1935).

# Measurements of the Mobility of Potassium Ions at High Field Intensity and Low Pressure

ALLEN V. HERSHEY
*University of California, Berkeley, California*

(Received July 12, 1939)

The mobility of potassium ions in the gases $H_2$, He, $N_2$, and A has been measured by the Townsend method, in which a beam of ions is deflected by a magnetic field. When the mobility is reduced to 760 mm of mercury and 20°C it should be expressible as a function of the ratio of electric intensity $E$ to the pressure $p$. This is true at the highest pressures investigated but not at the lowest, apparently because of a breakdown in the method. At small values of $E/p$ the results agree to within a few percent with the measurements by the Tyndall and Powell method. As $E/p$ is increased, the mobility is at first constant. It then rises, passes through a peak, and finally falls. Pronounced peaks appear in the curves for $H_2$, $N_2$, and A but not for He. The mobility is constant only in weak fields where the ions and molecules interact with a frequency which is independent of the drift velocity of the ions. The rise in mobility with increase in $E/p$ may be interpreted as the result of a decrease in the effectiveness of the forces of attraction between the ions and molecules. As the drift velocity exceeds the thermal velocities of the molecules, the collision frequency becomes greater, and the mobility finally falls. Langevin's theory of mobility may be generalized to express the variation with $E/p$. It is in qualitative agreement with the experimental results, but fails to account for more than a suggestion of the peaks. They are accounted for, however, by a generalization of Hassé and Cook's theory. The experimental data are bracketed by the two theories.

## INTRODUCTION

MEASUREMENTS of the mobility of ions of high velocity have been prevented in the past by experimental difficulties. It has not been possible to control the high frequency alternating potentials which are required by both the square wave and the electrical shutter methods. On the other hand, only constant potentials are required by the Townsend[1] method, and reliable data should be obtainable by its use.

The Townsend method consists in deflecting a beam of ions in a uniform electric field by an orthogonal magnetic field. The ion beam is received by three coplanar collecting plates which are separated by narrow slits. To obtain the magnetic intensity corresponding to a known deflection, the field is adjusted until the ion beam is centered over first one slit, and then the other. The use of two slits makes unnecessary an accurate knowledge of the position of the source of ions. The relation between mobility, deflection, and magnetic intensity does not explicitly contain the electric intensity.

Townsend and Bailey[2] have shown that the drift velocity of electrons may be expressed as a function of the ratio of electric intensity $E$ to pressure $p$, and numerous investigators[3] have demonstrated that the drift velocity of normal ions is inversely proportional to the pressure from a few mm of mercury to many atmospheres. Ions of high velocity are therefore to be found at large values of $E/p$. A limitation on the range of measurement is set by the sparking potential of the gas. The value of $E/p$ at which a glow discharge occurs is known[4] to increase with decrease in pressure. The mobility of potassium ions in the gases $H_2$, He, $N_2$, and A has accordingly been investigated at low pressures by the Townsend method.

The investigation of mobility in a given gas is restricted to low pressure by the magnitude of the available magnetic field, but if the pressure is too low, the ions must travel too great a distance before they reach a terminal energy. On the other hand, if the apparatus is evacuated, it may be used to measure the ratio $e/m$ of the ions under investigation.

## APPARATUS AND PROCEDURE

Details of the glass chamber with which the measurements were made are shown in Fig. 1.

[1] J. S. Townsend and H. T. Tizard, Proc. Roy. Soc. **A88**, 336 (1913).
[2] J. S. Townsend and V. A. Bailey, Phil. Mag. **42**, 874 (1921); **44**, 1033 (1922); **46**, 657 (1923).
[3] A. F. Kovarik, Proc. Roy. Soc. **A86**, 154 (1912); A. J. Dempster, Phys. Rev. **34**, 53 (1912); McLennan and Keys, Phil. Mag. **30**, 484 (1915); W. Todd, Phil. Mag. **25**, 163 (1913).
[4] Paschen, Ann. d. Physik **37**, 69 (1889).

The ions were emitted at $F$ in the form of a beam by a heated platinum filament which had been coated with Kunsman's[5] catalyst. The heated filament constituted a source of error since it maintained a density gradient in the gas. Error also arose from the finite distance through which the ions were accelerated. An attempt was made to eliminate both errors by mounting the source on a slide so that the ions could be made to traverse various distances in the gas. If the errors were constant, it should have been possible to cancel them out by making measurements at two different positions of the filament. Motion of the slide was transmitted through the wall of the chamber by an electromagnetic device at $A$ in Fig. 1.

The electric field was maintained constant by an Evans[6] stabilizer. It was maintained uniform by a series of brass guard rings. Electrical connections to each ring were lead directly out through the wall of the chamber by separate tungsten to glass seals, so that the gas would have as little opportunity to break down as possible. The space occupied by the field was closed at $F$ by a disk mounted on the slide. The filament occupied a slot in the disk and was coplanar with its surface. To avoid distortion of the field, the slide was always located in such a position that the face of the disk was coplanar with the median plane of the adjacent guard ring. The electric field was not uniform in the immediate vicinity of the edge of each guard ring, and the amount of deviation was estimated. It was less than one percent up to within one-half centimeter from the edge. The effectiveness of the guard rings as a shield against external fields was also investigated. Estimation of the greatest possible penetration of field showed that any distortion at the center of the chamber was negligible.

The ion beam was divided into sections by the three collecting plates 1, 2, and 3 in Fig. 1, which were coplanar with the last guard ring. The plates were all cut to the same width, so that the currents to two adjacent plates would be equal, if the beam were centered over the slit between them. The outer plates were fitted with projections to catch any ions that missed the center plate. Thus at low pressures the beam was divided by the edge

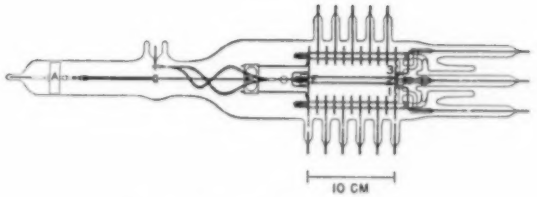


FIG. 1. The mobility chamber.

of the center plate. At high pressures, however, the ions followed the lines of force, and the beam was divided at the center of the slit between the plates. The division lines for intermediate pressures were found by a step by step integration of the equation of motion. The field of force was derived from the potential of a deep slot cut in a plane conductor. In $H_2$ and He at the lowest pressure investigated, the effective width of the center plate was equal to the true width for all values of $E/p$, and at the next intermediate pressure, for large values of $E/p$. At higher pressures in $H_2$ and He, and at all pressures in $N_2$ and A the effective width was equal to the distance between the centers of the slits, and exceeded the true width by four percent.

The currents to two adjacent collecting plates were compared by observing with an electrometer, the rate at which they charged free conductors. Details of the electrometer connections are shown in Fig. 2. The center plate was connected to one pair of quadrants, and one outer plate to the other pair. The idle plate was grounded. Complications from fluctuations in the ion emission of the filament were avoided by the use of a null method. Before measurement the system was so adjusted that the electrometer needle would remain stationary if the currents were equal. The coefficients of capacity and induction of the four conductors 1, 2, 3 and 4 in Fig. 2 were evaluated by a series of experiments in which selected conductors were charged, and the charges were then shared. The coefficients were adjusted by trial until they satisfied the conditions for balance. Allowance was made for the slow drift of the electrometer which resulted from leakage and radioactive contamination.

The magnetic field was maintained constant by a Thyratron regulator.* The intensity was

[5] C. H. Kunsman, J. Frank. Inst. **203**, 635 (1927).
[6] R. D. Evans, Rev. Sci. Inst. **5**, 371 (1934).

* The use of a sensitive method of control in this regulator made possible the omission of mechanical stages. A description may be published later.

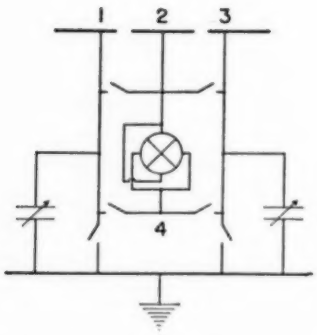


FIG. 2. Electrometer connections.

measured with a flip coil circuit whose electrical properties could be calculated accurately from geometrical dimensions. The field between the poles of the electromagnet was explored to determine the amount of deviation from uniformity. In the space occupied by the ion beam the deviation did not exceed one percent.

The gas pressure was measured with a pair of McLeod gages, each of which covered a different range. The gages registered only the partial pressure of the noncondensible component of the gas. The condensible component, mercury vapor, was excluded from the chamber by a liquid-air trap. The mean free path of the molecules of the gas was small by comparison with the dimensions of the system. The vapor pressure of mercury at the temperature of the gages was therefore added to the gage pressures to obtain the nearly uniform total pressure. The correction amounted at most to only a few percent.

The temperature was obtained with a thermometer just outside of the chamber. Heating of the gas inside by the filament set up a temperature gradient along the axis of the chamber. The temperature was estimated by a heat transfer analysis and corrections to the thermometer readings were calculated for a point midway between the filament and the collector system. They were tested on a discarded chamber into which thermocouples had been inserted. The corrections varied with pressure from 1° to 2.5° in $H_2$, and from 1° to 3.5° in He, but in $N_2$ and A they amounted to 1°.

All gases were obtained from commercial tanks and were purified. The hydrogen was passed first through a trap filled with copper at 350°, then one with potassium hydroxide. These did not remove traces of nitrogen which the hydrogen may have contained. The helium was passed over a liquid-air trap filled with charcoal, and was then exposed to a calcium arc to remove any traces of hydrogen or methane. The argon was also exposed to the calcium arc. The nitrogen was passed first through a trap filled with copper oxide, then one with copper, both at 350° to remove any traces of ammonia, oxygen, or oxides of nitrogen. The manufacturers of the gases claimed the purity of the hydrogen to be 99 percent; of the helium, 95 percent; of the argon, 99 percent; and of the nitrogen, 99.5 percent.

The chamber was baked out at 300° before insertion between the pole pieces of the electromagnet. The pressure recovered at a rate less than $10^{-4}$ mm of mercury per day. The chamber was continuously separated from the rest of the system by the liquid-air trap. Readings were taken with the filament located at 5 cm and at 10 cm from the collector system. The magnetic field was adjusted in each experiment to bring the electrometer needle nearly to rest, and the electrometer rate was noted. The magnetic intensity was measured with two consecutive flips of the flip coil and the average was obtained. The direction of motion of the electrometer needle was reversed by a slight shift in field, and the measurements were repeated. The field was reversed and the procedure was repeated for the other slit. That magnetic intensity was found by graphical interpolation, which would have made the electrometer drift at the same rate as it drifted in the absence of any ion current.

During the investigation of mobility, the molecular weight of the ions was checked occasionally, by measurements of the deflection of the beam in a vacuum. Measurements were first attempted with a sodium catalyst, but were upset by traces of potassium contamination. A pure potassium catalyst was finally prepared, which emitted ions with a molecular weight of $40\pm1$.

## METHOD OF ANALYSIS

An ideal theoretical interpretation of the experimental data would require a knowledge of the steady-state distribution in phase space of ions under the influence of electric and magnetic

fields. The interpretation may be simplified, however, in the case of heavy ions in light gases. The ions lose only a small fraction of momentum in each collision with a molecule, and almost continuous resistance is exerted upon them by the gas. They should therefore drift with a velocity $\mathbf{v}$, which is governed approximately by the vector equation

$$\mathbf{f}=e\mathbf{E}+(e/c)\mathbf{v}\times\mathbf{H}-(e/k)\mathbf{v}=m\dot{\mathbf{v}}. \quad (1)$$

In this equation the total force $\mathbf{f}$ is equated to the sum of the electric force $e\mathbf{E}$, the magnetic force $(e/c)\mathbf{v}\times\mathbf{H}$, and the resistance $-(e/k)\mathbf{v}$. When the ions reach the terminal velocity, the acceleration $\dot{\mathbf{v}}$ vanishes, and the velocity $\mathbf{v}$ makes with the electric intensity $\mathbf{E}$ an angle $\theta$, which is related to the magnetic intensity $H$ and the mobility $k$ by the equation[1]

$$\tan\theta=Hk/c. \quad (2)$$

If $H$ is expressed in gauss, $k$ is obtained in $(\text{cm})^2/(\text{sec.})(\text{volt})$ by the substitution of $10^8$ for $c$. In the absence of a magnetic field, $k$ is equal to the ratio $v/E$.

The ions describe a curved path as they leave the source, but at a distance they pick up the terminal velocity and the ion beam should approach a straight line. A curved beam is illustrated with great exaggeration in Fig. 3. If two points on the beam are known, and a straight line is drawn between them, the direction of the line is, by Rolle's theorem, the direction of the beam at some point between. The further the points are from the source, the more nearly is the direction defined by the mobility. If $x$ and $y$ are the Cartesian coordinates of the displacement of the ion, and the $x$ axis is taken parallel to the electric field, the straight line may be expressed by the equation

$$\tan\theta=y/(x-x_0)=Hk/c,$$

in which $x_0$ is the coordinate of the point of intersection of the line and the axis of the chamber. Measurement of $H$ for two values of $x$ would make possible the elimination of $x_0$. If $x_1$ and $x_2$ are the two values of $x$, and $H_1$ and $H_2$ are the corresponding field intensities, $x_0$ and $k$ are expressed by the equations

$$x_0=\frac{x_2H_2-x_1H_1}{H_2-H_1}, \quad (3)$$

$$k=\frac{yc(H_1-H_2)}{(x_2-x_1)H_1H_2}. \quad (4)$$

For a given value of $x$, $y$ is a linear function of $H$. Changes in $y$, $H_1$, and $H_2$ which correspond to deflections of the beam from one slit to the other may therefore be substituted for the variables themselves. The values of $k$ which are given by Eq. (4) may also be obtained by a linear extrapolation to $1/x=0$ in a plot of $yc/xH$ against $1/x$.

In a vacuum those ions that start from rest describe a cycloid. The equation of the cycloid may be found in terms of Cartesian coordinates from scalar equations equivalent to Eq. (1). Omission of terms containing $k$, integration, substitution of initial conditions, elimination of the time, and expansion in a power series lead to the equation

$$y=\tfrac{2}{3}x^{\frac{1}{2}}\left(\frac{eH^2}{2mc^2E}\right)^{\frac{1}{2}}+\tfrac{1}{5}x^{5/2}\left(\frac{eH^2}{2mc^2E}\right)^{\frac{1}{2}}+\cdots, \quad (5)$$

with which the ratio $e/m$ may be computed by successive approximations. In a vacuum also, uncertainty in the position of the ion source may be eliminated by two measurements. Eq. (5) may be modified by the substitution of $x-x_0$ for $x$, and $x_0$ may be eliminated from numerical equations containing experimental values of $x_1$, $x_2$, $H_1$, and $H_2$.

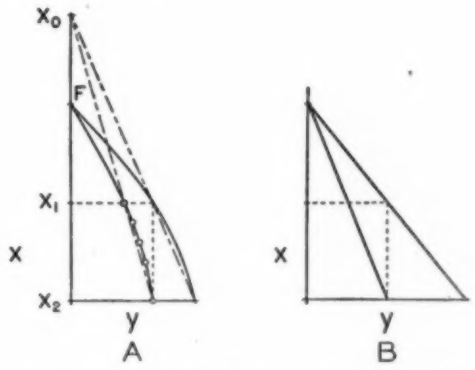


FIG. 3. The shape of the ion beam for two positions of the filament; $A$, if $y$ and $H$ were proportional; $B$, if the beam were straight. $H_1=1.53H_2$. $K^+$ in A; $p=0.1$ mm; $E/p=112$.

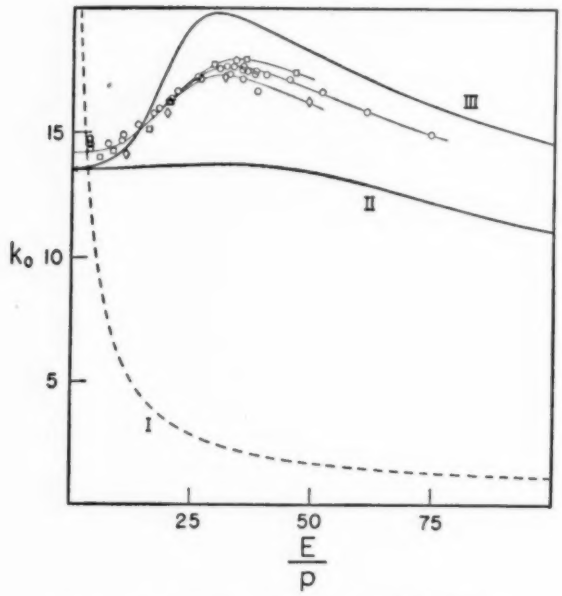


FIG. 4. The mobility of $K^+$ in $H_2$. ◇, 0.25 mm; ○, 0.85 mm; □, 2.7 mm.

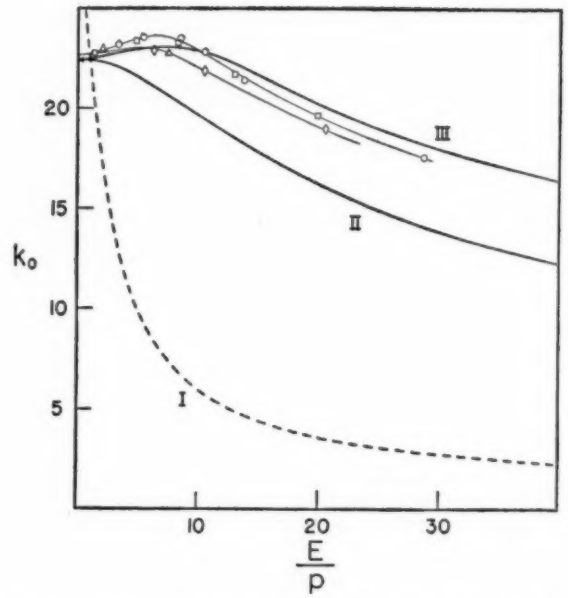


FIG. 5. The mobility of $K^+$ in He. ◇, 0.45 mm; ○, 0.95 mm; □, 1.95 mm; △, 3.8 mm.

## THE MOBILITY

Values of the mobility have been calculated from the experimental data by Eq. (4), and have been reduced to 760 mm of mercury, and 20°C by the perfect gas law. The reduced mobility $k_0$ is plotted against $E/p$ in Figs. 4 to 7. $k_0$ is expressed in $(cm)^2/(sec.)(volt)$, $E$ in (volt)/(cm) and $p$ in mm of mercury. Experimental values of the drift velocity $v$ at 20° may be obtained by the multiplication of $k_0$ with the factor $(760)(E/p)$. $k_0$ should therefore be expressible as well as $v$ as a function of $E/p$, and a single curve should appear at all pressures. Instead, the curves for various pressures are spread out to an extent which becomes progressively worse as the molecular weight is increased. There is internal evidence, however, that the experimental values are meaningless at the lowest pressure. Thus a nearly twofold increase in $H$ should accompany a decrease in $x$ to one-half. In argon at the lowest pressure and at the highest $E/p$, the factor of increase is only 1.53. The discrepancy may be attributed either to a strongly curved ion beam, whose deflection is proportional to $H$, or to a straight beam whose deflection is not proportional. The two alternatives are illustrated in Fig. 3 by the curves $A$ and $B$, which are based on measurements with the filament at 6, 7, and 8 cm as well as at 5 and 10 cm. The discrepancy disappears as the pressure is increased, and inspection of Figs. 4 to 7 shows also that $k_0$ approaches a limit. The conclusion may therefore be drawn safely that $k_0$ *is* a function of $E/p$, and that it would be represented in the figures by curves which would lie slightly above the highest experimental points. The appearance of several curves cannot be ascribed to the formation of complex ions, because the mobility would then be lower at higher pressure. It probably arises from a failure of the ions to comply with Eq. (1).

At small values of $E/p$ the results agree to within a few percent with the measurements by Tyndall and Powell,[7] and by Powell and Brata,[8] which are indicated for comparison in Figs. 4 to 7 by arrows at the border. As $E/p$ is increased the mobility is at first constant. It then rises, passes through a peak, and finally falls. Pronounced peaks appear in the curves for $H_2$, $N_2$, and A, but not for He. A constant mobility at low $E/p$ has been observed by Loeb[9] and by Yen[10] with normal ions at atmospheric pressure. The rise in mobility with increase in $E/p$ has been reported

[7] A. M. Tyndall and C. F. Powell, Proc. Roy. Soc. **A136**, 145 (1932).
[8] C. F. Powell and L. Brata, Proc. Roy. Soc. **A138**, 117 (1932).
[9] L. B. Loeb, Phys. Rev. **8**, 633 (1916).
[10] K. L. Yen, Phys. Rev. **11**, 337 (1918).

for alkali ions in $N_2$ by Mitchell and Ridler,[11] whose result with $K^+$ is indicated in Fig. 6 by curve *a*. The subsequent decrease has been found by Townsend and Bailey[2] with electrons.

### Comparison with Theory

The variation of mobility with increase in $E/p$ may be explained qualitatively in terms of the forces which act between the ions and molecules. At low field intensities the mobility would be two or three times higher if the ions and molecules were simple rigid elastic spheres. The mean free path, and hence also the mobility, are lowered by forces of attraction which arise from polarization of the molecule by the charged ions, and van der Waals interactions. As the speed is increased, the attractive forces have less time to act. The rise in mobility with increase in $E/p$ may be interpreted as the result of the decrease in the effectiveness of the attractive forces. The presence of peaks in the curves for $H_2$, $N_2$, and A may be associated with the greater polarizability of these gases.

Collisions with the molecules remove momentum from the ions as rapidly as they pick it up from the field. The momentum is transferred at a rate which is proportional to the product of the momentum, the fractional loss of momentum per collision, and the frequency of collision. At low field intensities the collision frequency is determined primarily by the temperature, and is independent of the drift velocity. The rate of transfer of momentum is directly proportional to the velocity, and the mobility is independent of $E/p$. At high field intensities on the other hand, the drift velocity of the ions is greatly in excess of the thermal velocities of the molecules. The collision frequency is then proportional to the product of the collision cross section and the velocity. If the ions and molecules were rigid elastic spheres, the collision cross section would be constant. The rate of transfer of momentum would therefore be proportional to the square of the velocity, and the mobility would vary inversely with the square root of $E/p$. Actually the ions and molecules are not rigid. The collision cross section continues to diminish as the velocity is increased, and the mobility varies more slowly than inversely with the square root of $E/p$.

A formula has been derived by Compton and Langmuir[12] to express the transition from independence of $E/p$ to inverse proportionality to

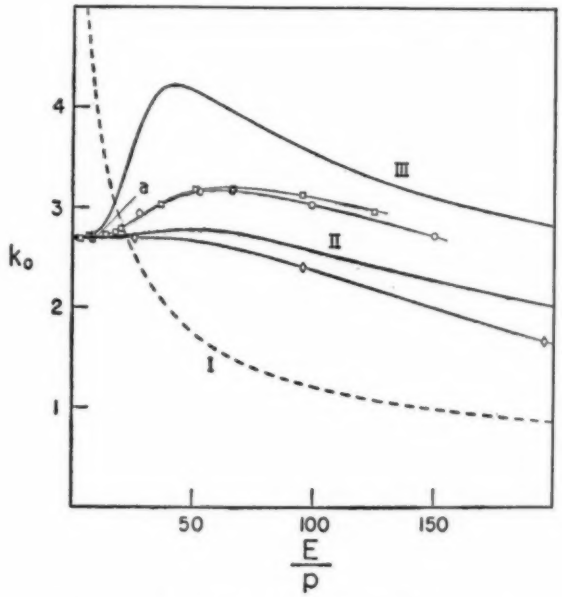


Fig. 6. The mobility of $K^+$ in $N_2$. ◇, 0.1 mm; ○, 0.3 mm; □, 0.7 mm.

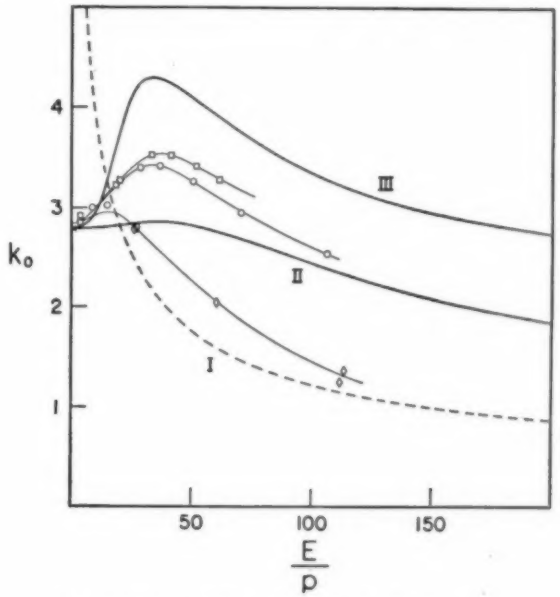


Fig. 7. The mobility of $K^+$ in A. ◇, 0.1 mm; ○, 0.3 mm; □, 0.7 mm.

[11] Mitchell and Ridler, Proc. Roy. Soc. **A146**, 911 (1934).

[12] K. T. Compton and I. Langmuir, Rev. Mod. Phys. **2**, 123 (1930).

the square root of $E/p$. It is given by the equation

$$k=\frac{(0.815)\lambda_0 e}{(2em_1\Omega)^{\frac{1}{2}}}\frac{\left[1+\dfrac{m_1/m_2}{\frac{1}{2}+\left(\frac{1}{4}+\dfrac{\lambda_0^2E^2(m_1+m_2)^2}{(6.57)\Omega^2m_1m_2}\right)^{\frac{1}{2}}}\right]^{\frac{1}{2}}}{\left[\frac{1}{2}+\left(\frac{1}{4}+\dfrac{\lambda_0^2E^2(m_1+m_2)^2}{(6.57)\Omega^2m_1m_2}\right)^{\frac{1}{2}}\right]^{\frac{1}{2}}},$$

in which $m_1$ and $m_2$ are the masses of the ion and molecule, $\lambda_0$ is the mean free path, and $e\Omega$ is the average thermal energy of a molecule. In Figs. 4 to 7 the curves labeled I are a plot of the formula. The curves are based on the kinetic theory radii given by Jeans.[13] A radius for the potassium ion was found by reducing the kinetic theory radius of the argon atom in the ratio between the radii calculated by Slater[14] from wave mechanics.

The formula of Compton and Langmuir does not take the attractive forces into account. Furthermore it is not applicable to heavy ions in light gases, since it is based on the assumption that the ions have a random energy which far exceeds the drift energy. On the contrary, the random energy is less than the drift energy. The formula gives too low a mobility since it assumes too high a collision frequency. The discrepancy between the formula and experiment amounts to a factor of nearly ten in $H_2$, but diminishes as the molecular weight of the gas is increased.

In Langevin's[15] theory of mobility, the ions and molecules are assumed to be rigid spheres which attract each other with a force inversely proportional to the fifth power of the distance of separation. The attractive force is assumed to arise solely from polarization of the molecules by the ions, and is expressed in terms of the dielectric constant of the gas. In Hassé and Cook's[16] theory, the rigid spheres are replaced by a repulsive force inversely proportional to the ninth power of the distance. Both theories are restricted to weak fields. Generalizations[17] of both to fields of any strength have been developed, which not only express the transition from a constant mobility to a mobility which diminishes with increase in $E/p$, but also take into account the attractive forces, and the dependence of the random energy upon the relative masses of the ions and molecules. In Figs. 4 to 7, the curves labeled II are a plot of the theory for the model with rigid spheres, and the curves labeled III, for the model with an inverse ninth power law of repulsion. The curves are based on molecular force data from the equation of state. Fowler's[18] calculations of intermolecular and interionic energies were extended to ion-molecule combinations. He has correlated the equations of state of gases and crystals in terms of a model with a repulsive energy inversely proportional to the ninth power of the distance, and a van der Waals energy inversely proportional to the sixth power. These correspond respectively to an inverse tenth power law of force, and to an inverse seventh power law. The combined potential energy $V$ between two molecules may be expressed in terms of the distance $r$ by the equation

$$V=\lambda/r^9-\mu/r^6.$$

Fowler has adopted the rule suggested by Lennard-Jones and Taylor[19] for estimating the coefficient $\lambda_{12}$ in the repulsive energy of two unlike molecules from the coefficients $\lambda_{11}$ and $\lambda_{22}$ for the two corresponding combinations of like molecules. The rule is given by the equation

$$\lambda_{12}^{1/9}=\tfrac{1}{2}(\lambda_{11}^{1/9}+\lambda_{22}^{1/9}).$$

He has expressed the coefficient $\mu_{12}$ in the van der Waals energy of two unlike molecules in terms of the coefficients $\mu_{11}$ and $\mu_{22}$ for like molecules by the equation

$$\mu_{12}=\frac{2(\mu_{11}^2\mu_{22}^2/Z_1Z_2)^{\frac{1}{2}}}{(\mu_{11}/Z_1^2)^{\frac{1}{2}}+(\mu_{22}/Z_2^2)^{\frac{1}{2}}},$$

which is derived from formulae proposed by Slater and Kirkwood[20] for the van der Waals

[13] J. H. Jeans, *The Dynamical Theory of Gases* (Cambridge University Press, third edition, 1921), p. 327.
[14] J. C. Slater, Phys. Rev. **36**, 57 (1930).
[15] Langevin, Ann. de Chimie et de Physique **8**, 245 (1905).
[16] H. R. Hassé and W. R. Cook, Proc. Roy. Soc. **A125**, 196 (1929); Phil. Mag. **12**, 554 (1931).
[17] A. V. Hershey, following paper.
[18] R. H. Fowler, *Statistical Mechanics* (Cambridge University Press, second edition, 1936), Chapter X.
[19] J. E. Lennard-Jones and P. A. Taylor, Proc. Roy. Soc. **109**, 476 (1925).
[20] J. C. Slater and J. G. Kirkwood, Phys. Rev. **37**, 682 (1931); J. G. Kirkwood, Physik. Zeits. **33**, 57 (1932).

energy. $Z_1$ and $Z_2$ are the numbers of extranuclear electrons in the molecules.

For ion-molecule combinations a polarization energy was added to the intermolecular energies. The total energy $V$ is expressed by the equation

$$V=-\frac{(\epsilon-1)}{8\pi n}\frac{e^2}{r^4}+\frac{\lambda}{r^9}-\frac{\mu}{r^6},$$

in which $n$ is the number of molecules per unit volume, and $\epsilon$ is the dielectric constant of the gas. Values of $\epsilon$ at 0°C and 760 mm were selected from the recent literature. They are 1.000270 for $H_2$,[21, 22] 1.000072 for He,[21] 1.000585 for $N_2$,[22] and 1.000553 for A.[21, 24] The energy in electron volts is plotted with heavy lines in Fig. 8 as a function of the distance in A. It is zero at a distance $\sigma_{12}$ of separation. The calculated values of $\sigma_{12}$ in A are 2.39 for $K^+$ in $H_2$, 2.48 in He, 2.77 in $N_2$, and 2.63 in A. They were retained in the subsequent selection of coefficients for the two models which are available to mobility calculations. Representation of the polarized molecule by an electric doublet of infinitesimal dimensions is basic to the calculation of polarization energy. Error arises from the finite distribution of charge which is induced by the powerful divergent field of the ion. Since, therefore, the energies plotted in Fig. 8 are not strictly accurate, the assumed magnitudes of the forces were freely adjusted to bring the calculated mobility into coincidence with the measurements by the Tyndall and Powell method. The energy which was selected for the model with

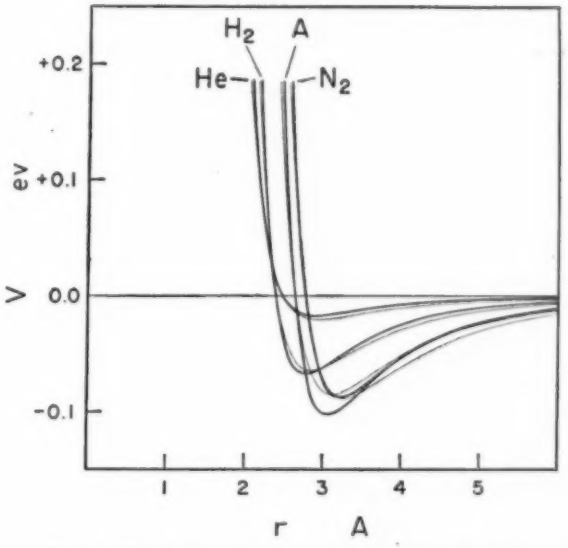


FIG. 8. The interaction energy between $K^+$ and $H_2$, He, $N_2$, and A.

an inverse ninth power law of repulsion is plotted in Fig. 8 with light lines.

The experimental results are bracketed by the two theories of mobility. The repulsive force, therefore, varies with distance to a higher power than nine, and, indeed, the crystal data[25] call for a tenth-power law. The same conclusion has been reached by Pearce[26] from a study of the temperature dependence of mobility. It is hoped that the theory will eventually be extended to a model in better agreement with experiment.

The writer gratefully acknowledges his indebtedness to Professor Leonard B. Loeb, at whose suggestion this problem was undertaken, and without whose continued encouragement it could not have been completed. It is a pleasure to thank Mr. Edward H. Guyon, for his able assistance in the construction of the chamber.

[21] Watson, Rao and Ramaswamy, Proc. Roy. Soc. **A132**, 569 (1931).
[22] Michels, Sanders and Schipper, Physica **2**, 753 (1935).
[23] H. L. Andrews, Physics **1**, 366 (1931); Michels, Jaspers and Sanders, Physica **1**, 627 (1934); C. E. Bennett, Phys. Rev. **45**, 200 (1934).
[24] G. Damköhler, Zeits. f. physik. Chemie **B27**, 130 (1934).
[25] M. Born, Ann. d. Physik **61**, 87 (1920).
[26] A. F. Pearce, Proc. Roy. Soc. **A155**, 490 (1936).

# A Theory for the Mobility of Ions of High Velocity

ALLEN V. HERSHEY
*University of California, Berkeley, California*

(Received July 12, 1939)

The theories of Langevin and of Hassé and Cook for the mobility of ions in weak fields have been generalized to fields of any strength. The random energy of the ions is assumed to have a Maxwellian distribution, and the drift and random energies are both evaluated by momentum and energy balances.

AN ideal theoretical treatment of the mobility of ions in gases would consist in the solution of the Boltzmann integral equation,[1] in which the laws of continuity are applied to the motion of ions in phase space. A solution may some day be found through the equations published by Pidduck[2] in 1915. He transformed the Boltzmann equation into a Fredholm integral equation with a symmetrical kernel and was able to perform one of the six required integrations. In the absence of an exact solution, however, an approximate distribution function may be chosen, and the parameters contained in it may be so adjusted that the equation is satisfied in the mean. Any solution must comply with the laws of conservation of momentum and energy, and these may be taken as criteria. The energy of the ions may be resolved into two parts, the drift and random energies, and these may be taken as the parameters. For simplicity the analysis is confined to elastic impacts, to steady distributions, to uniform densities in coordinate space, to low ion concentrations, and to uniform fields.

An approximate function which differs from the equilibrium distribution by a small added term has been used by Langevin[3] in his theory of mobility. In this theory the random energy is set equal to the thermal energy of the molecules, and the drift energy is evaluated by a momentum balance. The theory is thus restricted to weak fields. It is generalized to fields of any strength by the adoption of a Maxwellian distribution for the random energy of the ions which is free of any restriction as to the amount of deviation from equilibrium. The distribution is expressed by the equation

$$f_1=\frac{n_1}{(2\pi m_1 kT_1)^{\frac{3}{2}}}\exp\left[-\frac{(\mathbf{p}_1-m_1\mathbf{v})^2}{2m_1kT_1}\right], \quad (1)$$

in which $f_1$ is the density of ions in momentum space, and $n_1$ is the density in coordinate space. $m_1$ and $\mathbf{p}_1$ are the mass and vector momentum of an ion. $\frac{1}{2}n_1m_1v^2$ and $\frac{3}{2}n_1kT_1$ are the drift and random energies per unit volume, the sum of which is the total energy.

The molecules have the distribution of equilibrium. This is expressed by the equation

$$f_2=\frac{n_2}{(2\pi m_2 kT_2)^{\frac{3}{2}}}\exp\left[-\frac{\mathbf{p}_2^2}{2m_2kT_2}\right], \quad (2)$$

in which $f_2$ is the density of molecules in momentum space and $n_2$ is the density in coordinate space, $m_2$ and $\mathbf{p}_2$ are the mass and vector momentum of a molecule, and $T_2$ is the temperature of the gas.

The laws of conservation for steady motion are expressed by equating to zero the rates of change of the momentum and energy of the ions. In a field of intensity $\mathbf{E}$ the ions take up momentum at the rate $n_1e\mathbf{E}$, and energy at the rate $n_1e\mathbf{v}\cdot\mathbf{E}$. They give up the momentum and energy

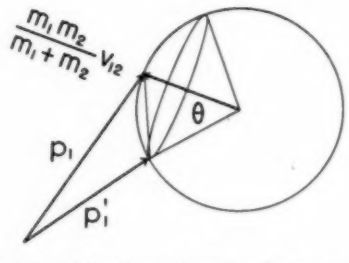


FIG. 1. The deflection of the ion by interaction with a molecule.

[1] L. Boltzmann, *Vorlesungen uber Gastheorie*, Vol. I, p. 114; J. H. Jeans, *The Dynamical Theory of Gases* (Cambridge University Press, third edition, 1921), p. 210.
[2] B. F. Pidduck, Proc. Lond. Math. Soc. **15**, 89 (1915).
[3] P. Langevin, Ann. de Chimie et de Physique **8**, 245 (1905).

to the molecules of the gas at rates which may be evaluated by integration over momentum space of the product of the change in each quantity per collision and the frequency of collision.

In a particular interaction the ion and molecule approach each other with a relative velocity $\mathbf{v}_{12}$, and separate after impact with a relative velocity which has the same magnitude as $\mathbf{v}_{12}$ but a different direction. The velocity of the ion itself is equal to the sum of the velocity of the center of mass, and the fraction $m_2/(m_1+m_2)$ of $\mathbf{v}_{12}$. The velocity of the center of mass is invariant in a collision. The velocity of the ion after impact therefore lies on a sphere whose center is at the center of mass. The deflection of the ion is illustrated in Fig. 1. The change in momentum $\mathbf{p}_1'-\mathbf{p}_1$ is equal to the product of the reduced mass $m_1m_2/(m_1+m_2)$, and the change in $\mathbf{v}_{12}$. The angle $\theta$ through which $\mathbf{v}_{12}$ is turned by impact is a function of the magnitude of $\mathbf{v}_{12}$, and of the distance $\sigma$ between the asymptotes of the trajectories which the ion and molecule describe about the center of mass. The magnitude of the change in $\mathbf{v}_{12}$ is equal to $2v_{12}\sin\frac{1}{2}\theta$.

If $p_{11}$, $p_{12}$ and $p_{13}$ are Cartesian components of $\mathbf{p}_1$, the number of ions whose momenta lie in the element $dp_{11}dp_{12}dp_{13}$ is equal to $f_1dp_{11}dp_{12}dp_{13}$, and if $p_{21}$, $p_{22}$, and $p_{23}$ are components of $\mathbf{p}_2$, the number of molecules with momenta in the element $dp_{21}dp_{22}dp_{23}$ is $f_2dp_{21}dp_{22}dp_{23}$. After impacts between these ions and molecules the relative velocities are distributed symmetrically about

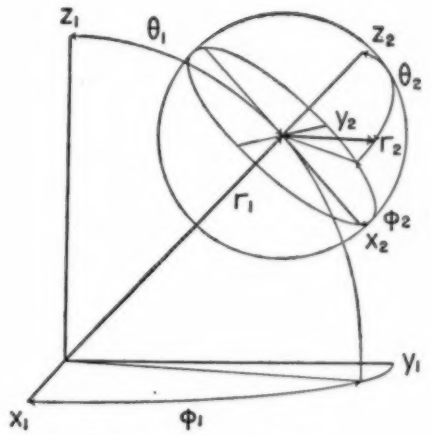


FIG. 2. Polar coordinates.

$\mathbf{v}_{12}$, and added vectorially form a vector collinear with $\mathbf{v}_{12}$. $\mathbf{p}_1'-\mathbf{p}_1$ may therefore be replaced in the integration by its component

$$-\frac{m_1m_2}{m_1+m_2}(1-\cos\theta)\mathbf{v}_{12}$$

along $\mathbf{v}_{12}$. Likewise, since $\mathbf{p}_1'^2-\mathbf{p}_1^2$ is identically equal to $(\mathbf{p}_1'-\mathbf{p}_1)\cdot(\mathbf{p}_1'-\mathbf{p}_1+2\mathbf{p}_1)$, it may be replaced in the integration by the expression

$$4\left(\frac{m_1m_2}{m_1+m_2}\right)^2\sin^2\tfrac{1}{2}\theta\mathbf{v}_{12}^2 - 2\frac{m_1m_2}{m_1+m_2}(1-\cos\theta)\mathbf{p}_1\cdot\mathbf{v}_{12}.$$

Interactions in which $\sigma$ lies in the range $d\sigma$ occur with a frequency equal to the number of molecules in a prism of volume $2\pi\sigma v_{12}f_1dp_{11}dp_{12}dp_{13}d\sigma$.

The completed momentum balance is therefore expressed by the equation

$$-\frac{m_1m_2}{m_1+m_2}\int\int\int\int\int\int f_1f_2\mathbf{v}_{12}Q(v_{12})v_{12}dp_{11}dp_{12}dp_{13}dp_{21}dp_{22}dp_{23}+n_1e\mathbf{E}=0 \qquad (3)$$

and the completed energy balance by the equation

$$\frac{m_2}{m_1+m_2}\int\int\int\int\int\int f_1f_2\left[\frac{m_1m_2}{m_1+m_2}\mathbf{v}_{12}^2-\mathbf{p}_1\cdot\mathbf{v}_{12}\right]Q(v_{12})v_{12}dp_{11}dp_{12}dp_{13}dp_{21}dp_{22}dp_{23}+n_1e\mathbf{v}\cdot\mathbf{E}=0. \qquad (4)$$

$Q(v_{12})$ is the diffusion cross section, and is defined by the equation

$$Q(v_{12})=2\pi\int(1-\cos\theta)\sigma d\sigma.$$

Five of the six indicated integrations may be performed after transformation to polar coordinates. The required transformation is illustrated in Fig. 2 and is defined by the system of equations

$$p_{11}=m_1x_1 \qquad p_{21}=m_2(x_1+x_2) \qquad x_1=r_1\sin\theta_1\cos\phi_1$$
$$p_{12}=m_1y_1 \qquad p_{22}=m_2(y_1+y_2) \qquad y_1=r_1\sin\theta_1\sin\phi_1$$
$$p_{13}=m_1z_1 \qquad p_{23}=m_2(z_1+z_2) \qquad z_1=r_1\cos\theta_1$$
$$x_2=+r_2\cos\theta_1\cos\phi_1\sin\theta_2\cos\phi_2-r_2\sin\phi_1\sin\theta_2\sin\phi_2+r_2\sin\theta_1\cos\phi_1\cos\theta_2$$
$$y_2=+r_2\cos\theta_1\sin\phi_1\sin\theta_2\cos\phi_2+r_2\cos\phi_1\sin\theta_2\sin\phi_2+r_2\sin\theta_1\sin\phi_1\cos\theta_2$$
$$z_2=-r_2\sin\theta_1\sin\theta_2\cos\phi_2+r_2\cos\theta_1\cos\theta_2.$$

$\mathbf{p}_1$ is expressed in terms of the position vectors $\mathbf{r}_1$ and $\mathbf{r}_2$ by $m_1\mathbf{r}_1$, $\mathbf{p}_2$ by $m_2(\mathbf{r}_1+\mathbf{r}_2)$, and $\mathbf{v}_{12}$ by $-\mathbf{r}_2$. The Jacobian of the transformation is $m_1^3m_2^3r_1^2r_2^2\sin\theta_1\sin\theta_2$. To facilitate the integration, parameters may be inserted into the integrands of Eqs. (3) and (4), and the integrands may be expressed as partial derivatives with respect to these parameters of simpler functions. The integration may then be carried out first, and the partial differentiation last since the order is immaterial. The parameters are finally eliminated by setting them equal to unity.

The momentum balance is reduced by integration to the equation

$$-\frac{8}{\pi^{\frac{1}{2}}}\frac{(m_1kT_2+m_2kT_1)}{(m_1+m_2)}n_1n_2\Sigma_1+n_1eE=0 \tag{5}$$

and the energy balance to the equation

$$-\frac{8}{\pi^{\frac{1}{2}}}\frac{n_1n_2}{(m_1+m_2)}v\left[\frac{m_1m_2}{m_1+m_2}k(T_1-T_2)\Sigma_2+m_1kT_2\Sigma_1\right]+n_1evE=0. \tag{6}$$

$\Sigma_1$ and $\Sigma_2$ are integrals. They are defined by the equations

$$\Sigma_1=\int_0^\infty Q(\lambda)\frac{(2\lambda\xi\cosh 2\lambda\xi-\sinh 2\lambda\xi)}{(2\lambda\xi)^2}\exp(-\xi^2-\lambda^2)\lambda^4d\lambda \tag{7}$$

and

$$\Sigma_2=2\int_0^\infty Q(\lambda)\frac{\sinh 2\lambda\xi}{(2\lambda\xi)^2}\exp(-\xi^2-\lambda^2)\lambda^6d\lambda. \tag{8}$$

$\xi$ and $\lambda$ are defined by the equations

$$\xi^2=\frac{m_1m_2v^2}{2(m_1kT_2+m_2kT_1)} \tag{9}$$

and

$$\lambda^2=\frac{m_1m_2v_{12}^2}{2(m_1kT_2+m_2kT_1)}. \tag{10}$$

Langevin's general formula is recovered if $v$ is made small. $T_1$ becomes equal to $T_2$, and $v$ is given by the equation

$$v=\frac{\pi eE[(m_1+m_2)/m_1m_2]^{\frac{1}{2}}}{(8/3)n_2(2\pi kT_2)^{\frac{1}{2}}\int_0^\infty Qe^{-\lambda^2}\lambda^5d\lambda}.$$

The last integration may be performed once the cross section $Q$ is known as a function of the relative velocity $v_{12}$. The relation between $Q$ and $v_{12}$ would be disclosed by measurements of the scattering or retardation of ion beams. Unfortunately, the experimental data[4] now available are not sufficiently precise to warrant a quantitative calculation. In any case they represent qualitative evidence that $Q$ decreases with increase in $v_{12}$.

Accurate theoretical values of $Q$ have been calculated for two models, which may be used in conjunction with molecular force data from the equation of state. In the theory of Langevin,

[4] Cf. C. Ramsauer and O. Beeck, Ann. d. Physik **87**, 1 (1928); F. M. Durbin, Phys. Rev. **30**, 844 (1927); R. B. Kennard, Phys. Rev. **31**, 423 (1928); I. W. Cox, Phys. Rev. **34**, 1426 (1929); R. E. Holzer, Phys. Rev. **36**, 1204 (1930); J. S. Thompson, Phys. Rev. **35**, 1196 (1930); K. H. Bracewell, Phys. Rev. **54**, 639 (1938).

the ion and molecule are assumed to be rigid elastic spheres which attract each other with a force inversely proportional to the fifth power of the distance of separation. The attractive force is assumed to arise solely from polarization of the molecule by the field of the ion, and is expressed in terms of the dielectric constant $\epsilon$ of the gas. The corresponding potential energy $V$ is expressed in terms of the distance $r$ by the equation

$$V=-\frac{\kappa_4}{r^4}=-\frac{(\epsilon-1)}{8\pi n_2}\frac{e^2}{r^4}.$$

In the theory of Hassé and Cook,[5] the rigid spheres are replaced by a repulsive force inversely proportional to the ninth power of the distance, and the equation for $V$ becomes

$$V=\kappa_8/r^8-\kappa_4/r^4.$$

The cross sections of the two models are functions of $v_{12}$, and of the energy coefficients $\kappa_4$ and $\kappa_8$. They may be expressed in terms of the distance $\sigma_{12}$, at which the potential energy is zero. If the ion and molecule are rigid spheres, $\sigma_{12}$ is the sum of the radii of the spheres, but if they repel with the inverse ninth power law, it is equal to $(\kappa_8/\kappa_4)^{\frac{1}{4}}$. For each model the ratio $Q/\pi\sigma_{12}^2$ may be expressed as a separate function of the ratio $\lambda/\mu$, in which the parameter $\mu$ is defined by either of the equations

$$1/\mu^2=\frac{8\pi p\sigma_{12}^4}{(\epsilon-1)e^2}\frac{(m_1kT_2+m_2kT_1)}{kT_2(m_1+m_2)}$$

and

$$1/\mu^2=\frac{\kappa_8}{\kappa_4{}^2}\frac{(m_1kT_2+m_2kT_1)}{(m_1+m_2)},$$

in which $p$ is the pressure of the gas. At low velocities, $Q/\pi\sigma_{12}^2$ for both models varies inversely as $\lambda/\mu$. At high velocities, it approaches unity if the ion and molecule are rigid spheres, but diminishes inversely with the square root of $\lambda/\mu$ if they repel with the inverse ninth power law. The quantity $(\lambda/\mu)(Q/4\pi\sigma_{12}^2)$ has been tabulated as a function of $\lambda/\mu$ by Hassé[6] for the model with rigid spheres, and the quantity $(1/\sqrt{2})(\lambda/\mu)^{\frac{1}{2}}(Q/2\pi\sigma_{12}^2)$ has been tabulated by Hassé and Cook[7] at small values of $\mu/\lambda$, and $(\lambda/\mu)(Q/4\pi\sigma_{12}^2)$ at large values for the model with an inverse ninth power law. Their results have been used in the evaluation of $\Sigma_1$ and $\Sigma_2$ by numerical integration.

For each model the ratios $\Sigma_1/\pi\sigma_{12}^2$ and $\Sigma_2/\pi\sigma_{12}^2$ may be expressed in terms of $\mu$ and $\xi$. These are functions of both $T_1$ and $v$, and $T_1$ cannot be eliminated from Eqs. (5) and (6). The variables $v$ and $E$ are separated, however, and expressed in terms of $T_1$ by the introduction of three parameters, $A$, $B$, and $C$, which are defined and related by the three sets of equations

$$\begin{aligned}A&=\tfrac{1}{2}\mu\xi(\pi\sigma_{12}^2/\Sigma_1)\\&=(v/E)\rho^{\frac{1}{2}}(\epsilon-1)^{\frac{1}{2}}\left(\frac{m_1}{m_1+m_2}\right)^{\frac{1}{2}}\\&=(\rho v/eE)(8\pi\kappa_4/m_2)^{\frac{1}{4}}\left(\frac{m_1}{m_1+m_2}\right)^{\frac{1}{2}},\end{aligned}\qquad(11)$$

$$B=(1/\xi)^2\frac{\Sigma_1}{\Sigma_2-\Sigma_1}=\frac{2k(T_1-T_2)}{m_2v^2},\qquad(12)$$

$$C=\frac{\Sigma_1}{\Sigma_2-\Sigma_1}=\frac{m_1k(T_1-T_2)}{m_1kT_2+m_2kT_1},\qquad(13)$$

in which $\rho$ is the density of the gas.

Values of $A$, $B$ and $C$ for various values of $\xi$ are tabulated as a function of $1/\mu$, in Table I for the model with rigid spheres, and in Table II for the model with an inverse ninth power law. Curves of $A$ and $B$ for various values of $1/\mu$ are plotted against $C$ in Figs. 3 to 6. $\mu$ and $C$ contain $T_1$ but not $v$ and $E$. The drift velocity $v$ and the mobility $v/E$ may therefore be calculated from the curves for a given value of $T_1$.

If $1/\mu$ is set equal to zero, the theory of small ions is obtained. The parameter $A$ has the value 0.5105 and $B$ the value $\frac{2}{3}$. The drift velocity $v$ is then expressed by the equation

$$v=\frac{(0.5105)E}{\rho^{\frac{1}{2}}(\epsilon-1)^{\frac{1}{2}}}\left(\frac{m_1+m_2}{m_1}\right)^{\frac{1}{2}}.$$

If $\mu$ itself is set equal to zero, the attractive forces are eliminated, and $\Sigma_1$ and $\Sigma_2$ may be

[5] H. R. Hassé and W. R. Cook, Proc. Roy. Soc. **A125**, 196 (1929); Phil. Mag. **12**, 554 (1931).

[6] H. R. Hassé, Phil. Mag. **1**, 139 (1926). $(\lambda/\mu)(Q/4\pi\sigma_{12}^2)$ is represented in his notation by $y$, and $\lambda/\mu$ by $z\lambda$.

[7] Reference 5. $(1/\sqrt{2})(\lambda/\mu)^{\frac{1}{2}}(Q/2\pi\sigma_{12}^2)$ is represented in their notation by $I_1/2\pi$, $\mu/\lambda$ by $k$, and $(\lambda/\mu)(Q/4\pi\sigma_{12}^2)$ by $Y_1$.

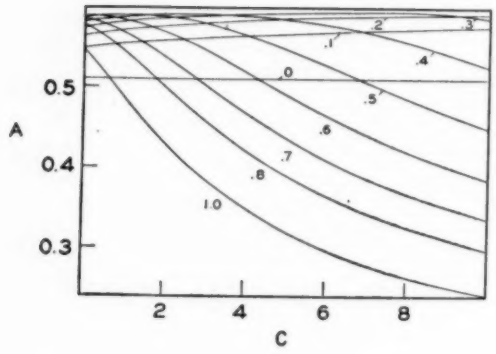


FIG. 3. The parameter $A$ for the model with rigid spheres, at various values of $1/\mu$.

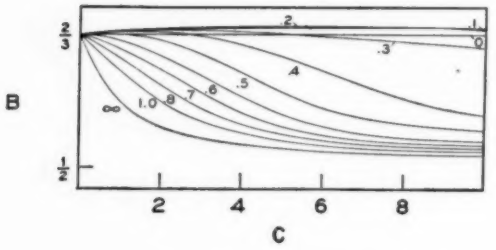


FIG. 4. The parameter $B$ for the model with rigid spheres, at various values of $1/\mu$.

TABLE I. *Parameters for the model with rigid spheres.*

| | $\xi=1.0$ | | | $\xi=2.0$ | | |
|---|---|---|---|---|---|---|
| $1/\mu$ | $A$ | $B$ | $C$ | $A$ | $B$ | $C$ |
| 0.1 | 0.553 | 0.669 | 0.669 | 0.561 | 0.673 | 2.69 |
| .2 | .570 | .670 | .670 | .579 | .674 | 2.70 |
| .3 | .581 | .669 | .669 | .589 | .672 | 2.69 |
| .4 | .588 | .669 | .669 | .592 | .667 | 2.67 |
| .5 | .591 | .667 | .667 | .584 | .650 | 2.60 |
| .6 | .588 | .663 | .663 | .559 | .628 | 2.51 |
| .7 | .577 | .657 | .657 | .523 | .611 | 2.44 |
| .8 | .559 | .649 | .649 | .486 | .592 | 2.37 |
| 1.0 | .509 | .636 | .636 | .416 | .574 | 2.30 |

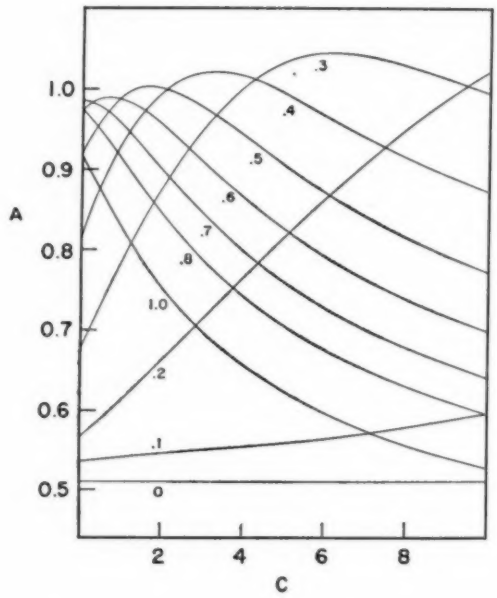


FIG. 5. The parameter $A$ for the model with an inverse ninth power law, at various values of $1/\mu$.

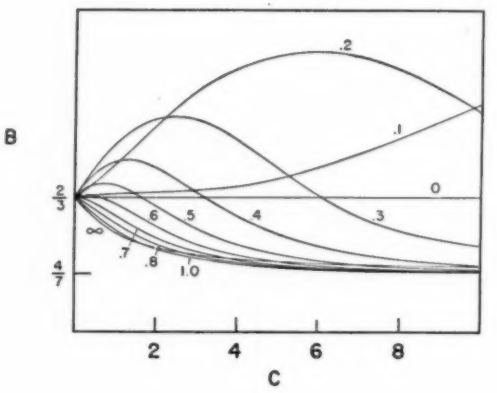


FIG. 6. The parameter $B$ for the model with an inverse ninth power law, at various values of $1/\mu$.

TABLE II. *Parameters for the model with an inverse ninth power law.*

| | $\xi=1.0$ | | | $\xi=1.6$ | | | $\xi=2.0$ | | | $\xi=3.0$ | | | $\xi=4.0$ | | |
|---|---|---|---|---|---|---|---|---|---|---|---|---|---|---|---|
| $1/\mu$ | $A$ | $B$ | $C$ | $A$ | $B$ | $C$ | $A$ | $B$ | $C$ | $A$ | $B$ | $C$ | $A$ | $B$ | $C$ |
| 0.1 | 0.541 | 0.670 | 0.670 | 0.546 | 0.673 | 1.722 | 0.550 | 0.675 | 2.70 | 0.568 | 0.710 | 6.39 | 0.639 | 0.873 | 13.96 |
| .2 | .600 | .693 | .693 | .661 | .751 | 1.921 | .726 | .803 | 3.21 | .931 | .835 | 7.51 | 1.052 | .715 | 11.44 |
| .3 | .760 | .718 | .718 | .875 | .763 | 1.952 | .954 | .761 | 3.04 | 1.043 | .669 | 6.02 | .999 | .608 | 9.72 |
| .4 | .908 | .705 | .705 | .990 | .707 | 1.809 | 1.018 | .682 | 2.73 | .978 | .612 | 5.51 | .883 | .583 | 9.33 |
| .5 | .977 | .684 | .684 | 1.002 | .665 | 1.703 | .988 | .640 | 2.56 | .891 | .593 | 5.34 | .787 | .576 | 9.21 |
| .6 | .989 | .667 | .667 | .968 | .641 | 1.641 | .931 | .619 | 2.48 | .814 | .585 | 5.27 | .714 | .574 | 9.18 |
| .7 | .969 | .654 | .654 | .919 | .627 | 1.605 | .872 | .608 | 2.43 | .750 | .582 | 5.23 | .656 | .573 | 9.16 |
| .8 | .933 | .647 | .647 | .869 | .619 | 1.585 | .817 | .603 | 2.41 | .698 | .580 | 5.22 | .609 | .573 | 9.16 |
| 1.0 | .854 | .639 | .639 | .780 | .612 | 1.566 | .728 | .598 | 2.39 | .618 | .579 | 5.21 | .539 | .573 | 9.17 |

expanded into rapidly converging power series in $\xi$. In the case of rigid spheres the drift velocity $v$ is given at small values of $\xi$ by the equation

$$v=\frac{eE}{(8/3)n_2\sigma_{12}^2(2\pi kT_2)^{\frac{1}{2}}}\left(\frac{m_1+m_2}{m_1m_2}\right)^{\frac{1}{2}},$$

which represents one form of the conventional kinetic theory formula. For other values of $\xi$ it is convenient to introduce a fourth parameter $D_\infty$, defined by the equations

$$D_\infty=\tfrac{1}{4}\pi^{\frac{1}{2}}\xi^2\left(\frac{\pi\sigma_{12}^2}{\Sigma_1}\right)=(\rho v^2/eE)(\pi\sigma_{12}^2)\left(\frac{m_1}{m_1+m_2}\right).$$

Values of $B$, $C$, and $D_\infty$ are tabulated in Table III as a function of $\xi$.

On the other hand, if the repulsive force varies inversely as the ninth power of the distance, $v$ is given at small values of $\xi$ by the equation

$$v=\frac{eE}{(5.789)n_2(\kappa_9kT_2)^{\frac{1}{2}}}\left(\frac{m_1+m_2}{m_1m_2}\right)^{\frac{1}{2}}.$$

For other values of $\xi$, it is convenient to introduce another parameter $D_9$, defined by the equations

$$D_9=\tfrac{1}{4}\pi^{\frac{1}{2}}\mu^{\frac{1}{2}}\xi^{\frac{1}{2}}(\pi\sigma_{12}^2/\Sigma_1)$$

$$=(\rho v^{\frac{1}{2}}/eE)\pi(2\kappa_9/m_2)^{\frac{1}{2}}\left(\frac{m_1}{m_1+m_2}\right)^{\frac{1}{2}}.$$

Values of $B$, $C$ and $D_9$ are tabulated in Table IV.

TABLE III. *Parameters for rigid spheres with no attractive forces.*

| $\xi$ | $B$ | $C$ | $D_\infty$ |
|---|---|---|---|
| 0.0 | $\frac{2}{3}$ | 0.0 | 0.0 |
| .2 | 0.663 | 0.0265 | 0.132 |
| .4 | .654 | .1046 | .258 |
| .6 | .639 | .230 | .373 |
| .8 | .623 | .399 | .474 |
| 1.0 | .607 | .607 | .560 |
| 1.2 | .592 | .852 | .632 |
| 1.4 | .578 | 1.133 | .691 |
| 1.6 | .566 | 1.449 | .739 |
| 1.8 | .557 | 1.803 | .778 |
| 2.0 | .549 | 2.19 | .810 |
| 2.2 | .542 | 2.62 | .836 |
| 2.4 | .537 | 3.09 | .858 |
| 2.6 | .532 | 3.60 | .875 |
| 2.8 | .528 | 4.14 | .890 |
| 3.0 | .525 | 4.72 | .903 |
| 3.5 | .520 | 6.36 | .926 |
| 4.0 | .515 | 8.23 | .942 |
| $\infty$ | $\frac{1}{2}$ | $\infty$ | 1.000 |

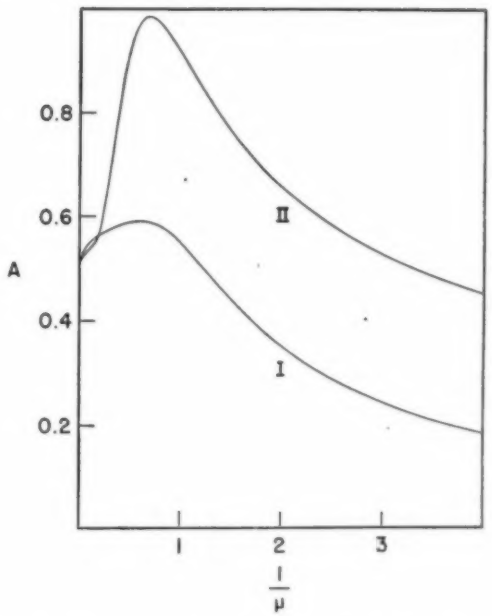


FIG. 7. The parameter $A$ for weak fields. Curve I, Langevin's theory for rigid spheres; curve II, Hassé and Cook's theory for the inverse ninth power law.

When the drift velocity is small, the mobility is independent of field intensity. Values of $A$ in this case have been tabulated by Hassé[8] as a function of $1/\mu$ for the model with rigid spheres, and values of the quantity $\frac{3}{16}\sqrt{2}(\mu^{\frac{1}{2}}/A)$ have been tabulated by Hassé and Cook[9] for the model

TABLE IV. *Parameters for an inverse ninth power law with no attractive forces.*

| $\xi$ | $B$ | $C$ | $D_9$ |
|---|---|---|---|
| 0.0 | $\frac{3}{4}$ | 0.0 | 0.0 |
| .2 | 0.665 | 0.0266 | 0.342 |
| .4 | .660 | .1056 | .478 |
| .6 | .653 | .235 | .574 |
| .8 | .644 | .412 | .648 |
| 1.0 | .635 | .635 | .704 |
| 1.2 | .626 | .902 | .747 |
| 1.4 | .618 | 1.211 | .781 |
| 1.6 | .611 | 1.564 | .807 |
| 1.8 | .605 | 1.961 | .827 |
| 2.0 | .600 | 2.402 | .843 |
| 2.2 | .596 | 2.887 | .856 |
| 2.4 | .593 | 3.416 | .866 |
| 2.6 | .590 | 3.990 | .874 |
| 2.8 | .588 | 4.61 | .881 |
| 3.0 | .586 | 5.27 | .887 |
| 3.5 | .582 | 7.13 | .897 |
| 4.0 | .580 | 9.28 | .904 |
| $\infty$ | 4/7 | $\infty$ | .9284 |

[8] Reference 6. $1/\mu$ is represented in his notation by $\lambda$.
[9] Reference 5. $\frac{3}{16}\sqrt{2}(\mu^{\frac{1}{2}}/A)$ is represented in their notation by $I(s)$. $1/\mu$ may be identified with their parameter $s$.

with an inverse ninth power law. Their results are reproduced in Fig. 7 for comparison. Curve I is a plot of $A$ as a function of $1/\mu$ for the model with rigid spheres, and curve II is the corresponding plot for the model with an inverse ninth power law.

As the drift velocity is increased, the parameter $C$ approaches the ratio $m_1/m_2$, $1/\mu$ becomes large, and the parameters $D_\infty$ and $D_9$ approach the corresponding values in Tables III and IV. In the case of rigid spheres, the velocity then varies directly, and the mobility inversely as the square root of $E/p$. If the repulsive force obeys the inverse ninth power law, the velocity varies directly as the two-thirds power of $E/p$, and the mobility varies inversely as the cube root of $E/p$.

Although the theory is not exact, the general formulae should not be seriously in error. Chapman,[10] Enskog,[11] and Pidduck[2] have shown that at low $E/p$ the error is no greater than a few percent. Comparison with experiment,[12] however, indicates that the repulsive force varies with distance to a higher power than nine. The correct law may eventually be found through accurate measurements of the scattering and retardation of ion beams. The use of classical cross sections also introduces error at low velocities, and at low temperatures, but this is less important at high velocities where classical and quantum theories converge.

The writer takes pleasure in thanking Professor Leonard B. Loeb for several stimulating discussions of this subject.

[10] S. Chapman, Phil. Trans. **A217**, 115 (1917).
[11] D. Enskog, *Kinetische Theorie der Vorgänge in mässig verdünnten Gasen*, Inaugural Dissertation, Upsala, 1917.
[12] A. F. Pearce, Proc. Roy. Soc. **A155**, 490 (1936); A. V. Hershey, preceding paper.

---

NOVEMBER 1, 1939 PHYSICAL REVIEW VOLUME 56

# Antiferromagnetism in Some Manganous Compounds*

CHARLES F. SQUIRE
*Department of Physics, University of Pennsylvania, Philadelphia, Pennsylvania*
(Received July 13, 1939)

The temperature dependence (300°K to 40°K) of the magnetic susceptibility of the following $Mn^{++}$ salts has been measured: MnO, MnS, MnSe, MnTe. A λ-point transition at low temperatures makes the susceptibility break away from a Weiss-Curie law and decrease with lowering temperatures. Each salt has its characteristic transition temperature, increasing with increasing molecular weight. Evidence for field dependence of the susceptibility and for magnetic hysteresis has been found. It seems likely that an exchange force is the cause of the transition from paramagnetism to antiferromagnetism.

## INTRODUCTION

THE paramagnetic susceptibility of salts usually obeys a Weiss-Curie law: $\chi = C/(T-\Theta)$ where the constant $C$ is the Curie constant, $T$ the absolute temperature, and $\Theta$ the point where the straight line $1/\chi$ intersects the temperature axis. Deviations from this law have been observed in several salts[1] at low temperatures. The experiments described in this paper are on the following $Mn^{++}$ salts: MnO, MnS, MnSe, MnTe. At a temperature, characteristic for each salt, the susceptibility breaks away from the Weiss-Curie law and decreases with lowering of temperature.

Kelley[2] has measured the specific heat of Mn, MnSe, and MnTe; in the latter two compounds he has found a hump or abnormal specific heat. Measurements on MnO and MnS by Millar[3] and Anderson[4] each show a hump in the specific

* The electrical conductivity as a function of temperature has been measured for these compounds. Details are described in a Letter to the Editor, Charles F. Squire, Phys. Rev., this issue.

[1] M. and B. Ruhemann, *Low Temperature Physics* (Cambridge, 1937), Chapter II.

[2] K. K. Kelley, J. Am. Chem. Soc. **61**, 203 (1939).
[3] R. W. Millar, J. Am. Chem. Soc. **50**, 1875 (1928).
[4] Anderson, J. Am. Chem. Soc. **53**, 476 (1931).

heat curve. The hump in each case is quite large and the transition temperature or λ point occurs at: 116°K for MnO, 140°K for MnS, 247°K for MnSe, 307°K for MnTe. It is evident that the temperature of the hump occurs higher the greater the mass of the combining atom.

Using the same sample of MnO and MnS as had been used for the specific heat studies, Ellefson and Taylor[5] looked for structure changes but found no change. Only an abnormal expansion in the λ region was detected. Ruhemann[6] independently made similar studies on MnO and reported a sodium chloride type structure above and below the transition with only a rapid but continuous expansion through the λ region.

The first accurate susceptibility measurements were made on MnO by Bizette, Squire and Tsai.[7] They showed that the susceptibility abruptly changed from the Weiss-Curie law at $T_\lambda$ and decreased continuously as the temperature was lowered. Below the transition the susceptibility varied with the measuring field. The sample was freshly prepared by reducing the manganese oxalate with hydrogen at a very high temperature. Analysis showed no impurities with respect to iron or sulfur.

## Experimental

The compounds MnS, MnSe, MnTe were obtained from Kelley.[2] The degree of purity is very satisfying—in particular Kelley reports the MnSe on analysis to be 99.35 percent pure, based on its manganese content; and 99.48 percent pure, based on its selenium content. The method for measuring the susceptibility was to determine the force on a sample placed in a nonhomogeneous field. The modification for low temperature measurements is due to de Haas, Wiersma and Kramers.[8] In these experiments, approximately 3 grams of the powder was placed in the weighing tube. The nonhomogeneous field was 700 gauss at its maximum intensity. The force pulling the sample into the field was of the order 100 milligrams; a force of 1 milligram could be easily detected on the balance. The calibration for the absolute value of the susceptibility was done with $NiCl_2$ whose value has been carefully determined.[9] With the calibration, measurements on $NiSO_4$ gave a value at 298°K which agreed with reported[9] values to within 2 percent. Temperatures were measured by thermocouples in all these experiments.

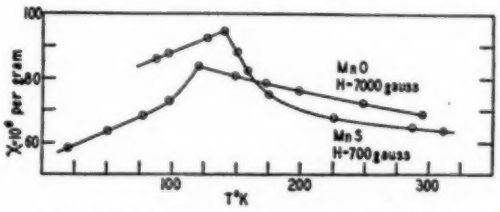


Fig. 1. Magnetic susceptibility per gram against temperature for MnO (from reference 7) and for MnS.

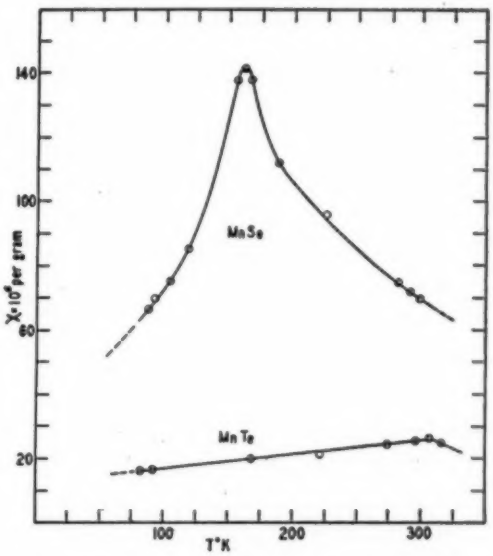


Fig. 2. Magnetic susceptibility per gram against temperature for MnSe and MnTe.

Figures 1 and 2 show the magnetic susceptibility plotted against the temperature for the $Mn^{++}$ compounds studied. A large number of points were taken and the experimental runs were repeated several times in complete agreement. Constant temperature baths of $CO_2$ in alcohol, of $O_2$, and of $N_2$ furnished fixed points at which temperature equilibrium was insured. Intermediate values were obtained by allowing the rate of cooling to proceed very slowly.

[5] B. S. Ellefson and N. W. Taylor, J. Chem. Physics **2**, 58 (1934).
[6] B. Ruhemann, Sow. Phys. **7**, 590 (1935).
[7] H. Bizette, Squire and Tsai, Comptes rendus **207**, 449 (1938).
[8] de Haas, Wiersma and Kramers, Physica **1**, 1 (1933).
[9] A. Serres, Ann. de Physique **20**, 441 (1933).

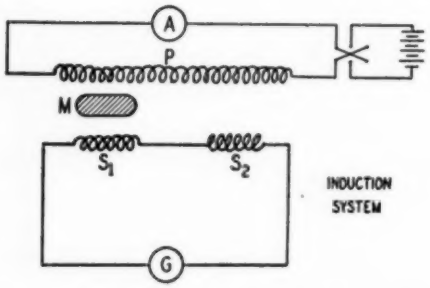


FIG. 3. Circuit for measuring magnetic susceptibility. The two secondaries, $S_1$ and $S_2$ are wound equal and opposite.

Supercooling—i.e., causing the transition point to occur at a lower temperature than reported for the $C_p$ values, is the result of rapid cooling. Kelley found similar supercooling effects on the $C_p$ measurements of MnSe.

The large change in the susceptibility of MnSe was easily detected by another technique. A 15-cm long solenoid of 2 cm diameter formed the primary coil ($P$) to an induction system (see Fig. 3). Two identical coils $S_1$ and $S_2$ (3000 turns each) were wound on the primary in such a way that their direction of winding was opposite to one another. When a current is passed through the primary coil, the induced e.m.f. of $S_1$ is equal and opposite to that of $S_2$. The induction system was placed in a liquid $N_2$ bath so that the resistance of the coils was reduced. Removing a single turn on one of the secondaries would produce an unbalancing action which could just be detected by the ballistic galvanometer $G$. Placing the paramagnetic salt, $M$, into the space of $S_1$ has the effect of increasing the induced e.m.f. of coil $S_1$. Thus with the coils perfectly balanced, the throw of the galvanometer is proportional to the magnetic susceptibility. Fig. 4 shows the deflection on the galvanometer scale plotted against temperature when 10 grams of MnSe is placed in coil $S_1$. With a current in the primary sufficient to give a field of 3 gauss, one obtains curve "$a$"; for 5 gauss, curve "$b$"; and for a 10-gauss measuring field, one obtains curve "$c$."

A reversing switch was put into the primary coil circuit for the purpose of detecting hysteresis effects.[10] In curve "$c$" of Fig. 4 the upper curve (marked with dashes) represents the throw of the galvanometer upon first reversing the primary current. All subsequent deflections caused by sending the primary current in the same direction fall on the lower curve. The magnitude of the current in the primary was kept constant. Similar upper and lower curves were observed in "$a$" and "$b$" but only the lower values are plotted. The measurements were taken every 5-degree interval on both curves and the curves were repeatedly reproduced. Measurements as low as 40°K were obtained by the adiabatic desorption of hydrogen gas from activated charcoal; the susceptibility continues to fall off at lower temperatures.

Figure 5 shows the same type of curve for MnSe measured with completely new coils. It is interesting to observe that the hysteresis effect vanishes after an appreciable temperature interval on each side of the transition. The points establishing the curves are not shown; the points plotted on the curve represent the observed deflection when an additional field of 7, 14, 21, 28, and 35 gauss was superimposed steadily by means of an external solenoid. Had a microscopic piece of soft iron been the cause of the hysteresis, it might possibly have become saturated in such an additional field. In any case the hysteresis arising from such an impurity would not vanish at low temperatures. It is difficult to see how the copper coils (Fig. 3) could give rise to the hysteresis; three different coils, wound on different Pyrex tubes, gave identical results.

Finally in Fig. 6 is shown one of the hysteresis loops which was measured close to the λ-point.

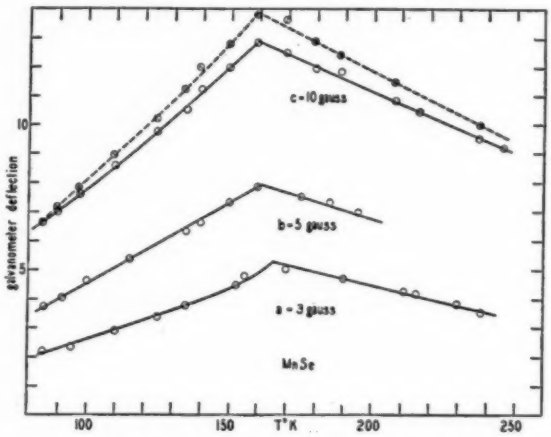


FIG. 4. Deflection of galvanometer in cm against temperature. MnSe.

[10] Kurti, Lainé and Simon, Comptes rendus **204**, 675 (1937).

The circle marks represent the first time around the loop and the $x$ marks the second time around. The coordinates are the galvanometer deflection against the measuring field of the primary. A similar loop was measured on MnS with the difference that the magnitude of deflection—i.e., width of the loop at the center, was about one-fifth as large.

## Discussion

The transition phenomenon appears to be the result of antiferromagnetism. Upon examining the susceptibility curves we may make the following remarks: Since the $Mn^{++}$ ions are in the $^6S$ state, the spin alone contributes to the paramagnetism. On the high temperature side of the transition, the spins are free to orient with the magnetic field; while on the low temperature side, they are locked antiparallel. Thus as one lowers the temperature towards 0°K the susceptibility approaches zero. The λ-point is simply a Curie point where paramagnetism becomes antiferromagnetism.

It seems likely that such antiparallel orientation can be identified with an exchange force; and as the temperature increases a point is reached where there is sufficient $kT$ energy to set free the spins. This means that the extra binding force due to the exchange will disappear and so the crystal expands during the liberation. The extra specific heat would naturally occur in such a process.

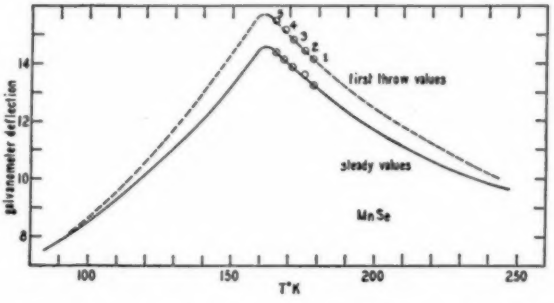


Fig. 5. Deflection of galvanometer in cm against temperature. MnSe. The points plotted have additional field in same direction as measuring field. 1, 7 gauss; 2, 14 gauss; 3, 21 gauss; 4, 28 gauss; 5, 35 gauss.

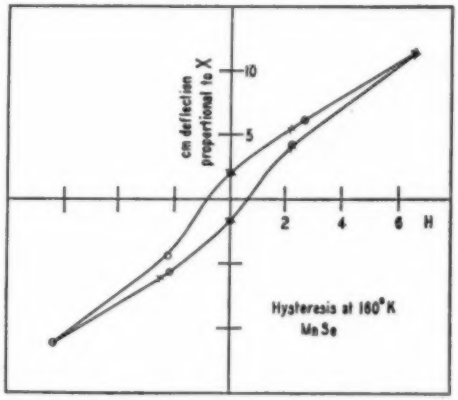


Fig. 6. Deflection of galvanometer in cm against measuring field in gauss. MnSe.

The hysteresis which is observed in the neighborhood of the Curie point cannot be explained on any such simple basis. Certainly with spins antiparallel there can be no permanent magnetic moment; at low temperatures well away from the Curie point there is no hysteresis. Just why the relaxation time should be abnormally long for the spin system to go from a state of magnetization to one of zero moment is not at all clear. Simon[10] has observed hysteresis effects in Fe—alum at 0.034°K.

Kramers[11] has pointed out the possibility of exchange coupling between magnetic ions being sometimes less drastic than an exponential function of their distance apart; coupling via the excited states of the intermediate (normally nonmagnetic) atoms is possible. The experimental fact that the Curie point is higher, the greater the mass of the combining atom indicates that the exchange force is perhaps not greatly diminished by increasing the distance between $Mn^{++}$ ions. It is not obvious that here is a transition of the third kind, corresponding to an order-disorder in spin space.

The author is greatly indebted to Dr. Kelley, Bureau of Mines, U. S. A. for the manganous salts used in this research, and for discussions with staff members at the University of Pennsylvania.

[11] H. A. Kramers, Physica **1**, 182 (1933).

# The Specific Heat of a Monatomic Liquid

WILLIAM J. ARCHIBALD*
*Yale University, New Haven, Connecticut*
(Received April 17, 1939)

The partition function for an atom in a monatomic liquid is evaluated by assuming that the atom is constrained by its nearest neighbors to move in a spherical region, and that the potential energy of the atom at any point within this region can be found if the law of force between two atoms is known. On the basis of this partition function an expression for $C_v$ is derived. The theory is checked by a comparison of the experimental and theoretical values of $C_v$ for liquid argon.

## I

MOST liquids of our common experience are too complex to enable the methods of statistical mechanics to be applied to them with any degree of rigor. A theoretical interpretation of the behavior of such liquids is for the most part still lacking. Of all liquids, those whose molecules possess spherical symmetry stand apart from the others because of their simple structure, and it is with these that we must deal at first in order to test our theoretical technique.

Both Eyring[1] and Lennard-Jones[2] have had singular success in their treatment of simple liquids of this sort. These investigators have devised a very definite and useful model for the structure of a liquid. Starting with a model as a basis it is possible to derive the properties of the system which the model represents by straightforward statistical methods.

Eyring considers a molecule or atom in a liquid to be imprisoned by its nearest neighbors in a nearly force free cell or cavity called the free volume. However, the molecule is not permanently confined to a particular cell but can wander occasionally from one to the next whenever it possesses sufficient energy to make the transition. In this way the total free volume of the liquid is available to any particular molecule and it is the sharing of the total free volume which differentiates the solid and the liquid states according to this model. This picture of the behavior of molecules has proved fruitful chiefly because it is possible to relate the free volume to many of the properties of the liquid. Subsequent elimination of the free volume leaves correlations between different properties of the liquid which are very satisfactory.

The method of Lennard-Jones is based upon the same conception of the liquid state as that of Eyring. However, he is more precise in detail in that he derives an analytical expression for the potential energy at all points of the cell within which the atom or molecule moves, whereas Eyring assumes the potential energy within the cell to be constant everywhere except at the boundary where the potential becomes infinite.[3] In order to calculate the potential at all points within the cell it is necessary to know the potential energy existing between two atoms or molecules of the liquid as a function of the distance between them. Consequently this second method, while giving a more precise description of conditions within a cell, is limited in its application to liquids such as neon, argon or nitrogen because only for such substances is the interatomic force known.

Let us assume that the analytical expression for the potential within a cell is known. It is then a simple matter to write down the partition

* Sterling Fellow.

[1] H. Eyring, J. Chem. Phys. **4**, 283 (1936); R. Newton and H. Eyring, Trans. Faraday Soc. **33**, 73 (1936); H. Eyring and J. Hirschfelder, J. Phys. Chem. **41**, 249 (1937); J. Hirschfelder, D. Stevenson and H. Eyring, J. Chem. Phys. **5**, 896 (1937).

[2] J. E. Lennard-Jones, Physica **4**, 941 (1937); J. E. Lennard-Jones and A. F. Devonshire, Proc. Roy. Soc. **A163**, 53 (1937); J. E. Lennard-Jones and A. F. Devonshire, Proc. Roy. Soc. **A165**, 1 (1938).

[3] Eyring has also considered the case where the potential wall at the boundary of the cell is not infinitely steep but has the form of the potential of the simple harmonic oscillator. The theory of an assembly of atoms moving in cells of this type gives a good representation of the properties of liquid mercury between its melting and boiling points. Cf. J. F. Kincaid and H. Eyring, J. Chem. Phys. **5**, 587 (1937).

function for an atom moving in such a cell. From this partition function it is possible in principle to derive all the equilibrium properties of the liquid. This is, briefly, the method of Lennard-Jones. It differs from that of Eyring in that a direct attempt is made to evaluate the integral occurring in the partition function, whereas Eyring substitutes for this integral the concept of the free volume.

The present paper is an application of the method of Lennard-Jones to the calculation of the specific heat at constant volume of a monatomic liquid. In order to check the formulae which are derived, the specific heat of liquid argon is computed and compared with the experimental values.

## II

An atom in a liquid is confined for the greater part of the time within a very restricted region by its nearest neighbors. We will assume that the possibility of escape from this cell in which it is imprisoned is negligible. Then its entire contribution to the specific heat will be that arising from its motion within the cell.

An atom at any point in a cell has a potential energy which is the algebraic sum of the potential energy existing between the atom in question and all the other atoms in the liquid. Consequently the potential at any point is a fluctuating quantity because of the ceasless, random motion of the atoms, but it has a certain definite average value which can be found as follows: we assume all the atoms in the liquid except one to be at rest in their equilibrium positions. Focusing our attention on this one atom we see that if it has sufficiently many near neighbors, the potential function has a high degree of spherical symmetry about the center of the cell in which the atom is confined. A slight adjustment in the actual potential function enables us to derive an approximate potential function which depends on "$r$" alone, where "$r$" is the distance from the center of the cell. Before deriving this approximate function we make the further assumption that only nearest neighbors contribute to the actual potential function. This assumption is not as drastic as it seems at first sight because the interatomic forces are of very short range and the contribution of atoms other than nearest neighbors to the potential function within a cell is small.

Let $\phi(x)$ represent the potential energy of one atom in the presence of another, where "$x$" is the distance between them. Then the potential at any point "$r$" in the cell (averaged so as to achieve spherical symmetry about the center of the cell) is given by[1]

$$W(r)=\frac{c}{2}\int_0^\pi \phi(z)\sin\theta d\theta, \tag{1}$$

where "$z$" is the distance from any point on the boundary of the cell to the point "$r$," $\theta$ is the angle which the line "$z$" subtends at the center of the cell and "$c$" is the number of nearest neighbors. If "$a$" is the radius of the cell (or the distance between nearest neighbors in their equilibrium positions) then

$$z=(a^2+r^2-2ar\cos\theta)^{\frac{1}{2}}. \tag{2}$$

The potential function $\phi(x)$ is known for a few substances from experimental data on the gaseous and crystalline state.[4] The most useful forms for the function are the two which follow:

$$\phi(x)=\lambda/x^s-\mu/x^6, \tag{3a}$$

$$\phi(x)=\lambda' e^{-px}-\mu'/x^6. \tag{3b}$$

All the quantities occurring in these expressions are determined empirically.

To evaluate $W(r)$ we introduce either of the expressions (3) into Eq. (1) and carry through the integrations. In what follows we shall perform the calculations for both forms of $\phi(x)$ and we shall adopt the convention that the primed quantities refer to an interatomic potential of type (3b) while unprimed quantities refer to an interatomic potential of type (3a).

$W(r)$ therefore depends on integrals of the form

$$I_1=\int_0^\pi \frac{1}{z^s}\sin\theta d\theta$$

and

$$I_2=\int_0^\pi e^{-pz}\sin\theta d\theta,$$

[4] R. H. Fowler, *Statistical Mechanics* (1936), Chapter X; R. A. Buckingham, Proc. Roy. Soc. **A168**, 264 (1938).

where "$z$" is given by (2). The integrations are simple and lead to the following results:

$$I_1=\frac{(1-\sqrt{y})^{2-\sigma}-(1+\sqrt{y})^{2-\sigma}}{2\sqrt{y}a^{\sigma}(\frac{1}{2}\sigma-1)}$$

and

$$I_2=\frac{2}{pa}e^{-pa}\left\{(pa+1)\frac{\sinh pa\sqrt{y}}{pa\sqrt{y}}-\cosh pa\sqrt{y}\right\},$$

where $y=r^2/a^2$. These expressions when introduced into (1) give $W(r)$ or $W(y)$, the potential field in which the atom in the liquid moves.

It is now necessary to assign a definite value to $\sigma$, and it has been found that $\sigma=12$ is the most satisfactory to choose.[2,4] With $\sigma=12$ the complete expression for $W(y)$ is

$$W(y)=m\left\{\frac{1+12y+25.2y^2+12y^3+y^4}{(1-y)^{10}}\right\}-n\left\{\frac{1+y}{(1-y)^4}\right\}, \quad (4)$$

where

$$m=c\lambda/a^{12} \quad \text{and} \quad n=c\mu/a^6.$$

It is evident that "$m$" and "$-n$" are the potentials at the center of the cell arising from the repulsive and attractive parts of $\phi$, respectively. The complete expression for $W'(y)$ is

$$W'(y)=\frac{m'}{pa}\left\{(pa+1)\frac{\sinh pa\sqrt{y}}{pa\sqrt{y}}-\cosh pa\sqrt{y}\right\}-n'\left\{\frac{1+y}{(1-y)^4}\right\}, \quad (5)$$

where

$$m'=c\lambda' e^{-pa} \quad \text{and} \quad n'=c\mu'/a^6.$$

An examination of (4) and (5) shows that while $W$ and $W'$ are relatively simple functions, they are much too complicated in their present form to be of service for the evaluation of a partition function. In the partition function they occur as the exponent of "$e$," and this expression must be integrated over a range of values of "$y$." Such an integral cannot be evaluated analytically. However both $W$ and $W'$ can be represented quite accurately, throughout most of the range of the liquid state, by the first few terms of their Taylor expansion in powers of "$y$." This expansion gives for $W(y)$

$$W(y)=E_0+E_1y+E_2y^2+E_3y^3+\cdots, \quad (6)$$

where

$$E_0=m-n, \quad (6a)$$

$$E_1=22m-5n, \quad (6b)$$

$$E_2=200.2m-14n, \quad (6c)$$

$$E_3=1144m-30n. \quad (6d)$$

The Taylor expansion for $W'$ takes a particularly elegant form because of the relation

$$\frac{1}{pa}\left\{(pa+1)\frac{\sinh pa\sqrt{y}}{pa\sqrt{y}}-\cosh pa\sqrt{y}\right\}=\sum_{\nu=0}^{\infty}\frac{(pa)^{2\nu-1}}{(2\nu+1)!}(pa-2\nu)y^{\nu}.$$

Thus we have

$$W'(y)=E_0'+E_1'y+E_2'y^2+E_3'y^3+\cdots, \quad (7)$$

where

$$E_0'=m'-n', \quad (7a)$$

$$E_1'=m'(pa/6)(pa-2)-5n', \quad (7b)$$

$$E_2'=m'[(pa)^3/120](pa-4)-14n', \quad (7c)$$

$$E_3'=m'[(pa)^5/5040](pa-6)-30n'. \quad (7d)$$

From this point the treatment for the two types of potential function will be identical because (6) and (7) are identical except for slightly different numerical values for the $E$'s. Furthermore, in what follows we shall assume the zero of potential energy to be that existing at the center of the cell. This is equivalent to dropping the term $E_0$ in the expression for $W(y)$. The term gives rise to no contribution to $C_v$ so we are justified in neglecting it. (However in computing some other properties of the liquid it would be necessary to retain $E_0$.) Therefore we take for $W(y)$

$$W(y)=E_1y+E_2y^2+E_3y^3+\cdots. \quad (8)$$

It is instructive now to study the function $W(y)$ in some detail. In the solid state the first term is the only one which is important. This is

because in a solid the amplitude of vibration of an atom or molecule is small and for small values of "$y$" the first term is by far the predominant one. (It is to be kept in mind that "$y$" varies from 0 to 1 and it is very seldom that an atom in a cell will have a value for "$y$" greater than $\frac{1}{4}$.) Thus for an atom in a solid we have

$$W(r)=E_1r^2/a^2=2\pi^2\mu\nu^2r^2,$$

where $\nu$ is the frequency of vibration of the atom, and $\mu$ its mass. This enables one to derive a relation between $E_1$ and $\Theta(=h\nu/k)$ the characteristic temperature of the solid: *viz*,

$$\Theta=(h/\pi ka)(E_1/2\pi)^{\frac{1}{2}}.$$

In the liquid state terms containing higher powers of "$y$" than the first begin to be important. For a considerable range of temperatures above the melting point the first two terms of (8) are sufficient to give a good representation of $W(y)$ for the values of "$y$" which are relevant. The first three terms are sufficient over nearly the whole range of the liquid state.

One other feature is to be noted: As the volume of the liquid increases the coefficients $E_1$, $E_2$, etc. steadily decrease. However, $E_1$ is the smallest of them all and it also decreases the most rapidly with increasing volume. Consequently there is a certain volume of the liquid at which $E_1$ becomes zero—at greater volumes $E_1$ is negative. This change in the sign of $E_1$ takes place just before the critical volume is reached. Then, $W(y)$, which usually increases with increasing "$y$," will at first decrease with increasing "$y$," giving rise to a region around the center of the cell in which the potential is lower than that at the center of the cell.

## III

With $W(y)$ given by (8), it is possible to handle the partition function for an atom in a cell without any great difficulty. In our first calculations it will be assumed that the first two terms of (8) are sufficient to give valid results. This will certainly be true for the region just above the melting point. With this form for $W(y)$ the partition function for a single atom is

$$f(T)=\left(\frac{2\pi\mu kT}{h^2}\right)^{\frac{3}{2}}2\pi a^3\int_0^1 e^{-(E_1v+E_2v^2)/kT}y^{\frac{1}{2}}dy, \quad (9)$$

where all the quantities have their usual meaning. Changing the variable in the integral from "$y$" to "$x$" by the transformation

$$y=kTx/E_1,$$

the partition function becomes

$$f(T)=S(V)T^3\int_0^{E_1/kT} e^{-x-\alpha x^2}x^{\frac{1}{2}}dx, \quad (10)$$

in which

$$S(V)=2\pi a^3N\left(\frac{2\mu\pi}{E_1}\frac{k^2}{h^2}\right)^{\frac{3}{2}}$$

(a function of the volume only) and

$$\alpha=E_2kT/(E_1)^2. \quad (11)$$

A numerical consideration of the quantities occurring in the integral on the right of (10) shows that the integrand becomes extremely small long before the upper limit of "$x$" is reached. Hence the upper limit can be replaced by infinity without introducing any noticeable error. Then the partition function takes the compact form

$$f(T)=S(V)T^3I(\alpha;\tfrac{1}{2}), \quad (12)$$

where

$$I(\alpha;s)=\int_0^\infty e^{-x-\alpha x^2}x^s dx.$$

For the Helmholtz free energy per mole we have[5]

$$A=-kT\ln[f(T)]^N,$$

where $N$ is Avogadro's number. (Strictly speaking the logarithmic part of the free energy should contain some such factor as $N^N/N!$ but we will not be concerned with such constant factors as they do not contribute to $C_v$.) The internal energy $E$ is related to $A$ as follows:

$$E=A-T\partial A/\partial T \text{ or } E=RT^2\partial\ln f(T)/\partial T, \quad (13)$$

where $R$ is the gas constant per mole. Using (12) for $f(T)$, we find for $E$ (neglecting the part arising from the term $E_0$)

$$E=3RT-RT\alpha\frac{I(\alpha;5/2)}{I(\alpha;1/2)}. \quad (14)$$

[5] R. H. Fowler, reference 4, Chapter VI.

Eq. (14) is obtained with the help of the relation

$$T\partial I(\alpha; s)/\partial T = -\alpha I(\alpha; s+2). \quad (15)$$

When $\alpha$ is zero ($E_2=0$), i.e., when the motion of the atoms is simple harmonic, (14) gives $E=3RT$ as it should. It is also easy to evaluate $E$ when $\alpha$ is infinite ($E_1=0$). This will correspond to conditions existing near the critical point. It is easy to show that

$$\operatorname{Lim}_{\alpha\to\infty} \frac{I(\alpha; 5/2)}{I(\alpha; 1/2)} = \frac{3}{4\alpha}. \quad (16)$$

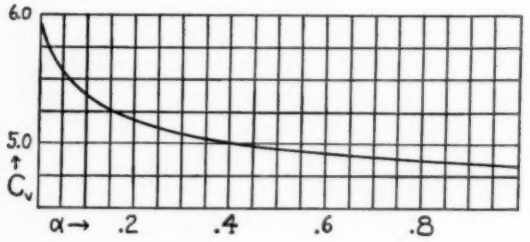


FIG. 1. $C_v$ as a function of $\alpha$ as computed from Eq. (17).

Consequently $E\to 9RT/4$ as $\alpha\to\infty$. Of course this method is only an approximation in the neighborhood of the critical point, but more refined calculations indicate that $E$ actually has a value very close to that given above. Thus we see that the internal energy per mole of a monatomic liquid ranges from a value near $3RT$ at the melting to a value near $9RT/4$ at the critical point.

The specific heat at constant volume is obtained from $E$ by differentiation with respect to $T$. The equation obtained for $C_v$ by this process is quite complicated but it can be simplified by the use of (15) and the following recurrence formula for the $I$ functions:

$$(s+1)I(\alpha; s) = I(\alpha; s+1) + 2\alpha I(\alpha; s+2).$$

In its simplest form the expression for $C_v$ is

$$C_v = 3R - R\{15/16 - (\alpha+1/4)\eta + \alpha^2\eta^2\}, \quad (17)$$

where

$$\eta = \frac{I(\alpha; 5/2)}{I(\alpha; 1/2)}.$$

When $\alpha=0$ Eq. (17) should give a value of $3R$ for $C_v$ since then we have an assembly of simple harmonic oscillators as pointed out above. It is easy to show that

$$\operatorname{Lim}_{\alpha\to 0} \eta = \frac{15}{4}$$

and with this value of $\eta$ it is obvious that $C_v=3R$ as required. Also when $\alpha$ is infinite $C_v=9R/4$. Thus we see that the specific heat of a monatomic liquid ranges from a value near $3R$ at the melting point to a value near $9R/4$ at the critical point. As before, the approximate nature of this result near the critical point must be borne in mind. Below we give a method for deriving a more correct result in this region.

The validity of formula (17) has been checked by a detailed calculation of $C_v$ for liquid argon. This calculation has been carried through for both types of interatomic potential (3a) and (3b). The values of the constants $\lambda$, $\mu$ and $p$ have been taken from a recent paper by R. A. Buckingham.[4] The first step is to find the value of $\alpha$ at different temperatures of the liquid. But $\alpha$ is a function of $E_1$ and $E_2$ and these are in turn functions of $\lambda$, $\mu$, $p$, $c$ and $a$. It has been assumed that "$a$," the distance between nearest

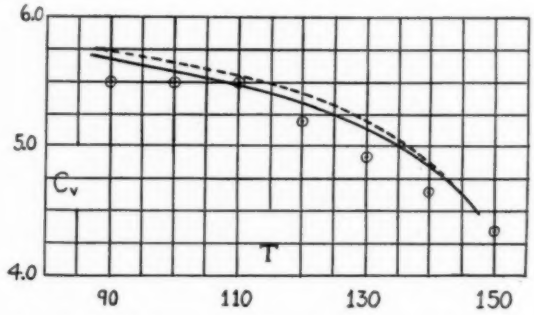


FIG. 2. Solid line gives $C_v$ calculated on the basis of (3a); dotted line on the basis of (3b). Circles represent experimental points.

neighbors when the atoms are at rest in their equilibrium positions, is given by

$$a = (V/N)^{\frac{1}{3}},$$

where $V$ is the volume of one mole of the liquid. The value of "$c$" is 12. We have obtained $V$ from the orthobaric densities of argon as given in the *International Critical Tables*. Having obtained a series of values of $\alpha$, it is next necessary to compute the functions $I(\alpha; 5/2)$ and $I(\alpha; 1/2)$

for these values. If $\alpha$ is less than about 0.5, it is necessary to resort to numerical integration, which however is not laborious, because of the simplicity of the $I$ functions. If $\alpha>0.5$ the following expansion is convenient:

$$I(\alpha;s)=\frac{1}{2(\sqrt{\alpha})^{s+1}}\sum_{n=0}^{\infty}\frac{(-1)^n}{n!}\frac{1}{(\sqrt{\alpha})^n}\times\Gamma\left(\frac{n+s+1}{2}\right). \quad (18)$$

For each value of $\alpha$ there is a definite value of $C_v$ given by (17). This functional relationship is shown graphically in Fig. 1. Such a curve is very useful because it gives $C_v$ immediately for any value of $\alpha$ up to $\alpha=1$, and most values of $\alpha$ lie within this range.

In Fig. 2 the experimental and calculated values of $C_v$ are plotted for comparison. The solid line gives $C_v$ calculated on the basis of (3a), the dotted line on the basis of (3b). The experimental values are those given by Eucken.[6] The agreement between theory and experiment is as good as could be expected when one recalls that only two terms in the expression for $W(y)$ have been included. The effect of including a third term in $W(y)$ would be to lower the theoretical values somewhat at the higher temperatures and to leave the values at the lower temperatures practically unchanged. It is of interest that an interatomic potential of the form (3a) with $\sigma=10$ and the values of $\lambda$ and $\mu$ given by Fowler does not give nearly as good agreement with experiment as the two forms which have been used.

## IV

The computations are considerably more complicated when three terms of $W(y)$ are introduced into the partition function. However, it is possible to calculate $C_v$ for this case at the point at which $E_1=0$ without undue difficulty. For liquid argon $E_1=0$ at about 148 degrees absolute. At this point the above theory gives $C_v=9R/4$.

[6] A. Eucken and F. Hanck, Zeits. f. physik. Chemie **134**, 161 (1928).

From the more complete partition function, we get

$$E=3RT-RT\left\{\alpha\frac{J(\alpha;\beta;5/2)}{J(\alpha;\beta;1/2)}+2\beta\frac{J(\alpha;\beta;7/2)}{J(\alpha;\beta;1/2)}\right\}, \quad (19)$$

where

$$J(\alpha;\beta;s)=\int_0^{\infty}e^{-x-\alpha x^2-\beta x^3}x^s dx$$

and

$$\alpha=E_2kT/(E_1)^2, \quad \beta=E_3(kT)^2/(E_1)^3.$$

Eq. (19) is obtained with the help of

$$T\partial J(s)/\partial T=-\alpha J(s+2)-2\beta J(s+3). \quad (20)$$

(The arguments $\alpha$ and $\beta$ will be omitted from the $J$ functions since no ambiguity arises from so doing.) Inspection shows that when $\beta=0$ ($E_3=0$), (19) is identical with (14).

The following recurrence formula for the $J$ functions

$$(s+1)J(s)=J(s+1)+2\alpha J(s+2)+3\beta J(s+3),$$

and Eq. (20) enable $C_v$ to be expressed in the form

$$C_v=3R-R\left[\frac{10}{9}\frac{J(3/2)}{J(1/2)}+\frac{4}{9}(\alpha-1)\frac{J(5/2)}{J(1/2)}-\frac{4}{9}\alpha\frac{J(7/2)}{J(1/2)}-\frac{1}{9}\alpha^2\frac{J(9/2)}{J(1/2)}+\left\{1-\frac{2}{3}\frac{J(3/2)}{J(1/2)}-\frac{1}{3}\alpha\frac{J(5/2)}{J(1/2)}\right\}^2\right]. \quad (21)$$

A useful check on this formula is the fact that when $\beta=0$ it goes over into Eq. (17).

For large values of $\alpha$ and $\beta$ the $J$ functions are given by the expansion

$$J(\alpha;\beta;s)=\frac{1}{(\sqrt{\alpha})^{s+1}}\sum_{n=0}^{\infty}\frac{(-1)^n}{n!}\frac{1}{(\sqrt{\alpha})^n}P(s+n), \quad (22)$$

where

$$P(m)=\int_0^{\infty}e^{-x^2-\gamma x^3}x^m dx$$

and

$$\gamma=E_3(kT)^{\frac{1}{2}}/(E_2)^{\frac{3}{2}}.$$

When $\alpha=\beta=\infty$ ($E_1=0$) the expression for $C_v$ assumes a very simple form. This arises from the fact that

$$\lim_{\alpha,\ \beta\to\infty} J(s)=\frac{P(s)}{(\sqrt{\alpha})^{s+1}}$$

as is immediately evident from (22). Thus for liquid argon at 148 degrees we have $C_v$ given by

$$C_v=3R-R\left\{\frac{4}{9}\frac{P(5/2)}{P(1/2)}-\frac{1}{9}\frac{P(9/2)}{P(1/2)}+\left(1-\frac{1}{3}\frac{P(5/2)}{P(1/2)}\right)^2\right\}. \quad (23)$$

A useful check can be applied to this formula because when $\gamma=0$ ($E_3=0$) it should give $C_v=9R/4$. Since for $\gamma=0$ we have

$$P(1/2)=\Gamma(3/4);\quad P(5/2)=\Gamma(7/4);\quad P(9/2)=\Gamma(11/4),$$

it can easily be shown that this is the case.

Equation (23) gives a value of 4.27 rather than 4.47 as given by the former theory for the specific heat of argon at 148 degrees. This indicates that the specific heat as calculated by the simpler method should be lowered by approximately two-tenths of a calorie per mole at the higher temperatures, thus making the agreement between theory and experiment considerably better than that indicated in Fig. 2. It should be emphasized that three terms give a very good representation of the complete function $W(y)$ throughout the range of temperatures considered here and it is not to be expected that the addition of further terms would lower the calculated values appreciably.

There is evidence which indicates that as the melting point of a monatomic liquid is approached, $C_v$ rises quite rapidly to a value above $3R$ at the melting point.[7] The experimental values of Eucken do not extend sufficiently close to the melting point to exhibit this phenomenon for liquid argon. However it is probable that a careful investigation would reveal behavior of this sort in this region. It is suggested that the "extra" specific heat near the melting point arises from the internal energy associated with the short range order which has been shown to exist at and above this point.[8] This internal energy is quite distinct from the internal energy calculated by the present theory and becomes insignificant at temperatures much above the boiling point.

---

[7] E. Bauer, M. Magat and M. Surdin, J. de phys. et rad. **7**, 441 (1936).

[8] J. E. Lennard-Jones and A. F. Devonshire, Proc. Roy. Soc. **A169**, 317 (1939).

# Magnetic Test for Superstructure in Permalloy*

S. T. PAN
*Massachusetts Institute of Technology, Cambridge, Massachusetts*
(Received July 27, 1939)

A search for indirect evidence of the existence of superstructures $FeNi_3$ and $Fe_2Ni_2$ by a magnetic method is described. In a preliminary test, it was found that annealing at a temperature around 450°C for two to three days followed by slow cooling at a rate of about 40°C per hour increased the saturation magnetization by 3.9 percent in Permalloy and 1.3 percent in Hipernik over the values found after the alloys were quenched from above 900°C. These increases were reproducible and the magnitudes depended somewhat on the exact way of heat-treatment. This makes it seem likely that at least partial order exists in the annealed alloys. Subsequent measurements taken after annealing at, and quenching from, different temperatures showed that the assumed ordering process takes place in temperature ranges 640°C–400°C and 800°C–400°C for the 76Ni–24Fe and 50Ni–50Fe alloys, respectively. The saturation magnetization *vs.* temperature curves for the quenched and the slowly cooled states of the 76Ni–24Fe alloy have also been taken. At a rather slow cooling rate, about 30°C per day from 700°C to room temperature, the increase in saturation value at room temperature is 6.0 percent. All these results agree very well with those just reported by McKeehan and Grabe, Sucksmith, and P. Leech and C. Sykes.

ALLOYS corresponding to the compositions $FeNi_3$ and $Fe_2Ni_2$ both belong to the $\gamma$-phase of the Fe–Ni series. Commercially they are known as Permalloy and Hipernik. Because of their remarkable magnetic properties after suitable heat-treatments, the existence of superstructures $FeNi_3$ and $Fe_2Ni_2$ were postulated long ago, particularly the former. Owing to the great similarity of the iron and nickel atoms, direct evidences of the existence of these superstructures by x-ray are very difficult to obtain. Up to the time when this work was partly carried out, no conclusion had been reached from x-ray diffraction results, while less direct and indirect evidences were somewhat ambiguous, though the works of Dahl[1] and of Kaya[2] strongly supported the existence of $FeNi_3$. Among the phenomena that can be used as indirect criteria for the existence of order and disorder transformation, the change of saturation magnetization at room temperature with heat-treatment is usually taken as an important one. It has been generally supposed that there are no changes of saturation magnetization in Permalloy and Hipernik with heat-treatment; no particular investigation had been made along this line when this work was partly completed. However, McKeehan and Grabe[3] reported lately in their work on the magnetic anisotropy of a Permalloy that they found a few percent change of saturation magnetization with heat-treatment.

The purpose of this investigation was to see whether there are some changes in saturation magnetization at room temperature with heat-treatment in Permalloy and in Hipernik, and, if there are some, whether they take place in definite temperature ranges. The approach to the problem was essentially the same as that used by Kussmann and Nitka[4] in the case of $PtNi_3$.

## EXPERIMENTAL

Very pure 76-percent Ni Permalloy was kindly supplied us by Dr. F. C. Nix of the Bell Telephone Laboratories. Commercial Hipernik was purchased from the Westinghouse Electric and Manufacturing Company. This is a 50 percent Fe-50 percent Ni alloy with a little Mn and Si added for forgeability. The specimens are in the form of wires of about 4 cm length and of appropriate diameters so that each gives a total saturation magnetic moment of 6 to 7 absolute units. These were made by first swagging small pieces of the materials into thin rods and then drawing into wires.

The measurements were carried out by an

* Part of the material is condensed from a thesis submitted in candidacy for the degree of Master of Science to the faculty of the Graduate School at the Massachusetts Institute of Technology, February, 1939.

[1] O. Dahl, Zeits. f. Metallkunde **28**, 133 (1936).

[2] S. Kaya, J. Faculty of Sci., Hokkaido Imp. Univ., Series II, **11**, 29 (1938).

[3] L. W. McKeehan and E. M. Grabe, Phys. Rev. **55**, 505 (1939).

[4] A. Kussmann and H. Nitka, Metallwirschaft **24**, 657 (1938).

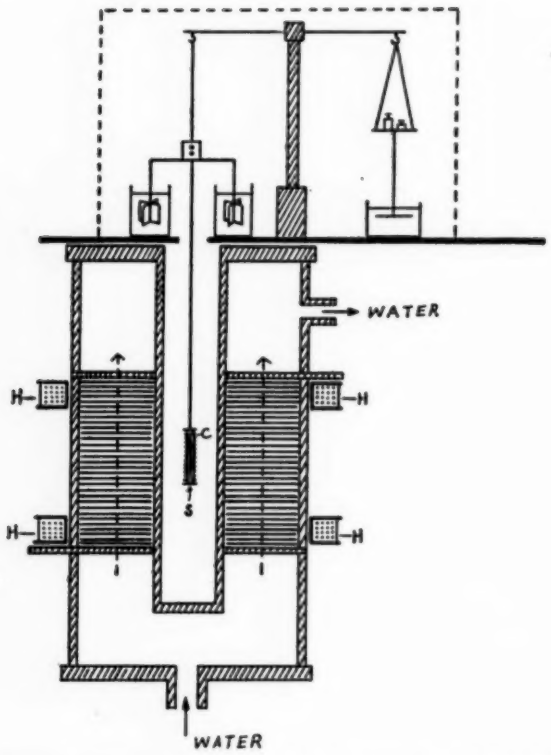


FIG. 1. Diagram of the magnetic balance. *H*—Helmholtz coils; *C*—compensation coil; *S*—specimen.

apparatus to be used for measuring ferromagnetic magnetization at high fields with the new air-solenoid type of electromagnet designed by Professor F. Bitter[5] in this laboratory. The construction of the apparatus is a combination of an ordinary balance and a torsion balance and is actually some modification of an apparatus designed by McKeehan.[6] A schematic diagram is shown in Fig. 1. It makes application of the well-known principle that when a small isotropic ferromagnetic body of volume $v$ is magnetized to a magnetization $I$ in a field $H$, which has a gradient along its direction $x$, say, then the body will experience a force in this direction given by

$$F = IvdH/dx.$$

If $v$ and $dH/dx$ are known, by measuring $F$, one can calculate $I$. In the present design, instead of measuring $F$, we use a null method. The specimen is placed in a hollow cylinder in the spool of a small coil of about the same length as the specimen. This coil is then suspended at the middle of the electromagnet from one arm of a lever, which in turn is supported at its center by a torsion ribbon. The weight of the coil, etc. is balanced by weights in a pan at the other arm of the lever. A uniform field gradient superposed on the main field is produced by a pair of Helmholtz coils connected in opposition. This gradient exerts force on the magnetized specimen and displaces the lever. A concave mirror attached on the lever together with a lamp-and-scale system magnifies the displacement. By passing a current through the coil surrounding the specimen so that the magnetic moment of the coil is equal and opposite to that of the specimen, the equilibrium position of the lever can be restored. Two vanes and a disk, all immersed in oil, are attached to the suspension for the coil and to the pan, respectively, to damp out the lateral and vertical motions of the coil. The system is very stable and a reading can be taken in a few seconds. With a specimen of total saturation moment of about 6 absolute units and a field gradient of 30 oersteds/cm, a sensitivity of 2 parts in 1000 is obtained without difficulty. The magnetization of the specimen is calculated in terms of the current through the coil, which current, as it is of the order of a few tenths of an ampere, can be easily measured to the fourth or fifth figure. Therefore, the final accuracy depends solely upon the equivalent area of the coil. In the present case, however, what we are interested in are relative changes only.

The magnet consists essentially of a cylindrical coil with square ends, the outer and inner radii being 4 inches and 1 inch, respectively. The field current goes from about 50 amperes up to 1000 amperes, giving fields from about 500 oersted to 10,000 oersted. Within an available space of 6 cm length and 3 cm diameter, the field is uniform to 1 percent.

As an example for the working conditions of the apparatus, two typical magnetization curves of a commercial nickel wire are shown in Fig. 2. One curve was taken after the wire had been filed down in the shape of an ellipsoid of revolution but was so reduced as though the specimen had had the original total saturation moment.

[5] F. Bitter, Rev. Sci. Inst. **7**, 479–488 (1936); **8**, 318 (1937). See also a paper by F. Bitter which will appear concurrently in the Rev. Sci. Inst., the magnet used here being designated as Magnet No. 2 there.

[6] L. W. McKeehan, Rev. Sci. Inst. **5**, 265 (1934).

The ordinates plotted are the currents through the compensation coil. These curves show that in the range of field we used, the magnetization differed very little, whether the specimen is a cylindrical rod or an ellipsoid.

Since the above apparatus cannot be used for high temperatures, we modified it for taking magnetization *vs.* temperature curves by hanging the specimen, which was sealed in vacuum in a quartz tube, from one arm of a chemical balance and measuring the force produced by a constant field gradient directly. A tube furnace was fixed in the available space of the magnet. The relative accuracy was only about 1 percent. A copper weight of about 40 to 50 grams had to be hung under the quartz tube to prevent the specimen from being attracted to the side.

## Results and Conclusion

By a suitable arrangement, the specimens could be annealed in hydrogen and quenched in water without being exposed to air. They were first quenched from a temperature between 900°C and 1000°C and measured. Then they were heated to above 900°C again, slowly cooled to about 450°C, remaining at this temperature for more than 48 hours and then cooled at a rate of about 40°C to 50°C per hour to room temperature. The saturation magnetizations were measured again. It was found that after the second treatment, the saturation magnetization increased by 3.9 percent in Permalloy and 1.3 percent in Hipernik. The same process repeated with the same specimens and also with other specimens showed that these increases could be reproduced, small differences in magnitude being explained by the fact that the annealing times and cooling rates were not exactly the same.

The next point of interest was to see in what definite temperature ranges, the increases found

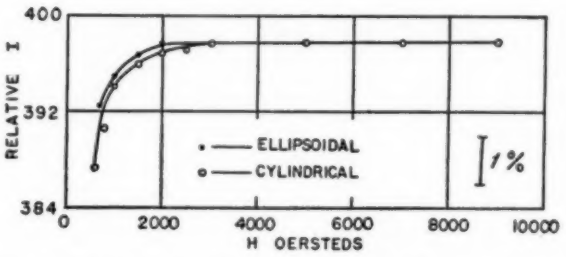


Fig. 2. Typical magnetization curves of a nickel specimen.

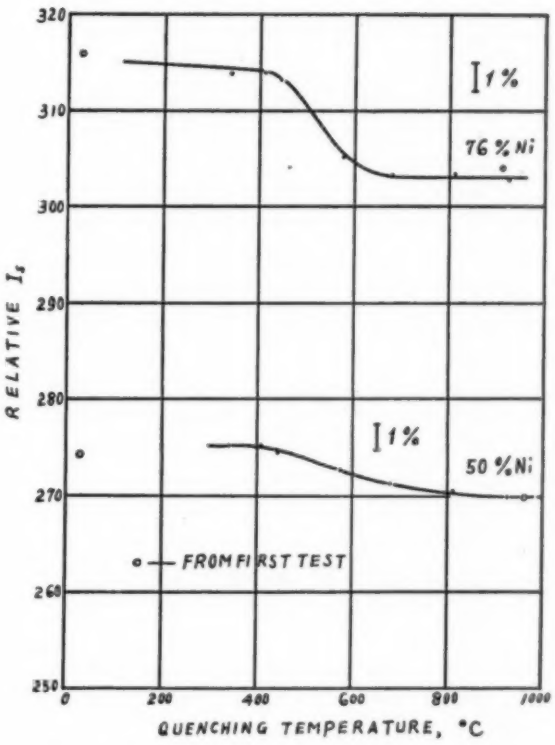


Fig. 3. Saturation magnetization *vs.* quenching temperature.

in saturation magnetization took place. This was done by annealing at, and quenching from, successive temperatures, starting from the highest temperatures, and measuring saturation magnetization after each quenching. Each temperature was of course reached from slow cooling and the time during which the specimens remained at that temperature depended upon the temperature, being from a few hours for the highest temperatures to 48 to 80 hours for temperatures below 700°C. The results are shown in Fig. 3, the ordinates plotted being again the current through the compensation coil. For each point, a complete curve was actually taken to make sure that saturation was approached. It is seen that the temperature range within which the saturation magnetization has any sensible increase is very conspicuous in the case of the Permalloy, being 640°C–400°C, but less conspicuous in Hipernik, being about 800°C–425°C. The values from the first test are also plotted in the same figure as circles.

The saturation magnetization *vs.* temperature curves for the Permalloy in the quenched and the

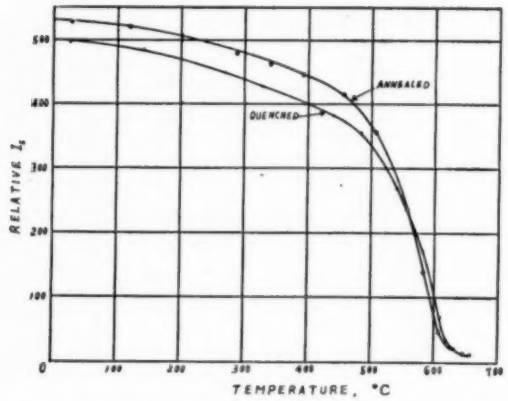


FIG. 4. Saturation magnetization of Permalloy *vs.* temperature.

annealed states were taken on nine pieces of length 1.3 cm from the same wire. They were sealed into the quartz tube after quenching from 1000°C. A curve was taken and then the specimen was annealed while it remained in the magnet. By cooling the specimen very slowly—about 30°C per day—from 700°C to room temperature—the increase in saturation magnetization was larger than ever before, being 6.0 percent at room temperature. The curves are shown in Fig. 4, the ordinate being the force on the specimens in milligrams. The weight under the quartz tube produced no error because it was hung at a place where the field gradient was negligible. In order to minimize errors due to ferromagnetic impurities, the thermocouple measuring the temperature was not fixed closely on the quartz tube, but was a few millimeters from the specimen, hence the temperature read might be a few degrees from the true temperature at the specimen. The curves show no marked abnormality. The interesting point is that they are almost coincident near the curie point. This is expected since it has been seen above that the increment of saturation magnetization after annealing disappears almost completely near 600°C. The crossing of the two curves may be due to a little displacement of the thermocouple or possibly be a true temperature hysteresis. We did not take similar curves for Hipernik because the apparatus was not sufficiently sensitive to warrant detailed measurements of the small effect in this alloy.

The changes in saturation magnetizations in Permalloy and Hipernik, though small in magnitude, are in every respect similar to those in $PtNi_3$[4] and $MnNi_3$.[7] This indicates probably that at least some partial ordering process exists in these alloys.

In a work just published by Leech and Sykes,[8] definite x-ray evidence for $FeNi_3$ was established for the first time, and was confirmed by Haworth.[9] Our result as to the temperature range within which the order-disorder transformation of Permalloy takes place agrees very well with Leech and Sykes' from specific heat measurements. Also, the saturation magnetization *vs.* temperature curves are about the same as those taken by Sucksmith reported in Leech and Sykes' paper. Since the change in saturation magnetization at room temperature is 5 percent as found by Sucksmith, and Leech and Sykes conclude that their samples are almost complete in the order-disorder transformation, a change of saturation magnetization of about 5 to 6 percent is probably the highest we can expect in Permalloy. Our experience also shows that the transformation in Permalloy is very sluggish and still more sluggish in Hipernik. It seems also justifiable to say that some degree of long range order is almost certain in the 50Ni–50Fe alloy.

In conclusion, the writer takes pleasure to express his indebtedness to Professor F. Bitter for suggesting this problem and for his advice and encouragement during the work; to Dr. A. R. Kaufmann for many valuable aids. Funds for carrying out this investigation were obtained in part from a grant made to Professor F. Bitter by the Joseph Henry Fund of the National Academy of Science for magnetic study of alloys.

[7] S. Kaya and A. Kussmann, Zeits. f. Physik **72**, 293 (1931).
[8] P. Leech and C. Sykes, Phil. Mag. **27**, 742 (1939).
[9] F. E. Haworth, Phys. Rev. **56**, 289 (1939).

# Energy Fluctuations in the Electromagnetic Field

P. MORRISON
*Department of Physics, University of California, Berkeley, California*
(Received September 5, 1939)

Born and Fuchs have recently pointed out that the energy fluctuations of the electromagnetic field contain terms, coming from the possibility of the emission and reabsorption of pairs of quanta, that do not occur in the energy fluctuations of a Bose gas. There are two such terms: One is a function of the occupation numbers which specify the state of the field, and is a surface term, proportional to the surface area of the volume in which the fluctuations are measured. The second term is a zero-point fluctuation, independent of the number of quanta in the field, and is infinite. The introduction of an essential indeterminacy in the time of measurement reduces the number of high energy quanta made by the rapidly varying time Fourier components of the charges and currents which make up the bounding walls of the test region, and makes the zero-point term a finite surface effect. With such a time indeterminacy and the use of a test volume of dimensions large compared to the wave-lengths involved, the fluctuations can be made as close as desired to those of the Bose gas.

## I

THE problem of the energy fluctuations of the electromagnetic field has been discussed from a quantum-mechanical point of view by many authors. Indeed, one of the early successes of the quantum mechanics[1] was the agreement between the quantum-mechanical formula and that calculated by Einstein using thermodynamical and statistical arguments appropriate to a Bose gas. Most of the quantum-mechanical calculations were made by exploiting the analogy between the electromagnetic field and a gas of Bose particles, writing the energy density of the field as the energy density of a Bose gas. Such a calculation was, for example, made by Heisenberg[2] in a one-dimensional case, using a non-relativistic connection between energy and momentum. He obtained a divergent result, which could be made to agree with the thermodynamic value by "smearing" the boundaries of the region in which the fluctuations were measured. The first straightforward calculations using the formalism of the electromagnetic field are those of Born and Fuchs.[3] Though their detailed results are misleading because of an error of calculation they have correctly pointed out the over-idealization of treatments like that of Heisenberg, which by making use of the analogy to the Bose gas miss some essential features of the present problem.

In the fluctuations of the electromagnetic energy, processes play a part which are not provided for in the formalism of an assembly of Bose particles. These are two-quantum processes, in which the contribution to the fluctuation energy is made by the simultaneous emission of two quanta, followed by their reabsorption. For the particles, only processes in which a single particle is created and destroyed occur. The two-quantum processes contribute nothing to quantities like the total energy and the total momentum of the field, where measurement involves contributions from the entire enclosure—for example, a metal box, in which the fields vanish at the walls. Then the analogy to the Bose particles is strict. But for quantities like the energy fluctuations within a volume which is only part of the box, the two-quantum terms contribute essentially.

We write $\bar{E}$ for the energy in the partial volume. $\bar{E}$ is the integral over a volume $V$ of the energy density. The energy density $u$ is expressed in terms of the quantized field strengths $\mathcal{E}$ and $H$, $u=(\mathcal{E}^2+H^2)/8\pi$. A given condition of the electromagnetic field is here specified by assigning a fixed number of quanta to every state. The measurement of $\bar{E}$ is repeated again and again with this specified condition of the field. The

[1] M. Born, W. Heisenberg and P. Jordan, Zeits. f. Physik **35**, 557 (1926).
[2] W. Heisenberg, Ber. sachs. Ges. (Akad.) Wiss., M.-P. Kl. **81**, 3 (1931).
[3] M. Born and K. Fuchs, Proc. Roy. Soc. **170**, 252 (1939). *Note added in proof.*—They have corrected this error in Proc. Roy. Soc. **172**, 465 (1939).

mean square fluctuation to be computed here is a direct measure of the broadness of the distribution of these repeated measurements around their average value. Formally we write $\Delta=\langle\bar{E}^2\rangle_{Av}-\langle\bar{E}\rangle_{Av}^2$ where $\langle O\rangle_{Av}$ means the expectation value of the quantity $O$ for the given state of the field, i.e., assignment of quanta.

We can write $\Delta=\Delta_s+\Delta_t$. Here $\Delta_s$ is the part of the fluctuation depending only on "single-quantum" processes, while $\Delta_t$ is the part in which two-quantum processes occur. $\Delta_s$ is identical with the fluctuations in the case of the assembly of Bose particles, but $\Delta_t$ has no analog in that problem. If we take a volume $V$ for the definition of $\bar{E}$ such that the linear dimensions contain many wave-lengths of the longest waves to be considered (a restriction essential for the measurement of wave-length), the term gives just the energy fluctuation in a given energy range that is expected from thermodynamics, the familiar result $\Delta_s(k)dk=8\pi N_k(N_k+1)k^4dk$. Here $N_k$ is the number of quanta in unit energy at the energy $k$, and is taken as slowly varying. The term $\Delta_s$ thus gives us what we expect for a gas of particles obeying the Bose statistics.

For any partial volume, however, the term $\Delta_t$ appears. It can be broken up into two parts, $\Delta_t=\Delta_n+\Delta_0$, with $\Delta_0$ independent of the occupation numbers assigned to the field. $\Delta_0$ is a kind of zero-point fluctuation. The contributions of the two-quantum term $\Delta_n$ are proportional, not to the volume $V$ like the normal term $\Delta_s$, but to the surface of that volume. Hence for sufficiently large linear dimensions for $V$, the result agrees with the thermodynamic as far as $\Delta_s$ and $\Delta_n$ are concerned.

The zero-point term requires special handling. For any physically possible assignment of occupation numbers, the terms $\Delta_s$ and $\Delta_n$, which depend on the occupation numbers, converge for high momenta, since the $N_k$'s must approach zero. The term $\Delta_0$ has no $N_k$; and its contribution to the fluctuations is in fact infinite, diverging like $\int k^3dk$. This divergence can be removed by modifying the conditions of measurement.

For definiteness, and in analogy to the problem of charge fluctuations in positron theory,[4] we think of measuring the energy content of the volume $V$ by measuring the normal component of the gravitational field over its surface. This is done by determining the acceleration of test masses distributed over that surface. If the test masses occupy a finite volume, the region in which the energy is being measured cannot be sharply defined; if the measurement of acceleration takes a finite time, the energy measured will be some time average of the energy in $V$. In the case of the charge fluctuations, a finite volume and time for these surface measurements is enough to give finite fluctuations in charge, fluctuations proportional to the surface of the region. In our problem of energy fluctuations, averaging the energy over a finite time, and "smearing" the volume, reduce the order of divergence but do not give finite zero-point fluctuations. Only by leaving the time of measurement essentially indeterminate do we get a finite result, because only in this case can the measurement be carried out without the creation of many quanta of infinitely high energy. Formally we may describe this by introducing a smeared time for the measurement, with an indeterminacy which we may take small compared to $V^{\frac{1}{3}}/c$, so that it affects the other terms $\Delta_s$ and $\Delta_n$ little. The fluctuations then turn out of the order $V^{\frac{1}{3}}(h/\tau)^2(1/c\tau)^2$, proportional to the surface of the region and not to its volume, and of course becoming infinite as $\tau$ vanishes. This corresponds to the creation of a surface density of quanta with energy $h/\tau$ equal to $(1/c\tau)^2$ quanta per unit area.

Another method of measurement is carried out by introducing reflecting walls which isolate the region $V$, removing it from the enclosure, and measuring its mass, say by weighing. Here there is no question of averaging the energy content of $V$ over a time interval, unlike the previous measurement, where the time average is clearly brought in by the measurement of acceleration. Here we measure the energy content of the box at the time it was isolated. On the other hand, the physical content of the indeterminacy in the time of measurement is clear. The charges and currents which make up the reflecting walls have time Fourier components which make quanta of all frequencies. The smearing of the time guarantees that Fourier components of arbitrarily high frequency do not come in; hence few such high

[4] J. R. Oppenheimer, Phys. Rev. **47**, 144 (1935).

energy quanta are made and the zero-point fluctuations are finite. The reason that the space "smearing" alone, which reduces the short wavelength Fourier components of the surface charges and currents, does not make the fluctuations finite, is that the processes involved are the emission and reabsorption of two quanta, which may be of high energy and still have low resultant momenta if they are nearly antiparallel.

It is worth noting that the infinite zero-point energy fluctuation is in principle measurable, unlike the purely formal difficulty of the infinite zero-point energy. The zero-point energy is independent of the occupation numbers, and therefore cannot affect the fluctuations in any way. Every term of the energy fluctuations that differs from the expected Bose gas result comes from the possibility of emitting and absorbing pairs of quanta. The divergent zero-point fluctuation corresponds to the infinite creation of quanta over the surface of the region to be studied by the instantaneous introduction of measuring devices.

## II

We consider the electromagnetic field quantized in plane waves in the open interval. The vector potential is:

$$\mathbf{A}(\mathbf{x},t)=\sum_k \mathbf{e}_k/(2\pi k)^{\frac{1}{2}}[c_k \exp(2\pi i(\mathbf{k}\cdot\mathbf{x}-kt)) + c^*_{-k}\exp(2\pi i(\mathbf{k}\cdot\mathbf{x}+kt))]$$

with

$$\sum_k \text{ written for } \int d\mathbf{k}\sum_\lambda,$$

and

$$\text{subscript } k \text{ for } \mathbf{k},\lambda;\ -k\rightarrow-\mathbf{k},\lambda,$$

where $\hbar$ and $c$ are taken as unity, and the $\mathbf{e}_k$ are unit vectors in two orthogonal directions of polarization, indexed by $\lambda$, forming with the propagation vector $\mathbf{k}$ a right-handed axis system. The electric and magnetic field strengths are:

$$\mathcal{E}=-\frac{\partial\mathbf{A}}{\partial t}=i\sum_k \mathbf{e}_k(2\pi k)^{\frac{1}{2}}[c^*_{-k}\exp(2\pi i(\mathbf{k}\cdot\mathbf{x}+kt) - c_k\exp(2\pi i(\mathbf{k}\cdot\mathbf{x}-kt))],$$

$$H=\operatorname{curl}\mathbf{A}=i\sum_k[\mathbf{n}_k\times\mathbf{e}_k](2\pi k)^{\frac{1}{2}} \times[c^*_{-k}\exp(2\pi i(\mathbf{k}\cdot\mathbf{x}+kt) + c_k\exp(2\pi i(\mathbf{k}\cdot\mathbf{x}-kt))]$$

with

$$\mathbf{n}_k=\mathbf{k}/k.$$

Here the operators $c$ and $c^*$ are independent of $(\mathbf{x},t)$, and obey the usual commutation laws $[c_k, c_{k'}{}^*]=\delta_{\lambda\lambda'}\delta(\mathbf{k}-\mathbf{k}')$. We form the expression for the energy density $u=(\mathcal{E}^2+H^2)/8\pi$, and compute $\bar{E}$, the integral of $u$ over a specified volume $V$.

$$\bar{E}=\tfrac{1}{2}\sum_k\sum_{k'}(kk')^{\frac{1}{2}}[k;k'][(c_kc^*_{k'}+c^*_kc_{k'})f(\mathbf{d}) - (c_kc_{k'}+c^*_kc^*_{k'})f(\mathbf{s})]$$

with

$$\mathbf{d}=\mathbf{k}-\mathbf{k}',\quad \mathbf{s}=\mathbf{k}+\mathbf{k}'$$

$$[k;k']=\mathbf{e}_k\cdot\mathbf{e}_{k'}+[\mathbf{n}_k\times\mathbf{e}_k]\cdot[\mathbf{n}_{k'}\times\mathbf{e}_{k'}],$$

$$f(\mathbf{k})=\int_V d\mathbf{x}\exp(2\pi i\mathbf{k}\cdot\mathbf{x}).$$

For a state of the field determined by the occupation numbers $N_k$, we find for the expectation value of $\bar{E}$,

$$\langle\bar{E}\rangle_{\text{Av}}=\frac{V}{2}\sum_k k(N_k+(N_k+1)).$$

The only terms in $\bar{E}^2$ which have equal numbers of $c$ and $c^*$ and can thus have a nonvanishing expectation value are:

$$\bar{E}^2=\tfrac{1}{4}\sum_k\sum_{k'}\sum_l\sum_{l'}(kk')^{\frac{1}{2}}(ll')^{\frac{1}{2}}[k;k'][l;l'] \times[(c_kc^*_{k'}c_lc^*_{l'}+c_kc^*_{k'}c^*_lc_{l'}+c^*_kc_{k'}c^*_lc_{l'} +c^*_kc_{k'}c_lc^*_{l'})f(\mathbf{k}-\mathbf{k}')f(\mathbf{l}-\mathbf{l}') +(c_kc_{k'}c^*_lc^*_{l'}+c^*_kc^*_{k'}c_lc_{l'})f(\mathbf{k}+\mathbf{k}')f(\mathbf{l}+\mathbf{l}')].$$

The first four terms form $\Delta_s$ and give just $\langle\bar{E}\rangle_{\text{Av}}{}^2$ for $k=k'$, $l=l'$. This we subtract to form the mean square fluctuation $\Delta=\Delta_s+\Delta_t=\langle\bar{E}^2\rangle_{\text{Av}}-\langle\bar{E}\rangle^2_{\text{Av}}$. They contribute also for other values with $k\neq k'$, $l\neq l'$. First and third terms contribute for $k=l'$, $k'=l$. Second and fourth terms contribute for $k=l$, $k'=l'$. If we compute the total energy, the integral $f$ is extended over all space and becomes singular, a Dirac $\delta$-function. Then the terms in $\Delta$ give nothing for $k\neq k'$, $l\neq l'$, and the mean square fluctuation vanishes. If we had quantized in a finite box, the boundary conditions on the elementary waves—fields vanishing at the conducting walls—would have led to the same result.

The last two terms in $\bar{E}^2$ constitute $\Delta_t$. They contribute for $k=l$, $k'=l'$; $k=l'$, $k'=l$ and also

for $k=k'=l=l'$. These give:

$$\Delta_t=\tfrac{1}{2}\sum_k\sum_l kl[k;l]^2[(N_k+1)(N_l+1)+N_kN_l)] \times f(\mathbf{k}+\mathbf{l})f(-(\mathbf{k}+\mathbf{l}))+\text{a term containing } \sum_k f(2\mathbf{k})f(-2\mathbf{k}).$$

We choose as the defining volume a sphere of radius $a$. Then

$$f(\mathbf{k})=\frac{1}{3}\left(\frac{2}{\pi}\right)^{\frac{1}{2}}V[J_{3/2}(ka)/(ka)^{\frac{1}{2}}].$$

We can take the $N_k$'s as slowly varying for any state of the field which can be compared with thermal equilibrium. Consider the term $\Delta_s$. If $a$ is chosen large compared to the maximum wave-length involved, $f(\mathbf{d})$ has a maximum for $\mathbf{k}=\mathbf{l}$. Here the bracket $[k;l]$ is a function only of the angle between the directions of polarization for the equal propagation vectors $\mathbf{k}$ and $\mathbf{l}$. We average over this angle, with the radiation taken as isotropic and unpolarized so that the $N_k$'s depend only on $|\mathbf{k}|$, getting:

$$\Delta_s\leqq V\sum_k N_k(N_k+1)k^2=V\int dk\cdot 8\pi k^4N_k(N_k+1).$$

For the term $\Delta_n$ the maximum in $f$ is for $\mathbf{k}=-\mathbf{l}$. But the bracket $[k;-k]$ behaves like $(1+\cos\theta_{kl})$, vanishing for $\mathbf{k}=-\mathbf{l}$. The major contribution to $\Delta_n$ comes for $\mathbf{k}+\mathbf{l}\neq 0$, and we can estimate this by using the asymptotic form $\cos ka/(ka)^{\frac{1}{2}}$ for $J_{3/2}(ka)$, since $k_{\min}a\gg 1$. Then the term is clearly proportional to $a^2$, and is thus a surface term, negligible when the linear dimensions of the volume are large compared to the wave-length.

The only remaining term is the zero-point fluctuation. Again the important integrals are those over $k$, $l$ and $\theta_{kl}$. Using an integral representation for the square of the Bessel's function, we integrate over $\theta$ and then over the parameter of the representation. We are left with

$$\Delta_0\leqq\int\int dkdlk^2l^2[H_{3/2}(2a(k+l))/(k+l)^2(a(k+l))^{\frac{1}{2}} -\text{same with } (k-l) \text{ for } (k+l)],$$

where the $H(ax)$ are Struve's functions, behaving like $(ax)^{\frac{1}{2}}$ for large $ax$. We put the asymptotic behavior in, introduce the sum and difference $k+l$, $k-l$ as coordinates, and obtain for large energies $k$ and $l$ an integral diverging like $\int k^3dk$.

We have now to remove this divergence. No reasonable smearing of the region will do it. We could take $f(k+l)$ as $V\cdot\exp(-\delta^2(k+l)^2)(f(\mathbf{k})$ must go to $V$ as $\mathbf{k}\to 0$). The angle integration is next, with $[k;l]$ behaving like $(1+\cos\theta)$. For the integral over $\theta$ with such an $f$ we get $\sim 1/(kl)^3\cdot\exp(\pm 2kl)$. Then the term $\Delta_0$ diverges like $\int dk/k$ at least. Following the discussion above, we introduce a time average. We redefine $\bar{E}$ as

$$\bar{E}=\int_{-\infty}^{\infty}dtS(t)\int_V d\mathbf{x}u(\mathbf{x},t).$$

If we use a sharply defined time interval, this too gives a divergent result. Only if we smear the time, which we may describe formally by taking $S(t)=\exp(-t^2/\tau^2)/\tau$, does the term converge. We estimate the magnitude of $\Delta_0$ in this case by integrating in $k$ and $l$ up to $1/\tau$. Since $k_{\min}a$ is large, we use the asymptotic form of $J_{3/2}$ as before. Then the term becomes another surface term of the order $a^2/\tau^4$, negligible if $a$ is large enough, and diverging as $\tau$, the measure of the indeterminacy in time, goes to zero. We can write this term $\Delta_0=a^2(h/\tau)^2(1/c\tau)^2$ as in the discussion above.

By taking a volume of dimensions large compared to the maximum wave-length involved, averaging over an indeterminate time interval short compared to the light transit time across the region, and taking the occupation numbers as a smooth function of the energy, we can obtain a value for the mean square fluctuation as close as we wish to the one expected on thermodynamic grounds.

It is a pleasure to thank Professor J. R. Oppenheimer for many helpful discussions.

# The Electrical Breakdown Strength of Ionic Crystals as a Function of Temperature*

R. C. BUEHL AND A. VON HIPPEL
*Electrical Engineering Department, Massachusetts Institute of Technology, Cambridge, Massachusetts*

(Received July 12, 1939)

It has been generally believed that the breakdown strength of an insulator is *constant* in the lower temperature range and decreases rapidly at high temperatures, indicating thermal breakdown. The authors show that, at least in ionic crystals like KBr, a very steep *increase* of breakdown strength with temperature is recorded in the lower range. This new phenomenon in insulators is apparently analogous to the temperature coefficient of the resistance in metals. It allows us to decide between the different theories of breakdown proposed.

SINCE Wagner,[1] Hayden and Steinmetz,[2] and Güntherschulze[3] proposed almost simultaneously that the electrical rupture of solid dielectrics is a phenomenon of overheating by current, the existence of a "thermal breakdown" has been accepted as one cause of the destruction of insulating materials. The insulator in this case is treated as a conductor of high resistance having a strongly negative temperature coefficient. Its breakdown voltage has been reached when the heat production by current begins to surpass the heat dissipation. This theory of thermal instability has been developed further by Rogowski,[4] v. Kármán,[5] and Dreyfus.[6] Fock[7] finally gave the complete mathematical solution, and Moon,[8] its formulation convenient for application.

Appropriate cooling or impulse testing will prevent the thermal decomposition of the dielectric; the material breaks down as a result of some other mechanism of electrical destruction. According to Inge, Semenoff and Walther,[9] the two fields of breakdown may be easily distinguished by the shape of the voltage-temperature characteristic (Fig. 1). Below a critical temperature the breakdown strength stays constant ("electrical" breakdown); above this point a steep decrease indicates the thermal nature of the process. Moon and Norcross[10] concluded later from extensive tests evaluated statistically that a third intermediate region of slower decay exists, but the independence of the "electrical" breakdown of temperature has become an axiomatic belief of the literature.

For several years one of us, in studying the properties of dielectrics under high field strength, has become increasingly doubtful of the simple conception presented above.[11] Not only is the numerical agreement between thermal theory and experiment in many cases insufficient, but the visual observation of the development of breakdown in ionic crystals and glass reveals directly that even at high temperatures the

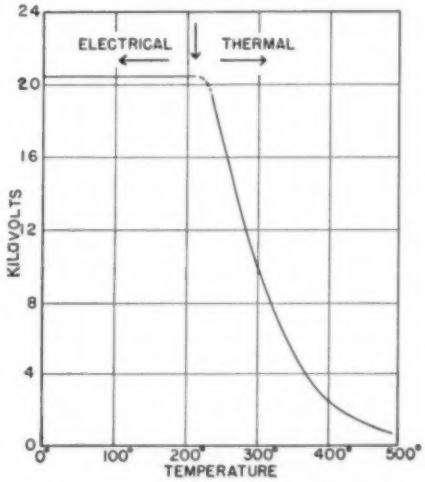


FIG. 1. Temperature dependence of the breakdown voltage through a 1-mm plate of NaCl. (Inge, Semenoff and Walther.)

* Paper N. 61 presented at the Washington meeting of the American Physical Society, April, 1939.

[1] K. W. Wagner, J. A.I.E.E. **41**, 1034 (1922).

[2] J. L. R. Hayden and Ch. P. Steinmetz, Elec. World **80**, 865 (1922).

[3] A. Günther-Schulze, *Jahrb. d. Radioakt. u. Elektr.* **19**, 92 (1922).

[4] W. Rogowski, Arch. f. Elektrot. **13**, 153 (1924).

[5] Th. v. Kármán, Arch. f. Elektrot. **13**, 174 (1924).

[6] L. Dreyfus, Schweiz Elektr. Verein Bull. **15**, 321, 577 (1924).

[7] V. Fock, Arch. f. Elektrot. **19**, 71 (1927).

[8] P. H. Moon, Elec. Eng. **50**, 676 (1931).

[9] L. Inge, N. Semenoff and A. Walther, Arch. f. Elektrot. **17**, 433 (1926).

[10] P. H. Moon and A. S. Norcross, J. A.I.E.E. **49**, 125 (1930).

[11] A. v. Hippel, Zeits. f. Physik **98**, 580 (1936).

Cathode← →Anode

FIG. 2. Spark proceeding in NaCl.

material is not destroyed primarily by a melting process.[12] In rocksalt, for instance, a spark path may be observed stepping forward from the anode towards the cathode in the [110] direction (Fig. 2). Furthermore, dendrite formation takes place as well as electron emission from sensitive spots activated by ionic conduction, effects depending on time and temperature and influencing the destruction of the material. Walther and Inge, even in their latest publication,[13] fail to recognize these phenomena published in clear photographs which make the calculation of the breakdown strength by the simple theory of thermal instability impossible. A clear insight into the mechanism of destruction is necessary before a mathematical treatment can be undertaken. A really convincing example of thermal breakdown has been reported recently by Fuoss,[14] in polyvinyl chloride.

Similar reservations have to be made against the claim that the breakdown characteristic (Fig. 1) in the lower temperature region shows independence of temperature. The absolute value of the breakdown strength given for rocksalt, for instance, is much too low (385 kv/cm[13] instead of 1500 kv/cm) indicating difficulties in the measuring technique. Furthermore if electronic impact ionization is responsible for the breakdown as seems probable from the work of one of us,[11, 12, 15] an *increase* in breakdown strength with increasing temperature might be expected in the low temperature field. This effect would be the analog of the temperature coefficient of metals as particularly pointed out recently by Fröhlich:[18] the interaction between conducting electrons and lattice rises if the regularity of the structure becomes damaged by heat vibrations. An effect pointing in the same direction was found by one of us several years ago[16] (Fig. 3): the breakdown strength of a mixed crystal plotted as a function of the composition passes over a maximum like the resistivity of metal alloys.

This parallelism of effects in metals and crystals does not necessarily imply, that in both cases an identical mechanism is acting. In metals the quantum-mechanical scattering of the electron waves belonging to the crystals as a whole is responsible. In insulators the disorder of the lattice produced by foreign matter, stresses or temperature creates deeper potential holes and this may increase the probability of capture.[12, 15]

How large the temperature dependence should be has not yet been calculated by the theory of Seeger and Teller.[17] The physical background of this theory is in accordance with our point of view. Fröhlich,[18] assuming an electronic ionization process without avalanche formation, gives a quantitative formula of the temperature dependence. Frenkel,[19] on the other hand, proposes a *decrease* of breakdown strength with

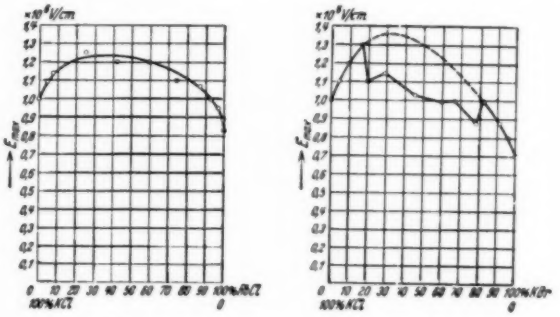

(a) (b)

FIG. 3. Breakdown strength as function of the composition. (a) KCl-RbCl; (b) KCl-KBr.

[12] A. v. Hippel, J. App. Phys. **8**, 815 (1937).
[13] A. Walther and L. Inge, Techn. Phys. U.S.S.R. **5**, 335 (1938).
[14] R. M. Fuoss, J. Am. Chem. Soc. **60**, 456 (1938).
[15] A. v. Hippel, Phys. Rev. **54**, 1096 (1938).
[16] A. v. Hippel, Zeits. f. Physik **88**, 358 (1934).
[17] R. J. Seeger and E. Teller, Phys. Rev. **54**, 515 (1938).
[18] H. Fröhlich, Proc. Roy. Soc., London **160**, 230 (1937).
[19] J. Frenkel, Phys. Rev. **54**, 646 (1938); Tech. Phys. U.S.S.R. **5**, 685 (1938).

increasing temperature, assuming that the material is destroyed by thermal ionization, facilitated by the high field strength applied. And Franz,[20] following a theory of Zener[21] that the high voltage transforms the insulator into a conductor by destroying the Bragg reflections of the electron waves, claims nearly independence of temperature for the breakdown strength.

The authors have sought an experimental decision among these contradictory opinions; their methods and first results are reported in this paper.

## The Breakdown Apparatus

A main source of error in testing insulating materials is the electrical field at the edge where the electrode bends away from the insulator. If a discharge starts at this boundary before the breakdown voltage of the sample has been reached, the originally homogeneous stress through the sample becomes distorted by surface charges, thus destroying the regularity of the shape of the electrodes. An early breakdown results as a consequence of the inhomogeneous field distribution produced. This edge effect is responsible for most of the erroneous data reported. It can be avoided,[22] by protecting the edge between insulator and electrode by a dielectric guard ring which by perfect contact fills the interspace between both boundaries. Beeswax, for instance, melted under vacuum in the interspace and then solidified and maintained under high pressure may be used in one temperature range. The application of pressure fulfills the second purpose of preventing corona from unprotected parts of the electrodes. Our apparatus was therefore constructed as a high pressure vessel.

Important information about the process of breakdown and the reliability of a measurement can be gained by recording the current through the sample during a test. This provision was made and a temperature range from about $-200°C$ to $+400°C$ became accessible by the following design (Fig. 4).

A copper block $A$ containing the crystal holder

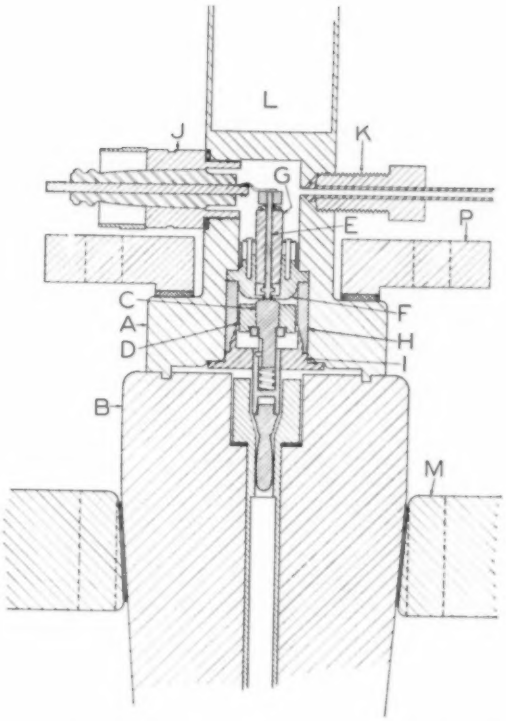


FIG. 4. Cross section through the breakdown apparatus.

in a central cavity serves as an electrical shield at ground potential and transfers heat from a temperature bath in $L$ and around $A$ to the sample. A metal pipe carries the high voltage up to the test piece through the porcelain insulator $B$, fitting a contact plug of the high voltage electrode $C$. $A$ and $B$ can be clamped together by a steel ring $P$ anchored with bolts to the steel plate $M$ which supports the porcelain cone. A groove cut into the upper surface of the porcelain insulator takes the gasket ring sealing the apparatus. At $K$ a nitrogen tank can be connected for raising the pressure inside up to 100 atmospheres if necessary. The chamber can be evacuated through the hollow high voltage line.

The crystal holder inserted into the copper block is a small tubular box. A copper tube $H$ forms its wall, and is closed at the bottom by an insulating piece $I$ which carries the high voltage electrode. A copper guard electrode is screwed to the other end, holding the glass insulator $G$ in place, which insulates the measuring electrode $E$ from the guard ring. Fig. 5 gives a front view of this ground-electrode arrangement with a crystal plate in place after a breakdown test. The

[20] W. Franz, Verh. d. deutsch phys. Ges. **19**, 113 (1938); **20**, 27 (1939).
[21] Ch. Zener, Proc. Roy. Soc., London **145**, 523 (1934).
[22] A. v. Hippel, Zeits. f. Physik **75**, 145 (1932).

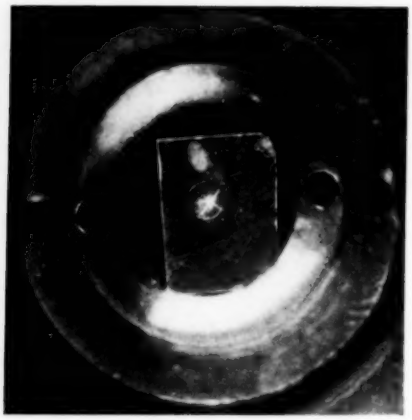

FIG. 5. Front view of ground-electrode arrangement with crystal (enlarged 1 : 2.5).

puncture in the center caused two cracks in the [110]-direction, progressing about to the edge of the center electrode. Guard and center electrode are separated by a spacing of only 1/1000 of an inch but are insulated from each other by a resistance of more than $10^{12}$ ohms. A spring contact transfers the current from the measuring electrode through a spark plug $J$ into the current amplifier connected outside by a coaxial cable.

After the crystal has been properly adjusted on the ground electrode a weak spring is released, pressing the high voltage electrode against the test sample. The sample is then surrounded by some drops of an appropriate insulating material, or the whole little chamber may be filled under vacuum with some embedding dielectric. The temperature of the sample is controlled by a thermoelement in the copper block $A$ very near to it, and by a thermometer in $L$, both readings being calibrated against a thermocouple which was inserted at the place of the test piece.

## THE ELECTRICAL CIRCUIT

D.c. high voltage up to 75 kilovolts, steady and smoothly controllable, is delivered by a condenser charged from a power pack through the resistor $r_1$ (Fig. 6). This voltage reaches the insulator through a protecting resistor $r_2$ of 100 megohms. Here it is measured by the current drained out through the precision resistor $r_3$ of 1000 megohms. An amplifier provides the different voltage ranges and the power necessary to record the voltage by a 5-ma Esterline-Angus recorder.

The current flowing through the central section of the test piece is amplified by a feedback micromicroammeter and fed into a second current recorder. The recorders are coupled together; therefore current-voltage-time characteristics are obtained. The range of the amplifier extends from $10^{-11}$ amp. to $5 \cdot 10^{-6}$ amp. full scale; the instruments have an accuracy of one percent of full scale. The amplifiers have been developed and built in our laboratory by Mr. S. Roberts who has published a detailed description recently.[23]

When breakdown of the insulator occurs, a glow discharge lamp connected across the current amplifier lights up, protecting the instrument and indicating the failure. Simultaneously the voltage falls back to the resistor $r_2$, and the voltage recorder notes the breakdown voltage by the point where a steep break of the characteristic occurs (Fig. 7). The reading accuracy thus achieved makes full use of the high sensitivity of our equipment.

Our resistors, $r_1$ to $r_3$, are of the spiral-wound MV type of I.R.C. Resistor $r_3$ has been carefully checked several times against a high voltage wire-wound precision resistor, and the lower ranges of the voltage amplifier have been calibrated by d.c. precision instruments. Our results should therefore be reliable to one percent of the full-scale reading of our instruments; that is, to between one percent and two percent of the values observed, so far as the electrical circuit is concerned.

## RESULTS

The dielectric strength of defined materials cannot be found by piling up many measure-

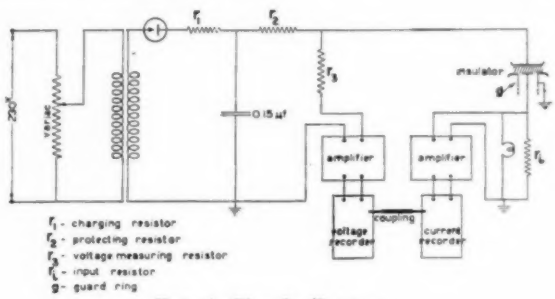


FIG. 6. Circuit diagram.

[23] S. Roberts, Rev. Sci. Inst. **10**, 181 (1939).

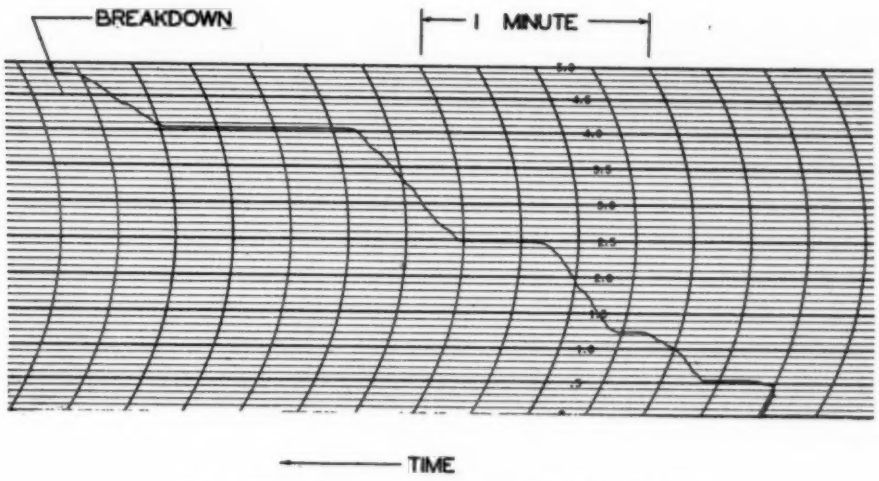


FIG. 7. Voltage record noting the breakdown voltage.

ments and averaging their results statistically. The current-voltage record during the test and the microscopic examination of the insulator afterwards give together the decisive evidence of whether or not an experiment was successful. We have not found a single case yet where the highest breakdown strength recorded was not at the same time the most reliable one. On the other hand, even the greatest care in preparing electrodes, sample, and guard ring did not prevent occasional erroneous low values produced by unnoticed faults in the test sample or in the arrangement. An extensive study of KBr single crystals revealed the principal aspects of the situation.

### CURRENT-VOLTAGE-TIME CHARACTERISTICS

Figure 8 gives a characteristic sequence of sections of a current-time record for a KBr crystal at room temperature. The charging resistor $r_1$ was omitted in order to demonstrate the effect of fluctuating line voltage. Between the first five sections less essential intermediate parts of the long record have been left out. The last three sections present one continuous curve with the corresponding voltage record above it. The voltage setting and time scale are indicated below.

Four facts are demonstrated very clearly: After each voltage rise the current drops rapidly.

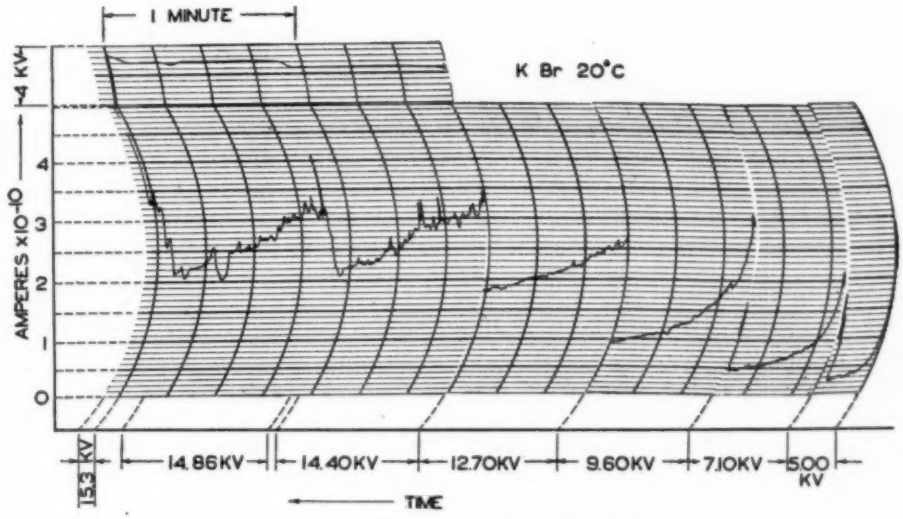


FIG. 8. Current-time record up to breakdown.

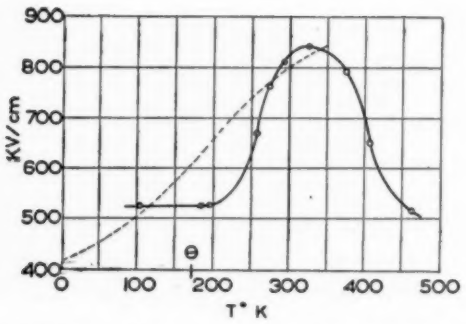


FIG. 9. The breakdown strength of KBr as $f(T)$. $\theta$ = Debye temperature.

With increasing field strength the decay becomes less steep and the curve shows more and more fluctuations. The breakdown itself appears as an abrupt discontinuity.

A comparison between current and voltage curves shows that the fluctuations are due partly to the line voltage. The deep hump about half a minute before breakdown, for instance, corresponds to a short voltage change of only one percent! Other fluctuations have their origin in the crystal itself, as one of us has found.[15] They are distorted in the record because our instrument needs about ½ second for a full-scale deflection. The existence of fluctuations due to shot effect has already been proved by Haworth and Bozorth[24] several years ago.

The decrease of the current with time is mainly caused by polarization. An experienced observer can predict from the current slope and its ripples when the breakdown voltage is approached, and in this way can detect early failures of the material. A detailed study of the current curve, its true shape and its composition of electronic and ionic conduction, will be given in a later paper.

## THE TEMPERATURE DEPENDENCE OF BREAKDOWN

In contradiction to the usual type of characteristic (Fig. 1) the temperature curve of KBr (Fig. 9) shows completely new and different aspects. The breakdown strength stays constant only below −80°C, increases sharply to a maximum at about +50°C, and decreases again. The current densities just before breakdown are plotted in Fig. 10.

These measurements give the decision we have sought (see p. 2): Frenkel's theory of thermal ionization can certainly not be true at temperatures below the maximum, because the slope of the voltage-temperature curve is contrary to his prediction. Also the current preceding breakdown has no direct connection to the breakdown phenomenon itself, as already stated recently.[15] The theory of Zener-Franz is ruled out, because a strong dependence of the breakdown strength on temperature has been found. The increase of breakdown strength with increasing temperature fits into the picture of electronic impact ionization given by one of us. The slope is much steeper than is predicted by Fröhlich's theory; the dotted line in Fig. 9 shows the temperature dependence according to his formula if the maximum is taken as reference point. It may be hoped that calculations of the temperature dependence on the basis of the avalanche theory results in a better agreement.

We have found a similar but even steeper characteristic for NaCl, while addition of AgCl to NaCl seems to quench the influence of temperature as should be expected. The measurements are not completed yet, because a new phenomenon was observed which delayed our program. At higher temperatures very low breakdown values with a clear indication of edge effect result if the voltage is not raised by small steps with large intervals of constant voltage between. Apparently some kind of progressive

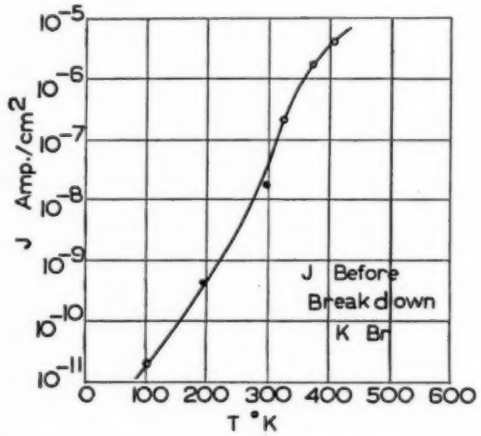


FIG. 10. Current density before breakdown of KBr.

[24] F. E. Haworth and R. M. Bozorth, Phys. Rev. **39**, 845 (1932).

formation of electrodes and sample takes place, the disturbances die down, and at last a reproducible highest breakdown value is reached, with the characteristics of a central breakdown. The formation once achieved seems to be permanent, because if a sample is treated in the way described and the voltage just before the expected breakdown value is cut down and after some time raised again very rapidly, the final high value results. It is hoped that a more detailed study of the current phenomena will give an understanding of this new effect. Until then the values published should be taken as preliminary results.

Simultaneously with our abstract for the Washington meeting a letter of Austin and Hackett appeared in Nature[25] reporting the breakdown strength of KBr as a function of temperature. The general shape of the curve given is in good agreement with our results. The absolute values lie lower than ours at the lower temperature end of the characteristic and have not been followed up above 350°K.

Some of the crystal samples used were kindly furnished by Professor D. C. Stockbarger, to whom the authors wish to express their gratitude.

[25] A. E. W. Austin and W. Hackett, Nature **143**, 637 (1939).

---

NOVEMBER 1, 1939 PHYSICAL REVIEW VOLUME 56

# On the Thermionic and Adsorptive Properties of the Surfaces of a Tungsten Single Crystal*

S. T. MARTIN‡
*George Eastman Research Laboratories, Massachusetts Institute of Technology, Cambridge, Massachusetts*†

(Received August 4, 1939)

The thermionic emission from a spherical tungsten single crystal has been observed. Photographs and diagrams show qualitatively the dependence of this emission on crystallographic direction. Nearly all the maxima and minima lie on a 110 zone. Similar observations have been made on the same crystal when caesium and barium were adsorbed thereon. Adsorption forces are largest for caesium on surfaces of highest work function. For barium the adsorption forces appear to be more dependent on surface structure as the force between the ion and its image contributes the major part of the adsorption energy. The behavior of adsorption as a function of crystallographic direction is such that the sphere surface may be approximated by that which would be obtained by carving the sphere from a perfect lattice. There is no evidence for a faceted or step-like microstructure. Emission from the spherical crystal when caesium is adsorbing on contaminated complex surfaces is more complicated in its dependence on crystallographic direction than when the surface is clean, and a map of the emission over the crystal changes its configuration with temperature. This behavior is not observed when the surface is clean or only slightly contaminated.

## INTRODUCTION

IT has been realized for some time that thermionic and photoelectric emission (in an accelerating field) from a clean metal surface in good vacuum may vary by some orders of magnitude depending on which surface of the crystal is studied.[1–3] Ordinarily, polycrystalline aggregates have been used for experiment in the past, and consequently the data represent some sort of an average of the emissions from a great variety of surfaces.[4, 5] Theories thus far pro-

* Part of a thesis presented for the degree of Doctor of Science from the Department of Physics, Massachusetts Institute of Technology, June, 1938.

‡ Coffin Research Fellow, 1937–38.

† Present address: Clark University, Worcester, Massachusetts.

[1] C. E. Mendenhall and C. F. deVoe, Phys. Rev. **51**, 346 (1937).

[2] E. W. Muller, Zeits. f. Physik **106**, 541 (1937).

[3] R. P. Johnson and W. Shockley, Phys. Rev. **49**, 436 (1936).

[4] L. H. Germer, Phys. Rev. **25**, 795 (1925).

[5] W. B. Nottingham, Phys. Rev. **49**, 78 (1936).

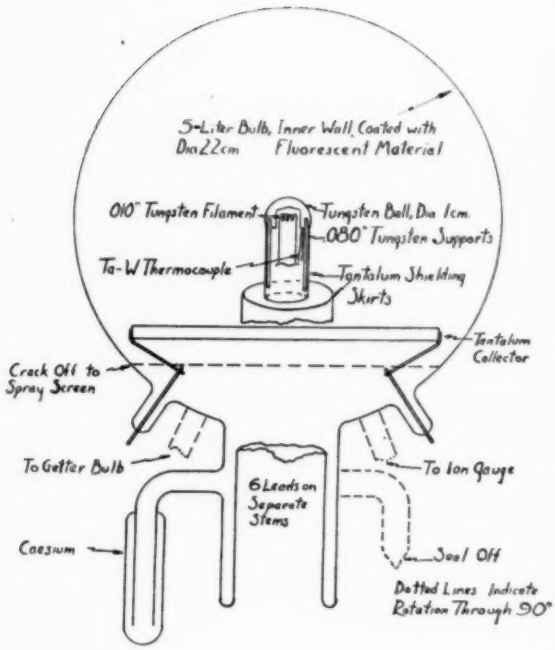


A

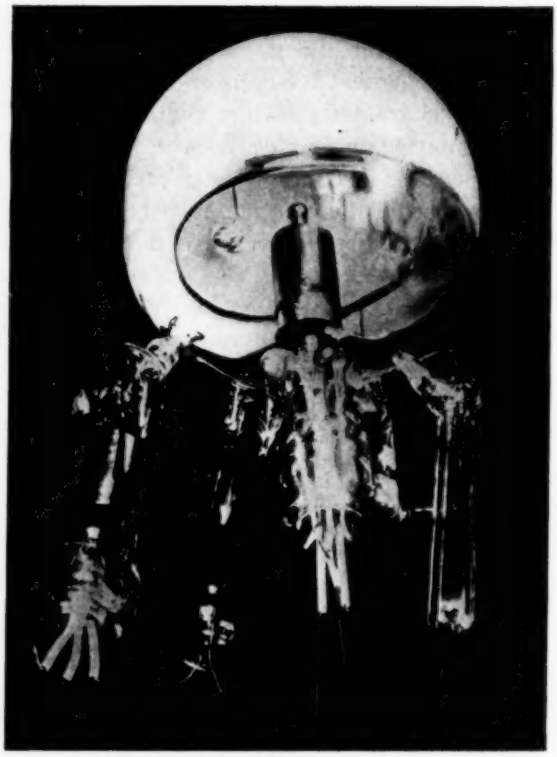

B

FIG. 1. Diagram and photograph of experimental tube.

posed,[6, 7] fail to consider the directional properties of the crystal structure of the emittor, as have the most precise experiments. Although an equation of the same form as the Richardson equation accurately represents the data,[5] in view of the known variation in emission from various surfaces, this is only fortuitous coincidence.

In order to proceed with further investigations, it is necessary to know which of the possible surfaces appearing on a metallic crystal are the most important in emission properties. After this information is established qualitatively, quantitative studies[8] may be made on the surfaces so selected.

Furthermore, present knowledge of the nature of the adsorbed phase of alkali and alkaline earth materials rests strongly on the work of Taylor and Langmuir,[9] Becker,[10] and deBoer and Veenemans,[11] who have determined the influence of the adsorbed metal on the thermionic emission from tungsten and nickel. It is desirable to investigate the nature of the variation in emission and adsorption over various crystal surfaces which were very likely present on their wires, as indicated by the work of Johnson and Shockley.[3] This is particularly true since the conclusions depend directly on a calculation of emission density with and without adsorbed materials. Unless a particular treatment has made the wire surface homogeneous, the average densities measured may deviate widely from those which should be considered.

One of the most provocative developments in this problem was the device of Johnson and Shockley, with which it is possible to compare visually the emissions from various parts of a single crystal filament. However, regardless of what surfaces may be developed or suppressed on such a filament, the information yielded by this apparatus can include no more than that pertaining to those directions* normal to the wire axis. Consequently from a single crystal

[6] S. Dushman, Phys. Rev. **21**, 623 (1923).
[7] L. Nordheim, Physik. Zeits. **30**, 177 (1929).
[8] M. H. Nichols, M.I.T., Doctor's Thesis, June, 1939.
[9] J. B. Taylor and I. Langmuir, Phys. Rev. **44**, 423 (1933).
[10] J. A. Becker, Phys. Rev. **28**, 341 (1926).
[11] J. H. deBoer and C. F. Veenemans, Physica **1**, 953 (1934).

* A crystallographic direction is defined by the unit vector normal to a crystallographic plane. Each is designated by the same Miller indices.

wire, only information about a single zone† is obtained.

Shockley recognized that it might be possible to obtain a qualitative map of the emission properties of all the surfaces of a crystal, by using an apparatus similar to that employed[3] previously except that the cathode would be a sphere instead of a cylinder, and corresponding changes made in the rest of the geometry of the tube. He constructed such an apparatus while at Massachusetts Institute of Technology but because of a limitation of time and an unsatisfactory etching treatment of the cathode, no significant results were obtained.

In this apparatus a spherical crystal was placed concentrically in a bulb whose inner wall was coated with a fluorescent material. When the sphere was heated and a strong accelerating field for electrons applied, these proceeded radially from the sphere to the bulb. Bright regions on the bulb were then in one to one correspondence with emission regions on the sphere. Because of the necessarily large size of cathode, magnification was not great. However, providing the surfaces developed on the spherical crystal were characteristic of the crystallographic directions normal to them, this was unimportant.

## Apparatus and Preparation

### Apparatus

The apparatus* is shown schematically in Fig. 1A, and a photograph of the assembled tube is shown in Fig. 1B. It will be seen that the cathode was really a truncated sphere, mounted on two 0.080″ tungsten rods. A 0.25″ hole (of the same depth) in the base accommodated a 0.010″ tungsten filament of 6½ turns, capable of giving an emission of about 0.5 ampere. This was insulated from the sphere and the high temperatures necessary for cleaning the sphere surface obtained by drawing emission from this filament to the sphere at about 1400 volts. (At 2800°K the sphere radiated about 500 watts.) A large tantalum strip circle served as collector for emission electrons from the sphere. When a voltage of about 5000 to 10,000 volts was applied between sphere and collector, electrons from the sphere surface went radially to the fluorescent screen and secondaries from this established conduction to the collector.[12, 13]

Other accessories shown in the diagram and photograph are the tantalum shielding skirts which suppressed unwanted electrons from the heating filament, and prevented field emission electrons from welds in the supporting structure, from reaching the screen. In some cases the edges of the outermost skirt also contributed field electrons, so that this was only partially successful. Also indicated are side bulbs with barium getter, ionization gauge, and caesium trap.

### Preparation of the sphere

Lacking definite information as to how to prepare a crystalline surface representative of the direction normal to its macroscopic area, the sphere was polished by metallurgical methods, after initial machining, to produce a smooth bright finish. As viewed under a microscope, it was seen to be covered with a multitude of small pits having glassy sides.

The machining was accomplished entirely by grinding. At first a large ingot of sintered tungsten,* consisting of a few very large crystals,

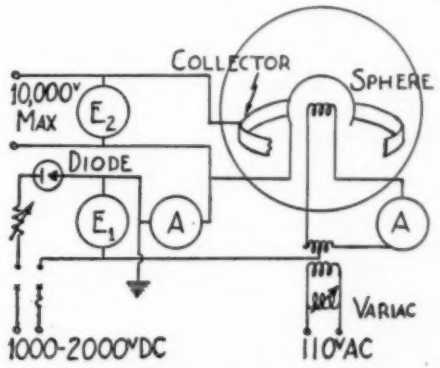


FIG. 2. Circuit diagram.

† A zone: The set of crystallographic planes containing a common direction. Since there is a difference between a crystallographic plane and the surface (ideal) defined by the same normal, a zone is here intended to mean the set of directions lying in a common plane. Surfaces will be designated by the indices of their respective normals.

* Basically this is the same as that made by Shockley, but there are several major differences in design and construction.

[12] W. B. Nottingham, J. App. Phys. 8, 762 (1937).

[13] S. T. Martin and L. B. Headrick, J. App. Phys. 10, 116 (1939).

* This was kindly furnished by Dr. P. P. Tarasov of the Cleveland Wire Works, General Electric Company. It showed large cleavage surfaces when broken. Although there is some change in density when such tungsten is drawn, it is very evidently far from being porous, and shows every indication of having reached an equilibrium lattice condition.

was ground cylindrical. The three holes used for support rods and filament were drilled in the base using Carbaloy drills. The largest was used to accommodate a mandrel, the two smaller for shear pins. Tantalum strips welded to the base were used to hold the assembly together. A hand grinder mounted on a turning lathe swivel, while the mandrel rotated in the lathe chuck, produced a roughly spherical surface. This was finished with successively finer grades of carborundum and a thick-walled copper tube as tool. In this operation, the tool rotated in the lathe, the mandrel in an electric hand drill. The sphere was pressed into the end of the tube and carborundum and oil painted on. The angle between the mandrel and the grinding tool axes was varied smoothly and randomly to produce a quite accurately spherical surface. The final polish was accomplished with a rouge-charged felt in place of the copper tube.

The finished sphere measured about 1 cm in diameter and required about four or five weeks to produce. Large crystals of tungsten are brittle and will shatter if subjected to undue mechanical shock.

**Preparation of the envelope**

The envelope consisted of a 5-liter Pyrex bulb opened as shown in Fig. 1A, on a small circle at about latitude 40°.* The collector was welded to previously inserted stems on the neck part, and a fluorescent screen sprayed on the interior of the globe part.

**Fluorescent screen**

In order to get a large uniform fluorescent screen, spraying was practically imperative. The fluorescent material, a mixture of willemite and calcium tungstate, was ball-milled from 8 to 16 hours with acetone in a porcelain ball mill using flint or mullite balls. To the resulting mix, just before spraying, was added nitrocellulose binder in diatol (commercial diethyl carbonate) in the proportions of a few drops of binder per 50 cc of suspension. This binder improved the suspension markedly and also helped the screen stick to the glass when sprayed. A spray gun made from two concentric glass nozzles with material feeding through the inner one was used. It was found necessary to make a very heavy coating so that direct light from the sphere would not reach the camera when photographing the emission of clean tungsten. When this was done, and a Wratten No. C 49 filter used in conjunction with motion picture positive film, the emission pattern of clean tungsten showed fair contrast, although there was a background of about 250 watts of continuous radiation at 2100°K from the sphere, only ten centimeters away from the fluorescent screen.

**Protection of the fluorescent screen**

It was found that caesium vapor not only destroyed the luminescence of the material, after a few hours, but had the effect of loosening it from the bulb wall. Under the action of high velocity electrons, the material acted as though charged positively and would flock back to the cathode. In an early tube, the entire screen left the bulb wall and coated the sphere with a hard eggshell-like coating.

To prevent this, the screen was treated with a 5-percent solution of pure potassium silicate. First the binder was burned out by baking in air to 550°C, then the potassium silicate was gently washed over the inside of the bulb. This was dried while rotating in an inverted position to assure a uniform coating (rather slight non-uniformities in this coating produce bothersome dark streaks and patches in the patterns). After wiping the crack, and its neighborhood, free of the silicate (otherwise the sealing properties of the glass are seriously affected), it was again baked to 550°C in air. Following this the screen was well washed with distilled water (much sloshing) to clean out poorly anchored particles, and the process repeated. When so treated the tube required an appreciably longer time for proper exhaust but no trouble was experienced with poorly anchored particles accumulating and decomposing on the hot sphere.

* The large size (7″ diameter) and inconvenient placement of this crack-off make the following a most effective procedure. A short section of the desired crack was scratched with a glass-knife. The scratch was heated with a hot iron, then wiped with a damp rag to start the crack, which tended to run away on a great circle of the globe if the iron was too hot. The crack was then led around the desired path with the hot tool. I am greatly indebted to Mr. Lawrence Ryan, assistant glassblower, for this effective technique.

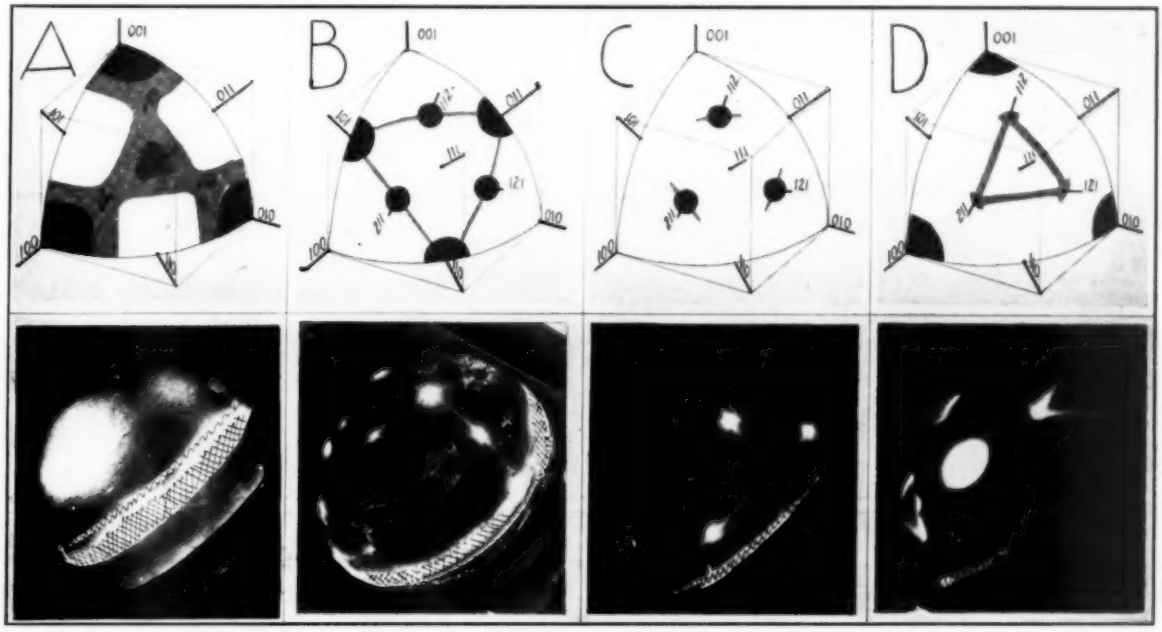


FIG. 3. A. Emission pattern of clean tungsten. B. Emission pattern of caesium on clean tungsten. Temperature range about 200°K. C. Emission pattern of caesium on slightly contaminated tungsten. Same temperature range as B. D. Emission pattern of barium on tungsten.

### Exhaust

The two parts were resealed and the blank given a preliminary exhaust with baking to 500°C and the collector cleaned by high frequency treatment. After assembling the tube it was exhausted for 60 to 70 hours with baking at 500°–510°C (trap and connecting tubing baked simultaneously) on a system which had a computed speed at the tube seal-off, of 15 liters/sec. At the end of this time the pressure was of the order of $10^{-7}$ mm of Hg with the ovens at full temperature.

Inasmuch as all metal parts were tantalum or tungsten, and alignment was not very critical, they were outgassed at 1600°–1800°K for about an hour per part (including ionization gauge), and the sphere run at 2600–2800°K for several minutes. An emission current of 15–20 ma at 6000–8000 volts (about the limiting potential of the phosphor) was drawn to the screen for 30 minutes to further outgas this. After flashing the barium aluminum getter (tantalum clad) the tube was sealed off from the pumps with the usual precautions.

### Pressure measurement

A constant check was kept on the pressure in the sealed-off tube. The tantalum and tungsten ionization gauge, when used in conjunction with a $10^{-10}$ amp./mm galvanometer, had a calibration such that a deflection of 2 mm on the scale with an electron current of 20 ma, corresponded to a pressure of $5\times10^{-9}$ mm of Hg. After the exhaust procedure outlined above, this was the recorded pressure in the tube No. 3, results from which are taken to represent caesium on clean tungsten. The ionization gauge had been checked for Barkhausen oscillations and photoelectric current from the plate.

## RESULTS

### Method of observation

At the temperatures at which clean tungsten emits sufficiently for this type of observation (2100°K), it was found that the sphere radiated enough power back to the heating filament to cause the circuit resistance to decrease with increasing power input. A diode, with tungsten filament operating on the knee of its *i vs. V* curve, in series with the sphere heating circuit, corrected this destructive tendency. The desired maximum current was fixed by adjusting the current in the diode filament, while manipulation of a load resistor and the generator voltage

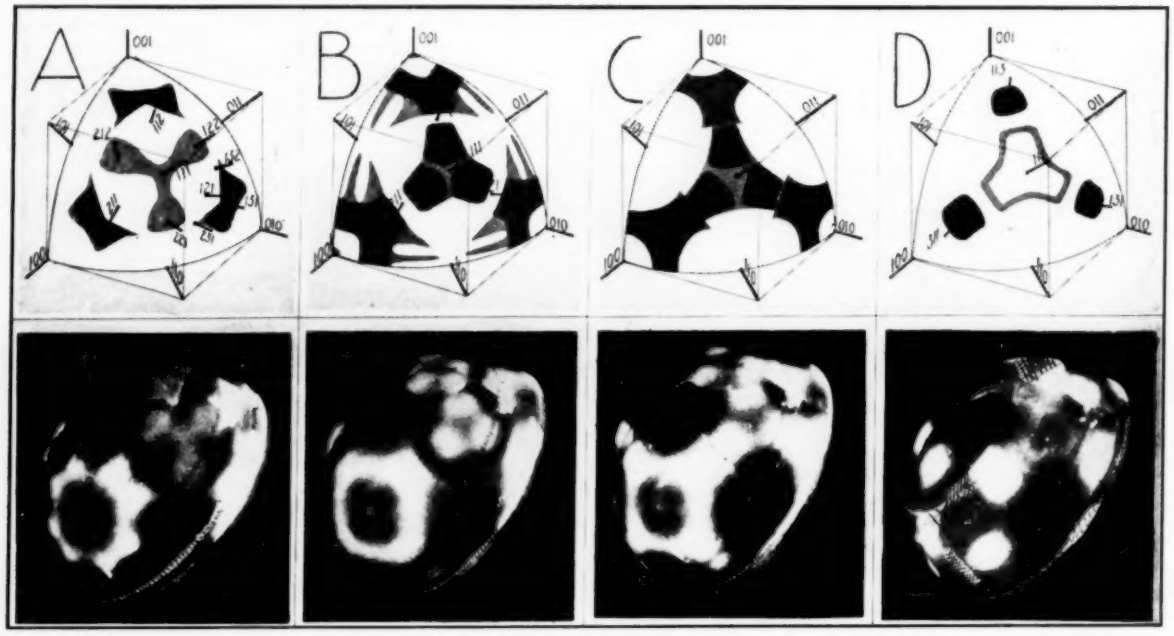


FIG. 4. Emission patterns of caesium on a contaminated complex surface, from tube No. 3, before flashing but after torching trap. Temperature increases from left to right. Temperature range about 300°K. Currents: *A* 0.20 ma; *B* 1.2 ma; *C* 0.85 ma; *D* 0.09 ma.

controlled the power input. Circuit diagram is shown in Fig. 2.

To observe the emission pattern of clean tungsten, the diode filament current was adjusted according to a previous calibration, then $E_1$ increased, and simultaneously the current in the sphere heating filament increased slowly until the sphere came up to its desired temperature. It was necessary to keep the emission from this filament "saturated" as this was the only convenient check on its temperature. After temperature was established, $E_2$ was applied and the pattern photographed.

To observe the emission pattern of caesium on tungsten, it was only necessary to remove liquid air from the caesium trap, warm this up gently, then after applying $E_2$, heat the sphere through the emission range for caesium activated tungsten by radiation alone from the sphere heating filament.

In the case of barium, which had to be evaporated on to the sphere from an exterior source, it was necessary to heat the sphere by electron bombardment and allow the barium to migrate and the excess to evaporate away ($T$ about 1200°K) before a significant pattern was observed. The temperature range of emission was also somewhat above that which could be reached by radiation from the heating filament alone.

**Explanation of observations**

For explanation of the results it is best to refer to Fig. 4, A, B, C and D. Fig. 3 will then be discussed. Currents are not given except in this case because of large extraneous emission from the sphere mount.

In Fig. 4, the bottom row consists of photographs of the tube exterior when emission was being drawn from the sphere with caesium adsorbed on the surface (as will be discussed, there are also contaminating agents present). Four different consecutive sphere temperatures are represented, the lowest being at the left. In the top row are diagrams corresponding to the photographs below. Because the symmetry of the patterns is that of the body-centered cubic lattice,* the orientation of the underlying crystal may be determined immediately. This orientation is specified in the diagram by the outlined

* Tungsten crystallizes in the body-centered cubic lattice, two atoms per unit cell, and so has the following elements of symmetry: three 4-fold axes, four 3-fold axes, six 2-fold axes, and nine reflection planes.

cube which represents the unit cell of the crystal. The map itself is the projection of an octant of a sphere whose center coincides with the backmost corner of the cube. Dark patches on the maps correspond to light patches on the photographs. The important crystallographic directions of each photograph are drawn in the diagrams as short black lines emerging from the surface of the octant. They are labeled with their Miller indices.

The diagrams appear to have more symmetry about the threefold axis than the photographs because the pattern of a neighboring crystal grain with somewhat different orientation appears in the upper part of each photograph. Since only an octant is drawn in the diagrams, the fourfold symmetry of the photographs is suppressed. Despite the fact that the whole sphere is not one single crystal, all the information that could be gained from one is to be found in the triangle defined by the 100, 110 and 111 directions. This triangle is repeated forty-eight times on a perfect spherical single crystal. The diagrams are drawn as though they were part of such a single crystal.

These patterns from a contaminated surface show the various symmetry axes so well that they are useful to fix the orientation of the crystal. Subsequent photographs are from nearly the same angle so that the various directions may be identified even though the patterns show much less detail. In general the orientation is much easier to see in the pattern on the bulb itself than in the photographs of it.

### Clean tungsten

Figure 3, A shows the emission pattern from clean tungsten (no adsorbent) at a temperature of about 2100°K. Emission is strongest from a large region around the 100 direction (but the 100 itself is somewhat weaker), next strongest around the 111 direction. The 211 is the next most important, and the 110 the poorest emittor. Surfaces ranked in order of decreasing work function are thus 110, 211, 111 and the group neighboring on the 100. Qualitatively this agrees with the results of Mendenhall and deVoe,[1] who found the 310 to have a lower photoelectric work function than the 211 surface, and the pattern is similar to some published by E. W. Muller[2] representing the field emission from a single crystal tungsten point. Except for some of the emission from the region around the 100 direction, all the maxima and minima lie on a 110 zone. This is fortuitous for quantitative thermionic studies as a drawn wire, recrystallized by slow heating in hydrogen to form large single crystals, contains this direction in the wire axis.[14]

Crosshatched regions on the photographs indicate spurious emission, either from electrons coming from the interior heating filament through a crack in the shielding skirt, or from field electrons drawn either from the edge of the base of the sphere, or from edges of the shielding skirts, or other points on the cathode support not sufficiently shielded.

### Caesium on clean tungsten

Figure 3, B shows the emission pattern when caesium is adsorbing on the clean sphere surface. Reference to the map shows that emission occurs from small regions at the 211 direction and somewhat larger ones at the 110 directions, and also along very narrow lines connecting these spots. These lines are zones whose axes are the 111 directions. (A set of directions will be specified by that one of the set whose indices are all positive and in order of decreasing magnitude.)

A very important feature of this observation is that the configuration of the pattern remains unchanged throughout the observable range of emission. Certain unfortunate accidents prevented measurement of the temperatures in this range, by means of a tantalum-tungsten thermocouple designed for this purpose. Extrapolation of a power input *versus* temperature curve established from 1100°K upwards shows the temperature range to be at least 200°K.

This pattern occurred in the third and best caesium tube constructed. Once it had been established by flashing the sphere to 2600–2800°K it did not change its configuration on subsequent flashings, and further, remained stable for a period of three hundred hours without intervening flashings or other treatment.

### Caesium on slightly contaminated tungsten

Figure 3, C is the emission pattern obtained immediately after flashing the sphere, and allow-

[14] R. B. Nelson, M.I.T., Doctor's Thesis, June, 1938.

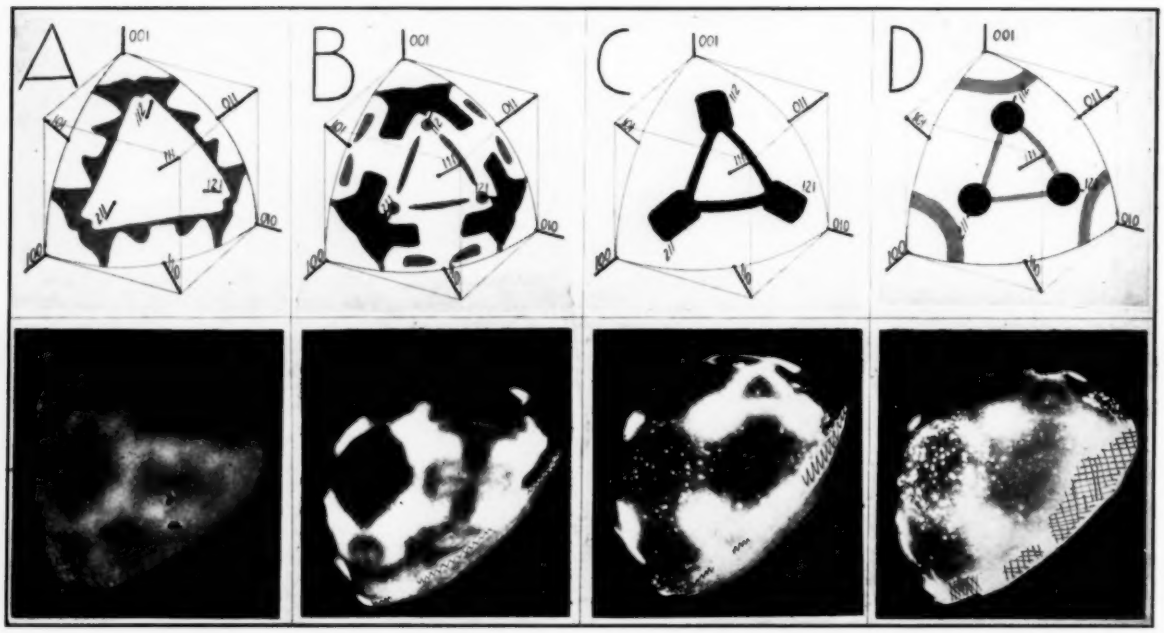


FIG. 5. Emission patterns of caesium on a contaminated complex surface, from tube No. 2, before flashing but after torching trap. Temperature increases from left to right. Temperature range about 300°K.

ing caesium to adsorb on it, in the *second* caesium tube constructed. The *very* extreme precautions used in the construction of the third tube were not exercised, although baking and outgassing were quite comparable. The configuration of this pattern was also invariant to temperature change, but under certain conditions other patterns would appear after a period of 24 hours (see Fig. 6). The two patterns are the same except that the emission from the 110 spots is suppressed as is also part of the 111 zones.

**Barium on tungsten**

The emission pattern from barium is shown in Fig. 3, D, after the barium had migrated to an equilibrium configuration. Contrary to evidence presented by Benjamin[15] no particular difficulty was experienced in getting the barium to migrate, although it takes some time as the distances involved are much larger than those normally encountered. Immediately after evaporation of barium on the sphere,* emission was observed to come from all portions of the sphere exposed to the source, and this emission was not related to the underlying crystal.

Successive observations were made as barium was evaporated. This was the only pattern having a symmetrical nature which was observed. After the pattern was established, there was no change in configuration on further evaporation until the emission was too small for further observation.

The important directions are indicated by the roundish patch at the 100 direction, and the triangle whose corners fall at the 211 directions. This triangle shows again in one of the patterns from caesium on a contaminated surface (Fig. 5, C). Ahearn and Becker[16] have found that thorium migrates preferentially along a 111 direction on a 211 surface. This direction would bisect the angles of the triangle.

The 100 direction spot was much stronger in emission than the rest of the pattern, held the

[15] M. Benjamin and R. O. Jenkins, Phil. Mag. **26**, 1049 (1938).

* This source of barium was developed by Dr. E. A. Lederer of the RCA Manufacturing Company, Radiotron Division, Harrison, New Jersey, and kindly loaned by Dr. G. R. Shaw. A double oxide of barium and beryllium is reduced by heating on a tantalum strip. Barium deposits so made are clean and bright. If used carefully, the ionization gauge shows a change of pressure of less than $10^{-9}$ mm of Hg when the process is started and stopped, provided it has been well outgassed. However, the presence of thermionically important quantities of oxygen or oxide in the deposit is not entirely ruled out.

[16] A. J. Ahearn and J. A. Becker, Phys. Rev. **54**, 448 (1938).

barium at higher temperatures, and when the pattern was first established, before too much evaporation had taken place, was visibly affected by the applied field.

**Caesium on contaminated complex surfaces**

The patterns of Fig. 4 (obtained in the third caesium tube before flashing) are emission patterns from caesium on contaminated complex surfaces. The contamination arises from gases released in the caesium trap by gentle torching necessary to drive caesium into the bulb proper. As the temperature increased the configuration changed gradually, and these are representative examples. The total emission passed through a maximum as the temperature was increased. Provided the temperature was not raised too high (roughly 1200°K) the same configurations appeared whether the temperature was increasing or decreasing. After flashing only the pattern of Fig. 3, B appeared.

Figures 5 and 6 represent observations made on the second caesium tube constructed. In Fig. 5 the caesium trap has been gently torched just before the observation. The observation of Fig. 6 is one of several made a few days later and represents an accumulation of contamination following flashing of the sphere to 2600°–2800°K after the observation of Fig. 5.

**Nature of contamination**

Both of these tubes were gettered with barium which is known to be effective for all manner of common gases. The long bake at high temperature seems to make the presence of water vapor unlikely but aside from these almost any other gas likely to remain in the Pyrex or in the caesium, the outgassing of which had received a great deal of attention, is a possibility for Figs. 4 and 5.

Dissociation of particles of screen material which have found their way back to the cathode is the most probable source of the contamination occurring in Fig. 6. This is one of many sets of observations made over a period of several days. With this and the preceding tube about twenty different sets of these observations were made by allowing the sphere to remain at about 1200°K overnight and taking the observations on successive days. Patterns were never duplicated. Some were of amazing complexity but all displayed the required symmetry. After a sufficient time a pattern having no discernible symmetry would occur indicating that the contamination

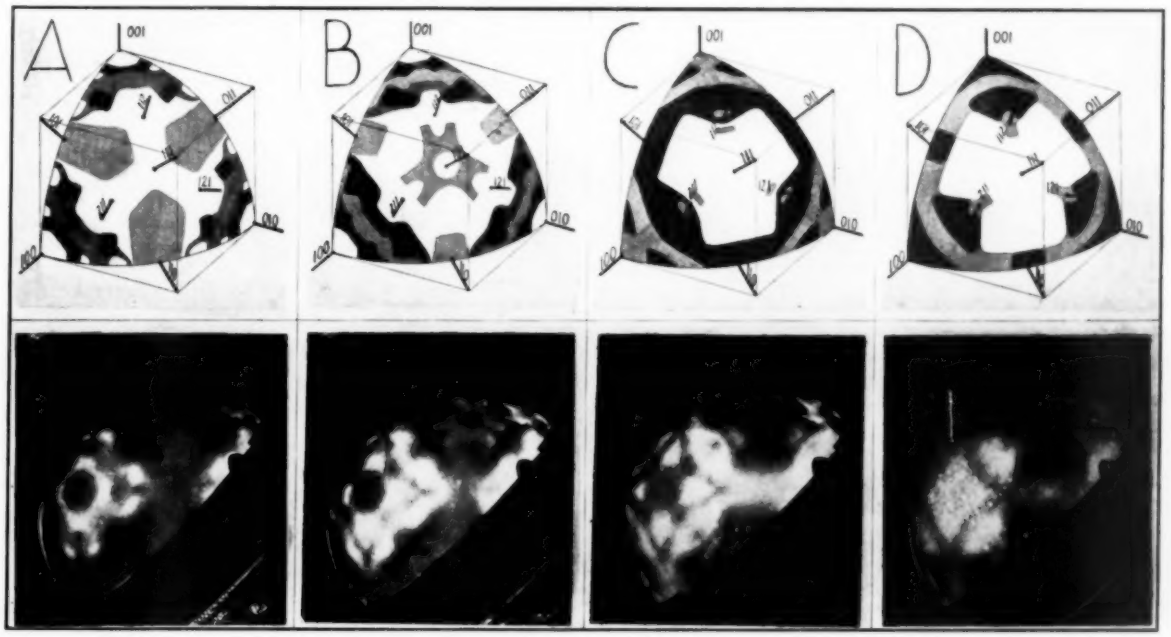


FIG. 6. Emission patterns of caesium on a contaminated complex surface from tube No. 2. This represents a moderate stage of contamination, probably by dissociation of particles of luminescent material drawn to the sphere. Temperature increases from left to right. Temperature range unknown.

had accumulated to an extent which obscured the effect of the underlying lattice. Flashing the sphere at this point invariably produced the pattern of Fig. 3, C.

Although only one crystal grain is shown in these photographs it was also observed that equivalent directions on other crystal grains on the side of the sphere away from the camera had apparently completely equivalent properties. Thus the contamination was not localized nor do the surface properties depend on the particular crystal selected.

A close inspection of Figs. 4, 5 and 6 will show that the patterns grow into one another in complicated ways as the temperature is varied. It will also show that some regions, at a given contamination, may have a comparatively low emission throughout activation, others a comparatively high emission. All that emit visibly exhibit a maximum with temperature increase, but the temperature of the maximum varies with the condition of contamination and the surface. No surface was observed to have a minimum of emission with temperature increase (over the temperature range of caesium activation).

Because the ionization gauge never showed a pressure greater than $10^{-7}$ mm of Hg at any time (pressure increases during flashing of sphere) after this tube (caesium No. 2) was sealed off, and generally registered a vacuum of the order of $10^{-8}$ (exclusive of caesium vapor), these figures are particularly interesting in showing the enormous effects of very minute amounts of gas or other contamination on adsorption studies.

### X-ray orientation

A Laue back-reflection picture[17] made with the x-ray beam normal to the sphere surface at the point determined by the center of the triangular pattern of Fig. 5, C unequivocably established this as the 111. The complete check between electronic and x-ray pattern justifies the assumption that electrons go radially to the fluorescent wall of the bulb.

[17] Alden B. Greninger, American Institute of Mining and Metallurgical Engineers, Institute of Metals Division **117** (1935).

## Discussion

### Nature of surfaces

Because of (1) the symmetry of the contaminated patterns, (2) the equivalence of emission from spots on the same or different crystals having the same or equivalent directions, and (3) the fact that under different conditions of contamination, different directions having very high Miller indices show properties distinct from those of nearby regions, it appears that the surfaces developed on the sphere are completely characterized by the crystallographic directions normal to the macroscopic surface of the sphere. No one surface can be said to dominate a very large fraction of the total area.

This latter point is borne out by the observation that the boundaries of the emission regions displayed on contaminated complex surfaces moved smoothly as the temperature was raised and lowered. That is, in general no one region gained or lost emission as a whole. Instead there was a gradual encroachment of an emitting area into a nonemitting one, or vice versa. Thus the considerable high temperature treatment for good outgassing in several tubes has not produced a polyhedron which approximated to the original sphere.

There remain two alternatives. (1) A given surface may have a faceted fine structure,[18] the facets being fundamental surfaces of simple structure. Such surfaces appear on metal crystals when etched with certain reagents. If more than one fundamental facet was produced, the relative area of each kind on a given surface would be a function of the direction normal to it. (2) A given surface may be approximated by that produced when all atoms are retained whose centers lie on one side of a plane passed through the crystal. This is termed an ideal surface.

If the first hypothesis were true, then the emission properties should change smoothly and monotonically in going from the normal which specified one of the fundamental surfaces to the other. Unless one is willing to accept very complicated surfaces as the fundamental ones, Fig. 5, B and Fig. 6, A and B, cannot be explained on this hypothesis. For instance, the small bright spots of Fig. 5, B near the 110

[18] L. Tonks, Phys. Rev. **38**, 1030 (1931).

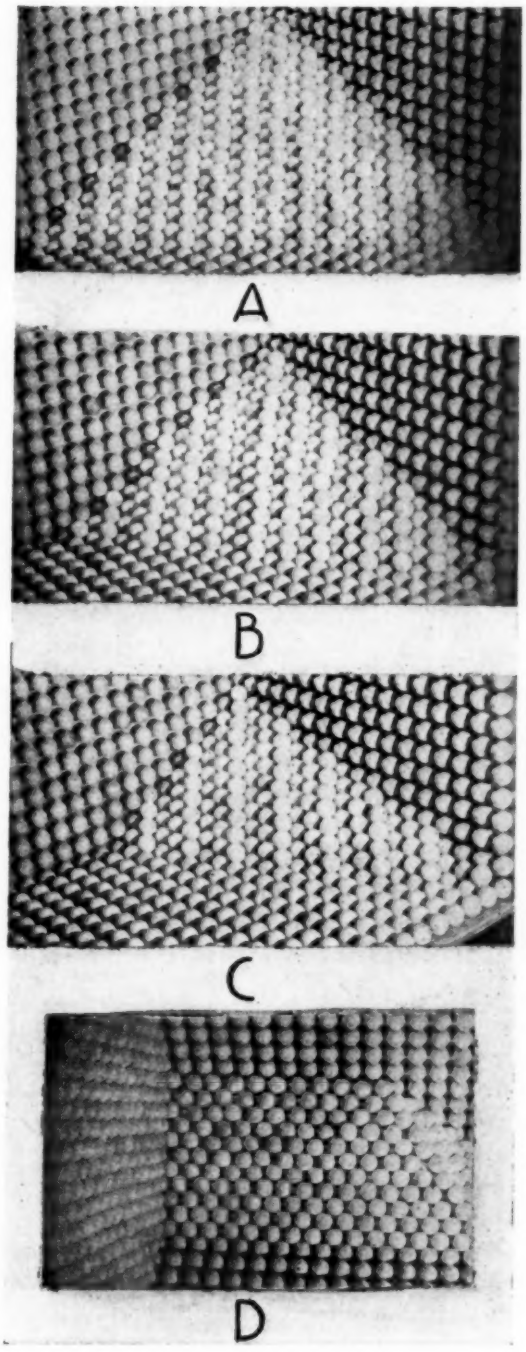


FIG. 7. Sample surfaces of $\bar{1}\bar{1}1$ zone. (*A*) 211; (*B*) 437; (*C*) 213; (*D*) 101. Floor and sides of model are 100 surfaces, except that underlying atoms are missing.

direction have indices approximately 12,9,2. Furthermore, the 110 surface has been proposed as one such fundamental facet for tungsten after high temperature treatment because of an early experiment of Langmuir's,[19] and because its high surface density of atoms and simple structure make it an appealing one. In this case it would certainly be expected that the sphere would show a step structure in a considerable region around the 110 direction with the tops of the steps consisting of 110 surfaces. The extraordinarily sharp variation of properties in this region shown in Fig. 5, B make this an unfavorable supposition. It is quite possible that Langmuir's result may be explained by etching of the surface, possibly by water vapor.

Alternative (2) is supported quite strongly by the above phenomena, and also by the fact that the line of emission extending between the 211 and 110 surfaces of the sphere in Fig. 3, B can be explained on this basis. Fig. 7, A, B, C and D, shows photographs of models of the ideal surfaces of the b.c.c. lattice whose normals are, respectively, the 112, 437, 213, and 101 directions.* These are sample surfaces of the $\bar{1}\bar{1}1$ zone.

The 211 surface consists of rows of atoms, at two different levels, forming long troughs and ridges. The 110 is a "flat" surface in that all atoms exposed are at the same level. The other surfaces of the 111 zone lying between these show a combination of these two types of structure and no other. Consequently it may be assumed that a structure sensitive property like adsorption should vary smoothly in going from the one surface to the other along this zone. If both of these give good emission under caesium adsorption, the intervening surfaces should do likewise. A tendency for this zone to behave as a unit can also be seen in Fig. 4. A similar tendency has been noted in other observations of caesium on contaminated tungsten although the cleancut behavior of uncontaminated surfaces is not expected.

### Differences in caesium and barium adsorption

*Caesium.*—Caesium adsorbs most strongly on surfaces of highest work function (best emitting surfaces at the highest temperatures of activation are considered to have the strongest adsorp-

[19] I. Langmuir, Phys. Rev. **22**, 374 (1923).

* In making this model advantage was taken of the fact that if spheres of diameter "$a$" are pegged out on a flat surface at the corners of a square grid whose distance of repetition is $(2/\sqrt{3})a$, subsequent spheres of this diameter laid thereon automatically build up a body-centered cubic lattice.

tion forces) when the tungsten surface is clean, although there is not an exact reversal of the clean tungsten pattern. This behavior is expected since the ionization energy of $Cs^+$ is 3.88 electron volts. This is lower than the work function of any tungsten surface[8] and the radius of the ion is so large (2.62A for coordination number 8)[20] that variations in the energy term arising from a varying image force on different surfaces may be neglected. The determining factor in the energy of adsorption is the difference between the ionization energy of the atom and the work function of the surface.

As mentioned before the invariance of configuration of the emission pattern of caesium on clean tungsten distinguishes it from that of caesium on a contaminated surface. It is generally accepted that the work function of a homogeneous surface must have a minimum with increasing concentration of adsorbed material. Consequently a "reversal" of the emission pattern was expected as the temperature was decreased, caused by the work function of poorly adsorbing surfaces reaching a minimum at a lower temperature than that corresponding to the minimum of the better adsorbing surfaces. Such behavior is noticeable in Figs. 4, 5 and 6.

It is quite possible that the expected reversal takes place at temperatures where emission from all surfaces is below the minimum observable. This minimum current density is computed to be about $10^{-6}$ amp./cm$^2$. From previous work it is estimated that the minimum observable current density at the fluorescent screen is $10^{-8}$ amp./cm$^2$ at the voltages of operation (8000v). Linear magnification is about 20. At a room temperature of 27°C, it may be computed from the data of Taylor and Langmuir[9] that this allows observation over a "coverage" range from $\theta=0.3$ to $\theta=0.7$.

*Barium.*—DeBoer has shown[11] that the adsorption of barium is possible (he considers only electrostatic binding forces for the ions, van der Waal's forces for the atom) only if the doubly charged ion is held to the tungsten surface by virtue of the image force, since the difference between work function and ionization energy is positive and energy must be supplied to the combination metal plus ion. This energy is more than supplied by polarization of the metal by the approaching ion if the radius of the ion is sufficiently small. This is not the case when the singly charged ion is used, but in spite of the great increase in energy needed to ionize the barium atom doubly, it is true in this case because of the smaller ionic radius. Computations were made for a plane surface.

Examination of models of surfaces in the neighborhood of the 100 show that these have a large percentage of their area occupied by groups of four neighboring atoms (refer to Fig. 7 for representations of ideal 100 surfaces) so that their adsorption properties should be similar to the 100. The radius of the doubly charged barium atom must be considerably smaller than that of singly charged caesium, so that the very strong emission from this region may be accounted for by supposing that the barium is adsorbed in these places. In such a position it is effectively in a small recess in the surface and the ion and its image are appreciably closer than they would be on any other surface, resulting in a larger image force.

Since the barium pattern of Fig. 3, D remains unchanged even after a considerable evaporation of barium has taken place (total emission declines steadily), the regions from which emission is occurring may be taken as those for which adsorption forces are the greatest. The triangular emission region is not easily explained with the model. The lines are portions of 311 zones, but the surfaces of these zones do not display the regularity of the 111 zone surfaces. It has not yet been discovered why only a portion of these zones display singular emission properties.

*Clean tungsten.*—The emission from clean tungsten did not show the spectacular variations with direction displayed by the others because (1) it is very likely not nearly so sensitive to change in configuration of the surface as is adsorption, (2) the high temperature of observation probably makes the surfaces more nearly alike because of thermal commotion of the surface atoms, and (3) the ratio of the emissions from two different surfaces are governed by terms of the form $\exp(-Ve/kT)$ where $V$ is the difference between respective work functions,

[20] W. Hume-Rothery, *The Structure of Metals and Alloys* (Institute of Metals Monograph and Report Series No. 1, 1936).

and the higher the temperature the more nearly does this approach unity for a given $V$.

Observations made on a polycrystalline wire recrystallized in the course of a few seconds by the treatment normally followed in thermionic experiments, probably represent the average of the emission of the sphere. A multitude of small randomly oriented crystals is known to result from such treatment. In such an average about half of the surface contributes at least 90 percent of the total emission. Consequently it is not remarkable that the constant $A$ in Richardson's equation has never been found to be in satisfactory agreement with experiment. There are, of course, other factors* which may cause deviations from the theoretical value, even though observations are made on a single homogeneous ideal crystal surface.

**Taylor-Langmuir and Becker experiments**

The quantitative work of Taylor and Langmuir,[9] and Becker[10] on caesium adsorbed on tungsten, is difficult to evaluate in the light of these experiments because it is not possible to say with certainty what surfaces dominated their wires. The Langmuir-Taylor theory, with which the Becker experiments agree, assumes that their wires had surfaces composed of 110 facets. It is doubtful if such a surface was produced by the vacuum treatment alone, as this was quite comparable to that given the cathode in this experiment. However, etching by preliminary treatment in wet hydrogen to bring the springs into a condition where they would not twist the wire, or other preliminary treatment may have done this.

It is possible to calculate from the Taylor-Langmuir paper[9] that the work function of the wires used was 4.62 ev.* This agrees with Nichol's best value of the 110 work function of 4.65 ev.[8] Consequently it seems likely that the data are representative of the 110 surface of tungsten, as supposed.

Since the work functions of all tungsten surfaces are greater than the ionization energy of caesium, the data of Taylor and Langmuir on ion and atom evaporation are quite unimpeachable whatever the state of the surface of their wires.

ACKNOWLEDGMENTS

I wish to thank Professor W. B. Nottingham, who directed this work, for his encouragement, advice and criticism. I wish to thank Dr. R. B. Nelson for much valuable help and criticism throughout the course of this work. To Mr. Walter Ennis, glassblower, and Mr. Lawrence Ryan, assistant glassblower, my sincere thanks for much difficult preparation without which this work could not have been accomplished.

For helpful suggestions and gifts of invaluable materials I wish to thank Dr. G. R. Shaw and Dr. L. B. Headrick of the Research and Development Section, RCA Manufacturing Company, Radiotron Division.

My sincere thanks to the Charles A. Coffin Research Foundation for a fellowship in the year 1937–38 for the continuation of this research.

* These are: A work function which varies linearly with temperature, and loss of low energy electrons by reflection at the surface potential barrier. See reference 5.

* Langmuir approximated the Richardson equation over the temperature range 600°–1000°K with one of the form $i=A_0 \exp(-b_0/kT)$ which fits the Richardson equation $i=AT^2 \exp(-b/kT)$ at the center of the temperature range in slope and magnitude. The necessary relations are easily derived as:

$A_0=A(T^2_M)(e^2)$ ($e$=base of natural logarithms)
$b_0/k=(b/k)+2T_M$ ($T_M$=center of temperature range).

Taking $T_M$ as 800°K and their value of $b_0=(4.76/300)\times(4.80\times10^{-10})$ we obtain the above.

# LETTERS TO THE EDITOR

*Prompt publication of brief reports of important discoveries in physics may be secured by addressing them to this department. Closing dates for this department are, for the first issue of the month, the eighteenth of the preceding month, for the second issue, the third of the month. Because of the late closing dates for the section no proof can be shown to authors. The Board of Editors does not hold itself responsible for the opinions expressed by the correspondents.*

**Communications should not in general exceed 600 words in length.**

## Electrical Conductivity as a Function of Temperature of Some Manganous Compounds

Recently the author[1] has studied the magnetic susceptibility of MnO, MnS, MnSe, and MnTe as a function of temperature. The anomalies observed has led to a study of the conductivity of these salts. The compounds were powders pressed firmly between two copper disks with electrical leads. For low resistance values a Wheatstone bridge was used; for high resistance values, the feeble current driven through the specimen was amplified by a Vance meter.

Plotting the log of the resistance against temperature for MnSe, MnS, and MnO one gets a series of straight lines one above the other. They behave like nonconductors in that the greater the temperature the lower the resistance (order of $10^6$ ohms at 298°K). The greater the molecular weight of the $Mn^{++}$ compound, the greater the specific conductivity. The resistance value of MnTe in Fig. 1 is very much smaller and the change in conductivity is unique.

The hysteresis effect which has been detected in the magnetic studies presents itself again as an abnormally long relaxation time for the conductivity to return to its characteristic value after the crystals had been transferred from one temperature bath to another. Thus in the case of MnSe, if one approached 200°K (solid $CO_2$ bath temperature) from the high temperature side (ice bath) it required approximately an hour before the resistance reached its final higher value. A similar long relaxation time was observed for MnTe around its λ-point.

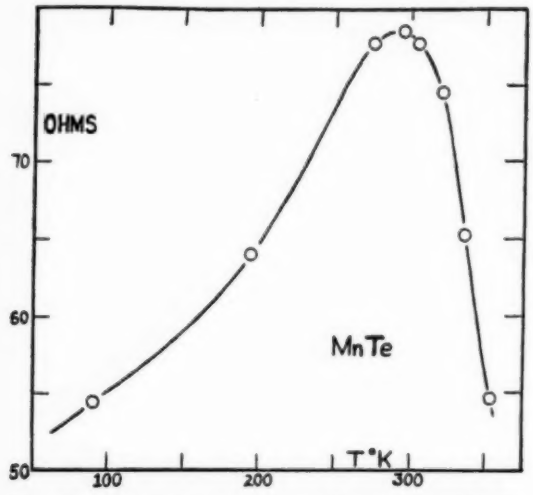


FIG. 1. Variation with temperature of the resistance of MnTe.

The fact that MnTe has a relatively high conductivity would lead one to classify it as a semi-conductor. The fact that the exchange force at the λ-point draws the crystal together, leads one to suppose that the electronic energy bands approach one another in going from high to lower temperature at the λ-point. One can reason from this, though it is by no means conclusive, that the conductivity anomaly of MnTe is associated with the change in the value of the excitation energy needed for an electron to enter the conducting energy band.

The theoretical problem which these experiments present is one which has already received some attention by L. Landau.[2] Hysteresis effects in third-order transitions have been measured in completely different phenomena than mentioned here.[3] The author is indebted to Professor Edward Teller for discussions of this research.

CHARLES F. SQUIRE

Department of Physics,
University of Pennsylvania,
Philadelphia, Pennsylvania,
August 22, 1939.

[1] *Physical Review*, this issue.
[2] L. Landau, Sow. Phys. Zeits. **4**, 675 (1933).
[3] A. Smits, Physik. Zeits. **36**, 367 (1935).

## Suggested Observation of the Zodiacal Light During a Total Solar Eclipse

Various features of the zodiacal light, such as the width and brightness of the zodiacal band, are known to within about 30° from the sun.[1] Because of the obscuration by sunlight scattered by the atmosphere no observations have been made closer than about 30°. It appears that observations might be extended to perhaps 5° from the sun during a total solar eclipse by an observer on the night side of the earth and within a few degrees of the sunset or sunrise horizon. In such a situation he would be shielded from the direct rays of the sun by both the earth and the moon, and his twilight sky toward the sun being shielded by the moon would be unusually dark although illuminated by the solar corona. Thus he would be in a position to examine with the unaided eye the width and brightness of the zodiacal band as near to the sun as possible and perhaps to see how the band merges into the corona. Since the brightness of the zodiacal light increases rapidly with decreasing angular distance from the sun plans might be made to photograph the light and to obtain its spectrum.

A total solar eclipse occurs on October 1, 1940, the path of totality extending across the northern part of South America and the southern part of South Africa.[2] The twilight regions most favorable to the foregoing

zodiacal observations are strips about 2° wide, one strip in about 3° north latitude and 80° to 100° west longitude in the Pacific Ocean off the coast of Colombia, and one strip in about 33° south latitude and 53° to 73° east longitude in the Indian Ocean about a thousand miles east of the Cape of Good Hope. The regions are entirely at sea and embrace no islands or land areas. This is an important advantage and in agreement with the view of Conrad who referred to the surface of the earth as "seven-eighths water, a fit abode for sailors."

E. O. HULBURT

Naval Research Laboratory,
Washington, D. C.,
October 3, 1939.

[1] E. O. Hulburt, Phys. Rev. **35**, 1098 (1930).
[2] *American Ephemeris and Nautical Almanac for 1940*, p. 586.

---

### Mass and Energy Levels of $S^{33}$

Among the lighter stable nuclei the mass of $S^{33}$ has not yet been determined. It was found that on bombarding a sulphur target with 3.1-Mev deuterons from a cyclotron a considerable yield of protons was observed corresponding to the absorption of a neutron by the sulphur nucleus and emission of a proton. An absorption curve was plotted for these protons which showed the presence of three very well-marked groups with energy change values +6.60, +3.70 and +1.02 Mev. The third group may perhaps be due to carbon contamination but the first two are definitely due to sulphur. If it is assumed that the observed protons are from the $S^{32}$ isotope which comprises 96 percent of the target, then the reaction occurring is

$$S^{32}+H^2 \rightarrow S^{33}+H^1$$

and since the mass of $S^{32}$ has been found by Aston we may deduce the mass of $S^{33}$. The value found is $32.9818 \pm 0.0030$. This agrees nicely with the value 32.9816 calculated by Barkas.[1] It is not likely that the isotope $S^{34}$ which is present to 3 percent is responsible for the observed protons, for this would require a mass of 34.978 which is stable with respect to beta-decay to $Cl^{35}$, contrary to experience. The $S^{33}$ isotope can virtually be eliminated on account of its very low abundance of 1 percent only.

The group at an energy-change value of 3.70 Mev indicates an excited state 2.9 Mev above the ground state and, if the third group is due to sulphur as its abundance indicates, a second excited state 5.58 Mev above the ground state. The probability of transition to the first excited state is three times that to the ground state. It is interesting to compare the above levels with the values 1.3, 2.8, 4.8 Mev above ground found for $S^{34}$ from the reaction

$$P^{31}+He^4 \rightarrow S^{34}+H^1.$$

I wish to thank Mr. W. L. Davidson, Jr., for his assistance in operating the cyclotron and preparing the target, and Professor E. O. Lawrence for the gift of the 27" acceleration chamber formerly used at Berkeley.

ERNEST POLLARD

Sloane Physics Laboratory,
Yale University,
New Haven, Connecticut,
October 16, 1939.

[1] W. H. Barkas, Phys. Rev. **55**, 691 (1939).

### Deviation from the Coulomb Law for a Proton

In a recent letter to the Editor of this Journal W. E. Lamb[1] has criticized our paper on the deviation from the Coulomb law.[2] In this paper we have discussed the possibility of short range forces between a proton and a point charge on grounds of the meson theory.

The total interaction energy between the proton and the point charge at a distance $R$ was shown to be of the following form:

$$V(R) = -\frac{e^2}{R} + \frac{e^2}{R}\int \rho d\tau - e^2 \int \frac{\rho(\mathbf{r})}{|\mathbf{R}-\mathbf{r}|} d\tau. \qquad (1)$$

Here $\rho(\mathbf{r})$ is the charge density of the meson field surrounding the proton according to the first approximation of the meson theory and is given in F.H.K. The third term (denoted in F.H.K. by $W_{\mathrm{I}}(R)+W_{\mathrm{II}}(R)+W_{\mathrm{III}}(R)$) arises from the third-order perturbation theory (corresponding to the three stages: emission of meson by proton, deflection of meson by point charge, reabsorption of meson by neutron). The second term of (1) represents the change of the second-order self-energy in the presence of the point charge as discussed in F.H.K., footnote on p. 274. It is due to the fact that the resonance denominators in this expression contain an additional term $e^2/R$. If one expands the expression for the second-order self-energy in powers of $e^2$ the term proportional to $e^2$ is exactly given by the second term of (1).

Both the second and the third terms of (1) diverge separately. The sum of the two terms, however, converges and was denoted in F.H.K. by $W'(R)$. A consistent application of the perturbation theory up to the third order gives therefore a converging result. At small distances, $W(R)$ was found to be larger than the Coulomb attraction $e^2/R$ and $V(R)$ is therefore repulsive at small distances.

Because of its proportionality to $1/R$ we have interpreted the second term of (1) as due to the absence of the Coulomb attraction of the proton during the "time of dissociation" the fraction of which would be equal to $\alpha = \int \rho d\tau$. This concept was used in our paper merely as an abbreviation for a term occurring in the perturbation theory.

Lamb's criticism is now based on the fact that according to (1) *a repulsive effect can only be obtained if $\alpha > 1$. This would seem unreasonable in view of the physical meaning of $\alpha$.*

In view of this result it is necessary to investigate the question as to what extent such a dissociation time has any physical meaning. In fact it seems that the only meaning one can attach to it is in the sense of a probability of finding the meson at a distance larger than $r$, say, from the nucleus. In its physical essence this is equivalent with the question of whether there is a "probability of finding the meson at a certain point or in a small volume $v$." As will be seen below this is not the case if the linear dimensions of $v$ are smaller than $\hbar/\mu c$ ($\mu$ = rest mass of meson).

The physical quantity which always has a physical meaning is the *charge density*. In our problem the charge density from which (1) is derived consists of two terms:

$$\rho' = -\delta(r)\int \rho d\tau + \rho, \qquad (2)$$

where the first term represents an infinite negative point

charge at the position of the proton. The total charge is zero (omitting the charge $+e$ of the proton). The charge contained in any small volume is finite but may be negative or larger than 1. Lamb's argument now runs as follows: Since the proton is capable of emitting only *one* positive meson at a time the charge contained in any volume of space must always be positive and smaller than 1.

This, however, appears to be quite false in a field theory describing Bose-Einstein particles. It is well known that in such a theory the *charge density is not positive definite.* This may even be the case if we have in *momentum space* a single free positive meson. Let its wave function be

$$\psi=\sum_i c_i\varphi_i, \qquad \sum_i |c_i|^2=1,$$

where $\varphi_i(\cdots n_j^+\cdots n_j^-\cdots)$ depends on the number of positive and negative mesons with wave numbers $k_j$. Let $\varphi_i=1$ if $n_i^+=1$ and all other $n=0$, and $\varphi_i=0$ for all other states. From the formulae of Pauli and Weisskopf the expectation value of the charge density at the point $\mathbf{r}$ becomes ($\epsilon_i$=energy in state $k_i$)

$$\bar{\rho}=\frac{e}{V}\left[1+\frac{1}{2}\sum_{i\neq j}\left(\left(\frac{\epsilon_i}{\epsilon_j}\right)^{\frac{1}{2}}+\left(\frac{\epsilon_j}{\epsilon_i}\right)^{\frac{1}{2}}\right)c_ic_j^*\exp\left(i(\mathbf{k}_i-\mathbf{k}_j,\mathbf{r})\right)\right]. \quad (3)$$

($V$=volume in ordinary space.) The total charge is $+e$. Yet $\bar{\rho}$ is negative in some points if at least one $\epsilon_i$ is large compared with another $\epsilon_j$. The regions of volume in which this is the case are always smaller than $\hbar/\mu c$. Thus there are small regions of volume in which the charge is negative or larger than 1. The result is connected with pair creation taking place if one tries to localize the meson in a volume smaller than $\hbar/\mu c$. It is clear that in such a small volume the position of the meson (and therefore the "dissociation time") has no longer any physical meaning.

Since even for a free positive meson the charge density may be negative in some points there is certainly *no legitimate reason for expecting that the charge density surrounding a proton according to the meson theory should not be negative in some points.*

It is true that for our result kinetic meson energies higher than $\mu c^2$ are required. It is doubtful whether the present meson theory can still be applied in this region. This was clearly emphasized in our paper. The fact, however, that some quantities diverge if kinetic energies $>\mu c^2$ are used is, in our opinion, not sufficient to postulate that the same "cutting off" rule should be applied for convergent effects. The purpose of our paper was to find convergent effects by which the limits of the theory can be checked experimentally.

H. Fröhlich
W. Heitler
B. Kahn

H. H. Wills Laboratory,
University of Bristol,
Royal Fort, Bristol 8, England,
September 24, 1939.

[1] W. E. Lamb, Phys. Rev. **56**, 384 (1939). We are indebted to Dr. Lamb for having sent us his manuscript before publication.
[2] H. Frölich, W. Heitler and B. Kahn, Proc. Roy. Soc. **A171**, 269 (1939) referred to as F.H.K.

**Coincidences Between Beta- and Gamma-Rays in $Na^{24}$**

Using a method previously described,[1] we have investigated the coincidences between beta- and gamma-rays in $Na^{24}$.

The beta-ray spectrum of $Na^{24}$ has been studied by several investigators, the most recent of which are Feather and Dunworth;[2] Kikuchi, Watase, Itoh, Takeda and Yamaguchi;[3] and Lawson.[4] Feather and Dunworth, measuring the range of the beta-particles in aluminum, concluded that the end point was $1.40\pm0.05$ Mev and that the spectrum was simple. Both Lawson and the Japanese investigators used a beta-ray spectrograph for analysis. The former, using very thin sources, concluded that the spectrum was

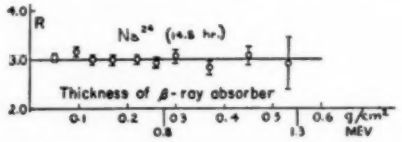


FIG. 1. Ratio $R$ of beta-gamma coincidences to beta-rays recorded ($\times 10^3$) as a function of the beta-ray energy.

simple and that the end point was at 1.40 Mev. The Japanese investigators, on the other hand, believe the spectrum to be complex and analyzable into three groups.

The gamma-radiation has been found to consist of three lines at 1.01, 2.04 and 3.00 Mev by Richardson and Kurie,[5] and Richardson.[6] On the other hand, the Japanese investigators suggest that there are gamma-rays of 2.97, 1.55, 0.8 Mev and possibly some of still lower energy.

In the present investigation, preliminary experiments were performed with a source of sodium fluoride bombarded by neutrons from a radium-beryllium neutron source but final results were obtained with the help of a strongly activated source of $Na^{24}$ from the Berkeley cyclotron. The end point of the beta-ray spectrum was obtained by measuring the range in aluminum. The results give an end point of $1.43\pm0.05$ Mev.

To measure beta-gamma and gamma-gamma coincidences, the source was mounted midway between two counters. Aluminum of 0.60 cm thickness, sufficient to stop completely all beta-particles, was placed between the source and one of the counters. Between the source and the other counter there was placed either 0.6 cm of aluminum for measuring gamma-gamma coincidences, or smaller thicknesses of aluminum for measuring beta-gamma coincidences as a function of the energy of the beta-rays. The resolving time of the coincidence circuit was $0.56\times10^{-7}$ min.

The number of gamma-gamma coincidences per thousand gamma-ray counts was found to be $1.72\pm0.05$. The beta-gamma coincidences were measured as a function of the energy and are shown in Fig. 1. As ordinate is plotted the number of beta-gamma coincidences per thousand beta-counts (the appropriate number of gamma-gamma coincidences subtracted) against the thickness of the beta-absorber, and therefore as a function of the beta-ray energy. It will be seen from the graph, that the number of beta-gamma coincidences per thousand beta-rays remains constant at 3.0 throughout the whole range of the spectrum. This means that *the beta-ray spectrum of* $Na^{24}$ *consists of a*

*single group*. Furthermore, it follows at once from the data that $Mg^{24}$ is formed in an excited state.

The existence of gamma-gamma coincidences means that in at least some cases there are two or more gamma-rays emitted per disintegration in dropping from the excited state of $Mg^{24}$ to the ground state. If one assumes that the sensitivities of the counter to the different gamma-rays emitted by the source is not very different from an average sensitivity $S_\gamma$, one may get an estimate of $K$, the average number of gamma-rays per disintegration. We have, from the beta-gamma coincidences data,

$$N_{\beta\gamma}/N_\beta S_\beta = S_\gamma K = 3.0\times 10^{-3}, \quad (1)$$

where $N_{\beta\gamma}$ is the beta-gamma coincidence rate, $N_\beta S_\beta$ the number of beta-rays recorded.

From the gamma-gamma coincidence data we have[7]

$$N_{\gamma\gamma}/N_\gamma S_\gamma = (K-1)S_\gamma = 1.72\times 10^{-3}. \quad (2)$$

Therefore,

$$K = 2.36.$$

The level scheme proposed by Richardson and Kurie permits the transition to the ground level to take place either in one jump by a 3-Mev gamma-ray or in two steps of 2 Mev and 1 Mev. This should result in an average value of $K$ less than 2. The scheme of Feather and Dunworth, on the other hand, calls for a 1-Mev gamma-ray followed by one of 3 Mev or alternatively a 2-Mev gamma-ray followed by another of 2 Mev. This should give $K=2$. Our value of $K=2.36$ suggests that in some cases the transition to the ground level may take place in even more than two steps.

The authors wish to express their thanks to Professor E. O. Lawrence for furnishing a strong source of radioactive sodium and to the Penrose Fund of the American Philosophical Society for a grant.

LAWRENCE M. LANGER
ALLAN C. G. MITCHELL
PAUL W. MCDANIEL

Department of Physics,
Indiana University,
Bloomington, Indiana,
October 12, 1939.

[1] L. M. Langer, A. C. G. Mitchell and P. W. McDaniel, Phys. Rev. **56**, 380, 422 (1939).
[2] N. Feather and J. V. Dunworth, Proc. Camb. Phil. Soc. **34**, 442 (1938).
[3] S. Kikuchi, Y. Watase, J. Itoh, E. Takeda, and S. Yamaguchi, Proc. Physico-Math. Soc. Japan **21**, 7 (1939).
[4] J. L. Lawson, Phys. Rev. **56**, 131 (1939).
[5] J. R. Richardson and F. N. D. Kurie, Phys. Rev. **50**, 999 (1936).
[6] J. R. Richardson, Phys. Rev. **53**, 124 (1938).
[7] This formula differs from that given in our previous papers. A full discussion will be given elsewhere. The use of this formula rather than the previous one makes no change in our conclusions on the spectrum of In, but necessitates a different interpretation of the value of $K$ in the case of Mn.

## The Use of Radioactive Forms of the Common Elements in Physiology

The use of radioactive forms of the elements as "tracers" for studying cell-wall permeability and metabolic processes is becoming increasingly common in physiology. For example, Cohn and Cohn,[1] using radioactive sodium, have recently reported that this form of the element readily traverses the wall of the red blood cell. They conclude, therefore, that ordinary nonradioactive sodium, contrary to what had generally been thought, passes as readily through the red cell membrane.

Since the red cell is known to have a charged surface[2] composed of a polar lipoidal substance probably of monomolecular thickness,[3] it is fair to raise the question as to whether (1) the charge on the limiting membrane of a red blood cell and (2) the polar properties of the lipoid molecules of which it is composed, might not be modified by the radiations (electrons and gamma-rays) emanating from the radioactive ion being studied. One would not expect electrically asymmetrical polar molecules in a monolayer to remain indifferent to bombardment by electrons and gamma-rays at short range and any change in the polar properties of the membrane would, according to Wilbrandt,[4] alter its permeability. Fricke[5] has shown that beta- and gamma-rays are capable of denaturing proteins. Radioactive sodium, once it has traversed the cell membrane, might, therefore, also denature the proteins in the vicinity of the cell surface and grossly modify surface conditions. Since the cell membrane is assumed to have a thickness of the order of one molecule, the radioactive sodium might even modify intracellular proteins while outside the cell, its radiations traversing the cell wall before the ion itself has penetrated. Any conclusions as to the permeability of the walls of a red cell for radioactive sodium ion cannot, therefore, be properly extended to embrace the behavior of the nonradioactive forms of the same element, until or unless it is first shown that the radioactivity is without effect on the membrane and on the proteins with which the latter is in contact.

The question raised here is, of course, broader than the illustrative case given. It applies to the general body of work now currently appearing in many journals and involving the use of radioactive forms of the common elements as tracers. Until it is answered, it will be fair to doubt the validity of conclusions drawn as to the corresponding behavior of nonradioactive forms of the same elements.

A. BARNETT

New York State Psychiatric Institute and Hospital,
722 West 166th Street,
New York, New York,
October 14, 1939.

[1] W. E. Cohn and E. T. Cohn, Proc. Soc. Exp. Biol. and Med. **45**, 445 (1939).
[2] E. Gellhorn and J. Régnier, *La Perméabilité* (Masson et Cie., Paris, 1936) p. 217.
[3] H. Fricke, J. Gen. Physiol. **9**, 137 (1926).
[4] W. Wilbrandt, J. Gen. Physiol. **18**, 933 (1935).
[5] H. Fricke, *Cold Spring Harbor Symposium* (1938) Vol. 6, p. 164.

## The Nature of Visual Observations at Low Light Intensities

We were led to conclude from visual observations that the minima reported by Allison in his magneto-optic method were reproducible. Our conclusions[1] are certainly wrong as we have not been able by any purely objective method to check these results. In order to clear up the record we wish to make this retraction.

There have been so many cases of erroneous deduction resulting from visual observations at very low light in-

tensities that the problem is worthy of serious consideration. In addition to the magneto-optic effect, we may list the numerous *N*-ray experiments,[2] the Davis and Barnes[3] experiments on the capture of electrons by $\alpha$-particles, and the Pokrovskii[4] experiments on the emission of $\alpha$-particles from lead by x-ray excitation.

In all of these cases the experimenters have been convinced that their observations are real and that their eyes cannot deceive them. This effect might be explained as arising from slight movement of the eye so that the light falls upon a less sensitive region of the retina. To the observer this would appear to be a change of intensity. There may also be some question as to the nerve centers which respond to low order stimuli and the possibility that such centers may be lacking in the usual power of discrimination. However, an element of suggestibility or hypnotism must also be present. Thus there were regions on the scale where we were never able to observe minima although we had expected to find them. Our initial readings appeared to set a pattern which was then reproducible. The observer had no knowledge as to the scale reading, so apparent reproducibility was due either to coincidence and would have disappeared when a sufficient number of readings were taken, or was due to some unknown mode of communication between the observer and his partner who recorded the scale readings and operated the trolley settings. In order to eliminate the possibility of inference from the tonal qualities of the voice, we used a system of buzzer signals as a means of communication. This, however, appeared to have no effect upon the reproducibility of the readings. We are inclined to question whether, under the conditions of these experiments, reproducibility has any physical significance when one member of the pair has knowledge of the previous result. Whatever interpretation one cares to make of this statement, it will at least be granted that this is a safe assumption to make in future observations of this character.

W. M. Latimer
H. A. Young

University of California,
Berkeley, California,
October 12, 1939.

[1] W. M. Latimer and H. A. Young, Phys. Rev. **44**, 690 (1933).
[2] Stradling, J. Frank. Inst. **164**, 177 (1908).
[3] B. Davis and A. H. Barnes, Phys. Rev. **37**, 1368 (1931).
[4] G. I. Pokrovskii, Phys. Rev. **38**, 925 (1931).

# THE AMERICAN INSTITUTE OF PHYSICS

INCORPORATED


## ADMINISTRATIVE STAFF

HENRY A. BARTON, *Director*

MADELINE M. MITCHELL, *Publications Manager*

*Office:* 175 Fifth Avenue, New York, New York

## JOURNALS

THE PHYSICAL REVIEW
REVIEWS OF MODERN PHYSICS
JOHN T. TATE, *Editor*
J. W. BUCHTA, *Assistant Editor*

JOURNAL OF APPLIED PHYSICS
ELMER HUTCHISSON, *Editor*

THE JOURNAL OF THE OPTICAL SOCIETY OF AMERICA
THE REVIEW OF SCIENTIFIC INSTRUMENTS
F. K. RICHTMYER, *Editor*

JOURNAL OF THE ACOUSTICAL SOCIETY OF AMERICA
FLOYD A. FIRESTONE, *Editor*

THE JOURNAL OF CHEMICAL PHYSICS
HAROLD C. UREY, *Editor*
JOSEPH E. MAYER, *Assistant Editor*

THE AMERICAN PHYSICS TEACHER
DUANE ROLLER, *Editor*

## GOVERNING BOARD

*For The American Physical Society:*

JOHN T. TATE, *Chairman*
University of Minnesota

GEORGE B. PEGRAM, *Secretary*
Columbia University

KARL T. COMPTON
Massachusetts Institute of Technology

*For The Optical Society of America:*

E. C. CRITTENDEN
National Bureau of Standards

A. C. HARDY
Massachusetts Institute of Technology

W. B. RAYTON
Bausch & Lomb Optical Company

*For The Acoustical Society of America:*

FLOYD A. FIRESTONE
University of Michigan

HARVEY FLETCHER
Bell Telephone Laboratories

WALLACE WATERFALL
The Celotex Corporation

*For The Society of Rheology:*

WHEELER P. DAVEY
Pennsylvania State College

MELVIN MOONEY
United States Rubber Products, Inc.

R. L. PEEK, JR.
Bell Telephone Laboratories

*For The American Association of Physics Teachers:*

PAUL E. KLOPSTEG
Central Scientific Company

FREDERIC PALMER, JR.
Haverford College

F. K. RICHTMYER
Cornell University


The American Institute of Physics is a membership corporation of which five societies are the founding members. These five societies are the principal national societies devoted to pure and applied physics in America. Their names, and those of their representatives who form the Governing Board of the Institute, are given above. The principal work of the Institute is the publication of journals sponsored by the societies or by itself. The names and the editors of the journals are also listed above.

The broad purpose of the Institute is to represent, in all matters of wide or common interest, the five thousand or more members and subscribers associated with the Founder Societies and the journals. It aims to advance the science and profession of physics, and to promote cooperation between pure research, the applied sciences and the industries. To achieve these aims, it is greatly in need of an endowment and is empowered by law to administer grants and funds of any kind.

# CONTENTS

PHYS. REV. 56 (1939) NOVEMBER 1

Internally Converted Gamma-Rays of Several Radioactive Elements . . . . . G. E. VALLEY AND R. L. MCCREARY 863

Radioactivities Produced by Proton Bombardment of Palladium . . . . . T. ENNS 872

Disintegration of Beryllium by Electrons . . . . . GEORGE B. COLLINS, BERNARD WALDMAN AND EUGENE GUTH 876

On the Scattering of Neutrons from the C+D Reaction . . . . . E. AMALDI, D. BOCCIARELLI, F. RASETTI AND G. C. TRABACCHI 881

Effects of Shape of Potential Energy Wells Detectable by Experiments on Proton-Proton Scattering . . . . . L. E. HOISINGTON, S. S. SHARE AND G. BREIT 884

Scattering of Photoneutrons from Deuterium by the Nuclei of Atoms of Light Elements . . . . . T. GOLOBORODKO AND A. LEIPUNSKI 891

Analysis of Proton-Proton Scattering Data . . . . . E. CREUTZ 893

Rotation-Vibration Energies of Tetrahedrally Symmetric Pentatomic Molecules. I . . . . . WAVE H. SHAFFER, HARALD H. NIELSEN AND L. H. THOMAS 895

Measurements of the Mobility of Potassium Ions at High Field Intensity and Low Pressure . . . . . ALLEN V. HERSHEY 908

Theory for the Mobility of Ions of High Velocity . . . . . ALLEN V. HERSHEY 916

Antiferromagnetism in Some Manganous Compounds . . . . . CHARLES F. SQUIRE 922

Specific Heat of a Monatomic Liquid . . . . . WILLIAM J. ARCHIBALD 926

Magnetic Test for Superstructure in Permalloy . . . . . S. T. PAN 933

Energy Fluctuations in the Electromagnetic Field . . . . . P. MORRISON 937

Electrical Breakdown Strength of Ionic Crystals as a Function of Temperature . . . . . R. C. BUEHL AND A. VON HIPPEL 941

On the Thermionic and Adsorptive Properties of the Surfaces of a Tungsten Single Crystal . . . . . S. T. MARTIN 947

Letters to the Editor:

Electrical Conductivity as a Function of Temperature of Some Manganous Compounds . . . . . CHARLES F. SQUIRE 960

Suggested Observation of the Zodiacal Light During a Total Solar Eclipse . . . . . E. O. HULBURT 960

Mass and Energy Levels of $S^{33}$ . . . . . ERNEST POLLARD 961

Deviation from the Coulomb Law for a Proton . . . . . H. FRÖHLICH, W. HEITLER AND B. KAHN 961

Coincidences Between Beta- and Gamma-Rays in $Na^{24}$ . . . . . LAWRENCE M. LANGER, ALLAN C. G. MITCHELL AND PAUL W. MCDANIEL 962

Use of Radioactive Forms of the Common Elements in Physiology . . . . . A. BARNETT 963

Nature of Visual Observations at Low Light Intensities . . . . W. M. LATIMER AND H. A. YOUNG 963

LANCASTER PRESS, INC., LANCASTER, PA.